Ratchetaxis and chemotaxis, or how to direct cell migration under confinement

Emilie Le Maout

UNIVERSITÉ DE STRASBOURG

ÉCOLE DOCTORALE DES SCIENCES DE LA VIE ET DE LA SANTE

Institut de Génétique et de Biologie Moléculaire et Cellulaire (IGBMC)

THÈSE présentée par :

Emilie LE MAOUT

soutenue le 5 Juillet 2018

pour obtenir le grade de : **Docteur de l'Université de Strasbourg**

Discipline/ Spécialité : Physique Cellulaire

Ratchetaxie et chimiotaxie, ou comment diriger la migration des cellules sous confinement

THÈSE dirigée par :
Dr RIVELINE Daniel — Directeur de Recherche, IGBMC, France

RAPPORTEURS :
Dr MARTINEZ FRAIZ Elena — Group leader, IBEC, Espagne
Dr STUDER Vincent — Chargé de Recherche, IIN, France

AUTRES MEMBRES DU JURY :
Dr RYCKELYNCK Michael — Maître de Conférences, IBMC, France
Dr DIDIER Pascal — Professeur, Université de Strasbourg, France
Dr OTT Albrecht — Professeur, Universität des Saarlandes, Allemagne

ACKNOWLEDGEMENTS

I would like to thank my PhD supervisor, Daniel Riveline for accepting me as a PhD student. In fact, I was fully trained as a biologist and arrived in the Cell physics lab having little knowledges about Biophysics. I am grateful for having discovered this field, for all the techniques I learned, the skills I acquired and for your support during this PhD.

I would like to thank all the jury members for accepting reviewing my PhD thesis. Elena Martinez Fraiz and Vincent Studer for being referees of the thesis. I also thank Michael Ryckelynck, Pascal Didier, Albrecht Ott and Erwan Pencreac'h for being part of the jury.

Un grand merci à Erwan Pencreac'h, avec qui le projet a commencé. Ton aide et tes conseils tout au long de cette thèse m'ont été très précieux.

I thank Daniel Riveline, Amélie Godeau, Raghavan Thiagarajan and Alka Bhat for commenting and criticizing the manuscript.

I want to thank my colleagues and former colleagues. Your presence was primordial for the success of this PhD thesis. I liked the moments spent with all of you. Every scientific and non-scientific discussions were stimulating. Jordi Comelles, you taught me the basics of techniques used in the lab, from microfabrication, microscopy images to microfluidics. You are a really good teacher, thank you for your patience and your good advices. Merci Amélie Godeau pour ton aide tout au long de la thèse. Tu m'as également appris beaucoup, entre autre immunomarquage et microcanaux, et tu étais toujours là pour répondre à mes questions. Merci pour ton soutien. Raghavan Thiagarajan, master in microcontact printing, you taught me the protocol. You are a really good teacher and always ready to help. You will definitively be a good PI☺. Alka Bhat, your support was really important to me. Many thanks for all the discussions we had and for being there. See you in India ;). Merci Simon Lo Vecchio pour ton dynamisme et ta bonne humeur! C'est un vrai plaisir de travailler avec toi. I would like to thank also David Caballero for his help and advices.

I would like to thank Marcel Boeglin from the imaging facility for his help in images analysis. Thank you also to the cell culture facility for providing me the different cell lines.

Je tiens aussi à remercier Ricardo et Youssef, anciens voisins à l'ISIS, pour leur gentillesse et constante bonne humeur.

Un grand merci à Carole, Anne-Sophie et Christophe, mes copains de master. On a traversé à peu de choses près les mêmes galères. Sans vous et votre soutien, ça aurait été beaucoup plus dur.

Merci à Caroline, partenaire de boxe et amie. Tu m'as fait aimer Strasbourg et encore plus la boxe.

Je remercie ma famille, mes parents, mes frères et mes grands-parents pour leur soutien et leur patience tout au long de cette thèse. La Bretagne est loin de Strasbourg… mais sans vous (et les colis de kouign amann), je n'aurai probablement pas pu réussir. Je remercie également ma belle-famille, toujours là depuis de nombreuses années. Vous m'avez aidé à garder les pieds sur terre.

Maël, merci pour ta patience depuis tout ce temps et de m'avoir supportée durant ces années de thèse. Merci de ta présence et de ton soutien. C'était difficile mais on a finalement réussi et sans toi je n'aurai pas pu y arriver.

RÉSUMÉ DE LA THÈSE

La migration des cellules est un processus clé qui a lieu aussi bien durant l'embryogénèse, la réponse immunitaire ou encore le développement de maladies comme par exemple le cancer[1–3]. Les nouvelles techniques d'imagerie permettent d'observer les cellules en temps réel et de mieux connaitre l'environnement dans lequel elles évoluent. Les cellules peuvent migrer au sein de la matrice extracellulaire, ou bien dans les capillaires qui irriguent les organes. Ces capillaires ont des diamètres de l'ordre de la dizaine de micromètres[4,5]. Ces études *in vivo* ont permis de révéler le mode de migration des cellules dans un environnement complexe et de mieux appréhender le développement de maladies, comme par exemple le cancer et la propagation des métastases. Cependant, en plus des études *in vivo*, les études *in vitro* sont nécessaires pour observer et comprendre dans un environnement simplifié, les processus conduisant à la migration cellulaire.

Traditionnellement, la motilité de cellule individuelle a été étudiée sur une surface 2D plane. En absence de facteurs extérieurs, la cellule migre de façon aléatoire sans direction privilégiée. Des tests utilisant des chambres de Boyden ont ensuite été développés pour étudier la migration des cellules: deux compartiments sont séparés par une membrane de 15µm d'épaisseur contenant des pores de 10µm de diamètre[6]. Les cellules sont ensemencées dans le compartiment supérieur et le compartiment inférieur contient un chimio-attractant. Les cellules répondent potentiellement à ce gradient chimique et traversent la membrane. Ces tests artificiels reproduisent difficilement les conditions dans lesquelles les cellules peuvent se trouver *in vivo* (confinement) ainsi que les distances sur lesquelles les cellules sont amenées à migrer (plusieurs centaines de micromètres). De plus, des nombreuses études *in vitro* ont notamment montré que les mécanismes et acteurs moléculaires impliqués dans la migration cellulaire étaient différents en surface plane et sous confinement[7–9]. Par exemple, le modèle d'Hawkins et al. (2009) montre qu'une cellule polarisée et confinée dans un micro-canal migre de manière spontanée et en absence de gradient chimique extérieur. Ce sont les forces de frictions entre les murs du micro-canal et la membrane de la cellule ainsi qu'une différence de pression exercée à l'avant et à l'arrière de la cellule qui conduit à son mouvement[10]. Ce mécanisme est indépendant de l'intégrité des contacts focaux alors qu'ils sont primordiaux pour une migration cellulaire sur surface plane.

C'est pourquoi, dans cette étude, nous avons voulu étudier la migration des cellules sur de longues distances et dans des environnements confinés, en présence de facteurs capable de diriger la migration des cellules: la *ratchetaxie* et la *chimiotaxie*. En effet, il est connu que les cellules peuvent détecter des gradients de molécules solubles et de migrer vers la plus forte concentration en molécules attractantes, un phénomène appelé chimiotaxie[11,12]. De ce fait, le développement de métastases dans le cas des cancers du sein et du côlon est attribué à la présence d'un gradient physiologique de la chimiokine CXCL12. En effet, les cellules de ces tumeurs primaires sur-expriment les récepteurs de la chimiokine, appelés CXCR4 et CXCR7[13,14]. Il est également connu que les organes dans lesquels les cellules du cancer du côlon et du sein métastasent (foie, poumon) produisent la chimiokine CXCL12. Pour expliquer ce phénomène, l'hypothèse d'un gradient de CXCL12 à proximité de ces organes a été retenue. Cependant, la présence de gradient soluble capable de diriger la migration des cellules cancéreuses n'a pas été reportée *in vivo*. Comme une alternative à la chimiotaxie, un nouveau mode de migration dirigée a récemment été reporté *in vitro*. La présence de motifs asymétriques et répétés dans l'environnement oriente la migration des fibroblastes NIH3T3 dans une direction et en absence de gradient chimique. Ce phénomène est appelé la *ratchetaxie*. Dans l'équipe, Caballero et al. (2014) ont imprimé des triangles de fibronectine, appelés *ratchets*, séparés d'environ 10 micromètres sur une lamelle en verre[15]. Ils ont observé la migration préférentielle des fibroblastes NIH3T3 vers la pointe du triangle, définit comme la direction positive "+". La cellule envoie des protrusions des deux côtés pour sonder son environnement. Cependant, la probabilité qu'une de ces protrusions s'attache au motif suivant et génère une force de traction est plus importante dans la direction "+", expliquant la rectification de la migration cellulaire en moyenne dans cette direction. Comelles et al. (2014) ont par ailleurs déposé les cellules sur une surface contenant des *ratchets* topographiques[16]. Dans ce cas, les cellules migrent le long des *ratchets* situés dans la direction "+". Le noyau positionne le fibroblaste NIH3T3 et rectifie sa migration. Dans cette étude, ils ont également opposé un gradient de fibronectine aux *ratchets* et ont observé que les cellules ne suivent en moyenne aucun des deux facteurs capable de diriger la migration des cellules. Ils ont donc prouvé que la *ratchetaxie* pouvait contrer l'effet attractant d'un gradient chimique.

L'objectif de cette thèse a donc été d'étudier la migration des cellules dans une nouvelle configuration, plus physiologique, en combinant grâce à des techniques de micro-fluidique, le confinement cellulaire, la *ratchetaxie* et la *chimiotaxie*.

Dans un premier temps, l'effet des *ratchets* sur la migration des cellules dans un espace confiné par des microcanaux en 3D a été étudié. Puis, nous avons combiné les *ratchets* confinés avec un gradient chimique de sérum pour tester l'effet mémoire des cellules. Enfin, nous avons testé la migration des cellules dans un gradient physiologique de la chimiokine CXCL12 et nous avons tenté d'observer la localisation de ses deux récepteurs, CXCR4 et CXCR7.

La première partie de ce projet a été de concevoir les *ratchets* en 3D dans lesquels les cellules doivent être confinées. Cela se fait par le biais de micro-canaux micro-fabriqués et consiste en une série de triangles connectés entre eux, appelés *ratchets*. Afin de respecter le confinement, le volume de chaque *ratchet* doit donc avoir le volume d'une cellule. Dans cette étude, nous avons utilisé les cellules NIH3T3 comme cellules de référence. C'est pour cela que nous avons mesuré le volume des fibroblastes NIH3T3. Il est de 1560±520µm^3 (n=388 cellules, moyenne et écart-type). Le volume d'un *ratchet* a donc été fixé à 1500µm^3. Nous avons également mesuré la hauteur du noyau avec un marquage au Hoechst. Il est de 8.5±1.4µm (n=199 noyaux, moyenne et écart-type). Cette valeur a permis de définir la hauteur des canaux micro-fabriqués à 5µm. Par déduction, l'aire du triangle à concevoir est donc de 300µm^2. Nous avons également mesuré l'axe court du noyau. Il est de 13.4±1.9µm (n=275 noyaux, moyenne et écart-type). Nous en avons déduit l'aire approximative de la coupe du noyau à 90µm^2. Afin de tester différents modes de migration plus ou moins confinés, nous avons varié l'aire i du goulot d'étranglement qui connecte deux *ratchets* successifs (10µm^2, 20µm^2 et 30µm^2) ainsi que l'angle α de la pointe du triangle (8°, 16° et 24°). Les *ratchets* sont nommés en fonction de l'angle α et l'aire i du goulot d'étranglement entre deux *ratchets*. Par exemple, un *ratchet* avec un angle de 16° et un goulot d'étranglement d'une aire i de 20µm^2 est appelé α 16i20. Les triangles sont alors conçus en conséquence. Les cellules sont confinées par les côtés et par le haut. C'est la configuration fermée. La migration des cellules est également étudiée en canaux droits de 20µm^2 et 30µm^2 d'aire de section et constitue les contrôles où les cellules migrent dans un environnement homogène.

Les micro-canaux sont alors micro-fabriqués grâce aux techniques de micro-fabrication en salle blanche et avec le polymère biocompatible, le PolyDiMethylSiloxane (PDMS). Après présentation des cellules à l'entrée des micro-canaux, leur migration peut être suivie au cours du temps par microscopie optique. En l'absence de gradient chimique, nous avons, dans un premier temps, observé que le confinement induit la migration de cellules cancéreuses du sein, appelé cellules MDA-MB-231, qui sont

immobiles sur surface plane. Cela confirme des études déjà publiées relevant que le confinement induisait la migration cellulaire[17,10,9].

Comme mentionné précédemment, le *ratchet* est asymétrique, les cellules peuvent migrer dans la direction du *ratchet*, définit comme la direction "+", ou contre la direction du *ratchet*, définit comme la direction "-". Cependant, en configuration fermée, c'est l'ensemencement des cellules d'un côté du micro-canal qui définit la direction de migration. Pour chaque cellule, différents paramètres sont mesurés : la longueur, le temps et la vitesse du premier mouvement persistant de la cellule. La persistance est définie comme la longueur, le temps et la vitesse durant lesquels la cellule migre sans s'arrêter plus de 30 minutes. La longueur de persistance est maximale lorsque la cellule traverse le micro-canal de part en part et est égale à 350µm. Nous avons testé la migration des cellules dans les différentes conditions présentées ci-dessus, α16i10, α16i20, α16i30 et α24i30 ainsi que dans les micro-canaux droits qui constituent les contrôles.

En micro-canaux droits de 20µm² et 30µm², les cellules migrent de manière persistante tout le long du micro-canal. La longueur de persistance est proche de la longueur maximale et est respectivement égale à 295±90µm et 269±77µm. Au contraire, dans les micro-canaux en *ratchet*, les longueurs de persistance sont significativement réduites, indiquant que les cellules sont gênées dans leur mouvement et marquent une pause avant de reprendre leur migration dans la même direction. Le noyau étant l'organelle le plus gros et rigide de la cellule, cela suggère qu'il gêne le passage efficace de la cellule[18]. Contrairement aux précédentes études publiées, nous n'observons pas de changement de direction de migration dans cette configuration fermée[19,16,15,20]. La polarité de la cellule imposée par l'entrée dans le micro-canal est conservée même si la cellule marque une pause. Cependant, nous notons que plus l'aire du goulot d'étranglement est petite, 10µm², 20µm² et 30µm², plus la longueur moyenne de persistance est faible. Nous avons, pour cette raison, choisit de poursuivre l'étude avec la dimension du goulot d'étranglement intermédiaire, c'est-à-dire le *ratchet* α16i20, qui déforme fortement le noyau sans pour autant empêcher la migration cellulaire.

Nous avons vu que la *ratchetaxie* en espace confiné affecte la migration des cellules mais ne la rectifie pas. Nous avons alors suggéré que le confinement important empêche les changements de direction de migration des cellules. Nous avons réduit le confinement cellulaire pour vérifier notre hypothèse. Pour cela, nous avons développé

la configuration en micro-canaux ouverts. Dans cette condition, les cellules sont confinées sur les côtés mais ne le sont plus par le haut. Les cellules sont déposées au centre des micro-canaux *ratchet* ou droits et peuvent migrer dans la direction du *ratchet* "+" ou contre la direction du *ratchet* "-" dès leur polarisation dans le micro-canal. La longueur du premier mouvement persistant de la cellule est mesurée. Nous observons que les cellules migrent plus loin dans la direction du "+" *ratchet*. La longueur moyenne du premier mouvement persistant de la cellule est égale à 169±151µm dans la direction du *ratchet* "+", 121±95µm contre la direction du *ratchet* "-" et 120±106µm dans les micro-canaux ouverts droits. Puis, nous avons voulu vérifié que la migration des cellules était dirigée dans la configuration en micro-canaux *ratchets* ouverts. Pour cela, la migration des cellules a été suivie pendant 12h et la position finale des cellules a été reportée en micro-canaux droits et *ratchets*. Nous observons que la distribution angulaire de la migration des cellules est asymétrique et orientée dans la direction "+" du *ratchet*, alors qu'en micro-canaux droits, la distribution angulaire est symétrique. Ces résultats sont confirmés par la position finale des cellules qui se situe en moyenne, après 12h de migration, dans la direction du *ratchet* "+". La même analyse pour le contrôle dans les micro-canaux droits ne révèle pas de direction privilégiée de migration. Cela montre que l'effet *ratchet* est bien vérifié pour diriger et rectifier la migration des cellules sur de longues distances en micro-canaux confinés ouverts.

En conclusion, ces résultats sont en accord avec les études de Comelles et al. (2014) sur la *ratchetaxie* topographique et de Le Berre et al. (2013) sur la *ratchetaxie* par le confinement asymétrique du noyau[16,20]. Nous avons montré, en plus, que dans un environnement confiné, plus proche de celui que la cellule peut rencontrer *in vivo*, la migration des cellules était dirigée en présence de motifs asymétriques et répétés présents dans son environnement et en l'absence de gradient chimique.

La deuxième partie de ce projet a consisté en l'étude de la migration des cellules dans des micro-canaux fermés avec un gradient de sérum, connu pour être chimio-attractant. Pour cela, la conception des canaux est modifiée pour pouvoir former le gradient. La forme en « échelle » permet l'introduction de deux milieux, l'un contenant le chimio-attractant et le Dextran couplé au fluorochrome TRITC et permettant la visualisation du gradient et l'autre ne contenant aucun des deux. Une pompe à seringues est nécessaire à la formation du gradient[21]. Celui-ci est visible au bout de quelques minutes après injection. Un gradient de 10% de sérum est formé dans les canaux fermés droits et en *ratchet*. Dans la condition canaux droits et *ratchet*, la longueur moyenne de

persistance est proche de la longueur maximale. Cela montre que ce gradient de sérum favorise la migration des cellules dans les micro-canaux en *ratchet*. De futures expériences devraient être réalisées en utilisant un gradient de sérum plus faible, par exemple de 2% de sérum dans les canaux en ratchet afin d'étudier la sensibilité des cellules à la *ratchetaxie* et *chimiotaxie*.

Cependant, en utilisant le gradient de 10% de sérum, nous avons voulu tester un effet plus significatif, l'effet mémoire des cellules du gradient chimique. Pour cela, la même configuration a été utilisée. Les cellules en présence de gradient entrent dans les canaux. Puis, lorsque les cellules sont dans les canaux, le gradient de chimio-attractant est enlevé. Les cellules sont alors libres de migrer dans la direction du précédent gradient, d'arrêter de migrer, ou bien de changer de direction de migration. Une fois encore, trois configurations existent, le gradient de chimio-attractant est dans la direction "+" des *ratchets*, dans la direction "-" des *ratchets* ou en canaux droits. De manière surprenante, après l'arrêt du gradient de chimio-attractant, les cellules continuent leur migration dans les micro-canaux droits et dans la direction "+" des *ratchets*. Au contraire, dans la direction "-" des *ratchets*, les cellules NIH3T3 arrêtent de migrer dès qu'elles rencontrent le goulot d'étranglement du *ratchet*. Cela suggère fortement que la géométrie du *ratchet* s'oppose à la migration de la cellule. Au contraire, dans la direction du *ratchet*, la migration des cellules est facilitée. Nous proposons l'existence d'une mémoire du gradient de sérum par la distribution asymétrique de protéines liée à l'organisation de l'actine dans les cellules NIH3T3. Par exemple la moesin, protéine liant le cytosquelette d'actine à la membrane plasmique, serait localisée à l'arrière de la cellule après retrait du gradient de chimioattractant de cellules migrant en micro-canaux[12].

L'étape suivante a consisté en l'étude la migration cellulaire dans un gradient physiologique de la chimiokine CXCL12 dont l'existence a été assumée *in vivo* dans le cadre du développement de métastases. Nous avons donc étudié dans un environnement plus ou moins confiné et en présence d'un gradient physiologique de CXCL12, le comportement des fibroblastes NIH3T3 ainsi que la relocalisation des récepteurs CXCR4 et CXCR7. Par surexpression du récepteur CXCR4 couplé à un fluorochrome ainsi que l'immunomarquage de CXCR4, nous avons observé sa localisation au bord de la cellule associée aux lamellipodes dans trois lignées cellulaires différentes, les fibroblates NIH3T3, les cellules cancéreuses du côlon SW480 ainsi que les neutrophiles dHL60. Cela suggère un lien entre CXCR4 et le cytosquelette d'actine. Le récepteur CXCR7 couplé à un fluorochrome est quant à lui observé sous forme de

vésicules qui migrent le long des microtubules dans les deux directions, suggérant un transport des vésicules via la dynéine et la kinésine. Nous soupçonnons que la localisation différentielle des récepteurs CXCR4 et CXCR7 puisse être responsable de la brisure de symétrie dans la cellule conduisant à sa migration dirigée.

Dans un premier temps, nous avons étudié la migration des fibroblastes NIH3T3 en présence de la chimiokine CXCL12 soluble à différentes concentrations et adhérentes à la surface. Pour cela, des expériences de micropipettes, de chambres de Boyden, de gradients en micro-canaux ainsi que la micro-impression de CXCL12 ont été réalisées mais n'ont pas permis de mettre en évidence la migration dirigée des cellules NIH3T3. Les études ont été menées avec les cellules NIH3T3 qui expriment CXCL12. Nous avons supposé que c'était pour cette raison que les cellules NIH3T3 n'avaient pas migré de manière directionnelle vers CXCL12. Nous avons alors utilisé une lignée cellulaire du cancer du sein, appelée cellules MDA-MB-231, et connue pour répondre à un gradient de CXCL12 en chambres de Boyden[14]. Des expériences préliminaires ont mis en évidence la migration des cellules MDA-MB-231 de manière directionnelle dans un gradient de sérum. Cependant, nous n'avons pas observé la migration des cellules du cancer du sein en présence de gradients de CXCL12 en micro-canaux. Cela soulève différents points qu'il reste à élucider : un trop fort confinement peut-il prévenir la migration des cellules en réponse à un gradient de CXCL12 ? Le gradient de CXCL12 a-t-il été choisi de manière optimale ? Un gradient de CXCL12 est-il capable de diriger la migration des cellules sur de longues distances ?

Cette étude a donc permis de tester la migration de fibroblastes dans des micro-canaux ouverts et fermés composés de motifs asymétriques et répétés. La configuration canaux *ratchets* ouverts, où les cellules sont confinées par les côtés, permet de diriger et rectifier la migration des cellules. La configuration canaux droits fermés dirige la migration des cellules. La configuration canaux *ratchets* fermés, où les cellules sont confinées par les côtés et le haut, perturbe la migration cellulaire mais ne permet pas de la rectifier. En condition fermée, la polarité de la cellule est apparemment fixée à son entrée dans les canaux et elle ne peut pas - ou très rarement - changer du fait du fort confinement. Dans les configurations ouvertes et fermées, la migration des cellules se fait de manière dirigée sur de longues distances et sans gradient chimique. Le gradient de sérum utilisé dirige la migration de la cellule quel que soit son environnement, c'est-à-dire canaux droits ou *ratchets.* Cependant, l'arrêt du gradient dans la direction du *ratchet* facilite la migration de la cellule. Au contraire, la direction opposée du *ratchet*,

empêche complètement la migration des cellules en bloquant le noyau à l'entrée du goulot d'étranglement. Cela suggère l'importance de l'environnement pour diriger la migration cellulaire et préserver leur effet mémoire. De plus, nous avons voulu utiliser, dans nos micro-canaux, un gradient physiologique de CXCL12, reconnu comme étant capable de diriger la migration des cellules cancéreuses en chambre de Boyden et d'être responsable de la dispersion des cellules métastatiques. Cependant, nous n'avons pas observé cette migration dirigée en micro-canaux en présence de gradients de CXCL12. Le manuscrit reprendra ces expériences et leurs enjeux, ainsi que les autres tests de motilité et de caractérisation biologique qui ont été réalisés pendant cette thèse.

THESIS SUMMARY

Single cell migration is a key process which occurs during embryogenesis, immune response and the development of diseases such as cancer[1–3]. New imaging techniques allow the visualization of cell migration in real time and to better understand the environment in which cells migrate. Cells can migrate within extracellular matrix, or in capillaries which irrigate organs. These capillaries have a diameter of tens of micrometers[4,5]. These studies report cell migration in a complex environment and allow to understand better the development of diseases, such as cancer and metastatic spread. However, in addition to *in vivo* studies, *in vitro* studies are necessary to observe and understand in simplified environment, the processes leading to cell migration.

For historical reasons, single cell migration has been extensively studied on 2D flat surfaces. In the absence of external cues, cell migrates randomly on surfaces without preferential direction. It is called "persistent random walk". Boyden chamber experiments have then been developed to study cell migration: two chambers are separated by a porous membrane whose thickness is equal to 15µm and pores have a diameter of 10µm [6]. Cells are seeded in the upper chamber and the lower chamber is filed with chemoattractant. Cells potentially respond to a chemical gradient and cross the porous membrane. These artificial experiments are far from the conditions in which cells migrate *in vivo*, in terms of confinement and migrating distances, *i.e.* hundreds of micrometers. In addition, several studies reported that migration mode as well as activated molecular actors are different on 2D flat surfaces and under confinement[7–9]. For example, Hawkins et al. (2009) modeled that a polarized cell confined in a microchannel migrates spontaneously and in the absence of chemical gradient[10]. Frictions between the channel walls and the plasma membrane and a difference of pressure at the front and at the back of the cell lead to cell migration[10]. Under confinement, focal contacts are not necessary whereas they are essential for cell migration on 2D flat surfaces.

For this reason, we decided to study cell migration over long distances, under confinement and in the presence of cues able to direct cell migration: *ratchetaxis* and *chemotaxis*. In fact, it is known that cells can detect gradients of soluble molecules and migrate towards the highest chemoattractant concentration. It is called chemotaxis[11,12].

It is widely accepted that metastatic spread of colon and breast cancer cells occurs due to the presence of a physiological gradient of the chemokine CXCL12. In fact, primary colon and breast cancer cells overexpress receptors of CXCL12, called CXCR4 and CXCR7[13,14]. It is also known that organs in which colon and breast cancer cells spread are CXCL12 producer (lungs, liver). To explain this phenomenon, the hypothesis of a gradient of CXCL12 at the proximity of these organs has been assumed. However, the presence of a soluble gradient able to direct cancer cell migration has never been shown *in vivo*. As an alternative to chemotaxis, a new mode of directed cell motion has recently been reported *in vitro*. The presence of asymmetric and repetitive motifs in the cell environment directs the migration of NIH3T3 fibroblasts in the absence of chemical gradient. It is called ratchetaxis. In our lab, Caballero et al. (2014) microcontact-printed, on a glass coverslip, triangular motifs of fibronectin called *ratchet*, and separated by ten micrometers gap[15]. They observed the preferential NIH3T3 cells migration towards the tip of the triangle, defined as "+" direction. Cells sent protrusions towards both sides of the motifs to probe its environment. However, the probability of a protrusion to adhere to the next motifs and generate a traction force is higher in the "+" direction, leading to the cell rectification on average in the "+" direction. Comelles et al. (2014) seeded NIH3T3 cells on topographical ratchet-like surfaces. In this configuration, NIH3T3 cells migrate along the ratchet axis and in the ratchet "+" direction. There, the nucleus position sets the direction of migration and rectify cell motion. They also opposed a gradient of fibronectin to the topographical ratchet. On average, the cells did not follow neither fibronectin gradient nor topographical ratchets, indicating that ratchetaxis can counter the attractive effect of a chemical gradient[16].

The aim of this thesis was to study cell migration in a new configuration, closer to physiological conditions, by combining with microfluidic techniques, cell confinement, ratchetaxis and chemotaxis.

First, ratchet effects on cell migration under confinement within 3D microchannels has been studied. Then, we combined confined ratchet to serum gradient in order to test cell polarity "memory". Finally, we studied cell migration in physiological gradients of the chemokine CXCL12 and we observed the localization of its both membrane receptors CXCR4 and CXCR7.

In the first part of this project, we designed 3D ratchets in which cells have to be confined. To do this, we microfabricated microchannels. 3D ratchets are composed of a

series of connected ratchets. To be sure that cells would be confined, the volume of each ratchet should have the volume of a NIH3T3 cell. NIH3T3 cell line in this project is used as a reference. Then, we measured the volume of NIH3T3 cells. It is equal to 1560±520µm^3 (n=388 cells, mean and standard deviation). The volume of a ratchet is set at 1500µm^3. We measured also the nucleus height by staining it with Hoescht. It is equal to 8.5±1.4µm (n=199 nucleus, mean and standard deviation). It allows us to define the height of the microchannel to 5µm. We deduced the area of the triangle to design at 300µm². We also measured the minor axis length of the nucleus. It is equal to 13.4±1.9µm (n=275 nucleus, mean and standard deviation). We roughly deduced the nucleus cross-section area equal to 90µm². To test the effect of different confinements to direct cell migration, we varied the bottlenecks area i connecting two ratchet units (10µm², 20µm² and 30µm²) and the angle α of the tip of the triangle (8°, 16° and 24°). Ratchets are named according to the angle α and the area of the bottleneck i. For example, a ratchet with an angle α equal to 16° and a bottleneck area i of 20µm² is called α16i20. Ratchets microchannels are then designed. Cells are confined from the sides and top. It is the closed configuration. The cell migration is also studied in straight microchannels of 20µm² and 30µm² cross-section area. They are control conditions in which cells migrate in an homogeneous environment.

Microchannels are microfabricated with microfabrication techniques in clean room and by using the biocompatible polymer, called PolyDiMethylSiloxane (PDMS). After cells seeding at the entry of the microchannels, their migration is followed across the time. Without chemical gradient, we first observed that confinement induced the migration of the breast cancer cell line, called MDA-MB-231 cells, which are non-motile on 2D flat surfaces. It confirms already published data which showed that confinement induced cell migration[9,10,17].

As previously mentioned, ratchet is asymmetric, cells can move in the ratchet direction, defined as "+" direction, or against the ratchet direction, called "-" direction. However, in the closed configuration, the cell seeding in one side of the microchannel defined the direction of migration. For each cell, different parameters are measured: the persistent length, time and speed of the first persistent cell motion. Persistency is defined as the length, time and speed the cell migrates without change direction of migration nor pausing for more than 30 minutes for NIH3T3 cells. The persistent length is maximum when the cell crosses the microchannels without pausing and is equal to 350µm. We followed the cell migration in the conditions presented above, in α16i10, α

16i20, α16i30 and α24i30 ratchet microchannels and in 20µm² and 30µm² straight microchannels which are the control.

In 20µm² and 30µm² straight microchannels, cells migrate persistently along microchannels. The mean persistent length is close to the maximal length and is equal to 295±90µm and 269±77µm respectively. In contrast, in ratchet microchannels the mean persistent lengths are significantly reduced, indicating that cell migration is impaired. Some of the cells pause before migrating in the same direction. The nucleus is the biggest and stiffest organelle in the cell[18]. It suggests that it prevents efficient cell passage in the ratchet microchannels. In contrast to previous studies, we did not observe change in direction of migration in closed configuration[15,16,19,20]. The cell polarity set by the entry in the microchannels is preserved even if the cell pauses. However, we observed that smaller is the bottleneck, 10µm², 20µm² and 30µm², lesser is the persistent length. For this reason, we selected the intermediate bottleneck, *i.e.* α16i20 ratchet, which strongly deformed the nucleus without preventing cell migration.

We showed that confined ratchetaxis affects cell migration but does not rectify it. We suggested that the strong cell confinement prevents cell to change direction of migration. Then, we reduced the cell confinement to check our hypothesis. We developed the open microchannel configuration. In this condition, cells are confined from the sides, but not from the top. Cells are seeded in the center of straight and ratchet microchannels. After polarization inside the microchannels, they can migrate in the ratchet "+" or against the ratchet "-" directions. The length of the first persistent cell motion was measured. We observed that cell persistent length increased in the ratchet "+" direction. The length of the first persistent move is equal to 169±151µm in the ratchet "+" direction, 121±95µm against the ratchet "-" direction and 120±106µm in straight microchannels. We observed also that cells change direction of migration while migrating in open microchannels. Then, we wanted to check if cell migration was directed is the open microchannels configuration. To do so, cell migration has been tracked for 12h and the final cell position has been reported in straight and ratchet open microchannels. In ratchet microchannels, we observed that the angular distribution of cell migration is asymmetric and oriented towards the ratchet "+" direction whereas in straight microchannels, the angular distribution is symmetric. These results are confirmed by the final cell position, which is, on average, and after 12h of migration in the ratchet "+" direction. The same analysis in the straight microchannel does not show any preferential direction of migration. It proves that ratchet effect exists to direct cell migration and rectify cell migration over long distances in open microchannels.

To conclude, these results are in agreement with Comelles et al. (2014) and Le Berre et al. (2013) studies which showed that ratchetaxis directed cell migration on topographical surfaces and through asymmetric nucleus confinement[16,20]. Then, we showed that under confinement, closer to *in vivo* conditions that cells can encounter, cell migration is directed due to the presence of asymmetric and repetitive motifs in its environment and in the absence of chemical gradient.

In the second part of this project, we studied cell migration inside microchannels and in the presence of a serum gradient, known to be a chemoattractant. To form chemical gradients, the design of the microchannels have to change. The "ladder" shape allows the injection of two mediums, one containing the chemoattractant plus Dextran coupled to the fluorophore TRITC allowing the visualization of the chemical gradient, whereas the second medium contains none of them. A syringe pump is necessary to the formation of the gradient[21]. It is visible few minutes after injection. A 10% serum gradient is formed in straight and ratchet closed microchannels. In the closed straight and ratchet microchannels, the mean persistent length was close to the maximal length. It showed that serum gradient favors cell migration in ratchet closed microchannels compared to in the absence of serum gradient. Future experiments could be performed to study the cell sensitivity to ratchetaxis and chemotaxis, for example by using a 2% serum gradient instead of 10%serum gradient.

However, by using 10% serum gradient, we decided to probe an effect more important, which is the "memory" effect of the cell to the chemical gradient. To do that, the same configuration is used. Then, once cells are inside microchannels, the 10% serum gradient is removed. Cells can then migrate in the previous gradient direction, migrate in the opposite direction or pause their migration. The same three conditions exist, the 10%serum gradient is in the ratchet "+" direction, against the ratchet direction "-" or in straight microchannels. Surprisingly, after 10% serum gradient removal, cells continue to migrate in straight microchannels and in the ratchet "+" direction. In contrast, in the ratchet "-" direction, cells stop their migration as soon as cells try to cross the ratchet bottleneck. It strongly suggests that ratchet geometry prevents cell migration. In contrast, in the ratchet direction, cell migration is favored. We proposed the existence of a serum gradient polarity "memory" due to the asymmetric distribution of proteins linked to actin reorganization. For example, moesin is a protein which linked actin cytoskeleton to plasma membrane and is localized at the back of the cell after chemoattractant gradient removal of neutrophil cells migrating inside microchannels[12].

The next part of this project was to study cell migration in the presence of physiological gradients of CXCL12 whose existence was assumed *in vivo* in the case of cancer spreading. We first studied NIH3T3 cells migration in microchannels and in the presence of physiological gradients of CXCL12. We observed also the relocalization of both membrane receptors.

In three different cell lines, NIH3T3 cells, the colon cancer SW480 cells and neutrophil-like dHL60 cells, we observed CXCR4 localization at the cell edges and linked to the lamellipodia by overexpressing CXCR4-coupled to a fluorophore and by immunostaining. It suggests a link between CXCR4 and actin cytoskeleton. In contrast, CXCR7 coupled to fluorophore is not observed at the lamellipodia but inside vesicles and migrating along microtubules in both directions, suggesting vesicles transport through dyneins and kinesins. We suspected that the differential localization of CXCR4 and CXCR7 could be responsible for symmetry breaking event leading to directed cell migration. First, we studied migration of NIH3T3 cells towards soluble and adhesive gradient of CXCL12 and at different concentrations. To this end, local CXCL12 injection with micropipette, Boyden chambers experiments and also CXCL12 gradients inside microchannels and CXCL12 microcontact-printed have been performed. But no directed NIH3T3 cells migration have been observed. However, NIH3T3 cells are CXCL12 producer[22]. We supposed that NIH3T3 cells did not migrate towards external CXCL12 gradients for this reason.

To overcome this problem, we used breast cancer cell lines, called MDA-MB-231 cells, known to migrate towards CXCL12 in Boyden chamber experiments[14]. Preliminary experiments showed that MDA-MB-231 cells were able to migrate towards serum gradients in confined microchannels. However, we did not observe MDA-MB-231 cells migration towards CXCL12 gradients in confined microchannels. Different hypotheses can be proposed to explain this absence of directed cell migration towards CXCL12: 1) Too strong confinement may prevent cell migration in response to CXCL12 gradients. 2) The CXCL12 concentrations used may not be optimal. 3) CXCL12 gradient may not be able to direct cell migration over long distances.

We tested the migration of fibroblasts in open and closed microchannels in the presence of asymmetric and repetitive motifs. The open ratchet microchannels configuration, in which cells are confined from the sides, allows the directed and rectification of cell migration. The closed microchannels configuration, in which cells are confined from the sides and top, directs cell migration. The ratchet closed microchannels impairs cell migration but do not rectify it. In closed configuration, cell

polarity is set at its entry in the microchannels and cell cannot change direction due to the strong confinement. Altogether, in closed and open microchannels, cell migration is directed over long distances and without chemical gradient. 10% serum gradient favors cell migration in ratchet closed microchannels. However, gradient removal in the ratchet direction favors cell migration. In contrast, against the ratchet direction completely prevents cell migration by blocking the nucleus passage at the entry of the ratchet bottleneck. It suggests the importance of the environment to direct cell migration and preserve the memory effect. In addition, we used in the microchannels, a physiological gradient of CXCL12, which is known to direct breast cancer cell migration in Boyden chamber and to be responsible for metastatic cancer spread. However, we did not observe any directed cell migration inside microchannels and in the presence of CXCL12 gradients. This PhD thesis presents the performed experiments and their implications.

LIST OF MOVIES

Movie 1: Migration of NIH3T3 cell on 2D flat surfaces. Time in hhmm.

Movie 2: Migration of dHL60 cells on 2D flat surfaces. Time in hhmmss.

Movie 3: Migration of MDA-MB-231 cell on 2D flat surfaces. Time in hhmm.

Movie 4: Migration of MDA-MB-231 cell in closed 20μm^2 straight microchannel. Time in hhmm. Scale bar 20μm.

Movie 5: Migration of NIH3T3 cell in closed 20μm² straight microchannel. Time in hhmm. Scale bar 20μm.

Movie 6: Migration of NIH3T3 cell in closed 30μm^2 straight microchannel. Time in hhmm. Scale bar 20μm.

Movie 7: Migration of NIH3T3 cell in closed α16i10 ratchet microchannel in the ratchet direction. Time in hhmm. Scale bar 20μm.

Movie 8: Migration of NIH3T3 cell in closed α16i10 ratchet microchannel against the ratchet direction. Time in hhmm. Scale bar 20μm.

Movie 9: Migration of NIH3T3 cell in closed α16i20 ratchet microchannel in the ratchet direction. Time in hhmm. Scale bar 20μm.

Movie 10: Migration of NIH3T3 cell in closed α16i20 ratchet microchannel against the ratchet direction. Time in hhmm. Scale bar 20μm.

Movie 11: Migration of NIH3T3 cell in closed α16i30 ratchet microchannel in the ratchet direction. Time in hhmm. Scale bar 20μm.

Movie 12: Migration of NIH3T3 cell in closed α16i30 ratchet microchannel against the ratchet direction. Time in hhmm. Scale bar 20μm.

Movie 13: Migration of NIH3T3 cell in closed α24i30 ratchet microchannel in the ratchet direction. Time in hhmm. Scale bar 20μm.

Movie 14: Migration of NIH3T3 cell in closed α24i30 ratchet microchannel against the ratchet direction. Time in hhmm. Scale bar in 20μm.

Movie 15: Migration of dHL60 cell in closed 10μm^2 ratchet microchannel. Time in hhmmss. Scale bar 20μm.

Movie 16: Migration of dHL60 cell in closed α16i10 ratchet microchannel. Time in hhmmss. Scale bar 20μm.

Movie 17: Migration of NIH3T3 cell in open straight microchannel. Time in hhmm. Scale bar 10μm.

Movie 18: Migration of NIH3T3 cell in open ratchet microchannel. Time in hhmm. Scale bar 10µm.

Movie 19: Migration of NIH3T3 cell towards a pipette delivering 10%serum. Dextran-TRITC allows the vizualisation of the gradient. Time in hhmmss.

Movie 20: Migration of NIH3T3 cell in 75µm^2 cross-section microchannels towards 10% serum vizualized with Dextran-TRITC. Time in hhmmss.

Movie 21: Migration of NIH3T3 cell in 20µm^2 straight microchannels towards 10% serum vizualized with dextran-TRITC. Time in hhmm. Scale bar 20µm.

Movie 22: Migration of NIH3T3 cell in α16i20 microchannels against the ratchet direction towards 10% serum vizualized with dextran-TRITC. Time in hhmm. Scale bar 20µm.

Movie 23: Migration of NIH3T3 cell in α16i20 microchannels in the ratchet direction towards 10% serum vizualized with dextran-TRITC. Time in hhmm. Scale bar 20µm.

Movie 24: Migration of NIH3T3 cell in 20µm^2 straight microchannels in the presence of 10% serum gradient and after gradient removal. Time in hhmm. Scale bar 20µm.

Movie 25: Migration of another NIH3T3 cell in 20µm^2 straight migration in the presence of 10% serum gradient and after gradient removal. Time in hhmm. Scale bar 20µm.

Movie 26: Migration of NIH3T3 cell in ratchet microchannels in the ratchet direct direction and in the presence of 10% serum gradient and after gradient removal. Time in hhmm. Scale bar 20µm.

Movie 27: Migration of NIH3T3 cell against the ratchet direction and in the presence of 10% serum gradient and after gradient removal. Time in hhmm. Scale bar 20µm.

Movie 28: Migration of another NIH3T3 cell against the ratchet direction and in the presence of 10% serum gradient and after gradient removal. Time in hhmm. Scale bar 20µm.

Movie 29: SW480 cell expressing LifeAct-mcherry and CXCR4-GFP. Time in hhmmss Scale bar 10µm.

Movie 30: NIH3T3 cell expressing Tubulin-GFP and CXCR7-mRFP. Time in hhmm. Scale bar 20µm.

Movie 31: NIH3T3 cell expressing CXCR4-GFP and CXCR7-mRFP and migrating on a coverslip with pipette delivering 100nM CXCL12. Time in hhmmss. Scale bar 10µm.

Movie 32: NIH3T3 cell expressing CXCR4-GFP and CXCR7-mRFP and migrating on a coverslip towards a pipette delivering 10% serum. Time in hhmm. Scale bar 10µm.

Movie 33: Migration of NIH3T3 cell in 20µm^2 microchannels in the presence of 16nM CXCL12 gradient. Time in hhmm. Scale bar 20µm.

Movie 34: Migration of NIH3T3 cell in 100µm² microchannel in the presence of 13nM CXCL12 gradient. Time in hhmm. Scale bar 20µm.

Movie 35: Migration of NIH3T3 cell in 100µm² microchannel in the presence of 85nM CXCL12 gradient. Time in hhmm. Scale bar 20µm.

Movie 36: Migration of NIH3T3 cell on Dextran-TRITC microcontact-printed. Time in hh:mm. Scale bar 100µm.

Movie 37: Migration of NIH3T3 cell on Dextran-TRITC and 6nM CXCL12 microcontact-printed. Time in hhmm. Scale bar 100µm.

Movie 38: Migration of MDA-MB-231 cell in 20µm² microchannels and in the presence of 10% serum gradient. Time in hhmm. Scale bar 20µm.

Movie 39: Migration of MDA-MB-231 cell in 20µm² microchannels and in the presence of 20% serum gradient. Time in hhmm. Scale bar 20µm.

Movie 40: Movie 34 Migration of MDA-MB-231 cell in 20µm² microchannels and in the presence of 50nM CXCL12 serum gradient. Time in hhmm. Scale bar 20µm.

Movie 41: Migration of MDA-MB-231 cell in 20µm² microchannels and in the presence of 100nM CXCL12 serum gradient. Time in hhmm. Scale bar 20µm.

CONTENTS

1. Introduction

Cell migration is a key phenomenon which starts during development and lasts the whole lifespan. During embryogenesis, in response to infection and the development of metastasis, single and collective cell migration are required[1–3]. In my PhD thesis, I am focusing on the migration of single cells in environments which mimic *in vivo* conditions. For historical reasons, cell migration has been widely studied on 2D flat surfaces. However, *in vivo* cell migration is mainly confined. To reproduce this confinement, the development of microfabrication techniques in the past decades made possible the study of cell migration in highly controlled environment. Therefore, it is a powerful tool to study single cell migration in confined microchannels whose dimensions and shape can be easily modified. In fact, the project focuses on two aspects: **cell confinement** and **directed cell migration**. Cell migration is directed due to the presence of cues in the environment which biased and rectified cell movement in one direction over long distances. In particular, we focused on **chemotaxis** and **ratchetaxis**. Chemotaxis is the way to direct cell migration through chemical gradients. Its efficiency has widely been proven *in vitro*[11]. However, the presence of chemical gradient has not systematically been shown *in vivo* and therefore we cannot rely only on chemotaxis to explain directed cell migration. Along this line, ratchetaxis has been described as a way to direct cell migration due to asymmetric and repetitive patterns in the cell environment and in the absence of chemical gradient[23]. It can direct cell migration on 2D flat surfaces but also on topographical substrates. Altogether in this PhD thesis, we aim at studying cell migration under confinement together with ratchetaxis and/or chemotaxis.

In this Introduction, I will first highlight the importance of studying cell migration under confinement, equally considering the mechanics of the migration modes and the biochemical signaling pathways activated, compared to cell migration on 2D flat surfaces. Then, I will present the different cues which can direct the cell migration *in vivo* or *in vitro*, from chemotaxis to ratchetaxis and I will report that competition and cooperation between two cues exist to direct cell migration. Finally, I will present the chemokine CXCL12 and its membrane receptors CXCR4 and CXCR7 and the potential role of a physiological gradient of CXCL12 to direct cell migration *in vivo*.

1.1 Differences between *in vitro* and *in vivo* cell migration: the need for new *in vitro* assays

In vivo, cells evolve and migrate in their endogenous environment. In order to better understand processes leading to *in vivo* single cell migration, *in vitro* experiments have been conceived. However, single cells migrating *in vitro* are often far from the conditions encountered by the cells *in vivo*. To start, I will first present the environment in which cells are evolving *in vivo*, then the classical experiments performed *in vitro* to study single cell migration and finally I will present ways to study *in vitro* cell migration closer to *in vivo* environment.

1.1.1. *In vivo*: cell migration and environment

1.1.1.1 *In vivo* single cell migration

Cell migration is a key biological process that plays an important role in embryogenesis, development, immune cell trafficking and wound healing[1,2,24]. This contributes as well to the spreading of cancer cells. Immune cells patrol the organism to check for pathogens infection. In response to malaria infection for example, the immune CD8+ T cells migrate directionally in the draining lymph node towards antigen presenting cells[25]. In Zebrafish, leukocytes are recruited to injury sites *via* the formation of gradient of hydrogen peroxide[1]. It has been observed that in the absence of infection, single dendritic cells migrate preferentially within lymphatic capillaries in the downstream direction of the flow[26]. Examples of cell migration during development can be found: in Zebrafish, a leader epithelial cell migrates to form intersegmental vessel during angiogenesis process[27]. In the chicken embryo, the elongation of the anterior posterior axis is due to a clear posterior-to-anterior gradient of cell motility. This is explained by the random motion of cells associated to tissue deformation[2]. In addition, cancer cells migrate, in particular during metastatic spread, where circulating tumor cells reach the secondary organs to form secondary tumor. This example will be developed in the next section.

1.1.1.1.1 Cancer metastasis: an example of *in vivo* cell migration

The spreading of cancer cells is associated to cell migration. Metastasis formation occurs in four steps: first, metastatic cells leave the primary tumor. Once the cells have reached the blood circulation, a phenomenon called intravasation takes place: cells migrate within blood vessels following the blood flow and finally reach a secondary site. Cells leave the blood vessel in a process called extravasation and potentially form a secondary tumor associated to angiogenesis[3]. These steps have been observed in live animals: fluorescent cancer cells allow imaging of cells inside the tumor, during intravasation process, inside blood capillaries, during and after extravasation process (Figure 1.1)[4,5,28].

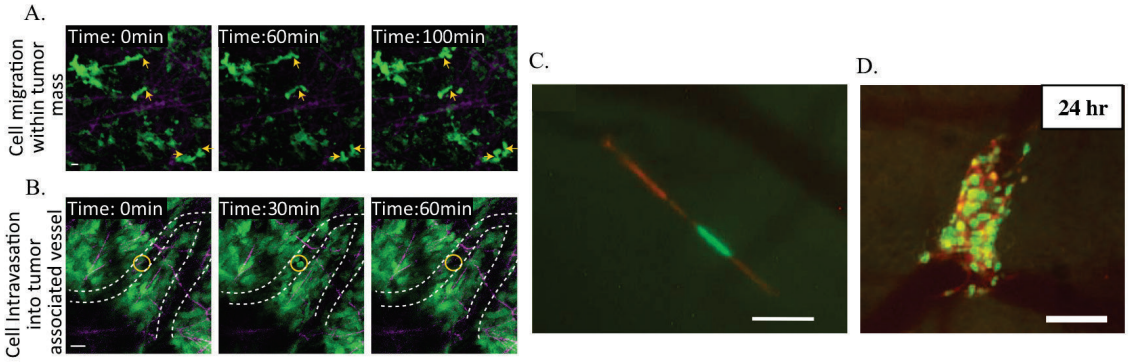

Figure 1.1: Examples of *in vivo* cell migration. Images show the migration of cancer cell within the tumor (A.) and the intravasation process of cell (B.) visualized in live mouse using intravital microscopy. (A.) Cancer cells are highly motile within the tumor mass. Yellow arrows indicate cell position. (B.) Intravasation of a cancer cell. At time 30min, the cancer cell is inside the blood capillary associated with the tumor (White doted lines). At time 60min, the cancer cell disappeares, transported by the blood flow. Green: Carcinoma cells and purple: second harmonic generation signal. Scale bars 10µm. Adapted from Beerling et al. (2011). (C.) Fibroscarcoma cell inside mouse blood capillary. Adapted from Yamauchi et al. (2005). (D.) 24 hours after injection of mouse mammary tumor cells, they extravasate, invade and proliferate around a blood vessel. Adapted from Yamauchi et al. (2006). (C.) and (D.) green Histone2B-GFP (cancer cells nuclei); red RFP (cancer cells cytoplasm). Scale bars 50µm.

Moreover, it is known that some primary tumors preferentially form metastases into specific organs, for example breast cancer metastasizes to bone, liver, lungs, lymph node whereas colon cancer metastasizes to the liver and lungs[3]. Nowadays, it is widely accepted that cancer cells migrate towards secondary sites using chemical gradients. If we consider the example of colon cancer, metastatic cells overexpress two membranes receptors, C-X-C chemokine receptor type 4 (CXCR4) and C-X-C chemokine receptor type 7 (CXCR7)[13,29]. The same chemokine bound these receptors. It is called C-X-C motif chemokine 12 (CXCL12 or SDF-1) and is produced by lungs and liver[14]. The hypothesis of a gradient of CXCL12 at the proximity of lungs and liver has been established. However, to date, the presence of *in vivo* CXCL12 gradient has not been proven. Therefore, we can doubt whether a gradient can direct migration of colon cancer cells. In fact, in 1889, Paget proposed the "seed and soil theory" to explain this bias in cancer spread: he suggested that a specific metastatic cell proliferates only if the environment favors its growth[30]. In addition, in the 1920s, Ewing suggested that the existence of blood flow pattern could explain the formation of organ-specific metastasis[31]. Blood from organs is transported to the heart and is pumped to the lungs to get charged in oxygen. Blood then returns to the heart and is distributed to all organs. However, for intestines, blood is first filtered by the liver before reaching the lungs[3]. Following the hypothesis of Ewing, circulating cancer cells after leaving the colon would first reach the liver where they would be trapped in liver capillaries. This hypothesis is supported by a recent review which reports that 62% of colon cancer patients present metastasis only in the liver[32]. Then, cells reach heart, lungs and distant organs. In addition, growing evidences show that cancer cells arrest at organs proximity by a passive process based on size restriction. Luzzi et al. (1998) highlighted the inefficiency of the metastatic process. Melanoma cells were intravenously injected at the liver proximity. 90min after injection, all the cells were arrested by size restriction in liver capillaries. Three days later, 82% of the injected cancer cells had extravasated into the surrounding tissue. However, only 0.02% of the injected cells had formed macroscopic tumors two weeks after injection. This shows that cancer cells successfully reach the targeted organ but the survival of these cells and the development of micro-metastasis within secondary site is an inefficient process[33].

These studies highlight the importance of *in vivo* cell migration in physiological and pathological processes. In the case of cancer cells spreading, the hypothesis of a chemical gradient at the secondary tumor site proximity is challenged by the lack of evidence for its existence. In contrast, it seems that circulating cancer cells mainly arrest at the proximity of secondary tumor sites by size restriction. Along this line and to better understand the process leading to cell migration *in vitro*, it is important to know in which environment cells are migrating *in vivo*.

1.1.1.2 *In vivo* environment: cell migration in confined spaces

In vivo, cells migrate in complex environments: they move along collagen fibers, in the ExtraCellular Matrix (ECM), inside blood vessels or along muscle fibers[34]. In the early 90s', several teams measured capillaries diameters ranging from 3µm to 8µm in diameter in the brain of mouse and from 4.1µm to 5.1µm in diameter in rat heart capillaries (Figure 1.2)[35,36]. Human

capillaries are in the same order of magnitude, with a mean diameter of 5.9±1.3µm for human brain capillaries[37].

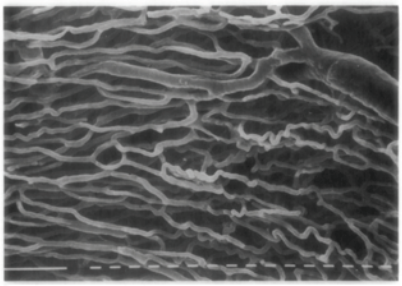

Figure 1.2: Scanning electron microscopy image of the capillary network cast from rat epicardial surface. It is mainly organized parallel to the muscle fibers. Scale bar 10µm. Adapted from Potter and Groom (1983).

The typical diameter of circulating cancer cells is 20µm[38]. Recently, the development of intravital two-photon microscopy and second and third harmonic generation microscopies (SHG and THG) allows the visualization of *in vivo* structures organization in live animals. Collagen form randomly loose network where pores up to 30µm in diameter can be observed, *i.e.* 707µm^2 in cross-section area (Figure 1.3A). Collagen organizes also in dense bundle-like network. Parallel fibers are separated by 3D longitudinal tracks from 5µm to 10µm in diameter, *i.e.* 20 µm^2 to 79µm^2 in cross-section area[39]. In the mouse and chicken dermis, pore size ranges from 3µm to 10µm in diameter[40]. Linear perineural tracks from 2µm to 5µm in diameter, *i.e.* 3 µm^2 to 20µm^2 in cross-section area, and longitudinal tracks along myofibers are structures where cells could migrate along (Figure 1.3B and C)[39]. In the tumor surrounding, alignment of dense fibronectin fibers in human prostate cancer tissues can be observed in fixed tissues[41]. Moreover, Yamauchi et al. (2005) measured the diameter of vessels and capillaries in live mice. The smallest capillaries diameter in which fibrosarcoma cells can migrate is around 8µm [4].

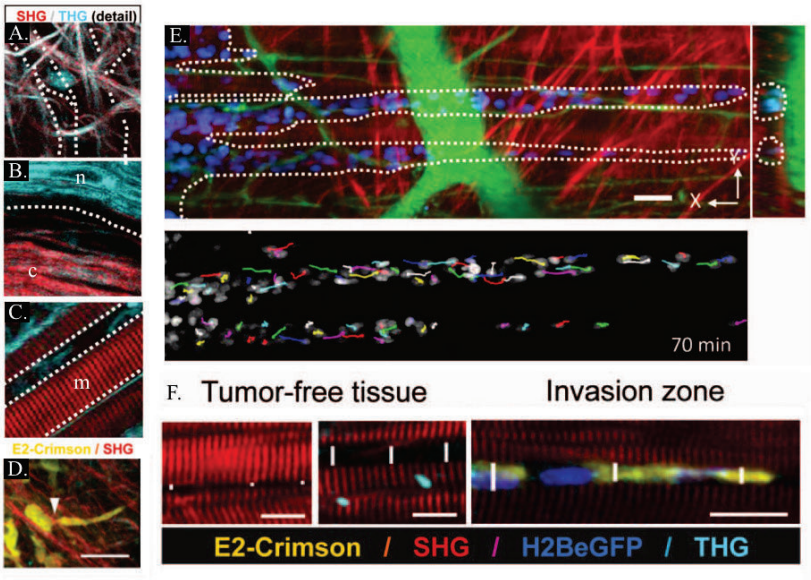

Figure 1.3 : *In vivo* environments and cell migration. 3D reconstruction of *in vivo* interfaces. White doted lines highlight the presence of longitudinal tracks within loose collagen network (A.), between nerve (n) and collagen fibers (c; B.) and along striated muscle fibers (m; C.). (D.) Individual cancer cell deforms its shape to invade collagen network. Scale bar 50µm. (E.) Top. Melanoma invasion at the interfaces of mouse dermal tissue. Bottom. Nuclei tracks of single cancer cells showing the dynamic process of cancer invasion. Scale bar 50µm. (F.) Cancer cells invade pre-existing tissue tracks along myofibers. Scale bars 20µm. light blue:THG (fat cells, nerve fibers); Red:SHG (collagen fibers); blue:histone-2B/eGFP (cancer cells nuclei); green:blood vessels ; yellow, E2-Crimson (tumor cytoplasm). Adapted from Weigelin, Bakker and Friedl (2012).

Below 8µm diameter capillary, cells cannot migrate at all and cytoplasm cleavage and cell death is observed. Above 8µm, cells adapt their shape to fit the capillaries dimensions (Figure 1.1C). In another study, they followed the extravasation process of breast cancer cells and their invasion and proliferation around blood vessels of mouse skin (Figure 1.3D). Weigelin et al. (2012) followed the collective migration of melanoma cells within tissue interfaces. They observed cell deformation within collagen networks (Figure 1.3D) and cells invasion along pre-existing longitudinal tracks; *i.e.* dermal tissue or myofibers (Figure 1.3E and F). They also revealed that within perineural tracks, fat tissue or collagen networks, the diameter of the cells inside tracks is similar to the width of the tumor-free tissue: cancer cells deform to fit pre-existing tracks[39].

In this part, we saw that cell migration is a key process *in vivo*, from a physiological to pathological point of view. Single cells evolve in a complex and heterogeneous environment where they mainly migrate in confined spaces. However, the complexity of *in vivo* environment studies challenges the elucidation of mechanisms leading to cell migration. For these reasons, *in vitro* systems have been developed. They allow the control of the cell environment and to understand better the mechanisms leading to cell migration. In the following section, I will present different *in vitro* systems used to study single cell motility: on classical 2D flat surfaces and in Boyden chambers. I will then introduce *in vitro* single cell migration under confinement, closer to the environment encountered by the cells *in vivo*.

1.1.2 *In vitro* studies: from classical to confined cell migration

1.1.2.1 Cell migration on 2D flat surfaces & in Boyden experiments

For simplicity reasons, migration of cells was first studied on 2D flat surfaces or Petri dishes[42]. Studies of cell motility on flat substrates reveal two modes of single cell migration: mesenchymal and amoeboid. Both modes differ in their adhesion to the surface, their speed, their morphology and their ability to degrade extracellular matrix[43]. Stromal cells such as fibroblasts or solid cancer cells migrate in a mesenchymal mode characterized by strong adhesions to the substrate, low speed (1µm/min) and degradation of the extracellular matrix *in vivo*[43]. They usually have an elongated shape. On the other hand, immune cells such as leukocytes migrate in an amoeboid mode. The term amoeboid referred to the migration of the protozoan *Amoeba proteus* which is characterized by regular changes in shape and migration direction[44]. *In vivo*, immune cells migrate between tissues to reach injury sites or patrol in the organism. They form weak attachments to the surface, migrate with a high speed (30µm/min) and without degrading their environment. They usually have a round shape[43].

On 2D flat surfaces, single cell migration has been extensively studied. It can be decomposed into five steps: cell polarization, cell probing at the front, attachments of the protrusions to the substrate, cell contraction and retraction of the cell's rear (Figure 1.4)[45]. The repetition of these steps leads to a net displacement of the cell.

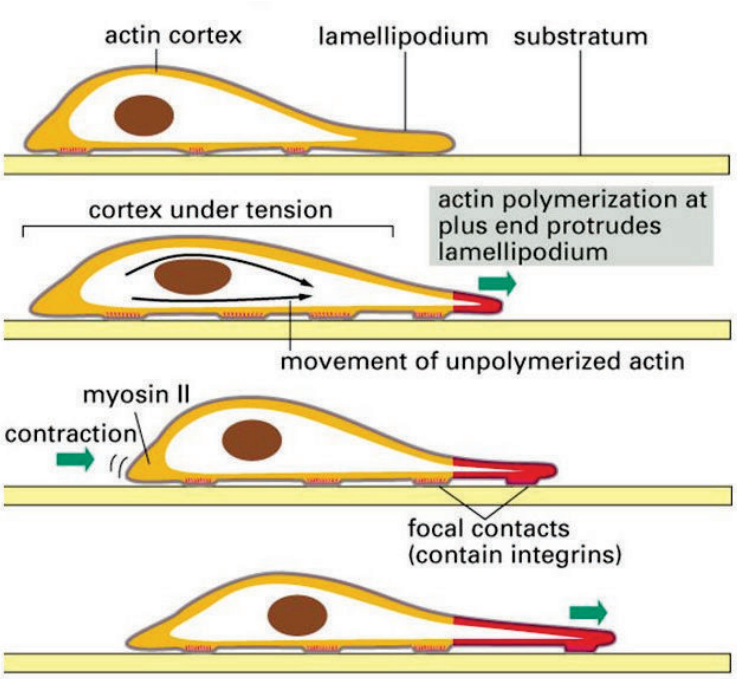

Figure 1.4: Schematics of the steps leading to net cell displacement on flat surface. A polarized cell sends protrusions at its front. Protrusions then attach to the substrate and form new focal contacts. The cell rear contracts leading to the detachemnt of the trealing edge[45].

Establishment of cell polarity implies to have a cell front characterized by a large lamellipodia or filopodia and a cell back[46]. This migration needs cell attachment and formation of adhesions to the substrates mainly through integrins[8]. They link the cell cytoskeleton to the proteins of the ECM present on the surfaces. At the cell front, actin polymerization leads to the formation of actin-based new protrusions which eventually attach and form new focal adhesions. At the cell back, the rear of the cell retracts due to myosin II contraction followed by focal adhesions detachment leading to the cell rear contraction. In a homogeneous environment and in the absence of external cues, cells change periodically polarity and therefore direction of migration. This is called the **"persistent random walk"**. This migration is characterized by a persistent time or length which is the migrating time or length the cell travelled without pausing or changing direction[46,47]. In the presence of external cues, cell polarity is biased and maintained in one direction, leading to an increase in persistent time and length and a directed cell migration[23].

This simple experimental configuration allows the understanding of important mechanisms leading to cell migration such as the role of molecular actors or signaling pathways involved. However, this is far from *in vivo* conditions where cells are confined and exposed to several cues at the same time. In addition to 2D flat surfaces studies, migratory potential of cell is usually evaluated through Boyden chamber also called transwell assays[6]. It is composed of two chambers separated by a porous membrane. Pore diameters vary from 3µm to 8µm and the membrane thickness is usually 15µm. Cells are seeded in the upper chamber and the chemoattractant is added to the lower chamber (Figure 1.5).

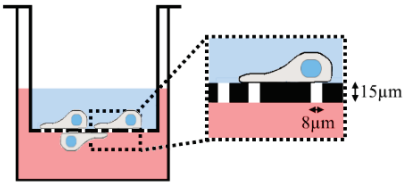

Figure 1.5: Schematics of a Boyden chamber. Chemoattractant gradient forms through the membrane pores and attracts cells to the lower chamber.

After 12h to 24h of incubation, cells which have actively migrated accumulate to the membrane in the lower chamber. Cells are counted and results are compared to conditions without chemoattractant[13,14]. Despite the fact that this experiment is widely used and accepted, it presents numerous drawbacks: first, the distance to cross is smaller than the size of a cell, 20µm. As a consequence, can this phenomenon really be defined as cell migration? Second, the stability of the gradient across the pores cannot be guaranteed for such long time period. Third, in the case of colon cancer cells, while it is accepted that cancer cells migrate towards gradient of the chemokine CXCL12, this chemotaxis has not been observed in Boyden chamber experiments[13,48]. For these reasons, we can doubt the reliability of Boyden chamber to specifically study cell migration.

These artificial experiments were and are still necessary to decipher basic cell migration processes. However, cell migration in Boyden experiment or on 2D flat surfaces is far from *in vivo* environment where cells are mainly confined. Therefore, new assays are needed to properly characterize cell motility.

1.1.2.2 Cell motility under confinement

Researchers developed methods to study cell migration in 3D environment, for example in extracellular network (collagen gel, fibronectin matrix) or in microchannels[11,49]. Properties/dimensions of each 3D environment can be tuned: microfabrication allows the fabrication of microchannels whose length, height and width are controlled and dimensions adjusted to micrometer size to mimic capillary[11]. Collagen matrix pore size can be modified by varying polymerization temperature, concentration or origin/type of collagen. It can vary from 5µm to 30µm in diameter according to experimental conditions used[49]. Other systems use the ability of some cells such as fibroblasts to secrete proteins. In certain conditions, this allows the production of Cell-Derived Matrix (CDM) mimicking the ECM found *in vivo*. More than purified collagen, CDM reconstitutes the complexity of *in vivo* environments in terms of molecular composition (collagen, fibronectin, growth factors bound to matrix) and organization (diversity of pores size, fiber orientation)[50]. Moreover, cells which are producing CDMs can be genetically modified to secrete fluorescent proteins of interest like fibronectin[51].

Cell migration in these environments has been extensively studied. Cells adapt their shape to their environment. Fibrosarcoma cells migrate within network containing narrow pores down to 5µm^2 in cross-section. Cell body and nucleus deform to cross pores with the support of proteolytic enzymes such as Matrix MetalloProteinases (MMP), secreted by the cells, which lyse proteins of the ECM and allow the passage of cell through narrow pores[49]. The absence of MMP

secretion leads to cell immobilization through 5µm^2 pores in cross-section and significant reduction of cell speed[49]. In 3D meshworks, different types of protrusions are observed. In dermal explant or in 3D CDM, human fibroblasts form lobopodia at the cell front and lateral blebs on the cell sides (Figure 1.6 3D CDM). Lobopodia are large cylindrical protrusions whereas blebs are spherical plasma membrane protrusions. They are both pressure-based protrusions and their formation is dependent on myosin II contractility. The same cells in 3D collagen meshworks form multiple long protrusions ending with small lamellipodia (Figure 1.6 3D collagen)[7]. This shows that environment may determine the type of cell migration.

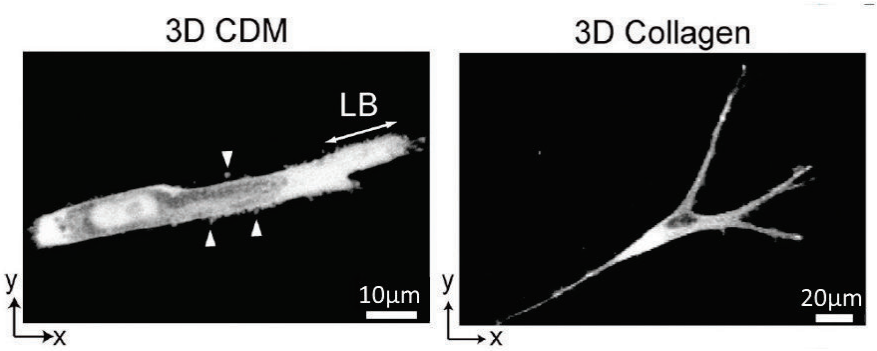

Figure 1.6: Fibroblasts adapt their migration mode to their environment. Human foreskin fibroblasts display lobopodia-based migration on stiff CDM (Right) and lamellipodia-based migration on soft collagen network (Left) LB: lobopodia. Arrowheads indicate blebs position. Adapted from Petrie et al. (2012).

Environmental changes, *i.e.* confinement, and cell properties, *i.e.* contractility and cell adhesion, can modify the migration mode of cells. For example, in contrast to wild type cells, dendritic cells which lack integrin cannot migrate on 2D flat surfaces whereas they can migrate while confined *in vitro* and *in vivo*[9]. Liu et al. (2015) showed that slow mesenchymal cells on flat surfaces can shift their migration mode to a fast amoeboid-like one's in high confinement and low adhesion conditions. There, focal adhesions cannot bind to the substrate and cells use frictions generated by the confinement to move. Interestingly, even non-migrating cells on flat surfaces migrate under confinement and low adhesion[17].

This process is named "chimneying" or "Pushing off the walls" and has been modeled for cells migrating in confined microchannels[10]. At low Reynolds numbers, cells need to exert constant forces to move, through gel polymerization and treadmilling or contractility. Hawkins et al. (2009) considered that a cell is an incompressible viscoelastic gel able to undergo polymerization. In the next part of this section, I will present their model. There, cell has both properties of viscous gel, *i.e.* at the cell front, and elastic gel, *i.e.* at the cell back. It is confined in a microchannel of height *b.* The cell migrates along the x-axis of the microchannel and the height of the microchannel is named *z. z* values ranged between 0 and *b* which constitute the channel wall positions (Figure 1.7).

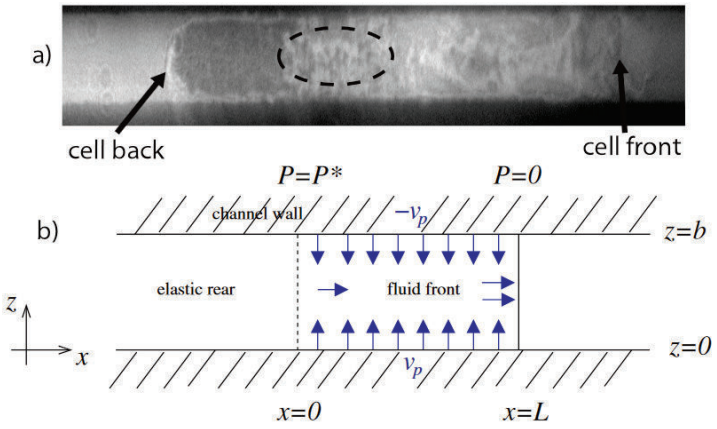

Figure 1.7: Migrating cell inside microchannel and schematic representation of the model. (A.) Top view. Microscopy image of a dendritic cell moving to the right inside microchannel. (B.) Side view. Schematics of the microchannel and model. Adapted from Hawkins et al. (2009).

The **velocity of the gel** is named υ_i. υ_i depends on the pressure P and the viscosity of the gel η. They defined P* as the critical pressure. Below this value, the gel is considered as viscous, above this value, it is an elastic gel. They next assumed that the gel polymerizes at the gel/substrate interfaces, *i.e.* z=0 and z=b, and defined the **gel polymerization speed** υ_p as $\upsilon_p \equiv \upsilon_z(x, z=0) = -\upsilon_z(x, z=b)$ (Figure 1.7 Blue arrows). In fact, it is known that actin nucleation proteins are located at the cell membrane. This is the reason why the vector $\boldsymbol{\upsilon_p}$ is normal to the cell migration. In this condition, the velocity field $\upsilon_i(x, z)$ is dependent on the pressure P and respects the force balance as $\partial_x P = \eta \partial_z^2 \upsilon_x$. It is important because it indicates that a difference of pressure along the x-axis is required to give velocity to the gel. In addition, at the gel/surface interfaces, *i.e.* z=0 and z=b, viscous frictions ξ are present at the channel walls. Then, they can determine the average velocity along the channel as Equation 1:

$$\text{(Equation 1)} \qquad \frac{d}{dx}\left[\left(1 + \tilde{\xi}^{-1}\right)\frac{dP}{dx}\right] = \frac{12\eta\left(2\upsilon_p - bk_d\right)}{b^3}$$

where k_d is the depolymerization speed of the gel and frictions $\tilde{\xi} \equiv \frac{\xi b}{6\eta}$ depend on the viscosity η and height of the channel b. Equation 1 indicates that the velocity along the channel is dependent on the pressure P, the viscosity η, channel height b and the friction $\tilde{\xi}$. More friction leads to reduce speed. To determine the pressure profile along the x-axis P(x), two boundaries conditions are required. They defined L the length of the viscous gel (Figure 1.7). At the gel front, *i.e.* x=L, the frictions with the fluid are neglected, P(L)=0. It is the first boundary condition. At the back of the viscous gel, *i.e.* x=0, the pressure is maximal, P(0)=P*. Altogether, in closed microchannel, they assumed that within the cell such as within the viscous gel, a difference of pressure at the back and front leads to cell movement and frictions play a key role. They assumed that velocity V at the front, *i.e.* for x=L, is equal to the calculated flow velocity plus the polymerization velocity at the front $V = \upsilon(\mathrm{L}) + \upsilon_P(\mathrm{L})$. The flow velocity is in the direction of the movement whereas the polymerization velocity is normal to the movement. However, this results in a velocity V in the direction of the movement.

In the Equation 1, they assumed that frictions are constant along the pressure gradient. However, it is not the case. To be more accurate, they next showed that it is the coupling between frictions and difference of pressure which leads to cell movement. First, they noted

that high frictions increased the attachment and decreased the detachment rate of the polymers at the interface gel/substrate, making the gel polymerization speed dependent on $\tilde{\xi}$ and P. More the pressure, more the friction and less is the polymerization speed. They defined $\tilde{\xi} = \tilde{\xi}_0 e^{\beta P}$ and $\upsilon_P = \upsilon_P^0 e^{-\alpha P}$ and assumed that for small α, υ_P is constant. They can integrate the Equation 1 and find the Equation 2,

(Equation 2) $$P^0 + \frac{\tilde{\xi}_0^{-1}}{\beta}\left(1 - e^{-\beta P^0}\right) = \frac{6\eta\left(2\upsilon_P^0 - bk_d\right)}{b^3}\left(L^2 - x^2\right)$$

and proposed a mechanism for cell motility under confinement (Figure 1.8).

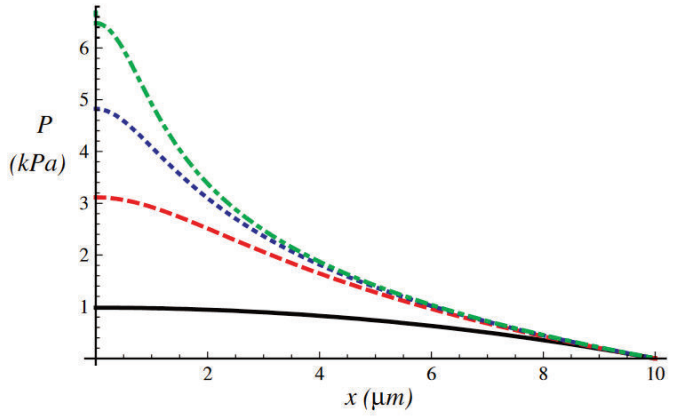

Figure 1.8: Pressure profile as a function of x. Red curve: numerical values for P^0 β=1 and α=0.01kPa^{-1}. Blue curve: analytical values Equation 2 β=1 and α=0. Green curve: numerical value for P^1 β=1 and α=0. Black curve: numerical values for P^0 β=0 and α=0.01kPa^{-1}. They used L=10µm, b=1µm, η=10kPa s, k_d=0.1s-1, v = 0,1µm.s^{-1}, ξ_0=0,1kPa.s.µm^{-1} taking from published data. Adapted from Hawkins et al. (2009).

β=1 indicates that $\tilde{\xi}$ is strongly dependent on the pressure P ($\tilde{\xi} = \tilde{\xi}_0 e^{\beta P}$). On Figure 1.8, this corresponds to the red, blue and green curves. The dark line is for β=0, *i.e.* frictions constant for any pressure. Altogether, they predicted a difference of pressure across the cell which increases by taking into account the frictions dependent pressure parameter. This phenomenon is possible due to cell confinement. In addition, they observed that contractility induced by myosin increases the flow velocity and thereby cell speed.

To conclude, in confinement, they showed that frictions between cell and channel walls forms a gradient of pressure within the cell and leads to spontaneous cell migration. This mechanism called "Pushing off the walls" is independent of focal adhesions. Myosin contractility increases cell velocity but is dispensable[10]. Moreover, this model is confirmed by *in vitro* dendritic cell migration in microchannels where myosin inhibition reduces cell velocity but does not prevent it[52].

Interestingly, cell under confinement reveals other modes of migration. To be closer to physiological conditions, it is essential to study cell migration under confinement. In the following section, I will present the main actors of cell migration, actin and microtubule cytoskeleton, their roles in cell migration and the signaling pathways involved in the migration process. Then, I will detail the differential signaling pathways according to the cell environment.

1.2 Molecular actors involved in cell migration

In the following part, I will present the main actors of the cell migration, actin and microtubule cytoskeleton, their role in cell migration and the signaling pathways involved in the migration process.

1.2.1 The cell cytoskeleton: key elements in cell migration

Cytoskeleton is a complex network which provides to the cell, a structure, rigidity, shape and is also necessary to control several processes including cell migration. It is a highly dynamic meshwork made of three types of biopolymers: intermediate filaments, actin and microtubules filaments. They are micrometers-size monomers which undergo polymerization and depolymerization cycles. In the following part, I will focus on actin and microtubule cytoskeleton, their role in cell migration and the signaling pathways involved in the migration process.

1.2.1.1 Actin cytoskeleton

Actin is found in all eukaryotic cells and is a highly conserved protein. It is present in the cells as monomer, called G-actin, or as filament, called F-actin. G-actin monomer is a polar protein of 4-7nm in diameter (Figure 1.9A). Actin can bind either Adenosine TriPhosphate (ATP) or its hydrolyzed form, Adenosine Diphosphate (ADP). The aggregation of three G-actin monomers, also called nucleation, is the first step of actin polymerization process (Figure 1.9B). New monomers linked to ATP are reversibly added to both ends of the aggregate to grow actin filaments[53]. Once a new monomer is bound to the filament, ATP is hydrolyzed into ADP. Both ends of the actin filament are different in terms of monomers polymerization: there is a fast growing-end called plus-end or “barbed-end”, rich in ATP-bound monomers and a slow growing-end called minus-end or “pointed-end”, rich in ADP-bound monomers and actin monomers.

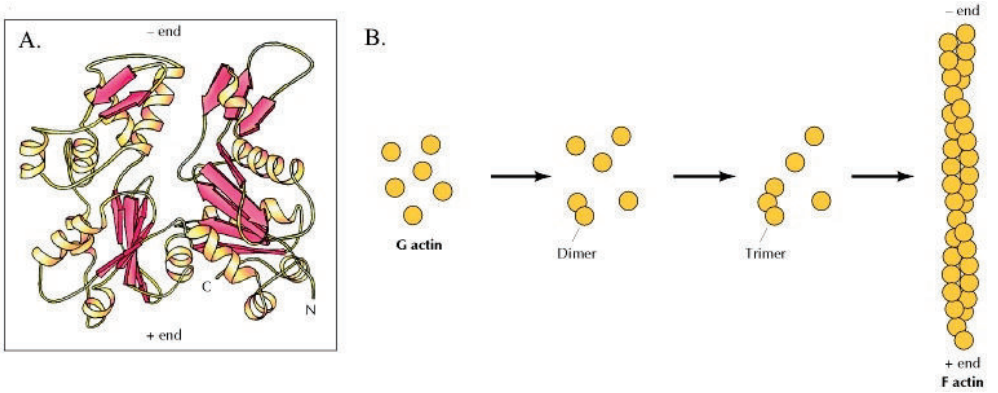

Figure 1.9: The actin monomer and filament. (A.) Structure of the polar actin monomer. (B.) Actin monomers (G-actin) polymerize to form actin filament (F-actin). Actin filament forms a helical polymer which has a plus-end and a minus-end. Adapted from Cooper (2000).

Actin polymerization is associated with actin depolymerization by dissociation of actin subunits from actin filament. ATP-actin dissociates less easily than ADP-actin. There is a difference in monomers concentration at both ends of the filaments resulting in a phenomenon called treadmilling where actin monomers polymerize at the plus-end of the filament and dissociate at the minus-end at the same rate[54].

F-actin is a double-stranded helical polymer which can organize in a variety of structures such as linear bundles, two dimensional networks or three-dimensional gels[54]. The actin layer located below the cell membrane is a three-dimensional gel called the actin cortex[53]. During cell motility process on flat surfaces, linear bundles and two-dimensional networks are found within the cell as filopodia and lamellipodia respectively. These are protrusions which are important in cell migration because of their role in environments probing and directed cell migration. Stress fibers are linear bundles of actin which are able to generate forces[55]. They are attached to the plasma membrane at focal adhesions and allow the cell to exert traction forces to the substrate[56].

In order to form this complex network and control actin polymerization and depolymerization, Actin-Binding Proteins (ABP) are necessary. They can either bind actin monomers, polymers or regulate actin filaments stability[57]. After nucleation, capping proteins such as gelsolin bind to the plus-end of the actin filament and prevent the addition of new G-actin monomers leading to the shrinkage of the filament length. Proteins such as profilin can induce actin polymerization: they bind to actin monomers, exchange ADP to ATP and the newly formed G-actins bound to ATP can then assemble into filament. In contrast, the Actin-Depolymerizing Factor (ADF)-cofilin binds to actin filament at the minus-end, accelerates the dissociation of actin monomers and stays linked to the ADP-actin resulting in monomer trapping and promoting filament disassembly. In response to the increase of free monomers, profilin promotes actin polymerization. Other proteins regulate the structure of the actin meshwork: for example, actin-bundling proteins such as fascin, fimbrin or α-actinin allow the formation of actin bundles, aligning parallel or anti-parallel actin filaments[57]. Actin cross-linking proteins such as filamin is a V-shaped dimer and is able to link perpendicular actin filaments. Filamin and α-actinin are most present in lamellipodium structures whereas fimbrin and fascin in filopodia structures[58]. Arp2/3 complex is an actin nucleator and allows the formation of new branching filaments. Arp2/3 complex binds to G-actin, generates a stable trimer and induces actin polymerization at the plus-end of the filament. It is responsible for the actin branched network in the lamellipodia. Proteins of the formin family are also actin nucleator proteins leading to fast actin polymerization at the plus-end of the filament. Formin and Arp2/3 complex are regulated by the members of the Wiscott Aldrich syndrome protein (WASP) located at the plasma membrane after their activation[55].

Another actin binding protein is the molecular motor called myosin. Several classes of myosin exist but the most studied myosin is the class II or Myosin II. They interact with actin filaments towards the plus-end, generate tension, exert contractile forces and play a critical role in several processes including cell migration[53,59].

Altogether, actin filaments and cross-linkers, which can be active, *i.e.* myosin II, or passive *i.e.,* filamin, generate highly dynamics structures such as actin cortex, stress fibers and protrusions.

Their roles in several processes are keys, from cell motility to environment probing and forces generation. In the next section, I will present the microtubules network.

1.2.1.2 Microtubules

Microtubules are structures which give rigidity to the cell and are necessary to several processes such as cell migration and division. The monomers of microtubules filaments are called α-tubulin and β-tubulin. They interact to form heterodimers and their polymerization gives rise to microtubules (Figure 1.10). In contrast to actin filaments, microtubules form hollow cylinders of 25nm outer diameters composed of 13 adjacent heterodimers. They can bind Guanine TriPhosphate (GTP) or Adenosine DiPhosphate (GDP). When a new tubulin monomer is added to the microtubule end, it is linked to GTP which forms the GTP cap and has microtubule stabilizing properties. As soon as GTP is hydrolyzed into GDP, the GTP-cap disappears and the microtubule becomes unstable. Like for actin filaments, microtubules are polar. They have a fast-growing end called plus-end where β-tubulins are exposed and a slow growing end called minus-end where α-tubulins are exposed[53]. Moreover, microtubules are unstable, a growing microtubule phase can switch to a rapid shortening of the microtubule, in a phenomenon called *catastrophe* or *dynamic instability* (Figure 1.10). Microtubules have an organized-center called centrosomes or Microtubules Organized Center (MTOC) and regroup the "minus-end" of the microtubules. The plus-end of the microtubules connects to the actin cortex towards the cell edge[60].

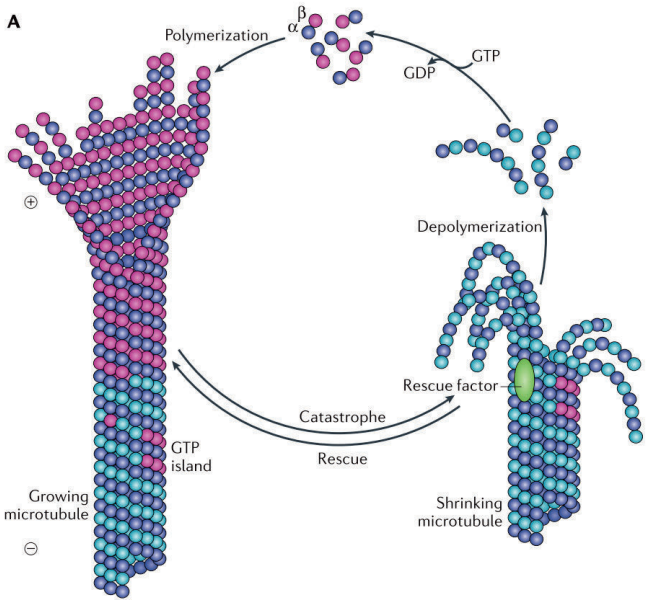

Figure 1.10: The cycle of tubulin assembly and disassembly. α- and β-tubulins heterodimerize to polymerize into microtubules. At the fast growing-end, heterodimers are linked to GTP which stabilizes the plus-end and form a GTP cap. When GTP is hydrolized into GDP, microtubules become unstable leading their rapid depolymerization in a process called catastrophe. Image from Akhmanova & Steinmetz (2005).

Microtubules are necessary to give rigidity to the cell and play a crucial role in cell division and cell motility. In addition, microtubules serve as tracks to transport cargos across the cell. Two groups of proteins have this function: kinesins, which move along the microtubules in the plus-end direction and dyneins, which move along microtubules in the minus-end direction.

Actin and microtubules are the major cytoskeleton elements which play a key role in cell migration. Moreover, attachments of cell protrusions to the substrate is essential for cell migration of flat surfaces. Therefore, a complex of transmembrane proteins link the cytoskeleton to the proteins of the ECM. This assemble is called focal contacts and I will present them in the next section.

1.2.1.3 Focal contacts as mechanosensors

As mentioned previously, protrusions attachment to the substrates play key role in the cell migration process. It is due to the formation of **focal adhesion**. In the next section, I will present focal adhesion, their formation and their role as mechanosensors.

Integrins link proteins of the ECM to cytoplasmic proteins such as tallin and paxillin. This assemble constitutes early focal complexes after attachment of the protrusions to the substrate at the cell front (Figure 1.11A). They are small dot-like structures and have a mean area equal to 0.5µm^2 [56]. Focal complexes are not stable, they can disassemble or mature into larger focal contacts, also called focal adhesions, by recruiting other proteins such as vinculin and α-actinin and connect to stress fibers[55]. They are larger and elongated structures, around 2µm^2 in area and are regulated by Rac1 and cdc42 which control actin fibers formation through Arp2/3 and formin recruitment. Stress fibers are contractile fibers composed of actin and myosin and are able to generate contractile forces leading to retraction of the cell rear following RhoA activation (Figure 1.11B)[53,55].

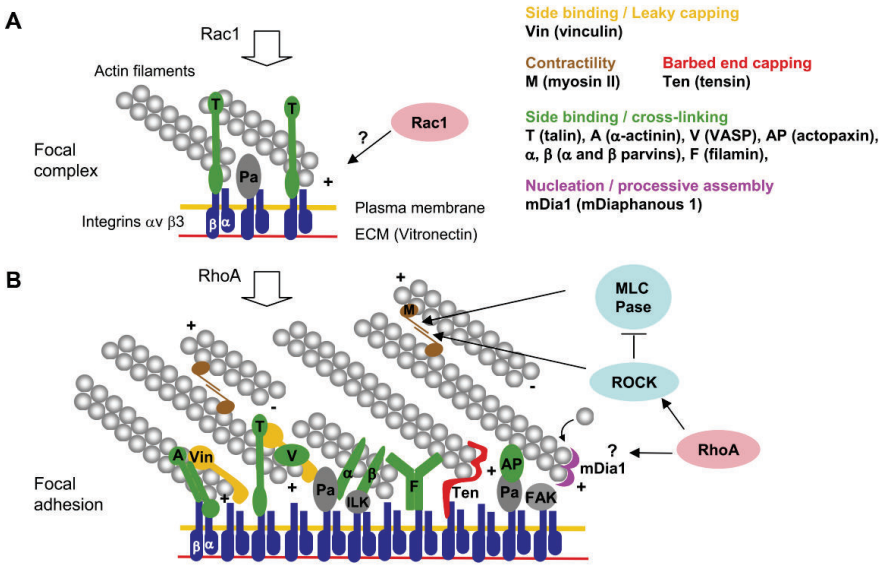

Figure 1.11: Focal adhesions formation and regulation (A.) Rac1 stimulates the formation of protrusions and early focal complexes. Integrins bind to the ECM and intracellularly to proteins such as talin and paxillin. (B.) Focal complexes mature into focal adhesions by recruiting proteins such as vinculin or α-actinin. Activation of RhoA leads to myosin and mDia activation generating contraction and actin polymerization. Focal adhesions connect the ECM to the cell cytoskeleton and can be used as traction sites following acto-myosin contraction. They can also serve as mechanosensors by sensing substrate rigidity. Adapted from Le Clainche and Carlier (2008).

In addition, cells are able to detect level of rigidity in the substrates. They migrate to the stiffer region in a process called durotaxis using focal adhesions as traction sites. They are also able to grow in response to contractile forces[56,61]. Focal complex mature locally into focal contact when a force is applied locally by a pipette tip on an adherent cell. In fact, it has been shown that a force applied to a cell leads to the reinforcement of the focal adhesions, revealing that focal adhesions are used by the cell as mechanosensors. Rho and therefore myosin activation generates actomyosin contraction and leads to focal adhesions growth. However, Rho activity is dispensable to the maturation of focal adhesion as external forces applied by a pipette tip cause the same focal adhesions growth. In fact, focal adhesion maturation is dependent on actin filament integrity and the activity of the formin mDia[56].

In order to migrate directionally and over long distances, cells are able to maintain their polarity and to tightly control actin cytoskeleton and microtubules through intracellular signaling molecules. I will present in the following part the Rho GTPases proteins which regulate cell migration as well as the different markers used to study the cell polarity.

1.2.2 Rho GTPases signaling pathways

Cell migration is a complex process which needs to be tightly regulated in order to produce a net cell displacement. Proteins belonging to the small GTPases family regulate this process. The main Rho GTPases regulating cell migration are named cdc42, Rho and Rac[62]. Cdc42, Rho and Rac act at different places within the cell and have a defined role. On 2D flat surfaces, cdc42 is required for the formation of filopodia, Rac for the formation of lamellipodia and membrane ruffles and Rho for the formation of acto-myosin contractile stress fibers (Figure 1.12)[62].

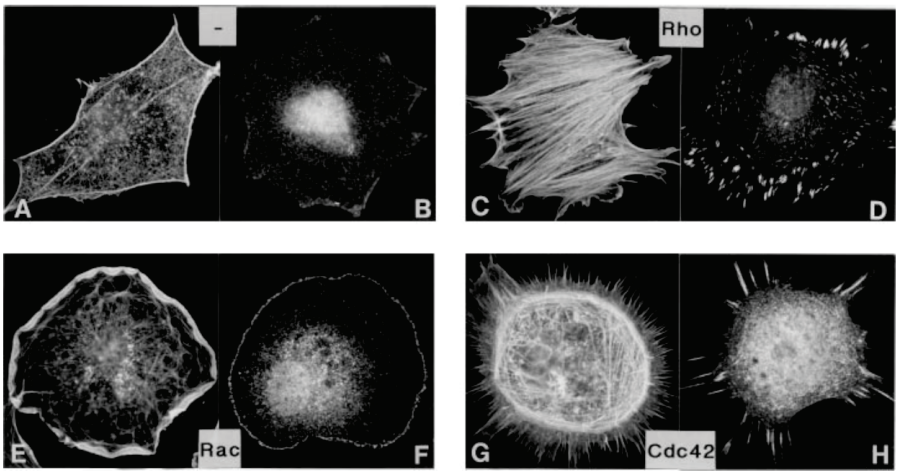

Figure 1.12 : Roles of Rac, cdc42 and Rho in cell migration on 2D flat surfaces. Quiescent 3T3 fibroblast shows few actin filaments (A) and focal adhesions (B). Activation of Rho leads to stress fibers formation (C) associated to focal adhesions formation (D). Activation of Rac leads to lamellipodia (E) and focal adhesions formations (F). Activation of cdc42 leads to filopodia (G) and focal adhesions formations (H). Adapted from Hall (1998).

These proteins exist in active and inactive forms. The active form is bound to GTP whereas the inactive form to GDP. Different upstream signals can regulate their activation (Figure 1.13). The Guanine nucleotide Dissociation Inhibitors (GDI) sequester the inactive form of the Rho GTPase

and prevent its activation. GTPase Activating Proteins (GAP) enhance the GTPase activity of the Rho GTPase protein leading to its inactivation. The Guanine nucleotide Exchange Factors (GEF) exchange GDP to GTP and activate the Rho GTPase proteins (Figure 1.13).

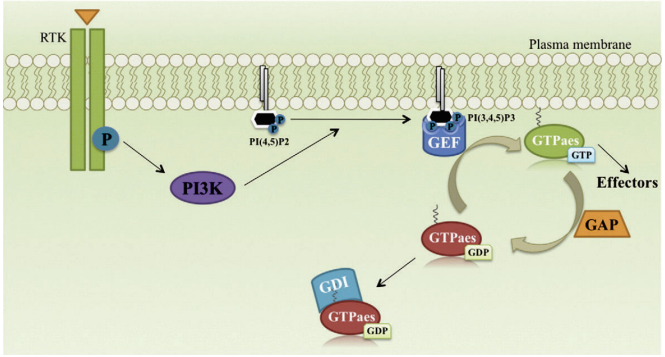

Figure 1.13: Schematics of Rho GTPases regulations and role of PI3K[63].

Once activated, each Rho GTPase binds to its effectors and generates a cell response: acto-myosin contraction through Rho activation, lamellipodia formation through Rac activation and filopodia formation through cdc42 activation[64]. It will be detailed in the next section.

1.2.2.1 Rho signaling

Three isoforms of Rho exist: RhoA, RhoB and RhoC which present high homologies. During the cell migration process, they play a key role in stress fiber formation generating tension and retraction of the trailing edge. RhoA is the most studied isoform. It has several downstream effectors. Rho-associated protein kinase (ROCK) is one of them and plays a key role in the formation of stress fibers and focal adhesions. In addition, it phosphorylates Myosin Light Chain (MLC) and inhibits dephosphorylation of MLC leading to myosin activation and acto-myosin contraction. Actin polymerization is promoted by ROCK, which activates LIMK whose function is to inhibit ADF-Cofilin, and by mDia, which belongs to the formin family and is an actin nucleator. mDia binds as well microtubules and stabilizes them (Figure 1.14)[65].

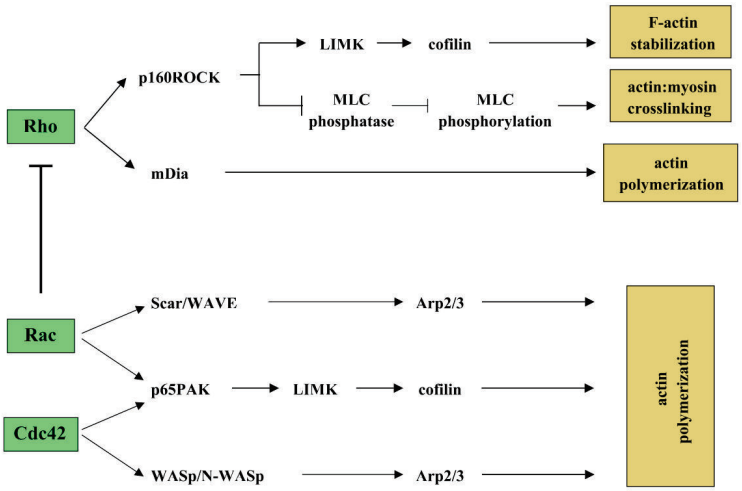

Figure 1.14 : Rho GTPases signaling pathway involved in cell migration. Image from Raftopoulou & Hall (2004).

Altogether, Rho activation leads to myosin contraction at the cell rear and actin polymerization at the focal adhesions level.

1.2.2.2 Rac signaling

Rac proteins have three isoforms Rac1, Rac2 and Rac3. During cell migration process, they play a key role in lamellipodia extension. Rac1 activation has different effectors. It can activate proteins of the WASP/WAVE/SCAR complex which lead to Arp2/3 complex activation, actin nucleation and the formation of actin filament branches at the lamellipodia edge. PAK is another effector of Rac1. It inhibits MLC activation and then contractility and activates LIMK leading to ADF-Cofilin inhibition and actin polymerization (Figure 1.14)[63]. In addition, Rac activates PIP-5 kinase, producing PIP2 which inhibits actin-capping proteins. Altogether, the activation of Rac at the leading edge leads to actin polymerization and regulates the formation of lamellipodia.

1.2.2.3 cdc42 signaling

Cdc42 plays an important role in environment probing, the first step of migration process. Cdc42 activation shares signaling pathways with Rac[63]. It induces actin polymerization and branching through ADF-Cofilin inhibition and Arp2/3 activation respectively. The formin mDia localizes at the tip of the filopodia[55] (Figure 1.14). In addition, cdc42 activates signaling pathways at the front of astrocytes promoting centrosome reorientation and microtubules stabilization[66].

Altogether, Rho, Rac and cdc42 activations lead to cell polarization and migration. As mentioned previously, a polarized cell on 2D flat surfaces has an asymmetric shape and is characterized by a large lamellipodia at its front. The localization of Rho GTPases can thereby indicate cell polarity. However, other markers such as the production of the Phosphotidylinositol (3,4,5)phosphate (PIP3) at the cell front or the localization of the centrosome or the Golgi complex, can be used to assess the cell polarity while cells are migrating. In a complex environment *in vitro*, this allows to understand better cell migration when there is a change in direction of migration.

1.2.3 Other markers of cell polarity

In vivo, tracking cell polarity is useful for assessing direction of collective cells migration. Often, the centrosome-nucleus axis or the Golgi complex position is studied. In single cell migration, the formation of PIP3 is followed. In this section, I will present these different markers and give some examples of their localization in single migrating cells.

1.2.3.1 PIP3 is produced at the leading edge of migrating cell

PIP3 is synthesized, upstream to RhoGTPases. Its production depends on the activation of the Phosphotidylinositol(3,4,5)phosphate kinase (PI3K) and the Phosphatase and TENsin homolog (PTEN). PIP3 production follows the activation of G-protein coupled membrane receptors in

Dictyostelium and neutrophil cells in response to chemical stimulations[67]. After its activation, it accumulates at the cell membrane, activates GEF leading to the activation of Rho GTPases (Figure 1.13)[63].

In fact, in *Dictyostelium* and neutrophil cells, PIP3 and PI3K accumulate at the cell front and the negative regulator PTEN at the rear of *Dictyostelium* cell[68,69]. It coincides with the recruitment at the cell front of actin regulators such as Rac, WASP and Arp2/3 complex and of proteins containing pleckstrin homology (PH) domain, such as Akt[67]. A PIP3 biosensor called PH-Akt is used to monitor PIP3 production or PI3K activation and is a good marker to follow cell polarization during cell migration[12,70,71]. In confined microchannels, dHL60 neutrophil-like cells are stimulated with chemoattractant gradients leading to PI3K accumulation at the cell front and directional cell migration. Then, the chemoattratant is removed: it leads to the loss of cell polarity, *i.e.* no PI3K accumulation at the cell front (Figure 1.15).

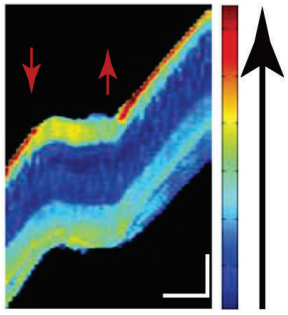

Figure 1.15: Kymograph of dHL60 cell migrating in microchannel and responding to chemoattractant stimulation. dHL60 cell expresses PH-Akt and activation level is false-color coded according to the color bar shown on the right. Red arrows indicate chemical gradient removal (Down) and reintroduced (Up). Vertical scale bar 15µm, horizontal scale bar 100s. Adapted form Prentice-Mott et al. (2016).

After addition of the chemical gradient, the cell polarizes, accumulates PI3K at the cell front and migrates towards the chemical gradient[12] (Figure 1.15). In chicken embryo fibroblasts, overexpression of active PI3K leads to an increase in lamellipodia and filopodia activity, a decrease number of stress fibers and increase in cell migration speed in a mechanism dependent on Akt activation[70].

PI3K activation leads to PIP3 accumulation at the leading edge of migrating cell. It is a good marker to assess cell polarity. However, centrosome position and reorientation as well as the Golgi complex position are other markers which can be used to indicate cell polarity.

1.2.3.2 Centrosome and the Golgi complex as markers of cell polarity

Microtubules are key elements which give rigidity and structure to the cell. The centrosome or MTOC position in migrating animal cells has been proposed to be a marker for cell polarity[72]. Centrosome position changes over time and depends on the nature of the substrate on which cells are migrating[73]. On glass coverslip, MTOC is mainly positioned at the front of nucleus fibroblasts whereas in 3D collagen gel, it is randomly oriented relative to the nucleus position[73]. Interestingly, centrosome position is cell type, substrates and migration mode dependent[72]. During wound healing and collective migration, 75% of the centrosome of migrating cell is positioned at the front of the NIH3T3 fibroblasts nucleus. However, on adhesive stripes, 95% of the centrosome of single NIH3T3 migrating cells is located behind the nucleus. In the same

configuration, the centrosome of single retinal pigment epithelial (RPE-1) migrating cells is located at the front of the nucleus (Figure 1.16A)[74].

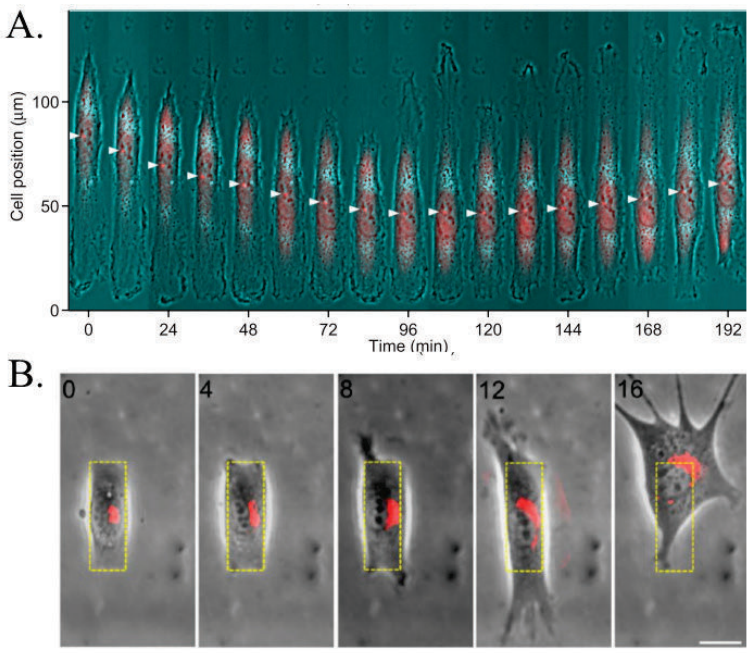

Figure 1.16: Centrosome and the Golgi complex localization in migrating cell. (A.) Time series of a RPE-1 cell expressing GFP-centrin (red dots) and migrating along adhesive line. Centrosome is located at the front of the cell (white arrowheads). After the cell stops its migration, the centrosome moves continuously towards the stalled leading edge. It becomes the new trailing edge after reversal of migration direction[74]. (B.) Time series of a NIH3T3 cell expressing Golgi-RFP and migrating after release from rectangular confinement. The Golgi complex reorients[75]. Scale bar 20µm. Time in hours.

Interestingly, a change in direction of migration is associated with centrosome repositioning (Figure 1.16A)[74]. The Golgi complex is another marker for cell polarity. Figure 1.16B presents the localization of the Golgi complex in a NIH3T3 migrating cell. The cell is first confined within rectangular shaped island. There, the Golgi complex is mainly oriented towards the long edges of the rectangular pattern. After confinement release, the Golgi complex reorients towards the short edges of the rectangle and is associated with an increased in lamellipodia activity and therefore cell migration in this direction (Figure 1.16B)[75]. In addition, it is possible to impose the position of centrosome and the Golgi apparatus at the nucleus front by imposing polarized shape to the fibroblasts[15,76,77]. On adhesive lines, the Golgi complex is located behind the nucleus of migrating epithelial kidney cells (Ptk2) and overlap with the centrosome. Both centrosome and the Golgi complex reorient themselves when there is a change in directional cell migration[78].

PI3K activation, centrosome and the Golgi complex localizations are examples of markers for studying polarity of migrating cell. However, centrosome and the Golgi complex positions vary according to the cell type and environment. To have a precise idea about the polarity state of the cell, it is recommended to look at different markers.

In this section, I have presented the actors of cell migration and signaling pathways activated during cell migration. In the following part, I will present that, according to the environment on which cells are migrating, there are not activated the same way.

1.2.4 Different mechanisms activated on cells migrating on 2D flat surfaces and in confined environment

A cell on 2D flat surfaces or in confined matrix or microchannels uses the same tools for its migration, *i.e.* acto-myosin and Rho GTPases proteins. However, activation of these different signaling pathways is tightly and differently regulated. In the following section, I will present first the symmetry breaking event which leads to spontaneous cell polarization on 2D flat surfaces without external cues. Then, I will compare mechanisms of cell migration on 2D flat surfaces and under confinement.

1.2.4.1 2D symmetry breaking mechanisms

1.2.4.1.1 From a theoretical point of view

In physics, to break the symmetry of a system, asymmetry is required[79]. Asymmetry could be intrinsic or extrinsic to the system. **Breaking symmetry** in cell biology is a common features and occurs during cell migration, cytokinesis or embryogenesis and leads to cell polarization[80]. This breaking event can occur spontaneously or be triggered by external cues such as chemical gradients. In the presence of external cues, the cell polarity is mainained in one direction. In this section, I will talk about the theories and models of cell symmetry breaking. In the next section, I will present the molecular actors involved in the spontaneous symmetry breaking.

How can a cell spontaneously break its symmetry? Alan Turing proposed in 1952, a theoretical model to explain symmetry breaking event leading to the formation of patterns in animals during embryogenesis[81]. He suggested that symmetry breaking is a result of the interplay between the local activation of a diffusive self-enhancing morphogen and its inhibition by a long-range inhibitor. A self-enhancing morphogen A activates a morphogen B which in turn inhibits the morphogen A (Figure 1.17). Taking into account this statement, from an initial homogeneous tissue, simulations reproduced the complexity of animal patterns (stripes, spots, waves) without any external cues (Figure 1.17)[81,82]. This local chemical activation and inhibition loops model can explain the symmetry breaking event in the cell migration process.

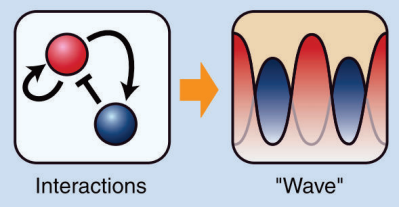

Figure 1.17: Self-regulation of two morphogen molecules. The morphogen A (pink) activates a morphogen B (blue) which in turn inhibits the morphogen A. The system can form a variety of patterns starting from an homogeneous state[82].

In contrast, Paluch et al. (2005) suggested that the mechanical instability of the acto-myosin network itself in the cell cortex could drive the symmetry breaking[83]. The cell cortex is a thin gel layer, *i.e*. from 100nm to 1µm thickness, located beneath the plasma membrane. It is composed of actin filaments cross-linked with actin-binding proteins and myosin II. High tension in the cell cortex is generated by myosin II contractility and by the actin gel architecture itself (Figure 1.18C)[84]. The breakage of the actin cortex leads to polarization events, such as bleb formation or cortex flows (Figure 1.18C and D)[83]. As a comparable system, actin gel formation around

beads can mimic symmetry breaking events of actin cortex (Figure 1.18A). Functionalized beads are placed in cell extracts containing all the proteins needed for actin assembly. An actin gel grows around the bead. Due to G-actin incorporation at the surface of the bead and actin polymerization, the gel forms homogeneously around the surface of the bead and is associated with an increase in tension within the gel. Above a threshold, the actin gel around the bead spontaneously breaks. The formation of an actin comet in the opposite side of the breakage site leads to bead polarization and movement (Figure 1.18B).

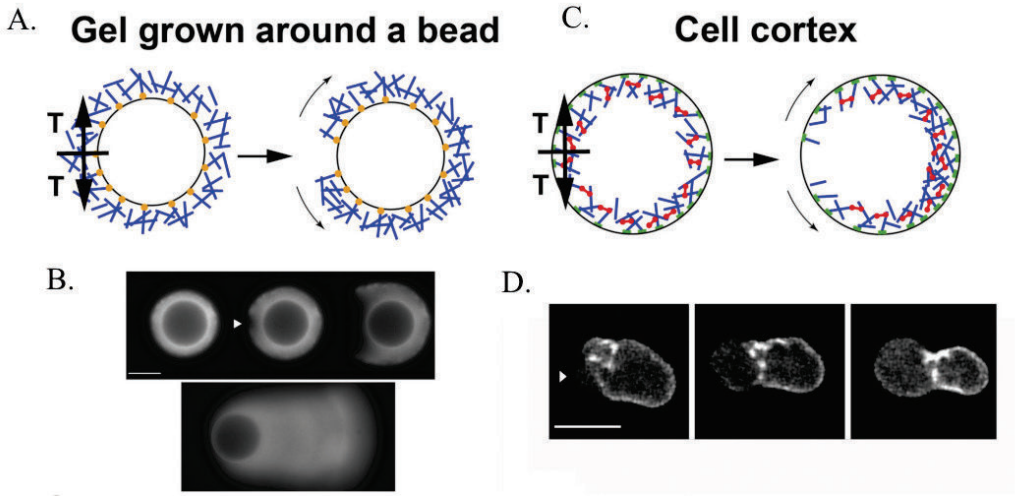

Figure 1.18: Similarities between actin gels growing around beads and beneath the plasma membrane of a cell. (A.) Actin gel grows around the bead until a certain tension (T). Above this threshold, the actin gel breaks. (B.) Time series of symmetry breaking event around a bead. Actin is fluorescently labelled. First, the actin gel grows, then it breaks, actin comet forms resulting in cell movement. Scale bar 10µm. (C.) Within cell, actin cortex breaks when the tension is too high. (D.) Time series of cortex breakage leading to the formation of bleb in cell. Actin is fluorescently labelled. Scale bar 5µm. Adapted from Paluch, Van der Gucht and Sykes (2006).

The above explained chemical and mechanical-based mechanisms can lead to spontaneous cell symmetry breaking. From a physics point of view, the introduction of any external cues in the environment can lead to the symmetry breaking event.

In a homogeneous environment, the migration of cell is called “persistent random walk”. The cell moves randomly on a surface as a single Brownian molecule. In 1963, the physicist Feynman explained theoretically how to bias movement in an asymmetric environment. To do that, he imagined a simple ratchet and pawl device which could orient gas molecule motion. An axle connect two boxes. One box contains vanes which jiggle due to the thermal agitation of the molecules hitting the vanes. The other box contains a ratchet and pawl system. It allows the rotation of the pawl only in one direction.

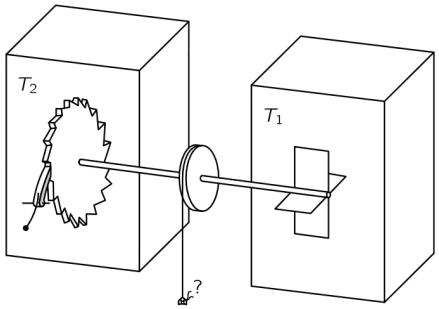

Figure 1.19: The ratchet and pawl device[85].

In theory, the jiggling of the vanes will turn the axel and then activate the ratchet and pawl mechanism leading to its motion in one direction[85]. The energy needed to move the pawl in the ratchet direction is lower than the one needed to move it against the ratchet direction. However, if both boxes are at the same temperature, (T1=T2), the system cannot move: the probability the pawl turns in the ratchet direction due to the action of the vanes is the same than the probability than the pawl turns in the ratchet direction spontaneously. If temperatures are different (T1>T2), then molecules are more agitating in the box containing the vane, leading to its rotation. In contrast, in the pawl and ratchet box, the low temperature makes the spontaneous rotation less frequent. Altogether, the probability to turn the pawl in the ratchet direction is higher than the probability to turn the pawl spontaneously or against the ratchet direction. This simple device shows that from on homogeneous state, a system could be poised and become polarized in one direction in an asymmetric environment. It could be applied to cell migration, where an external asymmetric cues could bias and direct cell migration by maintaining the cell polarity in one direction.

1.2.4.1.2 Biochemical

The previous section presented how symmetry breaking events occur from a theoretical point of view. Regarding cell migration, on 2D flat surfaces, the process has been studied. As previously mentioned (page 35), the first step of the migration process is called cell polarization. A “round” or non-polarized cell has a homogeneous distribution of cytoskeleton components such as actin, myosin or PIP3 within the cytosol (Figure 1.20)[71,86,87]. When symmetry breaking event occurs, cell polarizes and has a cell front characterized by lamellipodia and protrusions and a cell back[46]. In addition, the organization of the cytoskeleton becomes asymmetric, with actin accumulation at the cell front and myosin, formin and PTEN at the cell rear (Figure 1.20)[69,86,88].

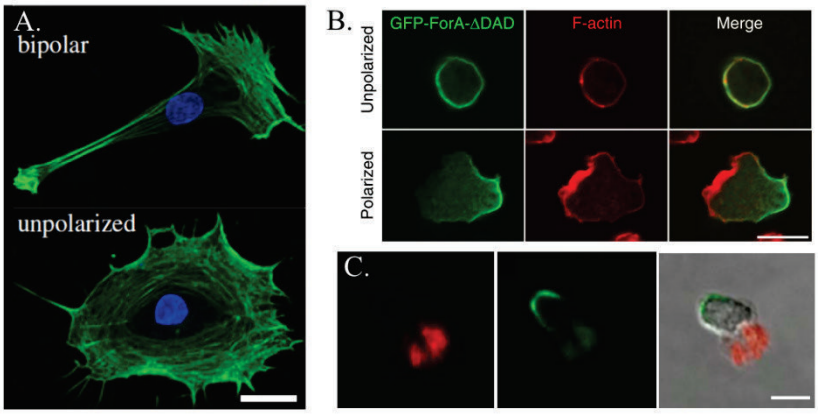

Figure 1.20: Examples of cytoskeleton organisation in unpolarized and polarized cells. (A.) Nucleus (blue) and Actin (green) distribution in Schwann cells. Scale bar 20µm. Adapted from Lopez-Fagundo et al. (2014). (B.) Formin (green) and actin (red) distribution in *Dictyostelium* cells. Scale bar 10µm. Adapted from Ramalingam et al. (2015). (C.) Human neutrophils stimulated by a uniform concentration of fMLP and fixed 2 min after stimulations. Actin (red) and myosin (green) distribution. Scale bar 10µm. Adapted from Wang (2009).

Study reports that PIP3 is the activator able to generate symmetry breaking within the cell[89]. They add a membrane-permeable ester of PIP3 (PIP3/AM) to unpolarized human neutrophil. Once inside the cell, it induces symmetry breaking forming the cell front first with accumulation

of F-actin in the lamellipodia and cell migration as efficiently as in the presence of a chemoattractant. PIP3/AM induces activation of PI3K in a positive feedback loop, supporting Turing theory[81,89].

In contrast to neutrophil, evidences suggest that in fibroblasts and keratocytes, the cell rear retracts first leading to symmetry breaking and is followed by cell migration[90]. Stationary keratocytes are symmetric. Spontaneously, the future rear moves towards the cell center before advancement of the front edge occurs[91]. It is associated with an increase in F-actin flow, induced by myosin activity at the cell rear. The role of myosin II in the polarization process is key: inhibition of myosin II by blebbistatin or activation of myosin II by CalyculinA prevents or strongly induces keratocyte polarization and migration respectively. Moreover, this symmetry breaking event is independent of PI3K activation[91].

However, in the presence of external cues, such as chemical gradients, substrate stiffness or electric field, symmetry breaking event is oriented according to the external factors: lamellipodia/protrusions grow in the direction of the highest concentration of chemoattractant, stiffer side of the surface or negative pole of an electric field respectively[12,61,92]. The external cues maintain the cell polarity across time leading to cell migration in one direction.

Symmetry breaking event as a spontaneous phenomenon has not been fully elucidated. However, its mechanism seems to be cell type dependent. External cues orient and direct cell migration. They will be detailed in the section Directed cell migration (page 55). In the next section, I will give few examples of differences in signaling pathways activated between cells migrating on 2D flat surfaces or in confined environment.

1.2.4.2 Signaling pathways on 2D flat surfaces versus 3D confined environment

Protrusion activity is different *in vivo* and *in vitro*: on 2D flat surfaces, cells send flat protrusions called lamellipodia, to probe their environment. Confinement does not allow the formation of flat protrusions but mainly filopodia, lobopodia or membrane blebs[7,8]. As lamellipodia formation is driven by Arp2/3 and Rac1 activation, they are required for Chinese Hamster Ovary (CHO) cells migration as well as focal adhesion[8]. Moreover, myosin II inhibition does not prevent cell migration on flat surfaces but is required under confinement[8]. In dermal explant or in 3D CDM, human fibroblasts form lobopodia at the cell front and lateral blebs on the cell sides (Figure 1.21). They are pressure-based protrusions and their formation is dependent on myosin II contractility. Thereby, lobopodia-cell migration is dependent on RhoA and myosin II activities. Moreover, lobopodia-based migration is independent of PIP3, cdc42 and Rac1 activation, *i.e.* no recruitment at the cell front. The same cells on 2D CDM or 3D collagen meshwork form lamellipodia or multiple branched protrusions with lamellipodia tips respectively (Figure 1.21). Their migration requires PIP3, Rac1 and cdc42 polarization in 2D CDM or 3D collagen[7].

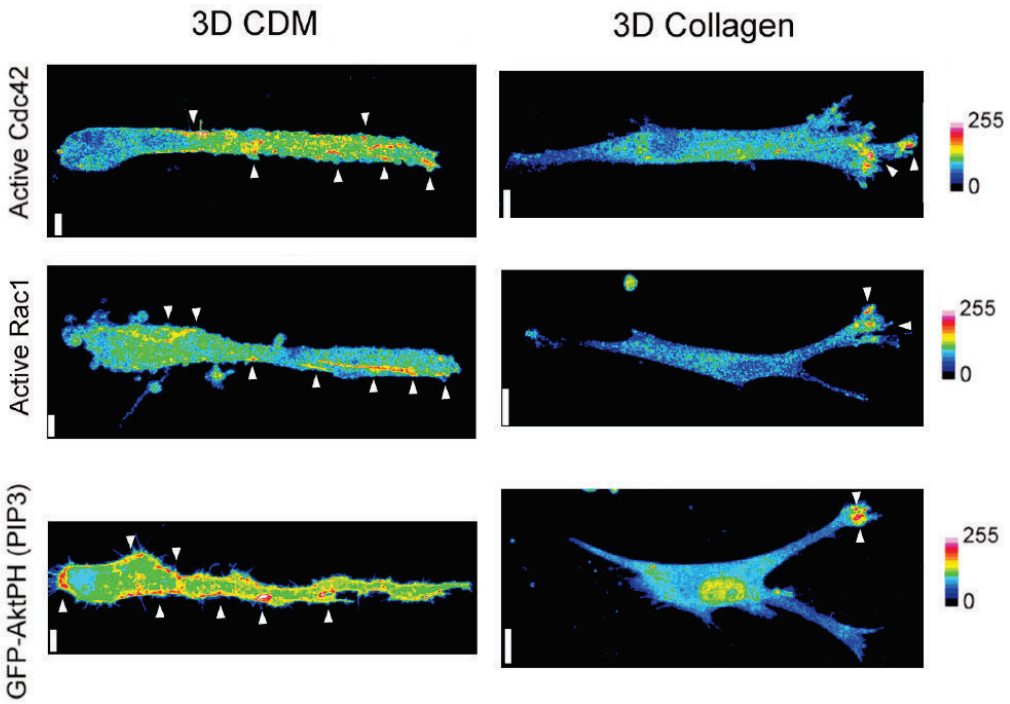

Figure 1.21: Lobopodia and lamellipodia-based cell migration and signaling pathways activated. In 3D CDM, cell migration is lobopodia-based. Cells are migrating to the right. PIP3, Rac1 and cdc42 are not polarized towards the cell leading edge. In 3D collagen gel, cell migration is lamellipodia-based. Cells are migrating to the right. PIP3, Rac1 and cdc42 are required for cell migration and polarized towards the cell leading edge Scale bars 10µm. White arrowheads represents peak activity of the polarity marker. Adapted from Petrie et al. (2012).

In confined 3D matrix, focal adhesions are present in large quantity but are thinner and more elongated than on flat surfaces, highlighting the ability of cells to sense their environment[93]. In collagen gel, mesenchymal cell migration is dependent on integrin and acto-myosin activity to generate efficient traction forces[49]. In contrast, integrins do not contribute to dendritic cell migration in confined collagen gel but myosin II activity is required for the cell passage through narrow pores[9].

Moreover, the actin nucleator formin (ForA) regulates *Dictyostelium* cell migration speed. ForA is located at the rear of the cell in the actin cortex and is involved in the acto-myosin contraction leading to cell motion. Inhibition of ForA in migrating cells on flat surfaces leads to faster motility compared to wild type cells. Under 2D confinement, ForA inhibition strongly impaired cells migration compared to wild type cells by altering the acto-myosin-based contractility machinery[86].

Altogether, these studies highlight differences in cell migration on 2D flat surfaces and in confined environment. On 2D flat surfaces, cell migration is protrusions-based and requires focal adhesions formation. It needs the activation of Rac1 and cdc42 as well as the production of PIP3 at the cell front. In confined environment, Rac1 activation is not essential. However, myosin II activity is important. Focal adhesions are not always required to allow cell migration under confinement. Altogether, a balance between protrusions activity and myosin contractility exists and regulates cell migration mode.

In this part, we saw that under confinement, cells display other modes of migration associated with the activation of different signaling pathways. *In vivo,* cells in a complex environment are exposed to different stimuli but are still able to migrate directionally. In the following section, I will present the cues which are able to direct single cell migration and highlight the fact that not only chemotaxis can direct cell migration but cues can compete or cooperate to direct the cell motion.

1.3 Directed cell migration

Directed cell migration plays a critical role in various processes such as immunity, embryonic development, wound healing or metastatic spread. A cell undergoing persistent motion is characterized by the stabilization of protrusion or lamellipodia at the cell front allowing the conservation of the cell polarity[46]. As mentioned previously, cells move *in vivo* in a complex environment where stiffness, chemical composition and confinement can vary and influence their migration. An increased in persistence time and length along a particular direction are characteristic of a cell which is migrating directionally. I will introduce in the following section the main cues which lead to directed migration of single cell *in vitro* and *in vivo*.

1.3.1 Contact guidance

Contact guidance is the phenomenon leading to cell shape modification and oriented cell migration due to particular geometry, organization and composition of the ECM. ECM is produced by cells, such as fibroblasts, and provides structural support for organs and tissues but as well for individual cell migration. It is composed of hundreds of proteins, the main one are collagen and fibronectin. ECM can also bind growth factors. In order to move, cells need to be polarized and attach to the substrate. I will report in the next section some studies which support the idea that contact guidance orient cell migration.

Human corneal epithelial cells are able to detect nano- to micro-topographical structures, elongate accordingly and orient their protrusions and lamellipodia activity along the structures direction[94]. Along this line, aligned collagen gels, synthetic fibers and fibronectin lines orient cell as well as actin filaments and focal adhesions[95–97]. An increased space from 3µm to 10µm between two fibronectin lines optimized the orientation of the cell body, actin filaments and focal adhesions distribution and its migration parallel to fibronectin lines (Figure 1.22A)[97].

In vitro, cancer-associated fibroblasts produce a highly organized meshwork allowing oriented cancer cell migration[41]. *In vivo,* they observed a parallelly-organized fibronectin network, linked to the presence of cancer-associated fibroblasts at the tumor proximity and promoting directional cancer cell invasion away from the tumor. Moreover, fibroblasts are by nature, CDM producing cells. *In vitro*, according to the topographical nature of the microenvironment on which cells are growing, organization of the CDM is modified: by culturing fibroblasts on micrometer size microgrooves, the cells aligned CDM parallel to the microgrooves leading to the cell migration along the aligned fibers (Figure 1.22B-C)[98].

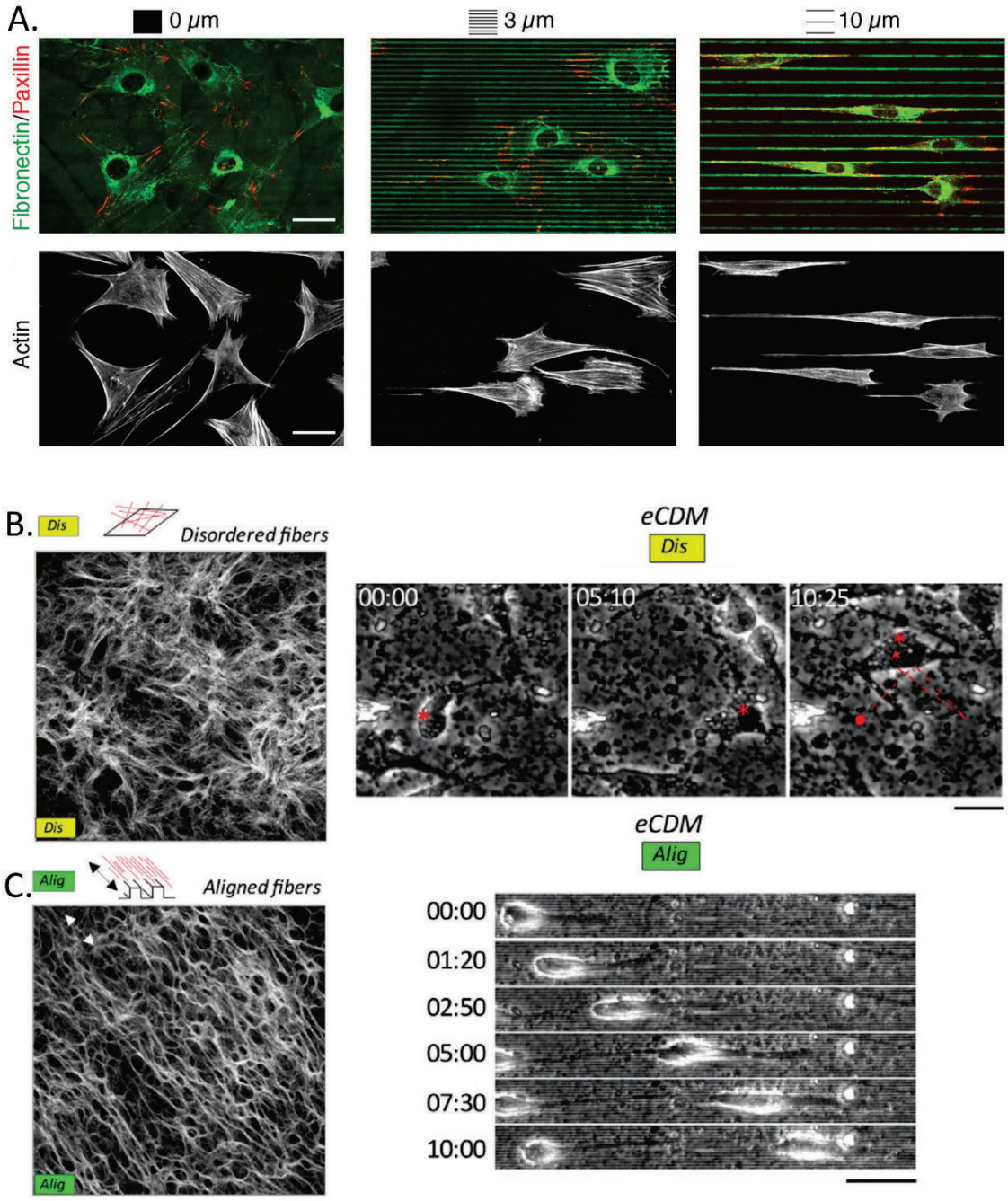

Figure 1.22: Fibronectin lines or aligned CDM orient cell migration. (A.) 2µm parallel lines of fibronectin are micropatterned with interline spacing of 0, 3µm or 10µm. Aligned actin filaments (grey) and focal adhesions sites (Paxillin in red) to fibronectin line (green) are observed leading to optimized directed cell migration at 10µm space interval. Scale bar 30µm. Adapted from Ramirez-San uan` akes` and Gardel (2017). (B.) Left. Image of a CDM produced on a homogeneous substrate. Collagen fibers (grey) are disordered. Right. Time lapse of a fibroblast migrating in the disordered CDM. No directional cell migration is observed. (C.) Left. Image of a CDM produced on a substrate containing parallel microgrooves of 1µm height as a guiding template. Collagen fibers (grey) are aligned. Right. Time lapse of a fibroblast migrating in the aligned CDM. Cells are directionnally migrating along collagen fibers. Scale bar 100µm. Time in hh:mm. (.)` and (.)` adapted from aballero` et al. (2017).

In this first part, we saw that cells detect nano- to micrometer structures size in their environment and orient their migration. There, cells do not migrate directionally. In the following sections, I will present cues which can direct cell migration. First, we will see that cells can detect substrate rigidity and migrate directionally.

1.3.2 Durotaxis

Durotaxis is the phenomenon leading to the directed cell migration along stiffness gradient. As mentioned previously, cell adhesion to the ECM is required for cell migration. Pelham and Wang (1997) observed that the shape of NIH3T3 cell changes according only to substrate rigidity, the chemical composition being constant. Differences in rigidity are obtained by varying the quantity of bis-acrylamide in a polyacrylamide gel. On stiff substrates, cells have the same elongated shape than on glass coverslip. On soft surfaces, cells are less spread and the number of stress fibers decreases. It is associated with a reduction of focal adhesion stabilization. They showed that cells detect the mechanical properties of the substrate and as a consequence adapt their shape[99].

Other studies formed a gradient of stiffness and followed the migration of NIH3T3 cells and Mesenchymal Stem Cells (MSC)[61,100]. NIH3T3 cells were placed on collagen-coated polyacrilamide substrates which contain gradient of rigidity ranging from 140kdyn/cm^2 to 300kdyn/cm^2. Cells on soft substrates migrate towards stiff substrates. It is associated with an increase in protrusions expansion onto rigid substrates. In fact, cells exert stronger traction forces on stiff substrates. They proposed that cells probe mechanical properties of its environment through protrusions. As a mechanosensor, focal adhesions form strong attachments on stiff regions and lead to strong mechanical feedbacks (actomyosin contractility) favoring cell migration in this direction[100]. In addition, recent study shows that cells follow rigidity gradient according to the extracellular proteins coated on the polyacrylamide substrate: cells migrate directionally on fibronectin coated substrate but do not on laminin coated substrates, highlighting that the matrix composition plays a crucial role for the cell to response to gradient stiffness in the environment[101]. Besides its role in directing cell migration, substrate stiffness plays a key role in cell differentiation: MSC cultured on substrates mimicking neural, muscle or bones stiffness differentiate into neurogenic, myogenic and osteogenic cells respectively[102,103].

To conclude, cells are able to detect mechanical properties of the surfaces and adapt focal adhesions formation accordingly. More interestingly, in a homogeneous chemical environment, cells migrate directionally towards the stiffer side of a rigidity gradient, a phenomenon called durotaxis. I will present now that cells are also able to detect electrical fields and to migrate directionally in response.

1.3.3 Electrotaxis

Electrotaxis or **galvanotaxis** is the phenomenon leading to the directed cell migration in response to an electrical potential gradient. Emil Du Bois Reymond (1849) detected and measured over 150 years ago, natural electric current in human skin wounds[104]. When a wound occurs, the tissue barrier is disrupted and produces a gradient of potential. *In vitro*, it has been shown that physiological electric fields (from 0.3V/cm to 3.0V/cm) applied to hamster ovary cells during wound healing process induced polarization of the Golgi apparatus followed by directional cell migration[105]. Corneal epithelial cells and lymphocytes are sensitive *in vitro* to

electrotaxis. They respond to a change in electric field directions and always migrate towards the negative pole. This mechanism is PI3K and Akt activation dependent respectively[92,106]. In addition, authors studied the migration of rat Walker carcinosarcoma cells in response to electrical fields. These cells under specific growing conditions exhibit lamellipodia or membrane blebs-driven migration. In physiological electric fields (1-3V/cm), both cells type migrate directionally towards the cathode. Lamellipodia-cell migration is dependent on Rac1 activation but independent of ROCK and myosin II activation. In contrast, bleb-driven cell migration is independent of Rac1, but cdc42, RhoA as well as ROCK and myosin integrity is required in response to electrotaxis[107].

Electrotaxis is another example of external cue able to direct cell migration. I will present in the next section, the well-established chemotaxis to direct cell migration.

1.3.4 Chemotaxis

Chemotaxis is the phenomenon leading to the directed cell migration along soluble gradient of chemical molecules. It has first been observed during the development of the amoeba *Dictyostelium.* It is a unicellular organism which grows separately. However, following starvation, cells group and form a multicellular structure. The clustering of these cells occurs trough an active process: individual cells directionally migrate towards a central point. In 1947, the phenomenon leading to directed cell migration has been attributed to the diffusion of a substance from a central point thereby forming a chemical gradient[108]. Later, they identified this substance as cyclic-AMP produced by cells[109]. *In vitro*, this directed cell migration has been reproduced: the migration of individual *Dictyostelium* cell is directed towards a pipette delivering cyclic-AMP (Figure 1.23)[110].

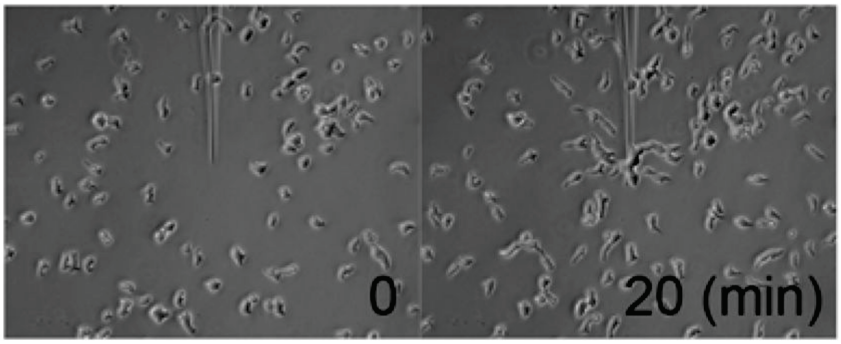

Figure 1.23: *Dictyostelium* cell migrating towards a pipette delivering cyclic-AMP[110] .

In addition, chemotaxis has proven its ability to direct migration of a large number of eukaryote cells *in vivo* and *in vitro*.

1.4.4.1 *In vivo* chemotaxis

In Zebrafish, Niethammer et al. (2009) detected the formation of hydrogen peroxide gradient in response to local injury. A ratiometric sensor is used to detect the presence of H_2O_2. After local injury of the tail, they observed the production of H_2O_2 followed by the recruitment and directed migration of single leukocytes at the injury site[1]. Other studies in Zebrafish reported the

formation of a gradient of the chemokine CXCL12 during primordium formation. It is generated across the primordium by the specific internalization of the chemokine at the back of the primordium leading to its migration to the highest chemokine concentration[24,111]. In live mammals, it is widely accepted that metastatic spread is influenced by chemical gradient. But often, the presence of this chemical gradient has not been shown. I will present now some studies which report *in vivo* chemical gradient associated with directed cell migration. Muinonen-Martin et al. (2014) revealed the presence of a gradient of lysophosphatidic acid (LPA) in mouse tissue close to melanoma site. The lowest concentration is located at the tumor site and the highest at the tumor periphery. *In vitro*, melanoma cells are attracted by LPA and are able to degrade it leading to the formation of a self-generated LPA gradient. This could potentially lead to metastatic spread *in vivo*[112]. In another study, authors injected growth factor at the tumor proximity in mouse and collected macrophages and carcinoma cells at the injection site. These cells respond to the chemical stimulation and migrate directionally[113].

In these specific examples, the presence of a chemical gradient associated with cell migration has been observed *in vivo.* However, directed cell migration is also reported without observing any chemical gradient, *i.e*. metastatic spread at specific organs. In such case, chemotaxis should not be used as a default mechanism to direct cell migration. In order to better understand the mechanism of chemotaxis and its potential relevance *in vivo*, *in vitro* experiments have been developed.

1.4.4.2 *In vitro* chemotaxis

In vitro chemotaxis experiments allow to understand better the mechanisms leading to cell migration, cytoskeleton organization and the activation of signaling pathways.
Classically, chemotaxis is studied in Boyden chamber experiments[6]. As previously described, it is composed of two chambers separated by a porous membrane. The chemoattractant is added to the lower chamber. This allows the study of cell migration on distances smaller than a cell size (15µm) in response to a chemoattractant.
Alternatively, pipette experiments are used to study single cell migration towards a pipette secreting a chemoattractant. After chemoattractant stimulation, *Dictyostelium* cells and neutrophils rapidly activate actin polymerization, protrusions formation and retraction at the cell rear through acto-myosin contraction leading to cell migration in the direction of the chemoattractant source[114,115].
Recently, other tools are used to study migration of chemotactic cells: microfluidic ladder chamber is useful to follow the cell migration in response to any chemical gradient in 2D or 3D environment[21]. The shape and geometry of the environment where cells migrate can be tuned to confine more or less the cells. Prentice-Mott et al. (2016) confined neutrophil cells in microchannels and followed the migration of these cells in different slopes of chemoattractant gradients[12]. Tong et al. (2012) used gradient of serum to introduce breast cancer cells inside microchannels and study their migration under different confinements[11]. They reduced the concentration of serum from 10% to 0% and observed a decreased percentage of cell entering (from 96% to 3%) and exiting (from 58% to 5%) from the microchannels respectively, revealing the importance of gradient slope to efficiency direct cell motion[11].

Soluble chemical gradients are powerful tools to direct cell migration. As mentioned previously, the slope of the gradient determines the efficiency of cell migration. However, adherent chemical gradients also exist and can direct cell migration.

1.3.5 Haptotaxis

Haptotaxis is the phenomenon leading to the directed cell migration along chemical gradients bound to the surface. The term haptotaxis was first introduced by Carter in 1965 when he observed fibroblasts motion in the direction of increasing adhesion on the substrate made of gradient of metal[116]. He observed directional cell migration in the direction of the gradient and longer cell tracks indicating more efficient motility[116]. Haptotaxis experiments were then performed by modifying Boyden chambers. Lower side of the membrane is coated with a solution containing the protein to be tested such as fibronectin or laminin. As a result, B16 mouse melanoma cells are migrating towards fibronectin and laminin[117]. On flat coverslip, a fast epithelial cell migration is observed at an intermediate concentration of fibronectin. In a too low concentration, cells form few adhesions and adhere weakly to the surface generating weak traction forces. Whereas in a high fibronectin concentration, cells adhere strongly to the surface leading to their immobilization[118]. More recently, microfluidic or microcontact printing techniques have been developed to study the migration of cells in response to any surface-bound protein gradient. Human microvasculature endothelial cells respond to different slope of fibronectin gradients. The slope of the gradient affects the cell speed: larger the slope, faster are the cells[119]. Zhang et al. (2015) formed lines of the chemokine CXCL12 to study the migration of neural progenitor cells. They observed directed cells migration towards CXCL12 lines associated with an increased and oriented actin polymerization and Rac activation[120]. *In vitro*, dendritic cells migrate towards adhesive gradient of CCL21[121] and *in vivo*, the presence of adhesive gradient of CCL21 has been detected within the lumen of lymphatic capillaries of mouse ear skin[26]. They managed to reproduce the adhesive gradient *in vitro* by culturing a monolayer of lymphatic endothelial cells (CCL21 producer) under a laminar flow similar to lymph flow.

Up to now, the cell migration was directed due to the presence biochemical cues in the environment, aligned fibers (contact guidance) or electrical (electrotaxis), stiffness (durotaxis), chemical soluble (chemotaxis) or adhesive (haptotaxis) gradients. For all the cues, the efficiency to direct cell migration depends on the slope of the gradient, usually much larger than the size of a cell. In the next section, I will present two types of directed cell migration based on physical cell properties at its scale, *i.e.* protrusions activity and nucleus confinement. Ratchetaxis will be presented first.

1.3.6 Ratchetaxis

Ratchetaxis has been reported recently as a phenomenon leading to the directed cell migration due to any local asymmetric cues in the environment[23]. A cell polarized on a coverslip has an asymmetric triangular-like shape, with a cell front characterized by a large lamellipodia and a cell back which constituted the trailing edge (Figure 1.24A). A migrating cell adopts this

morphology and moves in the direction of polarization. To better understand the influence of environment associated with asymmetric cues, initial studies imposed asymmetric shape to the cell in order to influence the direction of migration.

Jiang et al. (2005) imposed a teardrop shape to NIH3T3 fibroblasts. In fact, the positions of centrosome and the Golgi complex at the front of the nucleus match with the polarity imposed by the teardrop shape. This asymmetric polarity leads to an oriented cell migration to the blunt end of the teardrop (Figure 1.24A). Other asymmetric patterns (elongated teardrops, triangles, V-shape) are tested and they observed the same directed cell migration towards the blunt end. As a control, migration of cells from symmetric circle and square is followed and random motion is observed[77]. The asymmetrical unit has been called **ratchet**[23]. Without any external chemical gradient, asymmetric patterns, which have the size of a cell, force cell to polarize and influence locally the direction of motion. The next question is: does this ratchet is able to orient cell migration over long distances?

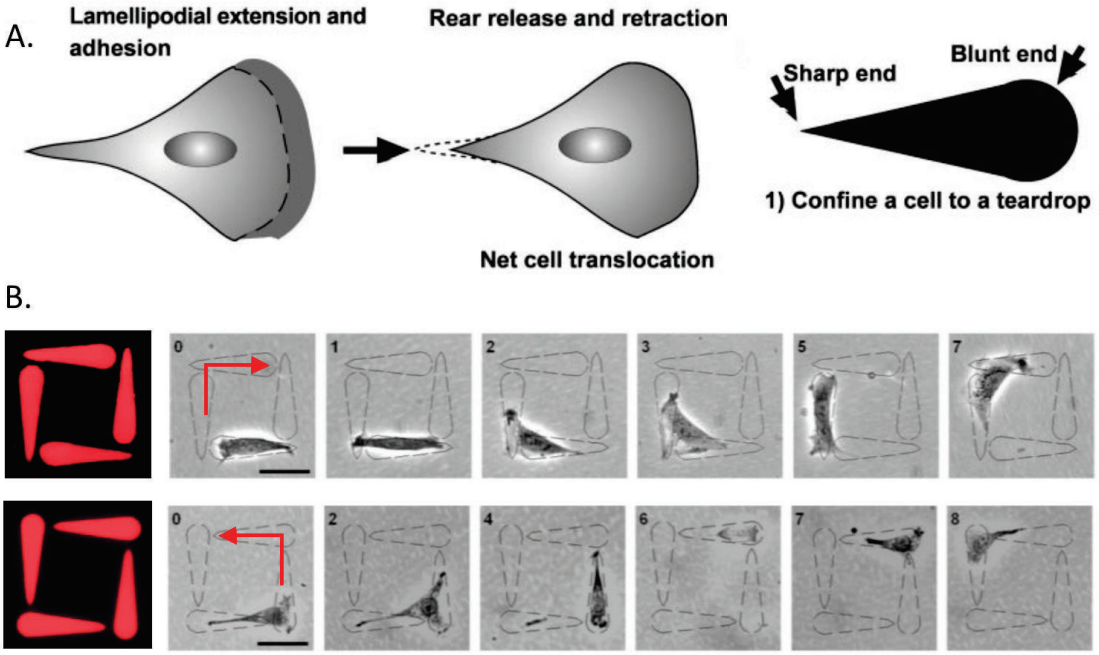

Figure 1.24: Imposing the shape of the cell allows the control of cell migration (A.) Left. Schematics of a migrating mammalian cell characterized by large lamellipodia at the cell front and retraction of the trealing edge. Right. Experimental configuration used. Teardrop shape imposes the polarity to the cell and migrates preferentially in the direction of the blunt end. Adapted from Jiang et al. (2005). (B.) The position of a teardrop ratchet relative to the next one challenges the lamellipodia activity of the cell and leads to its clockwise (Top) or counterclockwise (Bottom) migration. Scale 50µm Time in hours. Adapted from Kumar, Ho and Co (2007).

In fact, a long range directed cell migration is characterized by the conservation of the cell polarity[46]. Along this direction, several teams report directed cell migration over long distance by adjusting repeated asymmetric patterns [15,19,122]. The position of a ratchet teardrop relative to the adjacent one challenges the protrusion activity and plays a critical role to direct the cell motion. Figure 1.24B Top and Bottom shows that equal distance between motifs but difference in cells probing area in the blunt or sharp end direct the cell migration in opposite direction.

Cells migrate in the direction in which lamellipodia attachment is larger, *i.e.* Figure 1.24B First row. to the left and Figure 1.24B Second row. to the right of the initial cell position[122].

In addition, Mahmud et al. (2009) seeded cells on connected ratchets. After spreading, cells adopt the triangular shape of the motif[19]. They observed "funneling" lamellipodia in the direction of the tip of the ratchet associated with cell migration in the same direction (Figure 1.25A). Actin staining reveals an asymmetric distribution of actin cytoskeleton, with the presence of bundles at the cell back, perpendicular to the direction of motion (Figure 1.25B "P"). The perpendicular bundles prevent the formation of lamellipodia. On the cell sides, "funneling" bundles of actin favors lamellipodia growth in the sharp end of the motif and is associated with asymmetric distribution of focal adhesions. Therefore, it is less energy costly for the cell to form lamellipodia to the "funneling" direction than against it, the perpendicular bundles has to be broken before forming lamellipodia.

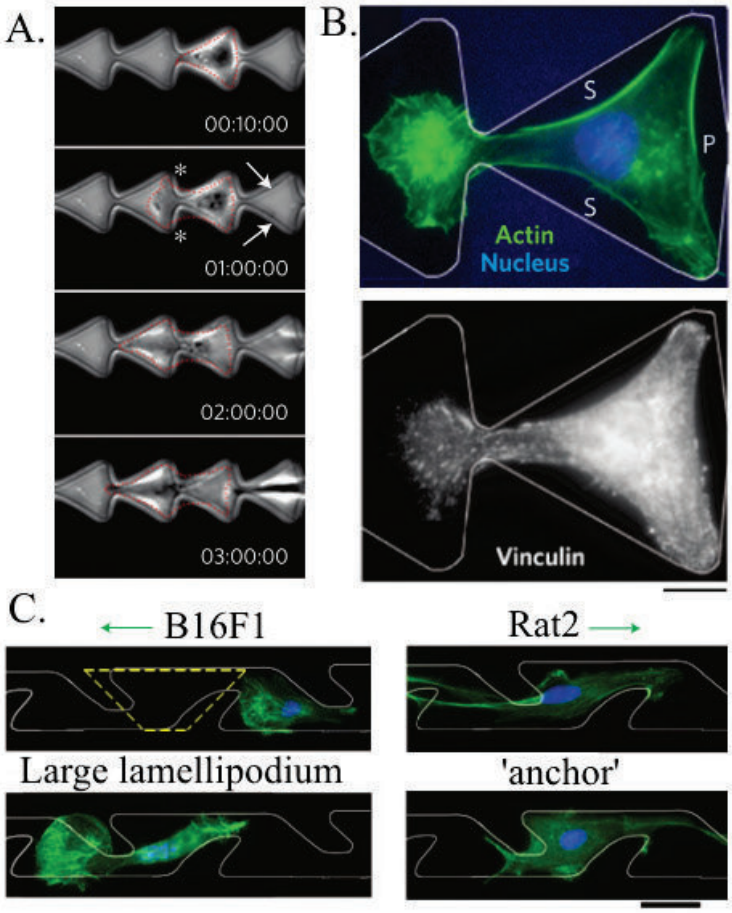

Figure 1.25: Protrusions activity directs cell migration. (A.) B16F1 melanoma cell migrating in connected triangles ratchets. The geometry of the pattern imposed the polarity to the cell. Cell is migrating toward the sharp end of the motif. Scale bar 50µm. Time in hh:mm:ss. (B.) Actin and vinculin distribution of a melanoma cell migrating in connected ratchets. Scale bar 12.5µm. (C.) Two cell lines migrating in an opposite direction on a line with asymmetric spikes ratchet motifs. In this configuration, B16F1 cell form large lamellipodia to the open narrow left side of the motif whereas Rat2 cell form long protrusions to the large open right side of the motif. Scale bar 30µm. Adapted from Mahmud et al. (2009).

In this study, they challenged the difference in protrusions activity of two cell lines to direct motion along asymmetric motifs. The cancerous B16F1 cells form large lamellipodia whereas the non-cancerous Rat2 fibroblasts form lamellipodia and long protrusions. This difference in

protrusion characteristics motivated them to investigate another ratchet geometry: line with asymmetric spikes motifs imposes an asymmetric polarity to the cell (Figure 1.25C). B16F1 cells form large lamellipodia towards the narrow part of the motif (left), leading to the cell migration in this direction whereas Rat2 cells extend long protrusions to the large side of the motif (right) leading to the cell migration in this direction (Figure 1.25C). It proves, but without explaining, that protrusions activity controls the directed cell migration.

Following this line, a previous work from our lab specifically investigated the role of protrusions activity to direct cell migration[15]. In this study, the basic ratchet motif is a triangle of fibronectin whose area is equal to the mean surface area of a NIH3T3 fibroblast. In contrast to Mahmud et al. (2009), a gap separates two ratchet motifs[15].

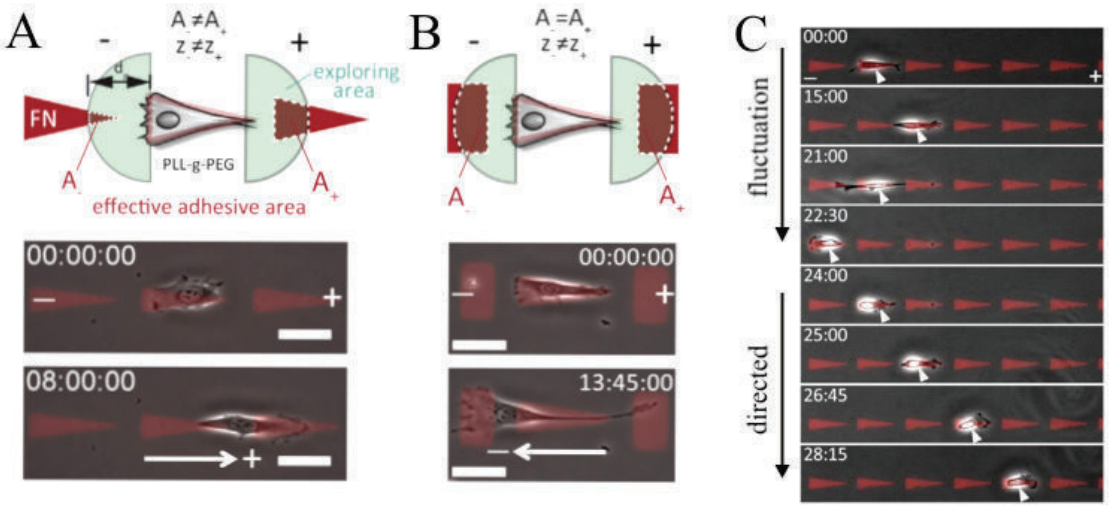

Figure 1.26: Efficient protrusion activity drives cell migration over long distances. Schematics and images of a NIH3T3 cell on a ratchet surrounded by two ratchets (A.) or two rectangles (B.). The efficient protrusion z is defined as the number of protrusions which adhere to the motifs, leads to a force transmission and is proportional to the effective adhesive area, called A. (A.) The protrusions frequency z and probing area A are different in the "+" and "-" sides leading to cell movement to the "+" direction. (B.) The protrusions frequency z is different and probing area A is equal leading to cell movement to the "-" side. (A.) and (B.) Scale bar 50µm Time in hh:mm:ss. (C.) Time lapse of a NIH3T3 fibroblast migrating on a line of fibronectin ratchet. The cells starts first to fluctuate and then migrate directionally towards the "+" direction. Scale bar 100µm. Time in hh:mm. Adapted from Caballero et al. (2014).

Caballero et al. (2014) used microcontact printing technique to print fibronectin motifs on a coverslip. As mentioned previously, the asymmetric shape of the asymmetric ratchet imposes a polarity to the cell[19,77,122]. In this set-up from Caballero et al. (2014), the cell polarity is imposed by the triangular shape. The cell send protrusions to both ends of the ratchet defined as "-" side to the blunt end, *i.e.* in the cell polarity, and as "+" side to the sharp end of the triangle, *i.e.* against the cell polarity (Figure 1.26). They defined the term efficient protrusion "z" as the protrusions which adhere to the neighboring motifs and potentially lead to force transmission in the "+" (z_+) or "-" direction (z_-). The parameter "z" is proportional to the effective adhesive area available (A): larger the area, larger is the number of efficient protrusions. "z" depends on the protrusion stabilization time τ, the frequency of protrusion probing ν and the rate of protrusion efficiency β and is equal to $z \simeq \beta\tau\nu$. They assumed β is equal in both directions, measure experimentally ν and τ and deduced z. Then they introduced the direction index

parameter $I_{dir} = \frac{Z_+ - Z_-}{Z_+ + Z_-}$ which described the asymmetry distribution of efficient protrusions. A negative I_{dir} indicates that more efficient protrusions are sent in the "-" direction. A positive I_{dir} indicates that more efficient protrusions are sent in the "+" direction. In contrast to previous study, Caballero et al. (2014) defined the parameter I_{dir} which predicts the direction of cell migration in different conditions. I will present now the two conditions tested. Condition 1, a triangle is surrounded by two rectangles of fibronectin (Figure 1.26B). The probing area is equal in both sides ($A_-=A_+$), but the triangular shape of the motifs imposes the cell polarity and leads to an asymmetric distribution of protrusions. More efficient protrusions are sent in the polarity direction, "-" side ($z_->z_+$). I_{dir} becomes negative and it is confirmed by cells movement in the "-" direction (Figure 1.26B). Condition 2, a triangle is surrounded by two fibronectin triangles (Figure 1.26A). More protrusions are sent in the "-" direction but the probing area is larger in the "+" direction ($A_-<A_+$) and the protrusion efficiency is asymmetric ($z_-<z_+$). I_{dir} becomes positive (Figure 1.26A). A cell movement to the "+" direction is observed (Figure 1.26A). On triangles line, this leads to the directional cell migration over a long range of time and length (Figure 1.26C).

In contrast to previous studies, Caballero et al. (2014) predicted the direction of migration by highlighting the role of efficient protrusions. The measure of protrusions frequency and stabilization time explained the directed the cell migration over short and long distances.

However, other studies showed that the nucleus is responsible to direct cell migration in an asymmetric environment[16,20]. Le Berre et al. (2013) studied the migration of the human dermal fibroblasts under non-adhesive tilted pillars (Figure 1.27A). The tilted pillars biased the cell migration in the direction of the tilt by asymmetrically and mechanically deforming the nucleus. Cells migrating against the tilted pillars have a reduced speed indicating that cells experience more frictions.

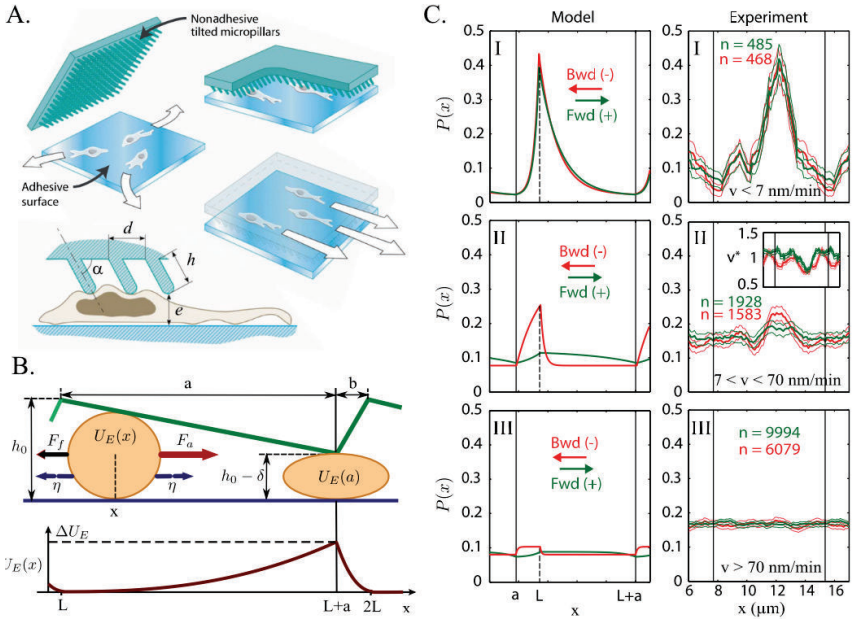

Figure 1.27: Tilted topographical ratchets direct cell migration. (A.) Schematics of the experimental set-up where cells are placed under non-adhesive tilted pillars. Cells are mainly migrating in the direction of the tilt. (B.) First row. Schematic of the nucleus deformation in ratchet profile. Nucleus is considered as an elastic sphere. Second row. Corresponding energy profile. (C.) Nuclei distribution predicted by the model and obtained experimentally for the 3 regimes. Vertical lines indicate position of the pillars. Adapted from Le Berre et al. (2013).

They modeled this phenomenon in a ratchet profile geometry and assumed that the nucleus is a spherical linear elastomer. Along the distance a, corresponding to the tilted distance, the nucleus squeezes progressively until reaching a maximal deformation where the distance between pillar and coverslip, called bottleneck, is minimal (Figure 1.27B). Then, over a distance b, they assumed that the nucleus at the bottleneck exerts a propulsion force which moves the cell forward and increases its speed in the tilt direction. The energy profile reveals that the nucleus is unstable at the bottleneck region resulting in a low probability to find the nucleus at this position (Figure 1.27). Moreover, in their model, they varied the energetic profile height, which experimentally would correspond to changing the height of the tilted pillars (Figure 1.27C). They predicted three different regimes: Regime I. at strong geometry constraints, *i.e.* long tilted pillars, small bottleneck, the nucleus is blocked between bottlenecks in the tilt direction (Fwd) or against tilt direction (Bwd) and the expected distribution is the highest at the minimal energetic constrain (Figure 1.27C First row Left). It results in a low velocity in both directions (Figure 1.27C First row). Regime II. at intermediate geometry constraints, *i.e.* intermediate tilted pillars, intermediate bottleneck, the cell nucleus has to overcome an energetic barrier lower in the tilted direction (Fwd) compared to against tilted pillars (Bwd). The expected distribution is the highest at the minimal energetic constrain in the Bwd direction. It is much less in the Fwd direction (Figure 1.27C Second row Left). This predicts a preferential direction in the Fwd and tilted direction at the intermediate regime. Regime III. at weak geometry constraints, *i.e.* small tilted pillars, large bottleneck, the energetics barrier are negligible in both directions and the nucleus is not confined to allow preferential direction (Figure 1.27C Third row Left). Experimentally, they assessed the position of cell nuclei according to the cell speed. The variation of nucleus position as a function of cell speed confirmed the three regimes. At low cell speed, Regime I, the nucleus distribution is the highest at the minimal energetic constrain in both directions. At high cell speed, Regime III, no preferential distribution is observed in both directions. However, at intermediate speed, Regime II, they observed a preferential direction of migration in the tilted direction. This indicates that the level of nucleus confinement plays a key role in directed cell migration under confinement: too confined prevents cell migration, no enough confined suppress directionality whereas intermediate confinement allows optimal mechanical interactions and geometric frictions and leads to directed cell migration[20].

I will now present in the next section, the work of Comelles et al. (2014) in our lab where the effect of topographical ratchet-like surfaces on cell migration has been studied (Figure 1.28A). They observed cell migration along the ratchet axis and in the ratchet direction (Figure 1.28B). The nucleus is setting the direction of cell migration. It interacts with topographical walls of the ratchets and aligns along them. As a consequence, the nucleus is mainly located in the bottom ratchet and has an oriented elongated shape. Then, to understand the role of cell cytoskeleton in the process of cell migration on topographical ratchet-like surface, they transfected the cells with Zyxin-RFP. In terms of protrusion activity, they did not observe differences between cells on the top and the bottom of the ratchets. However, they observed the formation of focal contacts along the topographical ratchet walls which disappear as soon as the nucleus moves forward. To explain this behavior, they assumed that the nucleus close to the substrate is sensitive to any changes in the substrates. On flat surfaces, they observed nucleus flattening associated with stress fibers suggesting the presence of forces to pull down the nucleus to the

surface. Variations on topographical surface could therefore influence nucleus height and cell migration. In fact, in the bottom ratchet, the nucleus is the most stable (Figure 1.28C) resulting in the lowest energy potential (Figure 1.28D) and the highest probability to find the nucleus at this position (Figure 1.28E). This is confirmed by experimental data.

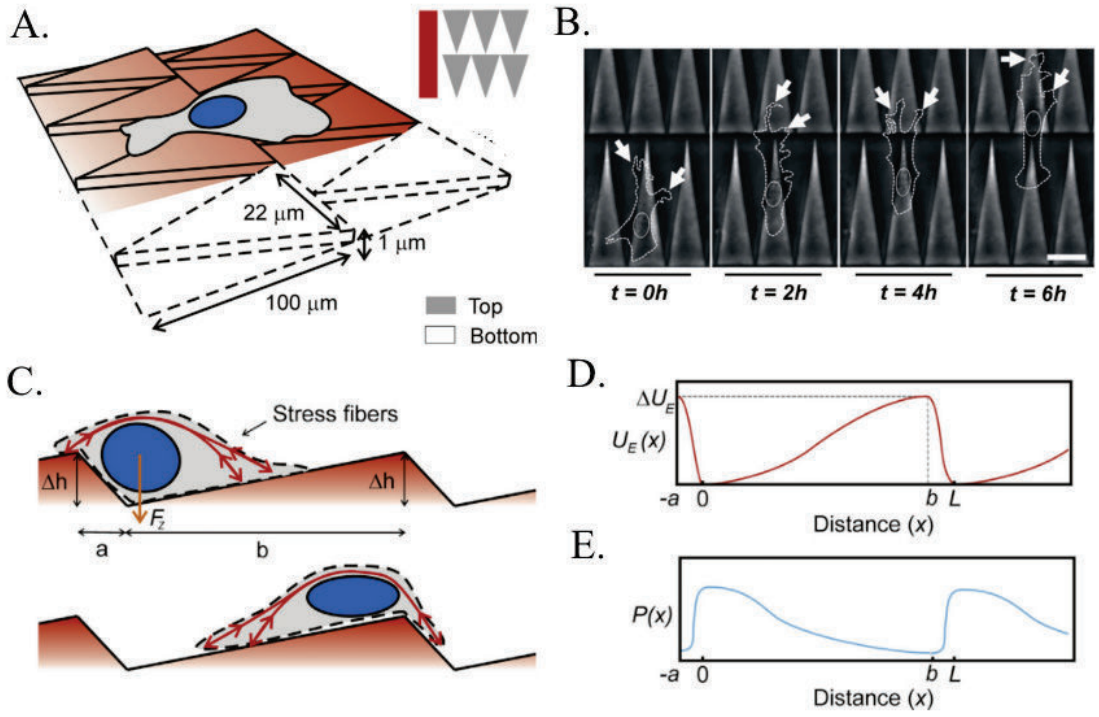

Figure 1.28: Topographical ratchet-like surfaces direct cell migration (A.) Schematic of the experimental set-up composed of topographical ratchet-like surface with 1µm height difference. Bottom triangles in white are pointed up, top triangles in grey are pointed down. (B.) Time lapse of a NIH3T3 cell migrating on the topographical ratchet-like surface. Cell is directionnaly migrating on the bottom triangles. White arrows indicate cell protrusions. Dash lines represent cell and nucleus contours. Scale bar 20µm (C.) Schematics of a cell in topographical ratchet-like surface. Nucleus deforms according to its position on the ratchet. (D.) Energetic potential of a cell on tographical ratchet. It is the lowest in the bottom ratchet and highest in the top ratchet. (E.) Probability distribution of the nucleus on topographical ratchet. Adapted from Comelles et al. (2014).

In this paper, Comelles et al. (2014) showed also that the mechanical interactions between the nucleus and the environment direct cell migration without chemical gradients.

These different studies showed that ratchetaxis directs cell migration on 2D surfaces due to asymmetric protrusions dynamics at the cell front and back. The protrusions activity plays a major role as their study predicts the direction of migration. In addition, tilted pillars and topographical ratchets lead to asymmetric deformations of the nucleus through its interaction with ratchet geometry. The strongest the nucleus deformation, *i.e.* bottleneck of tilted pillars or topographical obstacle, the highest is the nucleus instability leading to directed cell migration.

In the next section, I will present how cell and nucleus confinement by itself can orient or prevent cell migration.

1.3.7 Cell and nucleus confinement

In vivo, it has been shown that cells migrate mainly under confinement. As mentioned in the section "*In vivo* environment: cell migration in confined spaces" (page 33), longitudinal tracks exist *in vivo* and cancer cell migration along these preexisting tracks has been observed[39,41]. Capillaries are channels in which cells can migrate. Typically their size ranged from 3µm to 8µm in diameter[35]. Circulating cancer cells have a diameter of 20µm whereas immune cells have a diameter of 9µm[123]. It therefore indicates that cells are confined while migrating in these capillaries. In addition, *in vivo* study suggests that most of circulating cancer cells are arrested in small capillaries by size restriction[3].

Yamauchi et al. (2005 and 2006) followed the migration of cancer cells from large blood vessels to small capillaries in live mice[4,5]. They observed *in vivo* the extravasation process, starting with the sending of thin protrusions into host tissue, then cytoplasmic projections and finally the nucleus migrates until the cell is out of the vessel. Nucleus deformation is necessary to allow cell migration (Figure 1.29).

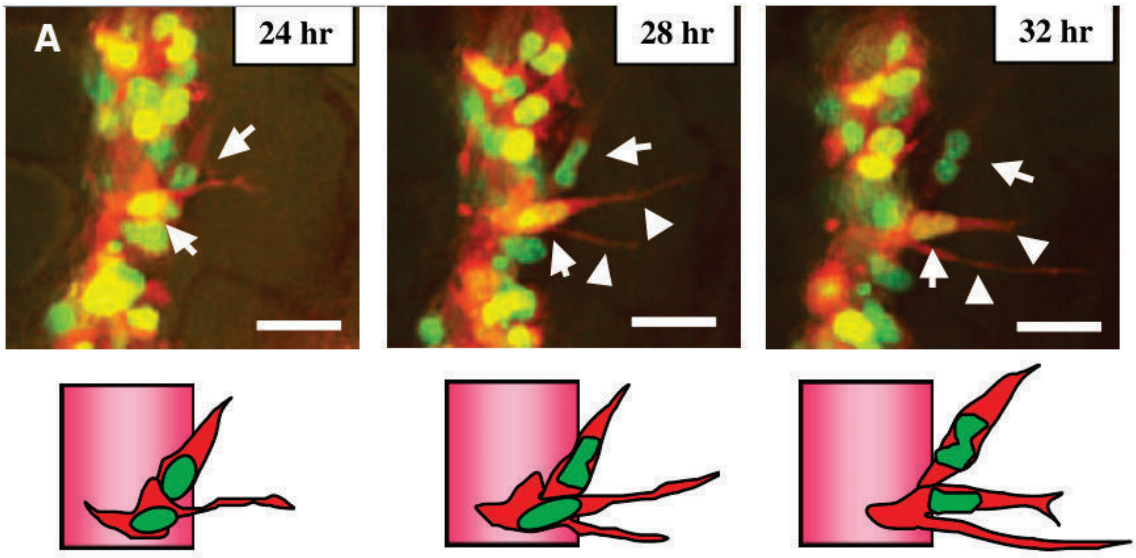

Figure 1.29: Time lapse images of extravasation process in live mouse of mammary tumor cells. Green Histone2B-GFP (cancer cell nuclei) ; red RFP (cancer cells cytoplasm). 24 hours after cancer cells injection, the cancer cell extend thin cytoplasmic projections into host tissue. At 28h, the nucleus migrates along cytoplasmic projections until the cell fully extravasates (32h). Below are schematics of the process. Scale bar 20µm. Images from Yamauchi et al. (2006).

As mentioned previously, cell adapts its shape and deforms its nucleus to fit capillaries dimensions: thinner capillaries lead to more elongated cells.

In vitro, several studies showed the effect of physical confinement on cell migration. I will present in the next section few examples of cell migration under confinement.

Researchers usually used gradients of serum to allow the cells entry into microchannels and studied their migration at different confinement level[8,11]. Tong et al. (2012) measured a decrease in human bone osteosarcoma cell speed correlated to a decrease in channel width whereas

Hung et al. (2013) observed an increase in migration velocity of CHO cells while channel width decrease. Other study combined both *in vivo* and *in vitro* experiments to understand dendritic cells migration in confined spaces. They showed that the migration of dendritic cell alternated between high and low motility phases corresponding to cell migration and antigen uptake respectively and is primordial to the immune response[52]. Liu and colleagues (2012) built a set-up allowing the control of cells confinement and adhesion. They placed epithelial and mesenchymal cells in low adhesion and high confinement conditions. On flat surfaces mesenchymal cells spread, form strong adhesion to the substrate and migrate at a low speed. Under confinement, the same cells became round and immobile. But surprisingly, some of them spontaneously polarized and migrated fast with an amoeboid like-morphology (round cell body and small leading edge) or even faster with a neutrophil like-morphology (ellipsoid body and large uropod). This transition is called mesenchymal-amoeboid transition (MAT). Under confinement and low adhesion, all the cell lines tested adopt one, the other or both fast migrating phenotypes. This suggested that spontaneous MAT could be used by cancer cells *in vivo* to adapt their migration mode to their environment. In these conditions, focal adhesions cannot bind to the substrates and cells used frictions generated by the confinement to move[17]. As detailed previously in the section "Cell motility under confinement" (page 38), this process called "chimneying" or "pushing off the walls" allows cell migration under confinement[10].

However, migration of cells is interrupted when the confinement increases: below 8µm in mouse capillary diameter and 5µm pores in collagen matrix, cells cannot migrate. In fact, the nucleus is the largest and stiffest organelle inside the cell[18]. Hence, limits of cell migration depend on the cell type, the nucleus deformability and the nature of the environment.
Inside collagen matrix, mesenchymal cells such as fibrosarcoma cells use MMP to degrade collagen in order to migrate through narrow pores (below 5µm). When MMP activity is abolished, cells embedded in 3D collagen matrix with pore diameters above 7µm (40µm^2 area cross-section) migrate and deform their all shape as well as nucleus shape. Nuclei of migrating cells adopt an hourglass shape to cross pore (Figure 1.30A). Smaller pore sizes do not allow cell migration independent of MMP[49].

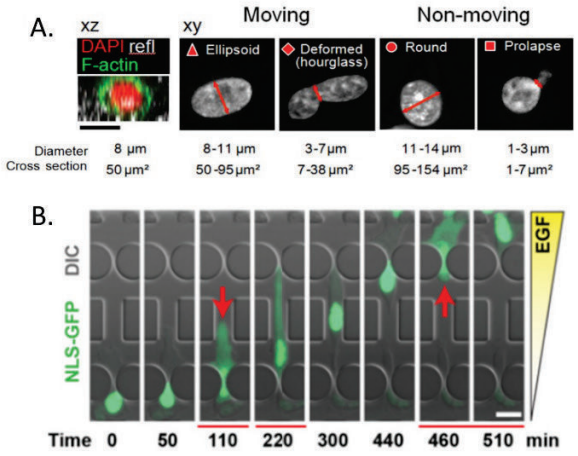

Figure 1.30: Cell and nucleus deformation in narrow pores (A.). Fibrosarcoma cell migrating in MMP independent in a collagen matrix Typical nucleus shape according to the pore diameter is depicted. Adapted from Wolf et al. (2013). (B.) Images sequence of a breast cancer cell migrating through 10µm² cross-section confinement. Green signal stains for Nuclear Localization Sequence and red arrows indicates nuclear envelope ruptures. Scale bar 20µm. Adapted from Denais et al. (2016).

Lautscham and colleagues (2015) designed microchannels that have a series of bottlenecks with decreasing cross-sections separated by larger chambers. They followed the migration of mesenchymal cancer cells along the microchannels. Below a cross-section of 30µm^2, the nucleus

started to be embedded and in the smallest bottleneck (6.5µm^2 in cross-section) the nucleus deformed dramatically. The nucleus velocity increased with confinement until reaching 18.5µm^2 bottleneck cross-section. The nucleus deformation is reversible[124]. However, Denais et al. (2016) reported that 10µm^2 cross-section confinement of the same cancer cells induced nuclear envelope rupture due to nuclear deformation associated with DNA damages (Figure 1.30B). In addition, they observed an increased number in nuclear envelope rupture in the absence of lamin proteins expressions. These proteins are highly expressed in mesenchymal cells and protect the nucleus to strong deformations leading to nuclear envelope ruptures. However, cells are able to repair nuclear envelope damages allowing cell survival but nuclear envelope rupture may promote cancer progression *in vivo*[125]. Thiam et al. (2016) followed the migration of dendritic cells through micrometric pores in microfabricated chambers. These cells migrate in an amoeboid-like manner and express intermediate level of laminA/C and laminB allowing cell migration through narrow pores (down to 7.5µm^2 cross-section). This process is possible due to the recruitment and polymerization of cortical actin around the nucleus at the constriction site and is dependent of Arp2/3 complex. There, actin accumulation exerts a pushing force leading to the cell passage through the constriction[126].

Altogether, the use of microfabrication allows the production of microchannels or microstructures which confine cell. As a consequence, cell migration can be followed in controlled and simplified environment: cell migration can switch from slow to fast migration modes under confinement and low adhesion, cell can strongly deform to fit capillaries or microchannels and nucleus is the limiting factor for cell migration. To conclude, it reveals that studying cell migration under confinement is a key feature to be closer to physiological cell migration.

In this part, I presented different ways to orient or direct cell migration, haptotaxis, electrotaxis, durotaxis and ratchetaxis. Chemotaxis is often referred as the best way to direct cell migration, and its efficiency has heavily been proven *in vitro*. But to explain cancer spreading, *in vivo*, the existence of soluble chemical gradient has so far not been observed. In addition, *in vivo* is a complex environment where cells have to integrate multiple stimuli to migrate directionally. Competition and cooperation between these different cues exist and I will present them in the next section.

1.3.8 Comparison of two types of directed cell migration

In vivo, cells are exposed to multiple cues while migrating. I will present in the following section, some reports which have challenged chemotactic cell migration efficiency by opposing or combining other cues able to direct cell migration. The slope of each cues thereby dictates the direction of cell migration.

Li et al. (2012) developed a microfluidic device in which they studied human T cell migration in the presence of electric fields and a soluble gradient of the chemokine CCL19. First, they validated the directed migration of the cell towards the cathode and the highest concentration of CCL19 separately. Then, they opposed chemotactic and electrostatic gradient. Surprisingly,

they observed a net migration of T cell only towards the cathode. In fact, it has been shown that electrotaxis polarize membrane receptors. As a consequence, membrane receptors are not available to respond to chemical gradient and cells preferentially migrate towards the cathode[127]. In another study, authors reported a cooperative effect of both electric field and CXCL12 gradient on the migration of retinal progenitor cells by increasing the cell directionality and by three-fold increasing the distance travelled by the cell, supporting Li et al. (2012) study[128].

Aligned fibers and VEGF gradient are challenged to study the migration of human umbilical vein endothelial cells (HUVEC). They observed cooperation in cell migration when fibers and chemical gradient are parallel. However, when fibers and chemical gradient are perpendicular, cells migrate along the fibers. This indicates that topographic environment is stronger to direct cell migration than chemical gradient[129].

Schwarz et al. (2016) compared the ability of cells to migrate towards two chemical gradients, one soluble (chemotaxis) and another one bind to the surface (haptotaxis) using a microfluidic device. Dendritic cells respond to haptotatic gradient of the chemokine CCL21 and chemotactic gradient of the chemokine CCL19. They formed three CCL19 soluble gradients, low, intermediate and high soluble gradient. The lowest CCL19 gradient did not induce directionality, whereas cells migrating at intermediate CCL19 gradient show a directional cell migration. This phenomenon is enhanced at the highest gradient of CCL19. To compete soluble and haptotatic gradients, they compared cell migration in constant haptotatic gradient of CCL21 and low or intermediate soluble gradient of CCL19. In low CCL19 soluble gradient, cells followed the haptotatic gradient of CCL21. In contrast, at intermediate CCL19 soluble gradient, cells followed the soluble gradient of CCL19. Although both chemokines bind to the same membrane receptor (CCR7) with the same affinity, these results indicated that cells are sensitive to gradient concentration and followed the highest concentration of chemical gradient[121].

Neutrophil-like cells sense hydraulic pressure and escape from high resistance channel in the absence of chemical cue. The mechanisms by which cells can detect difference in pressure is not known but they proposed that membrane tension sensors could detect small difference in pressure. To compete with chemical gradient, they uncaged the chemoattractant fMLP in the highest hydraulic pressure channel and observed that 75% of the cells migrated away from the chemoattractant even if the cells exhibit a strong polarization (through accumulation of PIP3) toward the chemoattractant[130].

Study from the lab has also explored the competition and cooperation of ratchetaxis in the presence of chemical gradients (Figure 1.31A)[16]. Fibroblasts seeded on topographical ratchets in homogeneous fibronectin coated surface migrated toward the ratchet direction (Figure 1.31B). A haptotatic gradient of fibronectin is superimposed to the topographical ratchet in the same direction of ratchet. In this case, the directionality and mean displacement vector of the cell trajectory increase compared to the effect of topographical ratchet or haptotatic gradient individually, suggesting cooperation between both cues (Figure 1.31C). When topographical ratchet and fibronectin gradient are opposed, absence of directionality and mean displacement vector close to zero is observed, revealing a competition between both cues (Figure 1.31D). As explained previously, nucleus of the cell is mechanically deformed by the ratchet and cell exerts

traction forces to the substrate to migrate directionally on fibronectin gradient. As a result, competition of both cues does not allow directed cell migration (Figure 1.31D).

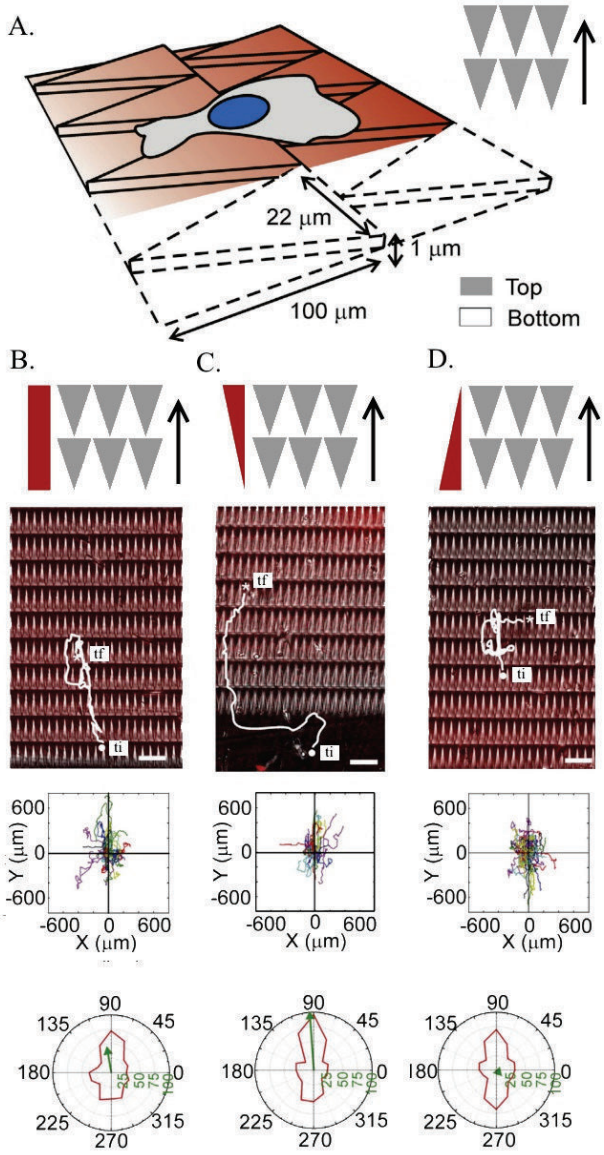

Figure 1.31 : Competition and cooperation of ratchetaxis and haptotaxis. (A.) Schematic of the experimental set-up composed of topographical ratchet-like. (B.) homogeneous distribution of fibronectin on topographical ratchet. (C.) fibronectin gradient in the same direction than topographical ratchet. (D.) fibronectin gradient in the opposite direction than topographical ratchet. (B.C.D) from top to bottom. Experimental configurations combining topographical-ratchet surface and fibronectin gradient (black arrows represent the direction of the ratchet), cells moving on topographical ratchet-like surfaces in the presence of the fibronectin gradient. ti represents initial time point, tf represents final time point. Cell trajectories are plotted. Angular distributions (red) and mean displacement vector (green vector). Scale in the length of the vector in µm. Adapted from Comelles et al. (2014).

Altogether, these studies reveal that rather chemotaxis, contact guidance, electrotaxis, haptotaxis and ratchetaxis are powerful ways to direct cell migration. They can cooperate, but more interestingly compete with chemical gradients to direct cell migration. The actors leading to cell migration are conserved, but their activation are specific to the cue tested, *i.e.* membrane receptors (chemotaxis, haptotaxis) or mechanical sensing (contact guidance, cell confinement, ratchetaxis). The directed cell migration will be dependent on the slope of each cue in the cell environment.

In this project, we want to compete chemical gradient to confined ratchetaxis. In order to be closer to *in vivo* conditions, we aim at using a physiological chemical gradient in microchannels and to follow cell migration. We choose a gradient of the chemokine CXCL12 because of its role *in vivo* to regulate cell migration, from organs development to immune cell trafficking. Its

involvement in the metastatic spread especially attracts our attention. Because it was accepted that cancer cells migrate to secondary tumor sites due to a chemical gradient, we wanted to test its relevance *in vitro*. In addition, the role and localization of both membrane receptors CXCR4 and CXCR7 to regulate cell migration is interesting to probe. First, I will introduce the chemokine CXC12 and its two membrane receptors CXCR4 and CXCR7. Then, I will present the signaling pathways activated following CXCL12 stimulation and finally the physiological and pathological roles of CXCR4-CXCR7/CXCL12 axis.

1.4 Using a physiological gradient: the chemokine CXCL12

1.4.1 CXCL12 and its membrane receptors CXCR4 and CXCR7

The chemokine CXCL12 plays key roles in various processes such as metastatic spread, hematopoiesis, development and angiogenesis[131]. CXCL12 binds two membrane receptors CXCR4 and CXCR7. They belong to the seven-transmembrane G-protein coupled receptors family (GPCR). CXCR4 was initially discovered as the co-receptor of CD4 for HIV virus entry into CD4+ T cells[132]. CXCR7 was recently discovered and first identified as a decoy receptor which does not activate signaling pathway associated to the G-protein. CXCL12 binds CXCR4 with a lower affinity (Kd=3.6nM) than CXCR7 (Kd=0.4nM) and these receptors can form homo- or heterodimers[133]. In physiological cases, CXCR4 is highly expressed by immune cells (monocytes, B cells and naïve T cells) in peripheral blood but as well by hematopoietic progenitor cell in bone marrow. CXCR7 regulates B cell development and differentiation[134]. Overall, both receptors are overexpressed in cancer cells such as colorectal cancer or breast cancer (Figure 1.32)[13,14].

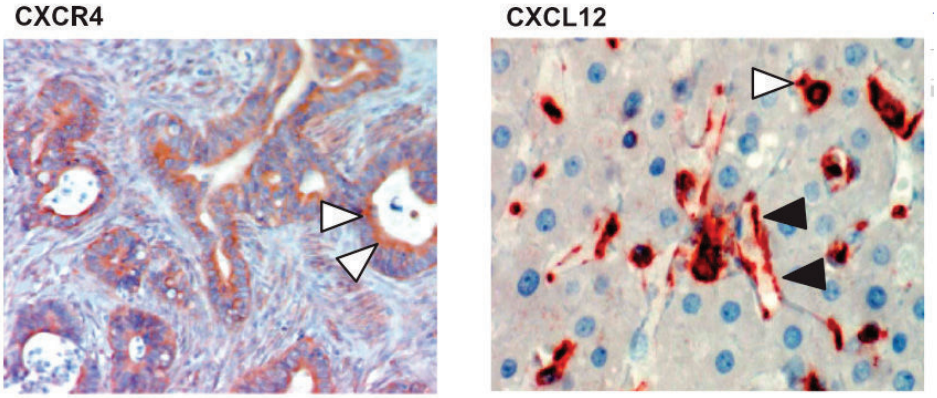

Figure 1.32: CXCR4 is overexpressed in human primary colon cancer and CXCL12 is produced by the liver. Left. Immunohistochemical staining of CXCR4 expression in a representative human primary colon tumor. White arrowheads: strong expression of CXCR4 by colon cancer cells. Right. Immunohistochemical staining of CXCL12 expression in normal human liver. Black arrowheads: CXCL12 expression located at the interface between the sinusoidal vessel and liver parenchyma. White arrowhead: isolated cell strongly expressing CXCL12. Likely this cell is a Kupffer cell, speciliazed macrophage located in the liver[135].

Lymph nodes, lungs, liver and bone marrow are main organs producer of CXCL12 (Figure 1.32)[14]. Six isoforms of CXCL12 exist and three isoforms are known to bind to the ECM with different affinities: CXCL12γ has the highest affinity for the ECM followed by CXCL12β and CXCL12α. In parallel, CXCL12α is the isoform produced in highest quantity by stromal and endothelial cells[134]. *In vitro,* NIH3T3 fibroblasts and cancer-associated fibroblasts are known to secrete CXCL12[22,136].

It is interesting to note that CXCL12 level can be detected into blood sample. In human patients, CXCL12 level in the serum of healthy donors (from 2 to 6.5ng/ml of serum) and pathological patients has been measured in different clinical studies. An increased in CXCL12 into serum patients is associated with recurrence ischemic stroke[137,138], severe sepsis or septic shock[139] and esophageal cancer[140]. In addition, CXCL12α level in the serum of human patients follows a circadian clock. The lowest CXCL12 level is measured at 1pm[141]. It is interesting to note that the concentration of CXCL12 within the serum of healthy patient is higher than the Kd of CXCR7 (CXCL12 from 2 to 6.5ng/ml versus Kd: 0,4nM corresponding to approx. 3ng/ml), thereby suggesting that CXCL12 presents in the serum would activate signaling pathways of circulating cancer cell through CXCR7. It raises some questions: Is it possible to form of CXCL12 gradient at the organs producer proximity? How long is this gradient? By taking into account the circadian clock, is the gradient sufficiently stable to direct cell migration? What would be the slope of this gradient? Are the cancer cells able to detect this gradient? Are the signaling pathways activated able to trigger a cell response?

In the next section, I will present the signaling pathways activated after CXCR4 and CXCR7 activation by CXCL12.

1.4.2 Signaling pathways

Once CXCL12 binds to CXCR4 or CXCR7, the membrane receptors activate intracellular signaling cascades leading to cell proliferation, survival or chemotaxis[142].
CXCR4 and CXCR7 are receptors coupled to the heterotridimeric G-protein composed of α, β and γ subunits. Four different Gα subunits exist: Gα_i, Gα_s, Gα_q or Gα_{12} and activate different signaling pathways. Once CXCL12 bound to CXCR4, Gα dissociates from G$\beta\gamma$. Gα_i inhibits Adenylate cyclase and the production of the second messenger cyclic-AMP, whereas Gα_s stimulates it. Gα_q subunit activates phospholipases (PLC) leading to the production of the second messengers diacylglycerol (DAG) and inositol triphosphate (IP3) (Figure 1.33). Gα_q activates the transcription factor NFκB. G$\beta\gamma$ subunits activate PI3K and lead to PIP3 production, whose role in cell migration has previously been described (Molecular actors involved in cell migration page 47). AKT activation through PI3K activation leads to cell survival and ERK activation favors cell proliferation. First, it was thought that CXCR4 was associated only to Gα_i[143]. However, data suggest that other Gα proteins could be linked to CXCR4, making the activation of signaling pathways even more complex. In addition, CXCR7 activation does not activate G-protein but rather stabilizes its association to β-arrestins. It was first through that its association only leads to receptor desensibilization. Now, it is accepted that CXCR7 is internalized after CXCL12 binding and acts as scavenger receptor of CXCL12 before being recycled back to the membrane and activates additional pathways[133].

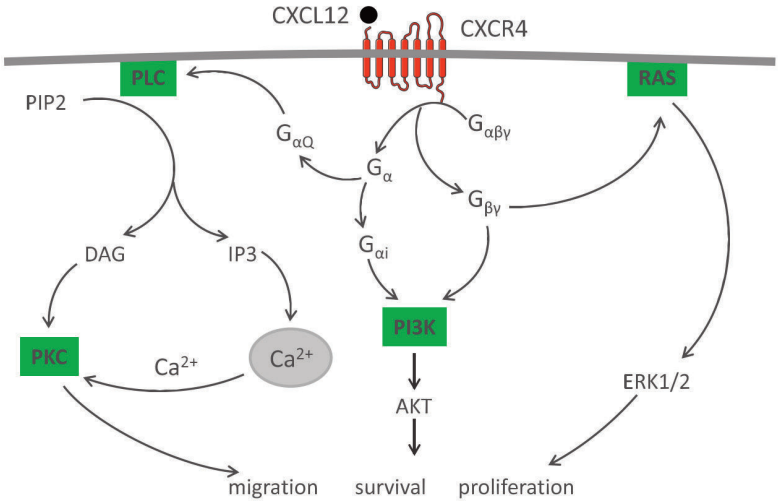

Figure 1.33: Schematics of the CXCL12/CXCR4 signaling pathways activated[29].

In this project, we are interested in the role of these membrane receptors in cell migration and their potential link with the cell cytoskeleton. I will present in the next section few examples which connect the activation of the membrane receptors to actin or microtubules within single cells.

After a short stimulation of breast cancer cells in suspension with CXCL12, an increase in F-actin polymerization is measured associated with cell polarization and redistribution of F-actin towards the cell leading edge[14]. In fact, in T cells, CXCL12 activates LIMK and cofilin leading to actin reorganization[144]. In human prostate cancer, drebrin is overexpressed[145]. Drebrin is known to bind actin filament and microtubules tips end and regulate axon branching[146]. For prostate cancer cell placed in a gradient of CXCL12, drebrin co-localized at the tip of filopodia, together with actin and microtubules. Its inhibition prevents cell migration and invasion[145]. In migrating interneurons, CXCL12 reduces actin and microtubules branching and consolidates actin and microtubules[147]. In neural progenitor cells, CXCR7 interacts with Rac1 in the presence of CXCL12 and leads to cell migration towards lines of CXCL12 in a mechanism independent of CXCR4[148]. In hepathocyte carcinoma cells, CXCL12 stimulation causes Rac1 activation associated with transient lamellipodia elongation[135]. In breast cancer cells, 5 min stimulation with CXCL12 leads to co-localization of CXCR4 and the formin mDia at the cell periphery. It generates blebs formation and cell morphology shift to amoeboid morphology in a mechanism RhoA-dependent[149]. β-arrestin was shown to play a role in CXCL12-induced migration of HeLa cells by interacting with and activating the Focal Adhesion Kinase that regulates cell migration through integrin signaling[150,151].

These studies reveals that CXCL12 can modify both actin and microtubules networks. The differential localization of the membrane receptors could be responsible for cell symmetry breaking and leads to directional cell migration.

As mentioned previously, CXCL12/CXCR4-CXCR7 axis play a key role during organs development, stem cell trafficking, immune response and angiogenesis[134,151]. In the following section, I will briefly present their role in physiological and pathological conditions.

1.4.3 Physiological and pathological roles

In Zebrafish, as previously mentioned, a gradient of CXCL12 forms around the primordium and directs the migration of this group of cells. Inhibition of either CXCR4, CXCR7 or CXCL12 impaired primordium migration[24,111]. In developing embryo, high level of CXCR4 is detected in the endothelial of developing blood vessels. CXCR4 or CXCL12 knock-out mice lack proper vascularization of the gastrointestinal tract[152]. CXCL12 is responsible for B-cell lymphopoiesis in bone marrow[153].

CXCR4-CXCR7/CXCL12 axis is as well evolved in the development of cancer. In the case of gastric cancer, high expression of CXCL12 within primary tumor is associated with poor prognosis[136]. Moreover, inhibition of CXCR4 or CXCL12 has been shown in numerous studies to reduce tumor size[154–156] as well as invasiveness of cancer cells[13,14,136,157,158]: it highlights the roles of CXCR4 and CXCR7 in the development of metastatic spread.
Typically, the colon and breast cancer cells overexpress the membrane receptors and metastasize in organs producer of CXCL12 (lungs, liver). It is accepted that cancer cells migrate towards the lungs or liver due to a chemical gradient of CXCL12. In fact, it has been modeled that a CXCL12 gradient of 0.002nM/µm should be large enough to direct cancer cell migration[142]. However, a gradient of CXCL12 has never been observed *in vivo* and the hypothesis of CXCL12 gradient was assumed. Some studies showed *in vitro,* through the controversial Boyden chamber experiments, the migration of cancer cells towards a gradient of CXCL12 in a dose-dependent manner[14,135]. But studies suggested as well that CXCL12 could promote cancer spreading by other ways: CXCL12 increases cell adhesion in an integrin-dependent mechanism[48,136,159] and/or promotes extravasation process *in vivo*[135,159]. CAF co-injected into mouse with breast cancer cells enhanced tumor growth by favoring angiogenesis. CAF produce higher CXCL12 proteins compared to counterpart fibroblasts leading to the recruitment of circulating endothelial progenitor cell and promoting angiogenesis[156]. Moreover, interestingly, *in vivo* study reveals that the number of arrested cancer cells along the liver sinusoid wall is the same in the absence of CXCR4 or in the presence of CXCL12[135]. It suggests that CXCR4-CXCL12 axis does not attract cancer cells to the liver but supports the statement that cells are arrested within capillary by size restriction and CXCR4/CXCL12 axis favors either extravasation process, adhesion or angiogenesis.

In conclusion, single cell migration has been widely studied *in vitro* in a simplified environment, on flat surfaces. Along this Introduction, we first saw that *in vivo*, cells are mainly migrating under confinement, between fibers or within capillaries. Mimicking this confinement *in vitro* triggers interesting features such as changing migration mode or preventing cell migration. In this project, we want to study single cell migration in a simplified and controlled environment under confinement. To do so, we built microchannels whose dimensions mimic capillaries. Second, we reported that *in vivo*, cells in complex environment are stimulated by different cues but are still able to migrate directionally. *In vitro*, we saw it was possible to direct cell migration with different cues. Here, we focusesd on ratchetaxis and chemotaxis whose efficiency to direct and rectify cell migration has been proven. Moreover, we formed physiological gradients of the

chemokine CXCL12 to direct cell migration and studied localization of the membranes receptors CXCR4 and CXCR7.

Altogether, this study aims at investigating cell migration under confinement and to compare two types of directed cell migration. We studied ratchetaxis in two degrees of confinement which constitute the novelty of this work. We studied chemotaxis in different configurations, from flat coverslip to confined microchannels with serum or CXCL12 gradients. Cooperation and competition between both cues revealed interesting features, showing the influence of the environment on cell migration in a chemically changing environment.

A precise question arises: ratchetaxis and chemotaxis, how to direct cell migration? To answer this question, we used an integrated approach with cell culture, microfabrication, microfluidics and microscope images and analysis. The Material & Methods used will be developed in the next section.

2 Material & Methods

I will introduce in this part all the experiments performed to study cell migration. First, I will describe the procedures for the cell culture and related experiments. Then, I will present the microfabrication process and techniques established to prepare closed, open microchannels configurations and to form chemical gradients inside microchannels. Finally, I will describe the experimental procedures to study cell migration in the different set-ups. Tables of products used and references are indicated in the Appendix.

2.1 Mammalian cells: experimental procedures

2.1.1 Cell culture maintenance

Mammalian cells are maintained at 37°C and in a 5% CO_2 humid incubator in appropriate medium and culture plates (Table 2.1). When reaching 70-90% confluency, adherent cells are replated using trypsin and 0.25% EDTA every 2-3 days. HL60 cells are in suspension. Their density should not exceed $1x10^6$cells/ml. In order to study cell migration, HL60 cells are differentiated in complete media supplemented with 1.3% DMSO (final concentration). They become neutrophil-like cells. Differentiated cells (dHL60 cells) for 5-6 days are used for cell migration experiments.

Table 2.1: Cell lines, origin, medium and growing plates

Cell lines	Cell type/source/ culture properties	Complete medium	Growing plate type
NIH3T3	mouse fibroblast ATCC n°: CRL-1658 adherent	DMEM 4,5g/l glucose + antibiotics[1] + 10% Bovine Calf Serum (BCS)	Petri dish
SW480	human primary colorectal adenocarcinoma ATCC n°: CCL-228 adherent	DMEM 4,5g/l glucose + antibiotics[1] + 10% inactivated Fetal Bovine Serum (FBS)	Cell culture flask
SW620	human lumph node metastasis of colorectal adenocarcinoma ATCC n°: CCL-227 adherent	DMEM 1g/L glucose + antibiotics[1] + 10% inactivated FBS	Cell culture flask
HL60	human promyeloblast ATCC n°: CCL-240 suspension	RPMI 1640 w/o HEPES + 40µg/ml Gentamycin +10% FBS	Suspension culture growing flask
MDA-MB-231	human breast cancer cells ATCC n°: HTB-26 adherent	RPMI 1640 w/o HEPES + 40µg/ml Gentamycin +10% FBS	Petri dish

[1] 100U/ml penicillin and 100µg/ml streptomycin

Nucleus of living dHL60 and NIH3T3 cells are stained by using DAPI at 4µg/ml for 4-6h or Hoescht at 0,4µg/ml for 2h.

2.1.2 Measure of cell dimensions

In this thesis, we want to study cell migration in confined ratchet microchannels. To do so, we have to design a ratchet unit which has the volume of a NIH3T3 cell. In addition, we need to know the nucleus dimensions of NIH3T3 cells in order to design the ratchet. I will present in the next section how to measure these different parameters.

2.1.2.1 Cell volume

Adherent cells at 90% confluent (NIH3T3, MDA-MB-231 and SW480 cells) were trypsinized to obtain round cells. Non differentiated HL60 cells are round in suspension. Phase contrast images are taken with x20 objective (0.40 Numerical Aperture N.A.). By using Fiji software, cells diameter (D_{cell}) is measured and the mean volume of the cells (V_{cell}) is deduced from the mean diameter of the cells using the formula $V_{cell} = \frac{4}{3}\pi \times (\frac{diameter_{cell}}{2})^3$.

2.1.2.2 Nucleus volume and dimensions

In order to measure nucleus dimension, nucleus of NIH3T3 cells are stained with Hoescht (0.4µg/ml) for 2h. Fluorescent images of nucleus in the middle plane are taken with x20 objective (0.40 N.A.). Fiji software is used to process images. After images thresholding, “Analyze particles” plugin of Fiji is used and “Ellipse fitting” option is selected to measure the major and minor axis of the nucleus. To measure its height and volume, stained nucleus is observed using x100 (1.4 N.A.) oil immersion objective on a spinning disk microscope (Nikon). Z-stacks of each nucleus are taken with a 0.5µm step by using the motor of the stage. “Orthogonal view” plugin of Fiji is used to determine the top and bottom limits of the nucleus, allowing the measure of the nucleus height. After image thresholding, analyze particle plugin of Fiji is used to measure the area of each nucleus cross section. Volumes of each cross section are obtained by multiplying the area of each cross section by the height of the z-step (0.5µm). Volumes of each cross section are then sum up to obtain the total nucleus volume.

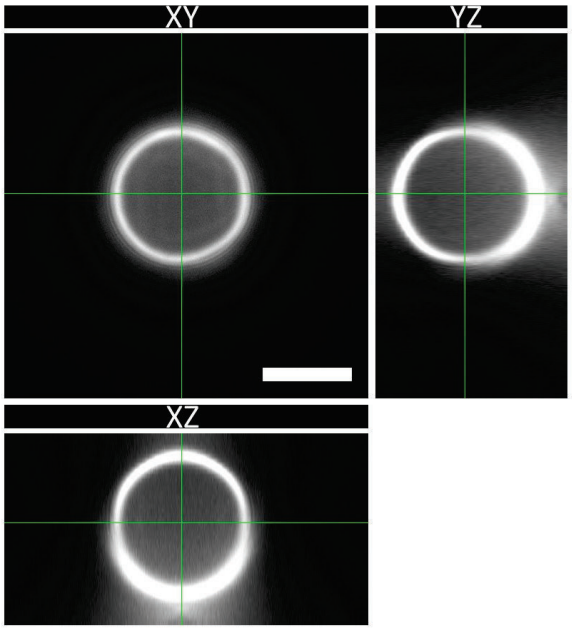

Figure 2.1: XYZ calibration of spinning disk microscope (Nikon). Scale bar 10µm.

To test the accuracy of the z-motor, we check the height and diameter of 15µm spherical fluorescent beads in the same spinning disk microscope (Figure 2.1). The 3D reconstruction indicates that in XZ and YZ axis, the bead diameter is equal to 15µm. It indicates that images taken with this microscope allow the proper measurement of nucleus dimensions in the XY, YZ and XZ axis.

2.1.3 DNA transfection and cell sorting

DNA transfection is a technique allowing insertion and expression of exogen DNA into cells. In this project, we transfected CXCR4, CXCR7, Life-Act, tubulin and centrine and information are listed in Appendix A.3. Transfection is performed with liposome complex using Lipofectamine™ 2000 Transfection Reagent. Manufacturer recommendations are followed, volumes below are indicated for one well of a 6 wells-plate.

- Replate NIH3T3, SW480 and MDA-MB-231 cells up to 4h before transfection at 50% confluency in one well of a 6 wells-plate.
- Dilute 2.5µg of DNA into 150µl Opti-MEM medium in a tube. If double transfection is required, the quantity of DNA for each plasmid is divided by two in order to have a total DNA quantity equal to 2.5µg.
- Dilute in a second tube, 10µl of Lipofectamine in 140µl Opti-MEM medium.
- Mix carefully both solutions and incubate at room temperature for 10min.
- Add the DNA-lipofectamine mix to the adherent cells in 2ml of complete medium.
- After 4-6h of incubation, medium is removed and 2ml of fresh complete medium is added.

18h after transfection, cells can be sorted based on Fluorescence-activated cell sorting (FACS) technology to obtain only fluorescent transfected cells.

Cells are trypsinized and resuspended at a density of $3x10^6$cells/ml into Leibovitz's medium (L-15) without phenol red to prevent autofluorescence from medium.
Cell sorter FACS ARIA is used to sort and collect fluorescent transfected cells based on the fluorophore used (mCherry or GFP).

These cells are then used for migration experiment.

2.1.4 CXCL12 down-regulation

In order to reduce CXCL12 expression into NIH3T3 cells, we used small interfering RNA (siRNA). They are small double stranded RNA (20-25bp) able to target a specific mRNA sequence and degrade it. As a result, the related protein is not translated. We tested two couples of siRNA to probe the efficiency of CXCL12 down-regulation and potential toxicity of the siRNA. The first siRNA couple used is a validated one (siCXCL12 n°10 and n°11). The second couple is a non-validated couple (siCXCL12 n°7 and n°16). A control scramble-siRNA (sc-siRNA) is also used. siRNA are co-transfected using Lipofectamine™ RNAiMAX Transfection Reagent. Manufacturer recommendations are followed. The siRNA preparation for 1 well of 24 wells-plate is found below:

- Mix in a tube 3µl of Lipofectamine RNAiMAX and 21µl of DMEM 4,5g/l glucose supplemented with antibiotics but without serum.
- Dilute in a second tube, 5pmol of each siRNA or 10pmol of sc-siRNA into 24µl of DMEM 4,5g/l glucose supplemented with antibiotics but without serum.
- Mix both preparations and incubate 20min at room temperature.
- Place 1ml of 30 000cells/ml in complete medium in 1 well and add siRNA mix on cells in suspension.
- After gently mixing, incubate at 37°C 5% CO_2 for 24h, 48h or 72h before mRNA extraction.
- Remove medium, add 200µl of Trizol to lyse the cells and place at -20°C until RNA extraction.

RNA extraction, Reverse transcription and quantitative PCR have been performed by Erwan Pencreach (Tumor Growth and micro-environment, Faculty of Medicine, Strasbourg) and protocols are indicated in Appendix A.3.1.

2.1.5 Immunostaining

Immunostaining is an antibody-based technique used to localize proteins in a sample. In this project, we used immunostaining to detect the endogenous expression of the membrane receptors CXCR4 and CXCR7, CXCL12 localization and f-actin distribution. Antibodies used in this work are listed in Appendix A.2. Following is the standard immunostaining protocol of cells in coverslips and within microchannels.

2.1.5.1 Immunostaining protocol for cells plated on glass coverslip

- Trypsinize a 90% confluent cells plate and seed the cells on a glass coverslip (#1) in order to have isolated cells and incubate the cells at least 2h at 37°C to allow the cells to adhere and spread.
- Remove the cell culture medium and add by 1ml of 3% Paraformaldehyde (PFA) solution. This allows the fixation of the cells.
- Rinse the coverslip 3x 5min with PBS1X
- Add 1ml of 0.5X Triton for 3min. This allows the cell membrane permeabilisation.
- Rinse the coverslip 3x 5min with PBS1X
- Add 1mL of PBS1X 5% Bovin Serum Albumin (BSA) for 1h at room temperature. It allows the saturation of non-specific sites.
- Rinse the coverslip 3x 5min with PBS1X.
- Incubate the cells with primary antibodies diluted in PBS1X 5%BSA for 1h at room temperature.
- Rinse the coverslip 3x 5min with PBS1X.
- Incubate the cells with secondary antibodies conjugated to a fluorophore (AlexaFluor-546 or Alexa-Fluor-488) diluted in PBS1X 5%BSA for 1h at room temperature. *The secondary antibody should be used carefully: it should recognize the host species used to produce the primary antibody.* During this step, it is possible to add to secondary antibody mix, phalloidin which binds filamentous actin and DAPI which stain for DNA.
- Rinse the coverslip 3x 5min with PBS1X.
- Mount the coverslip on a glass slide. Mounting medium is prepared by mixing glycerol: PBS1X (75:25 v:v). 16µl of mounting medium is deposited on glass slide. Cells on coverslip are then placed in contact with mounting medium.
- Seal the coverslip to the glass slide with nail polish.

2.1.5.2 Immunostaining protocol for cells plated inside microchannels

Standard immunostaining protocol is not appropriate to stain cells inside channels: medium in channels cannot be easily changed. It would be ideal to allow the cells to migrate inside the microchannels, fix them and then remove the biopolymer polydimethylsiloxane (PDMS) channels and perform standard immunostaining protocol. But plasma activation parameters used induces irreversible bonding of the PDMS channels to the coverslip (see page 83). Thiam et al. (2016) adapted immunostaining protocol to allow non-permanent bonding of the PDMS to the coverslip and immunostaining of cells which were inside channels.

- Activate with oxygen plasma only the glass coverslip. Place the PDMS on the coverslip. It is reversibly bond. Incubate the chip 3h at 65°C.
- Seed the cells at $30x10^6$ cellules/ml into the chip and incubate at 37°C for at least 12h to allow the cells to enter and migrate inside microchannels.
- Rinse PDMS chamber with PBS1x and immerse it into 3%PFA for 1h at room temperature.

- Remove carefully the PDMS chamber by inserting scalpel between the coverslip and the PDMS.

The shape of cells on coverslip is identical to the one they had before microchannels removal. Standard immunostaining protocol is then performed as explained in the previous section.

2.2 Microfabrication

2.2.1 Pattern design

Clewin® software is used to design motifs for the photolithography mask with proper dimensions.

2.2.2 Photolithography

Photolithography is the process which allows the fabrication of micrometer size motifs. To obtain the final template/mold, a resist sensitive to UV light and a mask containing desired motifs are used to transfer the motifs on a substrate called wafer. First, the photoresist is poured on the substrate. A mask containing the motifs protects or exposes the photoresist to UV light. The exposed motifs are then irreversibly bound to the substrate. Two photoresists are used according to the height of the motifs: for 5µm height, SU8-2005 is used, and for 25µm and 50µm height, SU8-2025 photoresist is used (MicroChem). The protocol is detailed in the following section and in Figure 2.2:

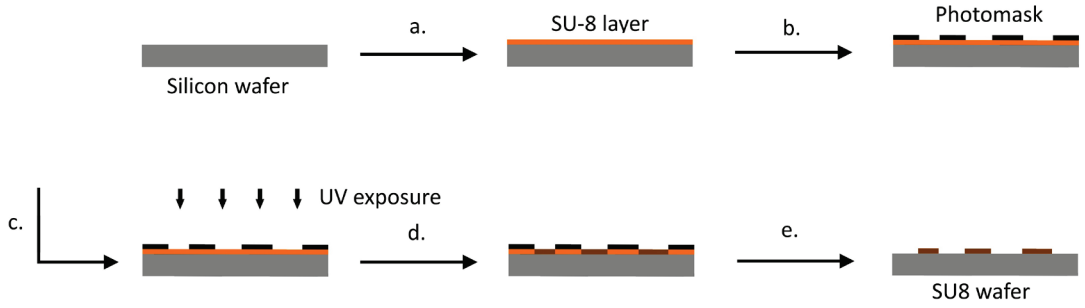

Figure 2.2: Photolithography process (a.) a SU8 photoresist layer is spin-coated on a Silicon wafer. (b.) wafer and SU-8 are pre-exposed baked at 65°C and 95°C and photolithography mask is placed in closed contact with SU-8 photoresist. (c.) mask and photoresist are exposed to UV during appropriate time to cross-link SU-8 exposed to UV. (d.) post exposure baked at 65°C and 95°C consolidate the cross linking. (e.) Uncrosslinked photoresist is removed by using SU-8 developer. If a second layer is needed, process starts again at step (a.).

- The silicon wafer is heated at 200°C to remove humidity traces which can prevent SU8 photoresist's fixation to the silicon wafer.
- Once the wafer cool down, SU8 photoresist is poured on the wafer and spin-coated at a certain speed to obtain SU8 layer thickness wanted. Here, 5µm, 25µm and 50µm thicknesses are required, corresponding respectively to a rotating speed of 3000 rpm with SU8-2005, 3000 rpm with SU8-2025 and 1700 rpm with SU8-2025.
- Wafer and photoresist are then pre-baked at 65°C and 95°C during the proper time according to the thickness wanted and following the manufacturer's instructions. This step allows the evaporation of solvents from the photoresist.

- The photolithography mask is pressed on the photoresist layer and both are exposed to UV light inside the mask aligner. Mask contains structures which protect the photolithography layer from UV light. SU8 is a negative photoresist, the photoresist exposed to UV light is cross-linked.
- The post exposure bakes of the photoresist at 65°C and 95°C allow the SU8 to fully polymerize. The photoresist unexposed to UV light is removed during the development step using SU8 developer.
- Wafer is then rinse with isopropanol and dry using nitrogen pistol. If white streaks appear, it means all SU8 photoresist has not been removed and developing step has to be repeated.

When a second layer is necessary, the process is repeated after the development of the 1st layer. A second layer of SU8 is spin-coated and prebaked. Before UV exposure, make sure the motifs of the first SU8 layer are aligned with the second motifs. After UV exposure, wafer is post-baked and developed using SU-8 developer.

Once the wafer obtained, the PDMS is used to get the replica molding. PDMS and curing agent are mixed in a 10:1 mass ratio. The PDMS mold bound to coverslip is then used to study the cell migration inside microchannels. In this work, two configurations exist: 1) open microchannels. One photoresist layer of 25µm thickness is needed. 2) closed microchannels. Two photoresists layers are needed. The first one, the microchannels, are 5µm height. The second one, main chambers and reservoirs, are 50µm height.
In the following section, I will explain how to obtain both configurations.

2.2.3 The open and closed microchannels configurations

In this PhD thesis, the cell migration in two levels of confinement is studied. In the closed configuration, the confinement is high, *i.e.* from the top and sides of the cell. In the open configuration, the confinement is low, *i.e.* from the sides of the cell. PDMS is poured onto the wafers. In order to remove air bubbles trapped in between SU8 microstructures, wafers are placed into desiccator for 1h. Then PDMS is cured at 65°C at least for 4h.

2.2.3.1 The closed microchannels configuration

The preparation of closed microchannels is presented in Figure 2.3Top.

- SU8 wafer contains 5µm height microchannels structures and 50µm height main chambers or reservoirs. PDMS is poured on the wafer.
- After curing, PDMS is removed from the wafer. Holes of 0.75mm are punched in the reservoirs or main chambers area.
- Tape is used to remove PDMS residues and dusts from the microstructures. Glass coverslip and PDMS are then activated with oxygen plasma and bond to each other's.
- The closed chip is then incubated at 65°C to consolidate the bonding. It is irreversibly bond.

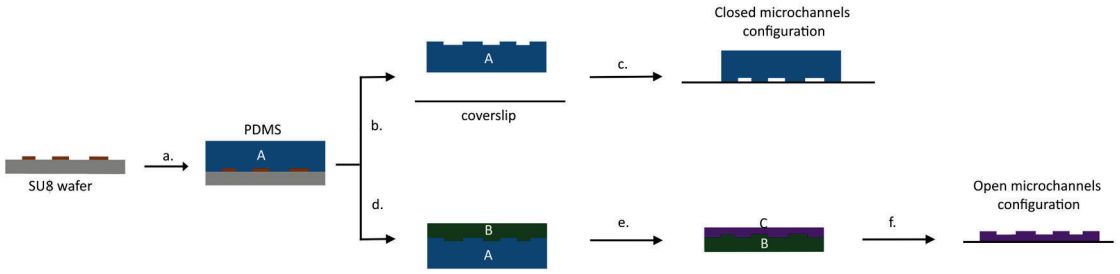

Figure 2.3: Fabrication process of PDMS molding, closed and open microchannels configuration. (a.) PDMS is poured on the SU-8 wafer and cured at 65°C for at least 4h. Closed microchannels configuration. (b.) PDMS (A) is removed from the Silicon wafer and bond to a coverslip after activation with oxygen plasma (c.). Open microchannels configuration (d.) PDMS (A) is used as a mold for the 1st replica molding step. It is silanised and PDMS is poured and cured (e.) PDMS (B) is used as a mold for the 2nd replica molding step. PDMS (B) is silanised and PDMS is spin-coated on top of PDMS (B) at 2000rpm to obtain 40µm PDMS layer. (f.) After curing at 65°C, PDMS (C) is bond to a coverslip after activation with oxygen plasma and PDMS (B) is peeled off.

I presented the way to obtain the closed microchannels configuration. In the following section, I will detail how to obtain the open microchannels configuration.

2.2.3.2 The open microchannels configuration

The preparation of open microchannels is presented in Figure 2.3Bottom.

- SU8 wafer contains 25µm height microchannels structures. They should be height enough to trap the cells inside the microchannels. PDMS is poured on the wafer.
- PDMS (A) is removed from the wafer. It is used as a mold: it is activated with oxygen plasma and silanized for 1h with chlorotrimethylsilane. PDMS is then poured and cured 4h at 65°C.
- The replicat (B) is removed from the PDMS (A). It is then used as a mold: it is activated with oxygen plasma and silanized for 1h with chlorotrimethylsilane. Liquid PDMS is then spin-coated at 2000rpm to obtain a PDMS layer of 40µm (Appendix A.3.2). It is cured at 65°C for 4h.
- Glass coverslip and PDMS (C) are activated with oxygen plasma. Surface of PDMS (C) is bond to the coverslip. It is incubated at 65°C to consolidate the binding.
- PDMS (B) is carefully removed by holding it with a tweezer.

The open microchannels configuration is obtained.

2.3 Cell migration study

In this PhD thesis, we used different techniques to induce directed cell migration. We studied chemotaxis by forming soluble chemical gradients with the pipette experiment, transwell experiment and microfluidic, or adherent gradients by microcontact-printing proteins. Ratchetaxis was studied using the open and closed microchannels configurations described in the previous section.
In this section, I will present protocols to prepare these different experiments, how to prepare the cells and how to analyze the data.

2.3.1 Cell migration on 2D flat surfaces

Before studying cell migration in complex environments, we studied their motion on 2D flat surfaces. It is important to determine how cells migrate without any external cues and to measure parameters which characterize their migration as persistent length, time and speed. We can then relate these values to the one obtained in the directed cell migration experiments. Confluent plate of adherent NIH3T3, SW480 and MDA-MB-231 cells are detached by using trypsin. Cells in suspension and trypsinized are seeded at low confluency on glass coverslip coated with fibronectin (50µg/ml) or non-coated coverslip respectively.
Start the acquisition on a CKX41 inverted phase-contrast microscope (Olympus). A cooled camera (Hamamatsu), ImageJ plugin Micromanager and 10x or 20x objectives (PhL, air, 0. NA, phase contrast, Olympus) were used to acquire images.

2.3.2 Cell migration on closed microchannels configuration

As explained previously, two microchannels configurations exist, open and closed configurations. In addition, in the closed microchannels configuration, a chemical gradient can be formed (Figure 2.4). The procedures to seed the cells and form chemical gradient is explained in the following section.

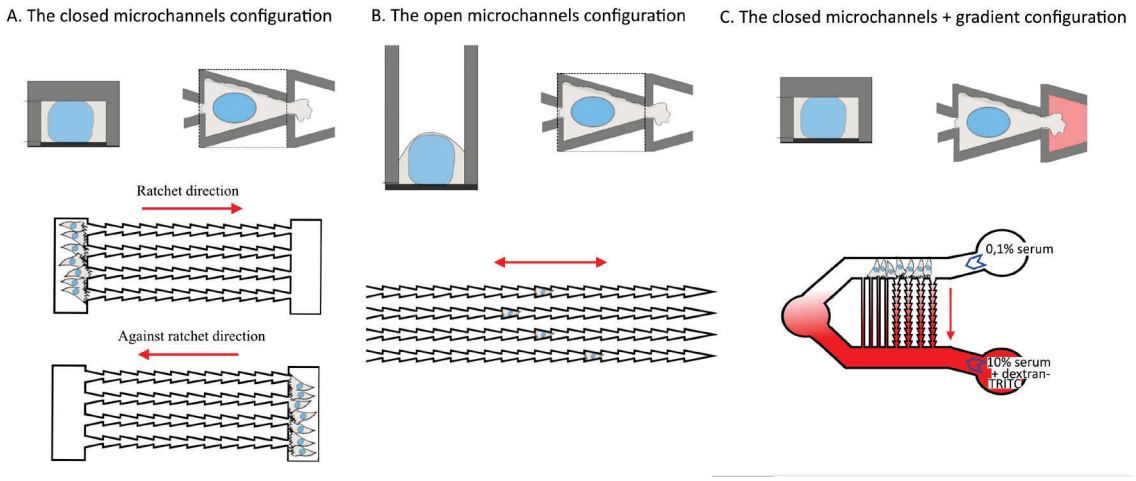

Figure 2.4: Schematics of the open microchannel configuration (A.), closed without (B.) and with chemical gradient microchannels configurations (C). Top, top and side view of the microchannels. Bottom cells seeding and gradient formation.

2.3.2.1 Cell migration on closed microchannels configuration

2.3.2.1.1 Without chemical gradients

This experiment has been performed with NIH3T3, SW480, SW620, MDA-MB-231, HEK-231-T and dHL60 cells (Figure 2.4B) and the protocol is described in the following section:

- Activate with oxygen plasma the chip to make it hydrophilic and ease the filling of the device with L15 10% serum (adherent cells) or 50µg/ml of human fibronectin in L15 (dHL60 cells). No bubbles should be present. Incubate 30min at room temperature.

- Trypsinize a 90% confluent adherent cells plate. 10µl of $30x10^6$ adherent cells/ml in L15 10% serum solution or 10µl of $10x10^6$ dHL60 cells/ml in L15 15% FBS are loaded into one of the inlet with an elongated tip. Aspirate medium from the other inlet to accumulate the cells at the microchannels entry. Make sure there are no bubbles inside inlets. Immerge chip into L15 10% serum.
- Incubate 2h at 37°C without oxygen to allow the cells to adhere and spread on the coverslip.
- Start the acquisition on a CKX41 inverted phase-contrast microscope (Olympus). A cooled camera (Hamamatsu), ImageJ plugin Micromanager and 10x or 20x objectives (PhL, air, 0. NA, phase contrast, Olympus) were used to acquire imagesImages are taken every 10min (adherent cells) or every 30s (dHL60 cells) in bright field. Keep acquiring for 24h for adherent cells and 4h for dHL60 cells.

2.3.2.1.2 With chemical gradients

This experiment has been performed with NIH3T3, MDA-MB-231 and dHL60 cells (Figure 2.4C) and the protocol is described in the following section:

- Activate with oxygen plasma the chip to make it hydrophilic and ease the filling of the device with L15 0%serum. No bubbles should be present.
- Trypsinize a 90% confluent cells plate. 10µl of $30x10^6$cells/ml L15 0% serum solution or 10µl of $10x10^6$ dHL60 cells/ml in L15 0% FBS are loaded into the outlet with an elongated tip. Aspirate medium from the two inlets to disperse and accumulate the cells at the microchannels entry. Make sure there are no bubbles inside inlets. Immerge chip into L15 0% serum.
- Incubate 2h at 37°C without oxygen to allow cells to adhere and spread.
- Prepare two 1ml syringes. The first one contains L15 0.1% serum and the second one L15 10% serum and Tetramethylrhodamine isothiocyanate Dextran (TRITC-Dextran) at 0.32mg/ml enabling the visualization of the chemical gradient. Connect the syringes to 23Gx1" syringe needles and Tygon tubing which have been rinsed with L15 0% serum. Make sure there are no bubbles into the tubing. During experiment, it can prevent a good flow and detach cells if bubbles enter the microfluidic device. Cut 20Gx1" syringe needles are used to connect tubing to microfluidic device. The outer diameter of the cut needles (0.9 mm) is slightly larger than the diameter of the hole punched, so when the cut needle is inserted into the hole, a seal is created.
- Use a syringe pump to flow medium inside microfluidic device at a rate of 10µl/h. The chemical gradient is formed into microchannels after few minutes and can be visualized with TRITC-dextran.
- Start the acquisition on a CKX41 inverted phase-contrast microscope (Olympus). A cooled camera (Hamamatsu), ImageJ plugin Micromanager and 10x or 20x objectives (PhL, air, 0. NA, phase contrast, Olympus) were used to acquire images. Images are taken every 10min (adherent cells) or every 30s (dHL60) in bright field and red fluorescent filter.
- Keep acquiring for up to 20h for stable gradient experiments.

In one variant of chemical gradients experiments, we removed the chemical gradient once the cells are inside microchannels. The process is explained as follow:

- For gradient removal experiment, acquire for up to 10h, to allow the cells entry inside the microchannels. To remove the serum gradient, take away the syringe containing L15 10% serum from the syringe pump and keep acquiring.

Several rules are followed to study migration of the cells in the closed configuration:

- No divided cells are tracked.
- Cell tracking starts once cell moves from the first ratchet or equivalent distance in straight microchannels: it is the first persistent motion.
- A cell pauses when it is not moving for more than 30min.
- A cell is tracked only when it is alone in the microchannels.

2.3.2.2 The open microchannels configuration

This migration experiment has been performed with NIH3T3 cells (Figure 2.4A) and the protocol is described in the following section:

- Activate with oxygen plasma activate the chip to make it hydrophilic.
- Place the microchannels under UV light for 10min to sterilize it.
- Trypsinize a 70-90% confluent cells plate.
- Resuspend the cells at a cell density of $0.1x10^6$cells/ml in DMEM 10%BCS. Place 100µl on the open microchannels. After 30min incubation at 37°C, cells enter spontaneously into the microchannels.
- Remove non adherent cells by washing the coverslip. Replace DMEM 10%BCS by L15 1%BCS.
- Start the acquisition on a CKX41 inverted phase-contrast microscope (Olympus). A cooled camera (Hamamatsu), ImageJ plugin Micromanager and 10x or 20x objectives (PhL, air, 0. NA, phase contrast, Olympus) were used to acquire images. Images are taken every 10min.

Several rules are followed to study migration of the cells in the open configuration:

- No divided cells are tracked.
- Cell tracking starts once cells move from the first ratchet or equivalent distance in straight channel. Do not consider the cells which start migrating outside the microchannels.
- A cell pauses when it is not moving for more than 30min.
- Track a cell only when it is alone in the channel.
- It is an open configuration. Cells can get out of the channels. Do not consider these cells.

2.3.3 Micropipette experiment

Micropipette experiment allows the delivery of chemical solution close to the cell. To allow quick cell migration, glass coverslip is treated to reduce cell adherence to the surface and pipette is carefully prepared to form a chemical gradient stable for few hours.
The first step consists on the preparation of the glass coverslip: it is first cleaned with "piranha" solution and then incubated with Poly-l-lysine-g-PolyEthylene Glycol (PLL-g-PEG):

Coverslip preparation:

- Under the hood, prepare the "piranha" solution by mixing carefully 7 parts of sulfuric acid with 3 parts of Hydrogen peroxide (v/v) in a glass Petri dish. Vapors will form, close the lead.
- Immerse the coverslips for 10min.
- Rinse coverslips with milliQ water and sonicate those 5min in milliQ water to remove any traces of "piranha".
- Dry with gas pulverization and incubate them at 65°C to evaporate the remaining liquids traces.
- Silanisation:
- Pour on a glass Petri dish 100µl of 3(mercaptopropyl)trimethoxy silane in a vaccum jar and place the coverslips.
- Create a silane atmosphere and incubate the coverslip for 1h.
- Place the coverslips at 65°C for 1h30 (minimum 30min).

Surface coating:

- For NIH3T3 cells, prepare a 0,1mg/ml solution of PLL-g-PEG. If cells are transfected with CXCR4 and CXCR7, prepare a solution of 0.075mg/ml PLL-g-PEG and 2.5µg/ml fibronectin. For dHL60 cells, prepare a solution of 200µg/ml human fibronectin.
- Incubate 20min the silanized coverslip in contact with the coating solution at room temperature in a humid chamber.

Cells seeding:

- For NIH3T3 cells, plate 1ml of 50 000cells/ml in complete medium and incubate 1h at 37°C. Coverslip is then placed into a holder, L-15 medium without serum is added and acquisition can start under the microscope.
- For dHL60 cells, plate 1ml of 50 000cells/ml in L15 without serum on the coverslip place into the holder. Cells are weakly attached to the coverslip.

Pipette preparation:

- Prepare home-made pipettes by stretching capillaries with a pipette puller.
- Prepare a solution of L-15 0.16 mg/ml TRITC–Dextran 10% serum or 6µg/ml dextran-AlexaFluor647 and 50ng/ml CXCL12. Filter the solution (Millex® 0.22µm filter unit) and fill the micropipette. Remove bubbles inside pipette by gently hitting it. Check under binocular the absence of air bubbles and rinse pipette with PBS1X.

- Check there are no bubbles into the Celltram® Vario filled with mineral oil.
- Carefully fix the pipette to the pipette holder.
- Find cells and pipette with x20 objective. Place the pipette as close as possible to the coverslip with manual screws and pipette holder motor.
- If cells are transfected with CXCR4 and CXCR7, carefully shift to x40 oil objective (N.A 1.3).
- Acquire images with 30s interval in a bright field microscope. The Celltram® Vario is a manual microinjector. Turn the screw to inject the chemical solution.

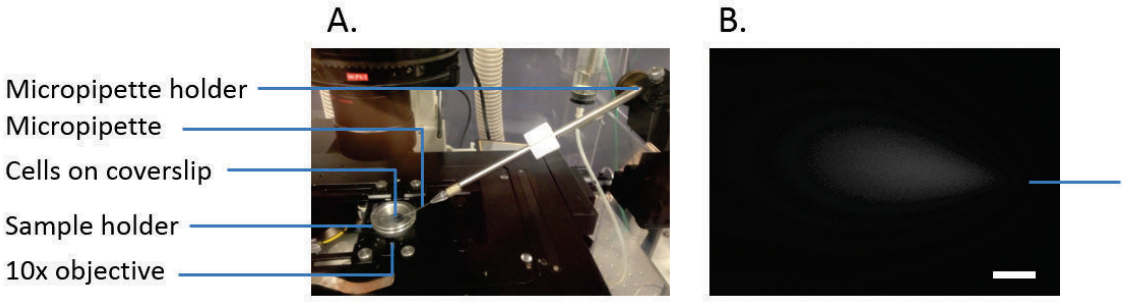

Figure 2.5: Pipette experiment set-up. (A.) Picture of experimental set up. Sample holder under a microscope with a micropipette injecting chemical solution. The micropipette is fixed to the pipette holder. (B.) Fluorescent image of the chemical gradient formed. Blue line shows the position of the pipette. Scale bar 10µm.

2.3.4 Transwell experiment in Boyden chamber

Boyden chamber experiment is used to study cells migration towards a specific chemoattractant[6]. Two chambers are separated by 15µm thick membrane containing pores of 8µm in diameter. Cells are seeded in the upper chamber on the membrane. Chemoattractant solution is added to the lower chamber. Cells attracted by the chemoattractant cross the membrane and accumulated in the lower part of the membrane. Following is the detailed protocol to perform transwell experiment:

- 4h before starting the experiment, remove complete medium and incubate NIH3T3 cells with DMEM 0% BCS to starve the cells.
- Seed 50 000 cells in DMEM 0%BCS in the upper chamber in a total volume of 200µl.
- In the lower chamber, place 600µl of DMEM 1% BCS (negative control), DMEM 10%BCS (positive control) or DMEM 1% BCS + 6nM CXCL12 or DMEM 1% BCS + 60nM CXCL12.
- Incubate 12h at 37°C 5%CO_2.
- Fix the cells with 3%PFA solution (17min) and stain nuclei with DAPI (1min at 1µg/ml).
- With a cotton bud, carefully remove cells in the upper chamber. They are the cells which did not migrate.
- Under a microscope with x10 objective, acquire 10 positions of the membrane with a DAPI filter.
- Count the nuclei which have actively crossed the membrane (Figure 2.6).

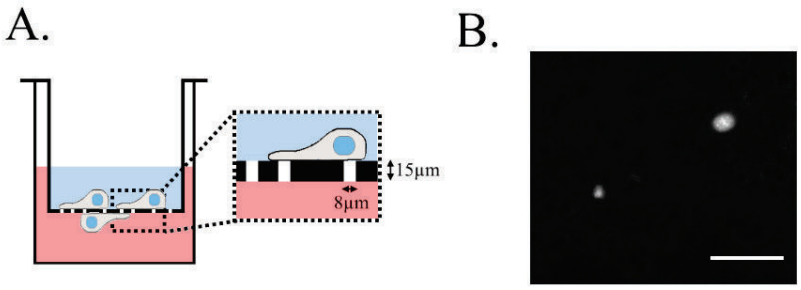

Figure 2.6: (A.) Schematic of Boyden chamber experiment. (B.) Example of Boyden experiment result. Nuclei which cross the membrane are stained with DAPI. Top. nucleus of a cell which has completely crossed the membrane. Bottom. nucleus of a cell stack inside the pore. Here, the size of the nucleus is equal to 8µm (size of the pore) and the nucleus is not counted as one which actively crossed the membrane. Scale bar 50µm.

The nucleus of cells which has not crossed the membrane are "stuck" inside the pore and therefore have the size of the pore.

2.3.5 Microcontact-printing of CXCL12

Microcontact printing (MCP) of protein is a method allowing the printing of microscale motif of a protein on a coverslip[15]. CXCL12 is microcontact-printed to study the directed cells migration towards adhesive motifs of CXCL12. The following protocol presents how CXCL12 is microcontact-printed on glass coverslip and visualized.

Silanisation of glass coverslip:

- All the glassware are cleaned with soap and dried into oven.
- Clean glass coverslips for 10min in a "piranha" bath made of 7 parts of sulfuric acid and 3 parts of hydrogen peroxide (v/v).
- Rinse coverslips with milliQ water, sonicate them in milliQWater in a glass beaker for 5min and dry with air pistol. All humidity traces are removed by putting coverslips 10min in a 65°C oven.
- Pour on a glass Petri dish 100µl of 3(mercaptopropyl)trimethoxy silane in a vaccum jar and place the coverslips.
- Create a silane atmosphere and incubate the coverslip for 1h.
- Place the coverslips at 65°C 1h30 (minimum 30min).

Stamp preparation:

- It needs to have PDMS molds and required SU8 master with proper structure and dimensions.
- Clean the stamp by sonication in ethanol and dry it.
- Activate with an oxygen plasma the PDMS stamp.
- Drop 100µl of 1.56µg/ml CXCL12 on the stamp and incubate 1h in a wet chamber.

Stamping and staining:

- Carefully remove the excess of CXCL12 solution from the stamp with a pipette and dry the stamp for 3min at room temperature.
- Place motifs on the stamp in contact with the silanized coverslip. A weight is placed on top of the stamp for 1h at room temperature.
- To check if CXCL12 has been transferred, a CXCL12 staining is performed. Coverslip is incubated for 1h with a mouse primary antibody against CXCL12 and then a secondary antibody against mouse coupled to Cy3 fluorophore is used. Fluorescence is checked under the microscope.

Cell seeding

- Seed 2000 NIH3T3 cells in DMEM 10%BCS on coverslip placed into holder. After 1h, change medium for L15 1% BCS.
- Start the acquisition on a CKX41 inverted phase-contrast microscope (Olympus). A cooled camera (Hamamatsu), ImageJ plugin Micromanager and 10x or 20x objectives (PhL, air, 0. NA, phase contrast, Olympus) were used to acquire images. Images are taken every 10min.

3 Results

In this PhD thesis, different cell lines have been tested to assess their migration ability on 2D flat surfaces, confined microchannels and later in the case of ratchetaxis and chemotaxis. We used the following cells: 1) NIH3T3 cells are fibroblasts and their migration has been widely investigated. In this PhD thesis, we used NIH3T3 cells as a reference cell line. 2) HL60 cells are neutrophil-like cells migrating in an amoeboid-like mode after differentiation. 3) Three epithelial cells, SW480, SW620 and MDA-MB-231 cells, for their implication in cancer cells spreading and the potential implication of the chemokine CXCL12 during this process[13,14]. SW480 cells were harvested from a patient diagnosed with colon cancer. SW620 cells are collected from the same patient but from metastatic site in lymph node. MDA-MB-231 cells have been collected from a patient diagnosed with breast cancer. We studied migration of these cells in different configurations: on 2D flat surfaces, in 2 levels of confinement, *i.e.* closed microchannels and open microchannels and in the presence of chemical gradients, *i.e*. serum or CXCL12 gradients. First, I will present the different abilities of these cells to migrate on 2D flat coverslip and on straight confined microchannels.

3.1 Cells migration: on 2D flat surfaces *versus* confined microchannels

Historically, cell migration has first been studied on 2D flat surfaces or Petri dishes[42]. As mentioned in the Introduction part page 35, it allowed the elucidation of the mechanisms leading to cell migration. In this PhD thesis, it is especially used as a control, where cells perform a "persistent random walk" characterized by a persistent length, time and speed, which are respectively the length, time and speed the cell migrates without pausing or change in direction of migration . In fact, persistent length, time and speed are measured throughout the thesis and will allow us to compare cell migration on 2D flat surfaces, in straight and ratchet microchannels and in the presence of serum gradient. To start with, the ability of these cells to migrate on 2D flat surfaces or confined microchannels has been assessed first.

3.1.1 Cells migration on 2D flat surfaces

To study cell migration on 2D flat surfaces, cells are seeded on coverslip as explained in the Material & Methods section page 85.

3.1.1.1 NIH3T3 cells migrate on 2D flat surfaces

NIH3T3 are mesenchymal cells which form strong adhesion points to the surface and are strongly motile on 2D flat surfaces. First row in Figure 3.1 is an example of a NIH3T3 cell migrating on 2D flat surfaces where cells perform a "persistent random walk" characterized by a persistent length, time and speed. In this case, we assume that cell is persistent if the cell migrates without pausing for more than 30 min or without changing direction of migration.

Therefore, during 24hours movies, a cell can change direction several times. We measured these parameters for cells migrating in medium containing 10% and 1% serum (Figure 3.1 Second row).

The persistent length, time and speed distributions of NIH3T3 cells migrating in 1% or 10% serum medium are similar (Figure 3.1 Second row). The mean persistent length in 1%serum is equal to 69±39µm and in 10%serum is equal to 75±47µm. The mean persistent time in 1%serum is equal to 1.9±1.5hours and in 10%serum is equal to 2.6±2.6hours. The mean persistent speed in 1%serum is equal to 43±28µm/h and in 10%serum is equal to 38±24µm/h.

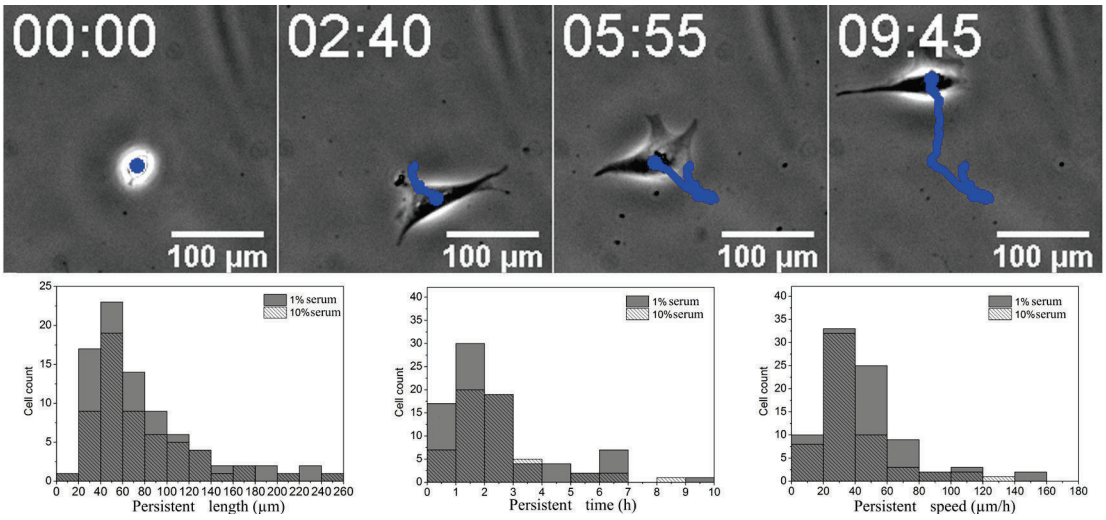

Figure 3.1: Characteristic of NIH3T3 cell migration on 2D flat surfaces. First row. Time series of a NIH3T3 cell migrating on a coverslip. Blue line represent the cell trajectory. Time in hh:mm. See Movie1. Second row. Persistent length, time and speed distributions of NIH3T3 cells migrating on a flat surface in medium containing 1% serum or 10% serum. Duration of experiments was 24hours. 1%serum n=22 cells, N=84 trajectories, 3 independent experiments. 10%serum n=22 cells, N=58 trajectories, 2 independent experiments. Statistical Test One-way ANOVA p>0,05.

There are not statistical differences between persistent length, time and speed distributions of NIH3T3 cells migrating in 1% serum and 10% serum containing medium.

3.1.1.2 HL60 cells migrate on 2D flat surfaces

HL60 are progenitor cells of the immune system. After differentiation with DMSO (1.3%), dHL60 cells become neutrophil-like cells. They have the morphology of amoeboid cells and form weak adhesion points to the surface.

As for NIH3T3 cells, their migrations are called “persistent random walk” and are characterized by a persistent length, time and speed (Figure 3.2). Images are taken every 30s (See Movie 2). The distributions of the persistent length, time and speed are presented in the second row of the Figure 3.2. dHL60 cells migrate roughly 13-fold faster than NIH3T3 cells: the mean persistent speed is equal to 9.1±2.9µm/min compared to 43±28µm/h for NIH3T3 cells. The mean persistent length for dHL60 cells is equal to 27±16µm and the mean persistent time, equal to 3.2±1.9minutes.

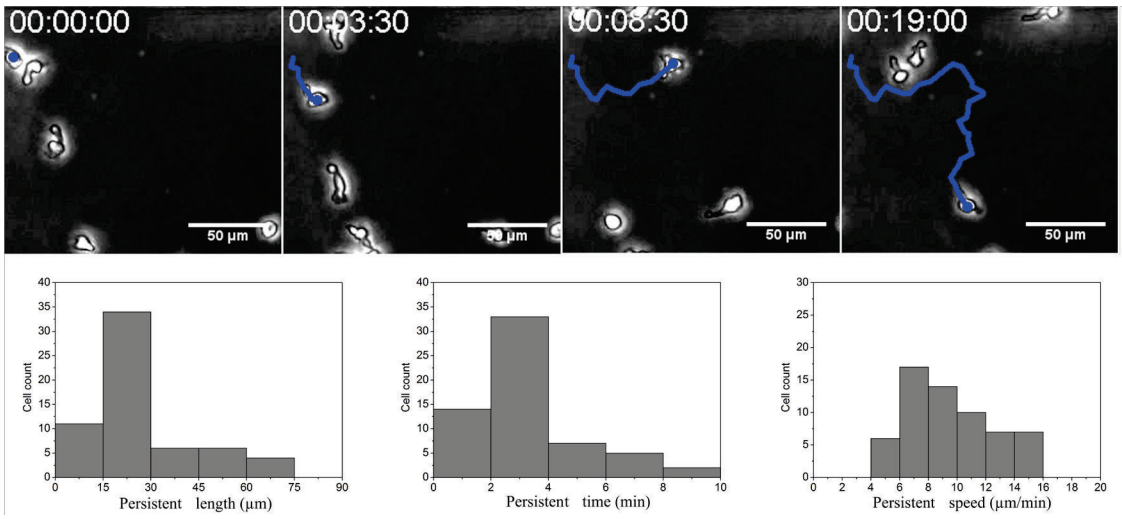

Figure 3.2: Characteristic of dHL60 cell migration on 2D flat surfaces. First row. Time series of a dHL60 cell migrating on a coverslip. Bleu line represnets the cell trajectory. Time in hh:mm:ss. See Movie 2. Second row. Persistent length, time and speed distributions of dHL60 cells migrating on a flat surface. Duration of experiments was 2hours. n=19 cells, N=61 trajectories, 2 independent experiments.

We then studied migration of epithelial cells on 2D flat surfaces.

3.1.1.3 Epithelial cells are non-motile on 2D flat surfaces

SW480 cells, SW620 and MDA-MB-231 cells are epithelial cells. On 2D flat surfaces, these cells are non-motile. During 10hours, MDA-MB-231 cell does not migrate compared to NIH3T3 cells (Figure 3.3).

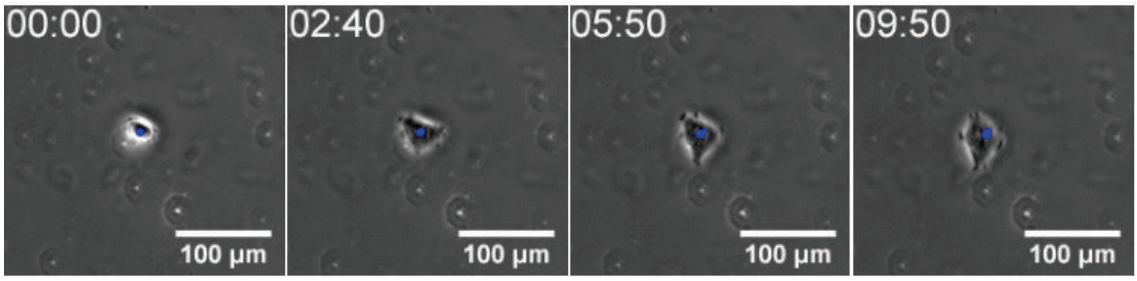

Figure 3.3: Time series of a MDA-MB-231 cell migrating on a coverslip. Duration of experiments was 24hours. Time in hh:mm. See Movie 3.

NIH3T3 fibroblasts and dHL-60 are motile cells, they move randomly on flat surfaces without external cues and perform "persistent random walk". As amoeboid cells, dHL60 cells migrate much faster than NIH3T3 fibroblasts. In this PhD thesis, we used NIH3T3 cells as the reference cell line. In addition, three cancer epithelial cells line have been tested for their ability to migrate on flat surfaces. SW480, SW620 and MDA-MB-231 cells are all immobile on 2D flat surfaces. As mentioned in the Introduction *in vivo* environment (page 33), *in vivo* surrounding is a complex environment where cells are mainly confined. Cells migration on flat surfaces is far from *in vivo* conditions. And studies report that non-motile cells can become motile under confinement[17]. Hence, in this study, we aim to copy *in vivo* conditions under confinement. To do so, we used

microfabrication. It is a powerful tool which allows the production of micrometer structures size. Microchannels mimic blood capillaries. The length, width and height of microchannel as well as its shape can easily be tuned. To study cell migration in confined environment, we first placed the cell in confined **straight microchannels**. I will present in the next section the migration of MDA-MB-231 and NIH3T3 cells in confined straight microchannels.

3.1.2 Cells migration in confined straight microchannels

As mentioned previously, we aimed to study cell migration under confinement in microchannels which mimic blood capillaries. Through microfabrication, we can tune the length and cross-section area of the microchannels; *i.e.* height and width of the microchannels. In closed microchannels, we set the microchannels length and height at 350µm and 5µm respectively. However, we changed the cross-section area from 10µm², 20µm² to 30µm² by modifying the width of the microchannels. In the following part, I will present MDA-MB-231 and NIH3T3 cells migration in confined straight microchannels.

3.1.2.1 The epithelial MDA-MB-231cells

The microchannels have been obtained as explained in Material & Methods section pages 82-83. Typically, cells are seeded in one reservoir (Figure 3.4A). Cells would enter the microchannels and reach the second reservoir and, critically, in the absence of any chemical gradient.
MDA-MB-231 cells are non-motile on 2D flat surfaces for up to 10h (Figure 3.3). However, as soon as these cells are confined in 20µm² microchannels, they can migrate. In this example, a MDA-MB-231 cell crosses 350µm in 8h (Figure 3.4B). This highlights the importance of studying cell motility under confinement.

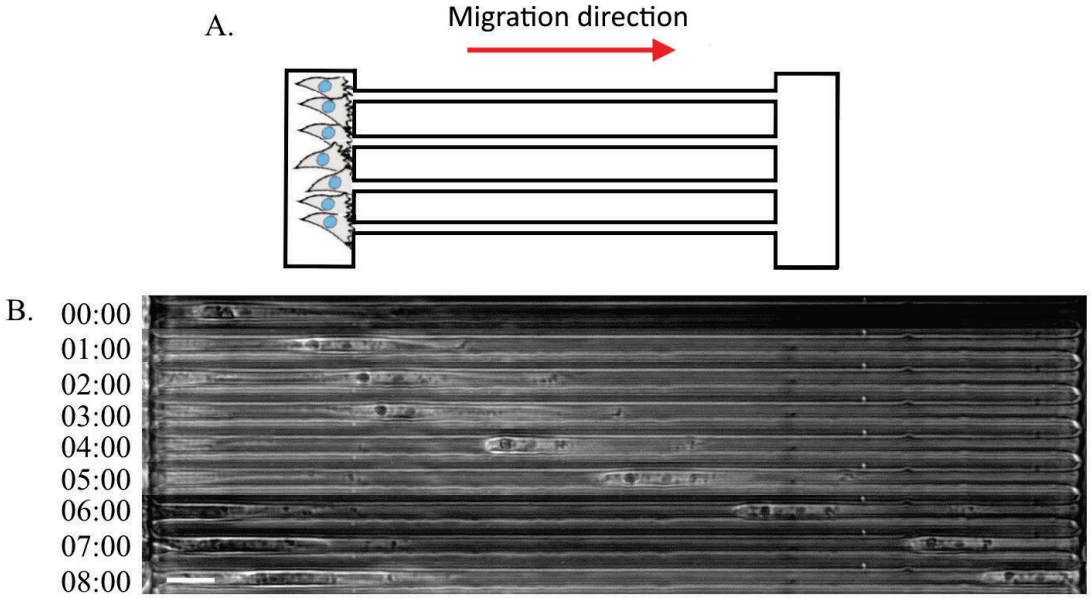

Figure 3.4: Straight microchannels configuration. (A.) Schematics of the closed straight microchannels. (B.) Time series of MDA-MB-231 cell migrating in 20µm² cross-section straight microchannels. Scale bar 20µm. Time in hh:mm. See Movie 4.

In the next section, I will present the migration of NIH3T3 cells in 20µm² and 30µm² cross-section area straight microchannels. These two straight microchannels are important because they constitute the control cell migration in closed microchannels. In this PhD thesis, we want to direct cell migration with ratchetaxis in closed microchannels, therefore preparing ratchet microchannels. Studying NIH3T3 cells migration in straight microchannels is a benchmark for cell migration in ratchet microchannel.

3.1.2.2 The mesenchymal NIH3T3 cells

As mentioned previously, I will detail now the migration of NIH3T3 cells in straight microchannels. In the next section I will present the ratchet geometry (page 101) and then the migration of NIH3T3 cells in the ratchet closed microchannels (page 106).
However, each time, I will present the time series of a representative cell migrating in the microchannel, the trajectory plot of the corresponding cell, the trajectories plot of a larger number of cells, and finally the persistent length, time and speed distributions of cell migrating in the microchannels. For each configuration, the initial position of the cell is set at 0 once the cell is inside the microchannel. We measured the persistent length, time and speed of the **first persistent cell motion.** We measured also the total time the cells need to cross the entire microchannel. It allows the fair comparison of cell migration between the different configurations.

3.1.2.2.1 20µm² cross-section in straight microchannel

As previously explained, I first show an example of a NIH3T3 cell migration in 20µm² straight microchannels and its corresponding trajectory (Figure 3.5).

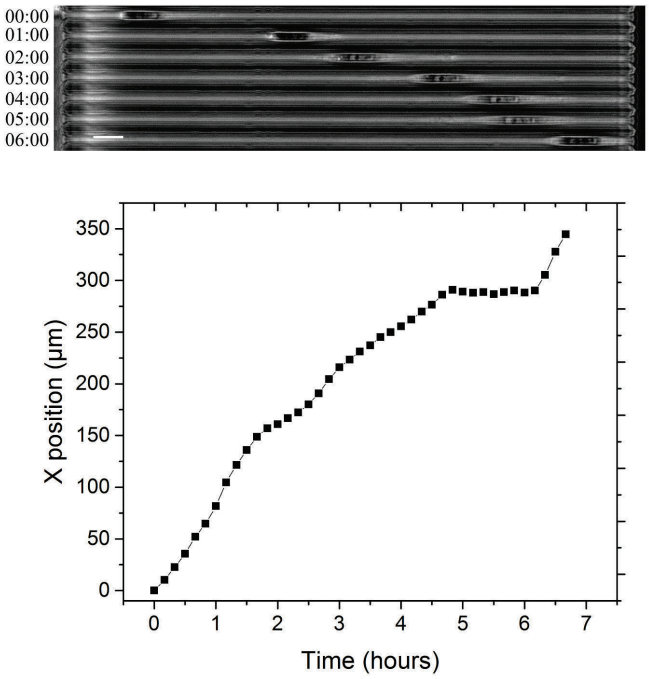

Figure 3.5: Example of a NIH3T3 cell migrating in 20µm² straight microchannels and its corresponding trajectory. Scale bar 20µm. Time in hh:mm. See Movie 5.

Then, we plot the trajectories of 8 cells tracked in 20µm^2 straight microchannels (Figure 3.6). Here, every cell crosses the entire microchannels in less than 12h. The mean total migrating time to cross the microchannels is equal to 6.0±2.8h. We observed here that cells did not change their directions of migration. Once the cell entered the microchannel, it migrates until the end of the channel without changing direction.

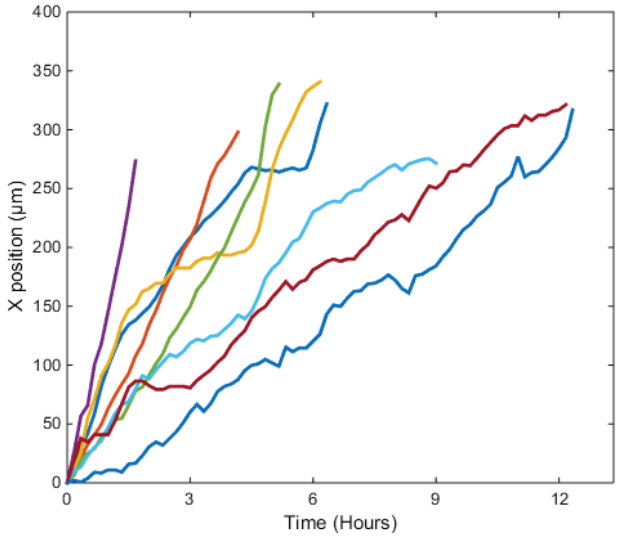

Figure 3.6: Trajectories of cells tracked in 20µm² straight microchannels.

Then, the persistent length, time and speed of the first persistent motion are measured. The distributions of persistent length, time and speed are presented in Figure 3.7. In straight microchannels, the mean persistent length was equal to 295±90µm, the mean persistent time was equal to 4.1±2.6h and the mean persistent speed was equal to 76±34µm/h. We observed a persistent length distribution which is shifted to the highest values, *i.e.* 300-350µm, it corresponds to the cells which migrate persistently until the end of the microchannel without pausing. In-between, lowest persistent lengths indicate that cells paused more than 30min. In 20µm^2 straight microchannels, few cells paused.

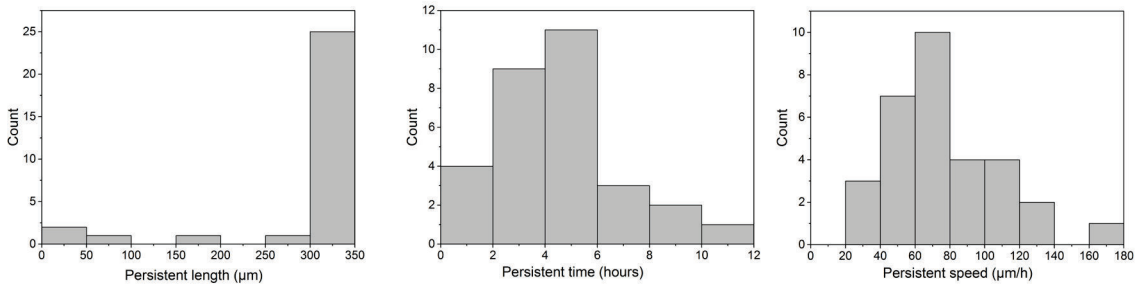

Figure 3.7: Persistent length, time and speed distributions of the first persistent motion of NIH3T3 cells migrating in 20µm² straight microchannels. 3 independent experiments n= 33 cells.

In 20µm^2 straight microchannels, we noted that the majority of cells crossed the microchannels without pausing. Cells did not change direction of migration. 30µm^2 straight microchannel is the second control used.

3.1.2.2.2 30µm² cross-section in straight microchannel

The same analysis as previously described is realized. Figure 3.8 shows an example of a NIH3T3 cell migration in 30µm² straight microchannels and its corresponding trajectory.

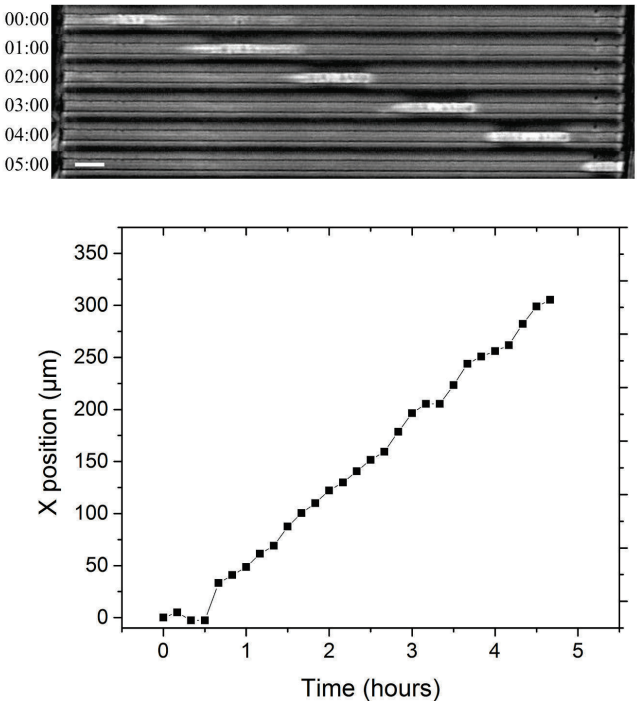

Figure 3.8: Example of a NIH3T3 cell migrating in 30µm² straight microchannels and its corresponding trajectory. Scale bar 20µm. Time in hh:mm. See Movie 6.

Then, we plot the trajectories of 8 cells tracked 30µm² straight microchannels (Figure 3.9). Here, every cell crosses the entire microchannels in less than 12h. The mean total migrating time is equal to 8.8±7.6h. We observed here that cells did not change direction of migration. Once the cell entered the microchannel, it migrated until the end of the channel without changing direction.

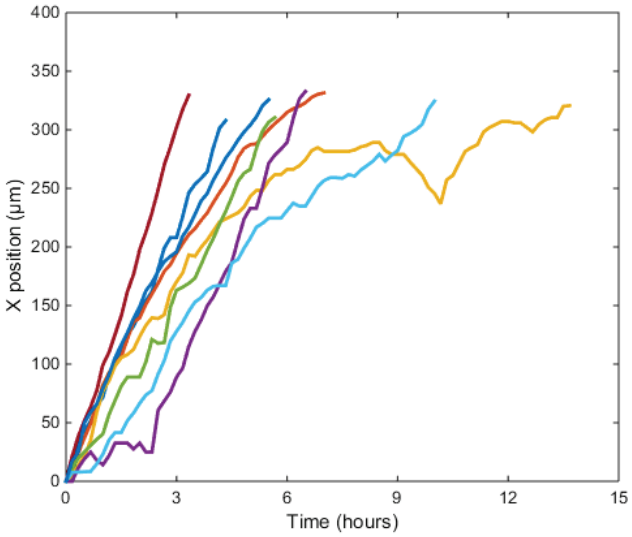

Figure 3.9: Trajectories of cells tracked in 30µm² straight microchannels.

Then, the persistent length, time and speed of the first persistent motion are measured. The distributions of persistent length, time and speed are presented in Figure 3.10. In straight microchannels, the mean persistent length was equal to 269±77µm, the mean persistent time was equal to 5.6±3.6h and the mean persistent speed was equal to 58±32µm/h. The persistent length distribution is similar to the one in 20µm^2 straight microchannels, we observed a peak in the persistent length distribution between 300-350µm, corresponding to the cells which migrate persistently until the end of the microchannel without pausing. In-between, lowest persistent lengths indicate that cells paused. Few cells paused in 30µm^2 straight microchannels.

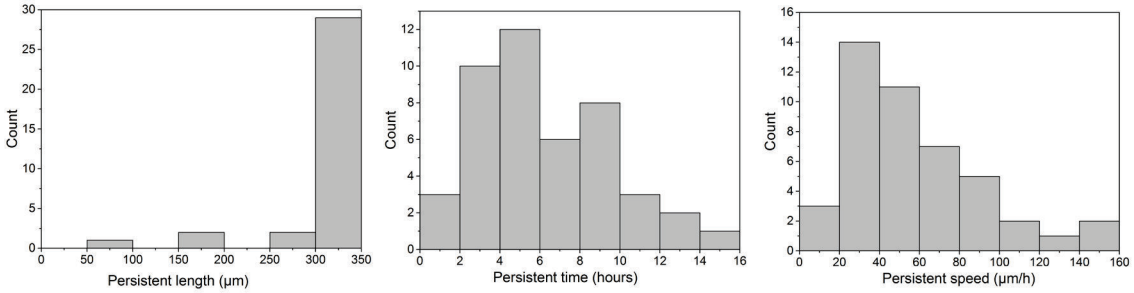

Figure 3.10: Persistent length, time and speed distributions of the first persistent motion of NIH3T3 cells migration in 30µm² straight microchannels. 4 independent experiments n= 34 cells.

As for 20µm^2 straight microchannels, in 30µm^2 straight microchannels, we note that the majority of the cells cross the microchannels without pausing. In addition, cells did not change direction.

The mechanism driving cell migration inside confined microchannels is called “Pushing off the walls”. In the model proposed by Hawkins et al. (2009), frictions generated between the cell and channels walls are at the origin of cell motion (page 38). Under confinement, and in contrast to 2D flat surfaces cell migration, focal adhesions are not required. For this reason, we stained for focal adhesions in cell migrating inside straight microchannels.

3.1.2.2.3 Focal adhesion distributions

We observed the focal adhesions distributions with two methods: transfection of a DNA construct which overexpressed proteins of the focal adhesion coupled to a fluorophore such as Zyxin-mCherry. We can observe cell migration inside microchannels and focal adhesions distributions (Figure 3.11 First and Second row). Focal adhesions can be stained also in fixed sample after cell entry inside microchannels (Figure 3.11 Third row). In both configurations, we observed the presence of focal adhesions in NIH3T3 cells migrating inside 20µm² and 30µm² straight microchannels. However, it does not mean that focal adhesions are required for NIH3T3 cells migration inside microchannels. Alternatively, experiment could be performed by coating the microchannels with PLL-g-PEG which prevents the formation of focal adhesions. We should be able to observe still cell migration.

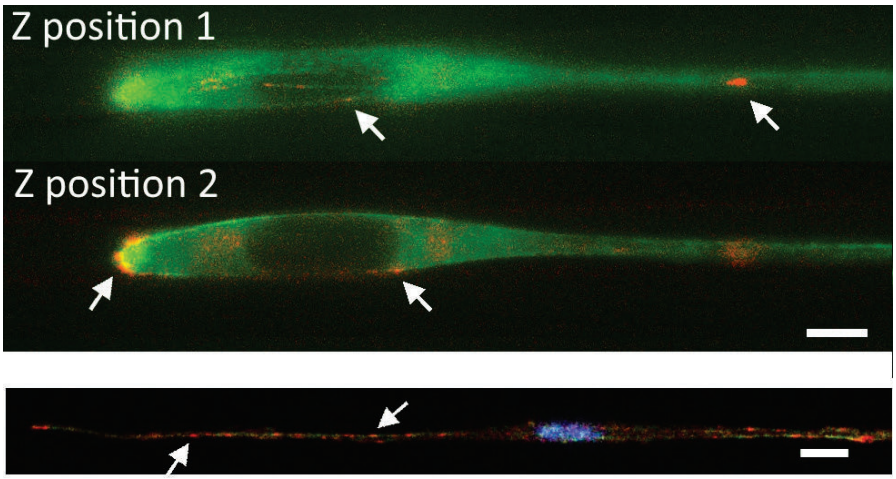

Figure 3.11: Focal adhesions distribution in NIH3T3 cells migrating in straight microchannels. First row. NIH3T3 cell expressing Zyxin (focal adhesion in red) and myosin (green) and migrating inside 30µm² microchannel. Z position 1 focuses on the coverslip. Z position 2 focuses in the middle cell position. Images from Godeau (2016). Scale bar 5µm. Third row. NIH3T3 cell migrating in 20µm² microchannel, fixed and stained for Vinculin (focal adhesions in red) and nucleus (DAPI in blue). Scale bar 10µm.

Moreover, 20µm² and 30µm² straight microchannels are important conditions because they constitute the control cell migration in closed microchannels. Later in the thesis page 106, I will present how NIH3T3 cells migration is impaired in the ratchet microchannel and I will summarize the migration of cells in straight and ratchet microchannels page 114.

Altogether, non-motile MDA-MB-231 cells on 2D flat surfaces become motile in confined environment. The mechanism leading to migration under confinement is different than on 2D flat surfaces as explained in the Introduction section, “Pushing off the wall” page 38. In addition, we saw that NIH3T3 cells migrate persistently in straight microchannel. Ratchetaxis has proven its efficiency to rectify cell migration on 2D flat and topographical surfaces[15,16]. There, the ratchet unit was a triangle motif, which is the shape of a polarized and migrating cell on 2D flat surfaces. In this project, in addition to orient cell migration in confined environment, we want to rectify it. In fact, “confined ratchetaxis” is a series of confined and connected triangle ratchet unit. To do so, we designed a triangle ratchet unit in which cells will be confined. It is presented in the next section. In confined environment, it has never been done and this is what we want to study in this PhD thesis.

3.2 Ratchet design

As mentioned in the previous section, cells are able to migrate persistently in straight microchannel. To rectify cell migration, we want to confine cell in 3D triangle ratchet, which recapitulate the shape of polarized cell on 2D flat coverslips. To confine cell in a closed ratchet unit, the ratchet should have the volume of a cell. As mentioned previously, we used NIH3T3 as a reference cell line. The dimension of the ratchet is therefore designed according to NIH3T3 cell dimensions.

3.2.1 NIH3T3 cell dimensions to design the ratchet unit

3.2.1.1 NIH3T3 cell volume

After detaching the cells from the surface, we measured diameter of perfectly circular cell in suspension and we assumed that cells were spherical. The cell diameter distribution is presented in Figure 3.12. We measured a mean NIH3T3 cell diameter of 14.4±1.6µm (n=388 cells, 3 independent experiments) and deduced the mean cell volume. It is equal to 1560±520µm^3.

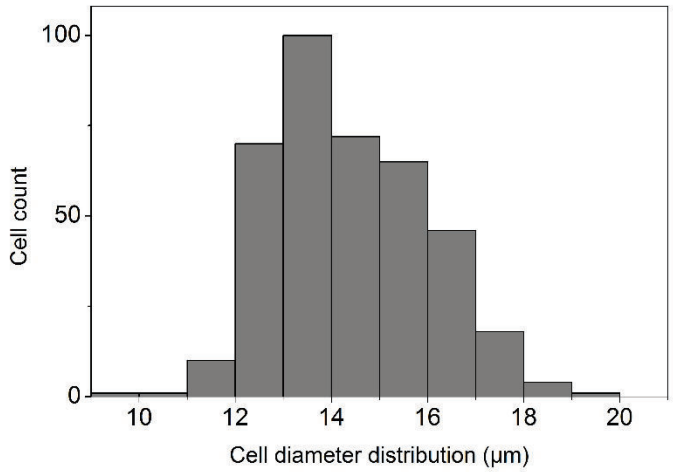

Figure 3.12: NIH3T3 cell diameter distribution right after detaching and before cell adhesion. n=388 cells, 3 independent experiments.

We measured as well the mean diameter of HL60, SW480 and MDA-MD-231 cells. They are equal respectively to 11.5±1.0µm, 12.1±1.8µm 17.0±2.5µm and correspond to a mean volume of 800±210µm^3, 940±420µm^3 and 2590±1140µm^3. The respective cell diameter distributions are presented in Appendix A.4.1.

The mean NIH3T3 volume is equal to 1560±520µm^3. We set the ratchet volume to 1500µm^3. Then, in order to even more confined the cells while migrating from one ratchet unit to another one, we decided to measure the dimensions of the nucleus, *i.e.* nucleus height, axis lengths and nucleus volume.

3.2.1.2 Nucleus dimensions

To measure nucleus dimensions, we stained for the nucleus of adherent NIH3T3 cells with DAPI or Hoechst as mentioned in the Material & Methods section page 78. Confocal microscopy allows the measurement of height, major and minor axis lengths of the nucleus. Figure 3.13 shows typical images of a NIH3T3 nucleus and the distributions of the nucleus volume, height, major and minor axis length and the nucleus angle. The volume and height of the nucleus have been measured and their means are equal to 720±180µm^3 and 8.2±1.4µm respectively. The major and minor nucleus lengths have been measured and their means are equal respectively to 17.0±2.2µm and 13.4±1.9µm. We measured also the mean cross-section area with the mean nucleus height, minor axis length values. It is roughly equal to 90µm^2. With the minor and major

axis measurements, we can deduce the nucleus angle, plot the nucleus angle distribution and obtain the mean nucleus angle. It is equal to 75±7°. In order to further confine the cells and to be closed to *in vivo* capillaries dimensions, we set the microchannel height at 5µm. There, the cells will be confined from the top. This configuration is called **closed microchannels**.

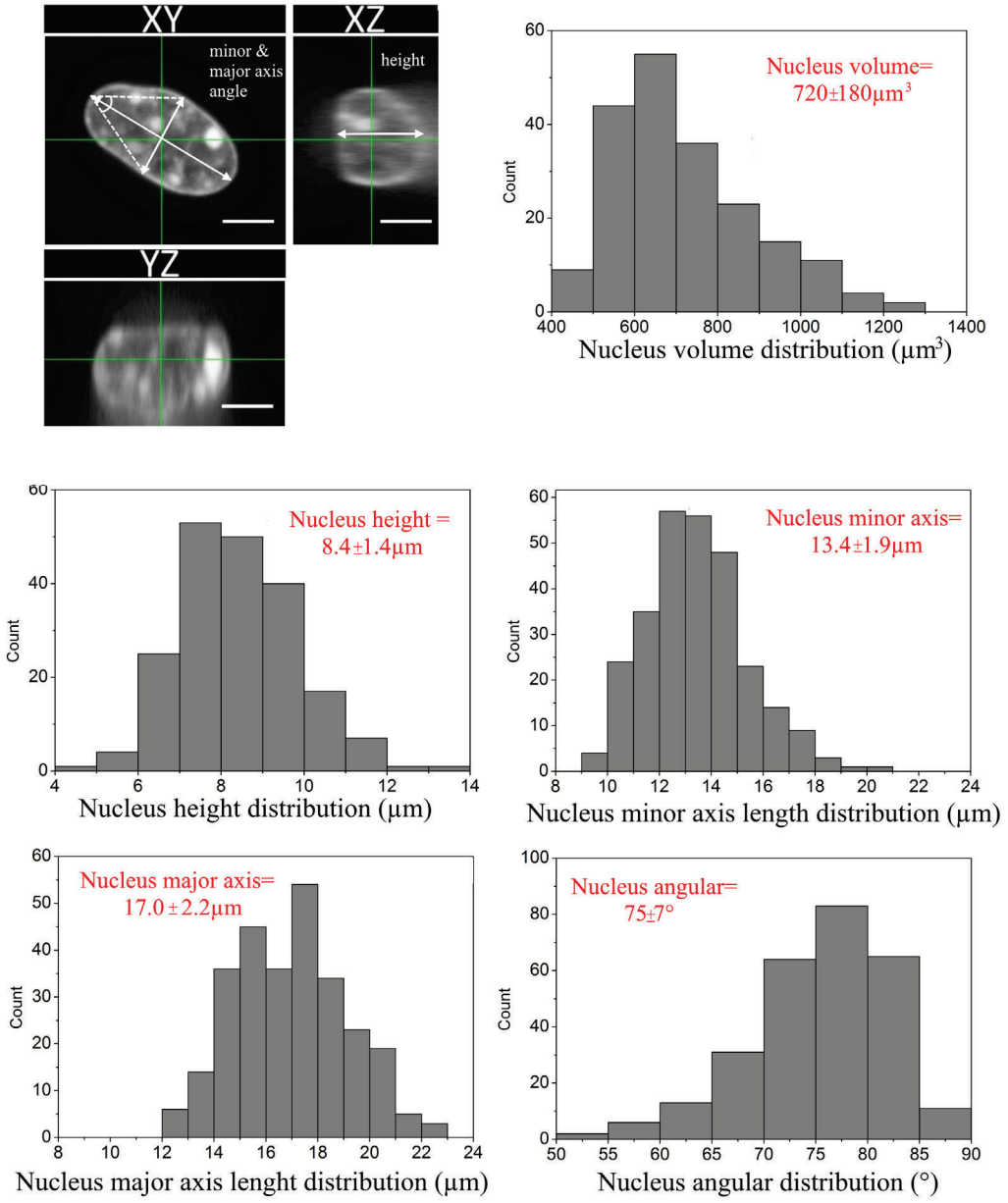

Figure 3.13: Measurement of NIH3T3 nucleus dimensions. Example of a NIH3T3 adherent cell in which the nucleus is stained. Spinning disk images. XY image allows the determination of the nucleus minor and major axis lengths, equal here respectively to 8.5µm and 15.9µm. XZ and YZ images allow the determination of nucleus height, equal here to 8µm. In this example, the nucleus volume is equal to 719µm. Scale bar 5µm. Distributions of nucleus volume, height, major, minor axis and angle. Nuclei were stained with Hoescht. Nucleus volume and height; n=199 nucleus, 3 independent experiments. Nucleus major and minor axis; n=275 nucleus, 2 independents experiments.

From volume measurements, we observed that on average, nuclei occupy a large volume of NIH3T3 cells. Nucleus is the biggest and stiffest organelle of the cell and can potentially prevent the cell passage from one ratchet to another one. We decided to keep the ratchet volume and height constant for a triangle ratchet unit, *i.e.* 1500µm^3 and 5µm, respectively. We deduced the

area of each ratchet motif equal to 300µm^2. The geometry of the closed triangle ratchet can be tuned by mainly taking into account the nucleus cross-section area. This is what I will present in the next section.

3.2.2 Design of the closed ratchet microchannels

Keeping the volume and the height of the ratchet constant, we can modify the geometry of the triangle ratchet by changing two parameters, the **angle α** and the **bottleneck area i** by changing opening width which connect two triangle units (Figure 3.14). It will probe the ability of the nucleus to deform and adapt its shape to the ratchet geometry. In addition, it will allow us to determine how the cell geometry influences its migration.

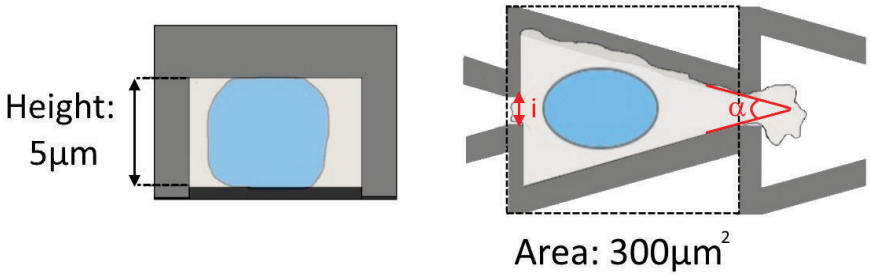

Figure 3.14: Schematics of the closed ratchet design with a cell trapped. The nucleus is in blue and the cell, in beige. The height and area XY are constant but the angle α and bottlneck area i connecting two ratchet units change.

To vary angle α, we first check the angle of ratchet used in other papers: 16° angle is the one used in Caballero et al. (2014). Others used more obtuse or shaper angles and still observed the ratchet effect of directed cell migration[15,16,75,160]. On average, the nucleus angle is equal to 75°.We therefore set the angle α of the ratchet to 8°, 16° or 24°, which will force the nucleus to deform.

To vary the bottleneck area i, the first point was to make sure that the nucleus will have to deform to go from one ratchet to another one. We know due to *in vivo* studies that nucleus can strongly deform to fit capillaries dimension (8µm in diameter, 50µm^2 in cross-section) and *in vitro* studies have shown than cells can migrate through micrometer size constriction (down to 6.5µm^2 in cross-section)[5,124]. Moreover, we measured a mean nucleus cross-section area equal to 90µm^2. In addition, we used previous data from the lab which show that NIH3T3 cells are able to migrate persistently for up to 200µm in straight microchannels whose cross-section area is as small as 10µm^2 [51]. By taking into account these statements and results, we set the bottleneck area between ratchet i units to 10µm^2, 20µm^2 and 30µm^2. We named the ratchet according to the parameters α and i. For example, the ratchet condition of 16° angle (α) and 20µm^2 bottleneck (i), is named α16i20.

In the next sections, we will study the cell migration in different ratchet configurations, *i.e.* different α and i, in two different levels of confinement, *i.e.* closed and open microchannels and in the presence of chemical gradients. But to start with, I will detail in the following section, the migration of NIH3T3 cells in different closed microchannel ratchet.

3.3 Cell migration in closed ratchet microchannel

As mentioned in the previous section for cell migration in straight microchannel (page 96), cells are seeded inside the reservoirs of the different closed ratchet microchannels conditions. Figure 3.15 is a schematic of the ratchet microchannels and the two reservoirs. I will present here the critical points for the rest of this study to define the sense of cell migration:

-we defined the **+ direction** for cell migrating in **ratchet direction** (as presented page 60 and in [15,16]).

-we defined the - direction for cell migrating against the ratchet direction.

For each configuration, the initial position of the cell is set at 0 and correspond to the cell position in the first ratchet or equivalent distance in straight microchannel. As a consequence, when a cell is tracked, the trajectory of the cell migrating in the ratchet direction (+ direction) will have positive values, whereas the trajectory of the cell migrating against the ratchet direction (- direction) will have negative values. For each configuration, we measured the persistent length, time and speed distribution of the **first persistent cell motion.** As a reminder, in the closed microchannel, the maximal persistent length is set by the length of the microchannel.

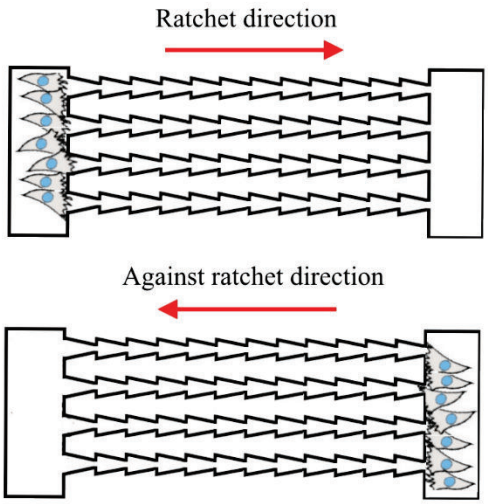

Figure 3.15: Schematics of the closed microchannels configuration. Cells are seeded in one reservoirs and enter in the microchannels. Ratchet direction: in the direction of the tip of the ratchet. Against ratchet direction: in the direction of the base of the ratchet.

In the next section, I will compare in details four different ratchets microchannels conditions and also straight microchannels used as a control. I will first present the ratchet geometry. As mentioned in the section “Cells migration in confined straight microchannels” page 96, I will present the time series of a representative cell migrating in the ratchet direction or opposite direction, the trajectory plot of the corresponding cell, the trajectories plot of a larger number of cells, and finally the persistent length, time and speed distributions. It will be exhaustive and repetitive figures and I will sum up the main results in the section “Sum up of the closed microchannels conditions presented and choice of α16i20 ratchet microchannels” page 114.

3.3.1 Cell migration in different ratchets dimension

This part is first divided according to the angle α used, *i.e.* 8°, 16° and 24° and then according to the bottleneck area i, *i.e*. 10µm², 20µm² and 30µm².

3.3.1.1 α= 8°

Here, we set the angle α at 8°. 10µm² and 20µm² connecting area are tested and microchannels are represented in Figure 3.16.

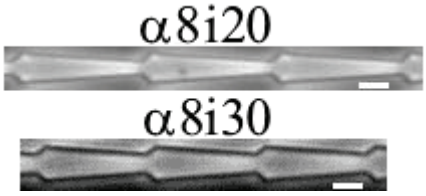

Figure 3.16: Images of α8i20 and α8i30 ratchet microchannels. Scale bar 10µm.

NIH3T3 cells migration has been experimented in these two configurations. Only few cells have been tracked and to not overcrowd this presentation, the results have been placed in the Appendix A.4.2.1 and A.4.2.2.
These both conditions are too restrictive and do not allow the migration of the cell over long distances.

3.3.1.2 α=16°

Here, we set the angle α at 16°. Different opening widths are tested. Figure 3.17 shows images of the α16i10, α16i20 and α16i30 ratchet microchannels.

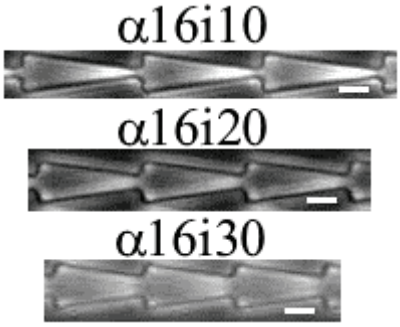

Figure 3.17: Images of α16i10, α16i20 and α16i30 ratchets geometry. Scale bar 10µm.

3.3.1.2.1 α16i10

As explained previously, we tracked trajectories of cell migrating in the ratchet direction or against the ratchet direction. We defined the ratchet direction as the + direction. Figure 3.18 shows examples of NIH3T3 migration in α16i10 microchannels in the ratchet direction (left) or against the ratchet direction (right) and their corresponding trajectory. Each sudden increase in X position represents the nucleus passage through ratchet bottleneck.

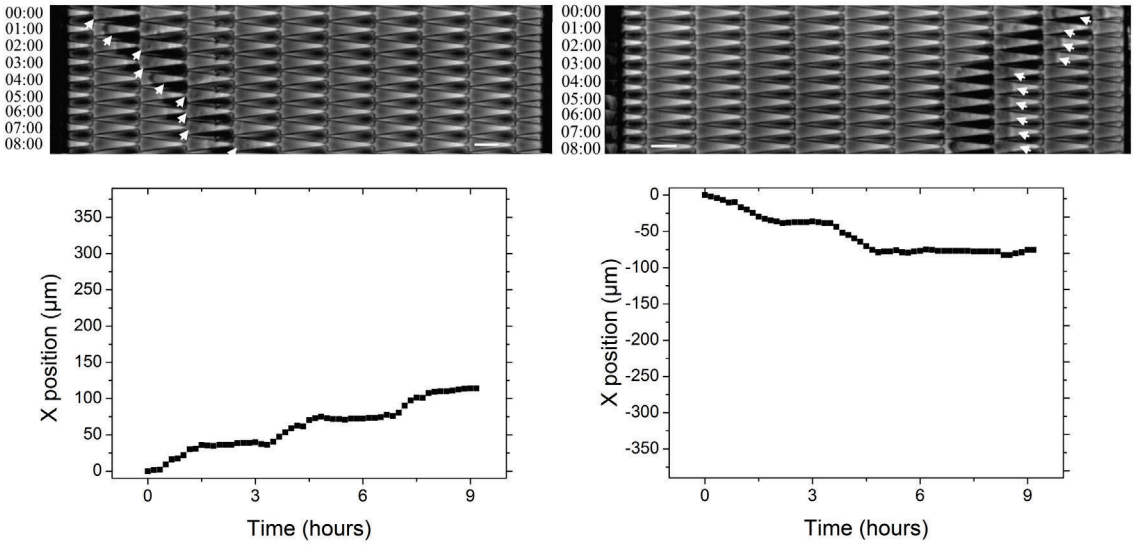

Figure 3.18: Example of a NIH3T3 cell migrating in α16i10 ratchet configuration and its corresponding trajectory. Left. In the ratchet direction. Right. Against the ratchet direction. White arrows show cell position. Scale bar 20µm. Time in hh:mm. See Movie 7 and Movie 8.

When we plot the trajectories of all cells tracked, we observed that none of the cells cross the entire microchannels in 24h: after moving, cells are "stuck" or died (Figure 3.19). For NIH3T3 cells, a bottleneck of 10µm^2 between ratchets is too constraining to allow proper cell migration.

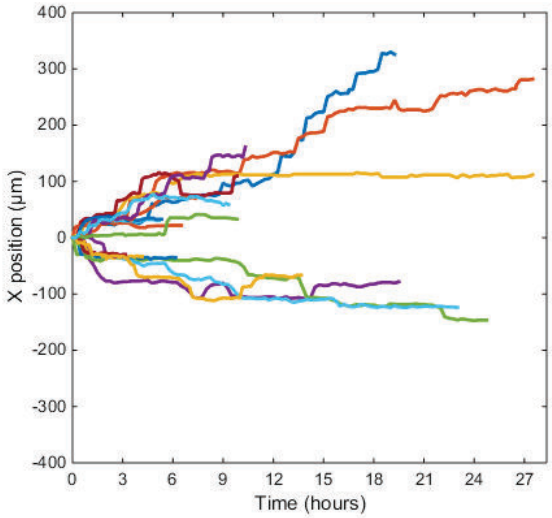

Figure 3.19: Trajectories of all cells tracked in the α16i10 ratchet configuration.

In the ratchet + and - directions, the persistent length, time and speed distributions are similar (Figure 3.20). In the ratchet + and – directions, respectively, the mean persistent length is equal to 39±14µm and 40±24µm, corresponding to the length of α16i10 ratchet unit, the mean persistent time is equal to 1.7±1.1h and 2.1±1.8h and the mean persistent speed is equal to 33±26µm/h and 30±20µm/h.

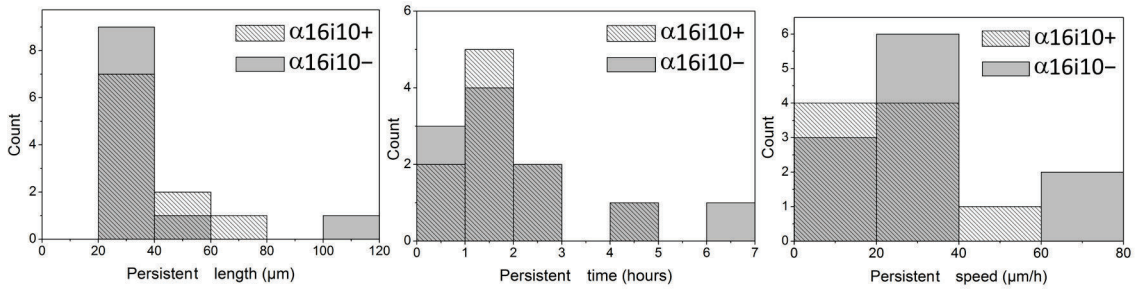

Figure 3.20: Persistent length, time and speed distributions of the first persistent motion of NIH3T3 cells migration in α16i10 microchannels in the ratchet direction (+) and against the ratchet direction (-). 3 independent experiments n+= 10cells, n-=11cells.

In this condition, we saw that 10μm^2 bottleneck between ratchets is too small to allow cell migration over long distances. In addition, we cannot see any differences in terms of persistent length, time and speed distribution for cells migrating in the ratchet direction (+) or against the ratchet direction (-).

3.3.1.2.2 α16i20

As explained previously, we tracked trajectories of cell migrating in the ratchet direction or against the ratchet direction. Figure 3.21 shows examples of NIH3T3 cell migration in α16i20 microchannels in the ratchet direction (left) or against the ratchet direction (right) and their corresponding trajectories.

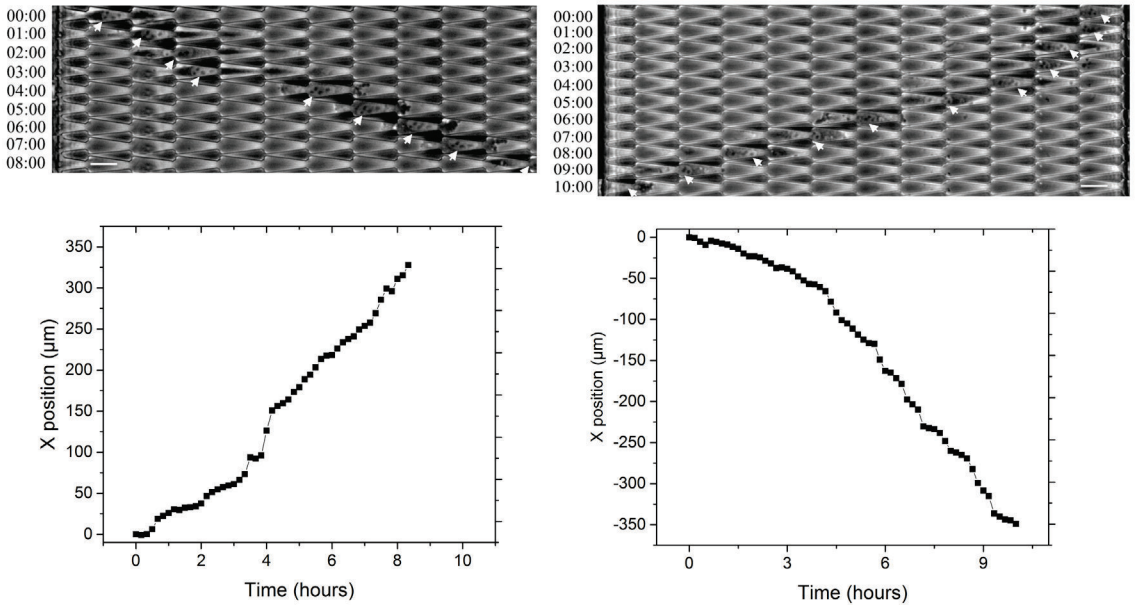

Figure 3.21: Example of a NIH3T3 cell migrating in α16i20 ratchet configuration and its corresponding trajectory. Left. In the ratchet direction. Right. Against the ratchet direction. Scale bar 20μm. Time in hh:mm. See Movie 9 and Movie 10.

We plot the trajectories of 8 cells tracked in the ratchet direction or against the ratchet direction (Figure 3.22). Here, all of the cells cross the entire microchannels in less than 15h. In fact in the + direction, the mean total migrating time to cross the entire microchannels is equal to 7.7±3.6h and it is equal to 8.5±4.6h against the ratchet direction: there is no statistical difference between the total migrating time in the ratchet + and ratchet – directions (One-way ANOVA p>0.05). As

for cells migrating in straight microchannels, we observed that cells did not change direction of migration. Once a cell entered the microchannel, it migrated until the end of the microchannel without changing direction.

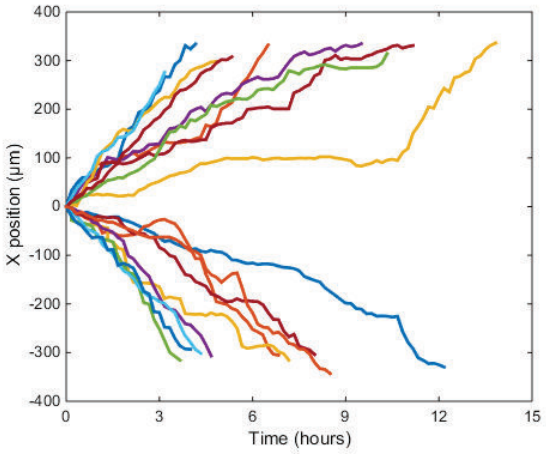

Figure 3.22: Trajectories of cells tracked in the α16i20 ratchet configuration.

Then, the persistent length, time and speed of the first persistent cell motion are measured. The distributions of persistent time and speed are similar in the ratchet + and – directions (Figure 3.23). In the ratchet + and – directions respectively, the mean persistent time is equal to 3.6±2.6h and 4.2±3.1h and the mean persistent speed is equal to 54±27µm/h and 54±28µm/h. The persistent length distributions show differences in the ratchet + and – directions and compared to straight microchannels. In the + direction, the persistent length distribution presents three peaks, between 0-50µm between 100-150µm and 300-350µm. In the – direction, the persistent length distribution also presents three peaks, between 0-100µm between 150-250µm and 300-350µm. The last peak from 300-350µm in persistent length corresponds to the cells which migrate persistently until the end of the microchannel without pausing. Intermediate peaks of persistent length correspond to cells which pause in the microchannel. However, despite this difference in persistent length distribution, the mean persistent length is equal to 203±126µm and 197±121µm in the ratchet + and – directions, respectively. There is no statistical difference in the persistent length distribution in the ratchet + and – directions (One-way ANOVA). We did not observe any preferential direction of migration neither rectification of cell migration.

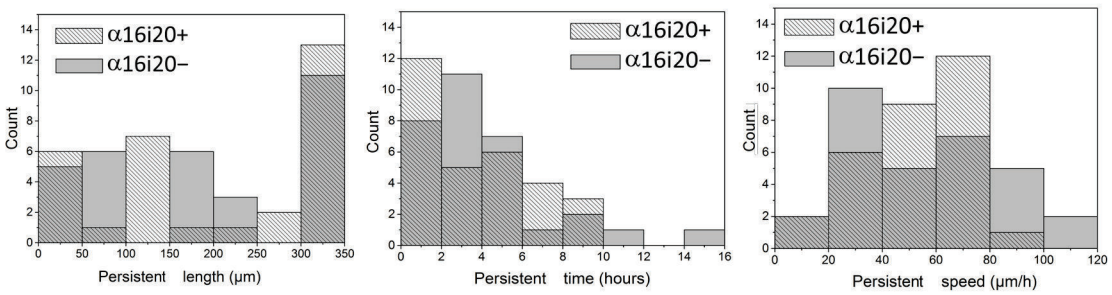

Figure 3.23: Persistent length, time and speed distributions of the first persistent motion of NIH3T3 cells migration in α16i20 microchannels in the ratchet direction (+) and against the ratchet direction (-). 7 independent experiments n+= 31 cells, n-=31 cells.

In contrast to α16i10, α16i20 ratchet condition did not prevent cell migration. Compared to the cross-section of the nucleus on flat surfaces, *i.e.* 90µm^2, 20µm^2 bottleneck between ratchet units allows some cells to cross the entire microchannels whereas other cells pause in-between. However, the cell migration is impaired the same way in the ratchet + and – directions and no change direction of migration is observed indicating that none of the direction is preferred. We did not see rectification of cell migration in α16i20 condition.

3.3.1.2.3 α16i30

As explained previously, we tracked trajectories of cell migrating in the ratchet direction or against the ratchet direction. Figure 3.24 shows examples of NIH3T3 cell migration α16i30 microchannels in the ratchet direction (left) or against the ratchet direction (right) and their corresponding trajectory.

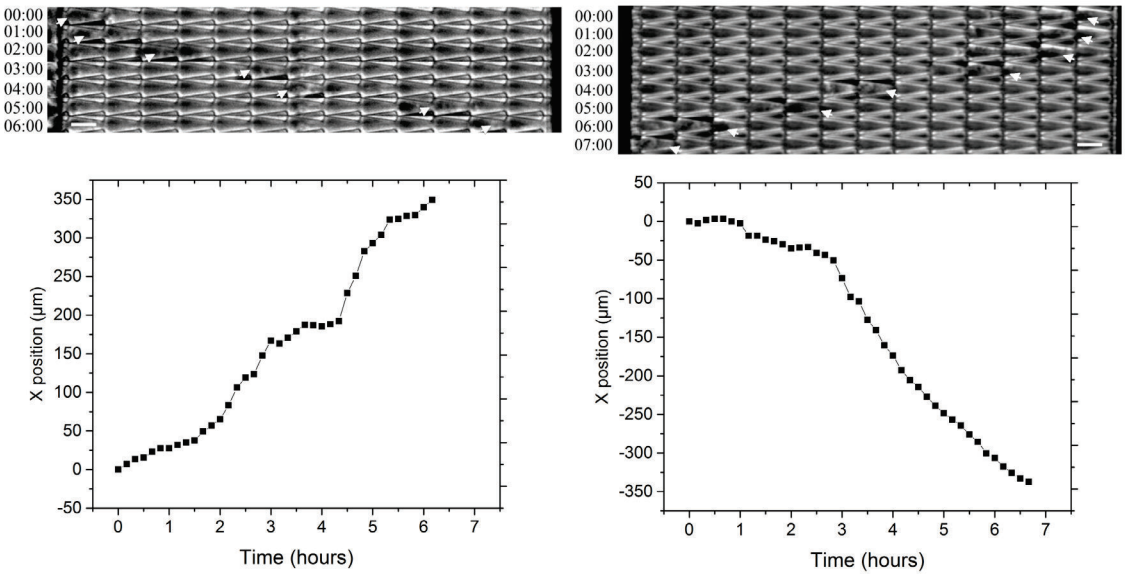

Figure 3.24: Example of a NIH3T3 cell migrating in α16i30 ratchet configuration and its corresponding trajectory. White arrow represents cell position. Left. In the ratchet direction. Right. Against the ratchet direction. Scale bar 20µm. Time in hh:mm. See Movie 11 and Movie 12.

We plot the trajectories of 7 cells tracked in the ratchet direction or against the ratchet direction (Figure 3.25). Here, all of the cells cross the entire microchannels in less than 10h. In fact, in the + direction, the mean total migrating time to cross the entire microchannels is equal to 8.6±7.7h and 9.0±4.3h against the ratchet direction: there is no statistical difference between the total migrating time in the ratchet + or ratchet – directions (One-way ANOVA, $p>0.05$). We observed here that cells did not change direction of migration. Once the cell entered the microchannel, it migrated until the end of the channel without changing direction.

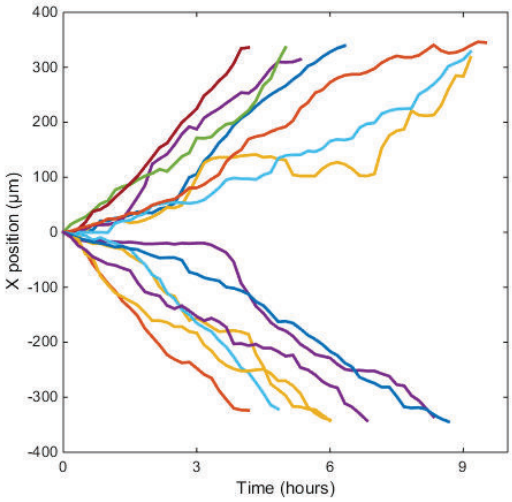

Figure 3.25: Trajectories of cells tracked in the α16i30 ratchet configuration.

Then, the persistent length, time and speed of the first persistent cell motion are measured. The distributions of persistent length, time and speed are similar in the ratchet + and – directions (Figure 3.26). In the ratchet + and – directions respectively, the mean persistent length is equal to 215±127µm and 233±119µm, the mean persistent time is equal to 4.6±3.2h and 5.5±3.3h and the mean persistent speed is equal to 52±25µm/h and 46±25µm/h. There are no statistical differences in the persistent length, time and speed distributions between the + and – directions. Like for α16i20 condition, we observed a peak in the persistent length distribution between 300-350µm. It corresponds to the cells which migrate persistently until the end of the microchannel without pausing. In-between, the distributions in persistent length are homogeneous. We did not observe any preferential direction of migration.

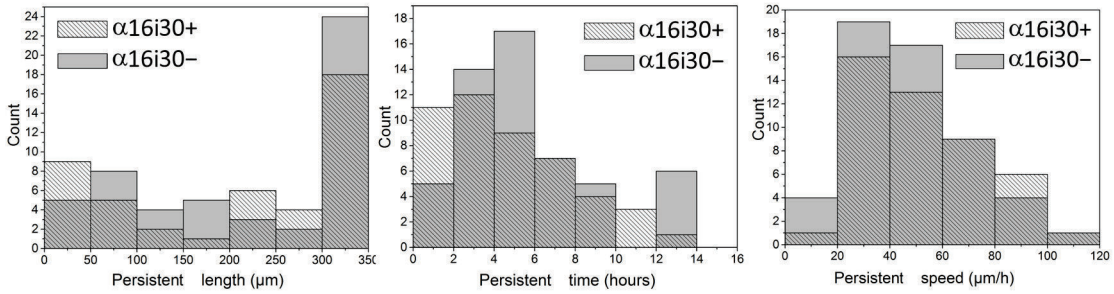

Figure 3.26: Persistent length, time and speed distributions of the first persistent motion of NIH3T3 cells migration in α16i30 microchannels in the ratchet direction (+) and against the ratchet direction (-). 6 independent experiments n+= 47 cells, n-=54 cells.

30µm^2 bottleneck area, allows some cells to cross the entire microchannels whereas other cells pause in between. However, the cell migration is impaired the same way in the ratchet + and – directions and no change in direction of migration is observed indicating that none of the direction is preferred. We did not see any rectification of cell migration with α16i30 condition.

3.3.1.3 α= 24°

Here, we set the angle α at 24°. Different bottlenecks are tested. Figure 3.27 shows images of the α24i20 and α24i30 ratchet microchannels.

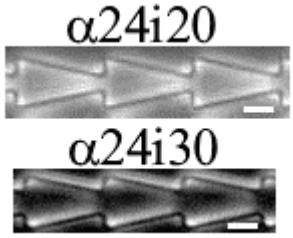

Figure 3.27: Images of α24i20 and α24i30 ratchets geometry. Scale bar 10µm.

3.3.1.3.1 α24i20

NIH3T3 cells migration has been followed in the α24i20 configuration. Only few cells have been tracked and to not overcrowd this presentation, the results are presented in the Appendix A.4.2.3. Experiments have to be repeated before concluding on the effect of this ratchet geometry on NIH3T3 cell migration.

3.3.1.3.2 α24i30

The same analysis as previously described is realized. Figure 3.28 shows examples of NIH3T3 cell migration in α24i30 microchannels in the ratchet direction (left) or against the ratchet direction (right) and their corresponding trajectory.

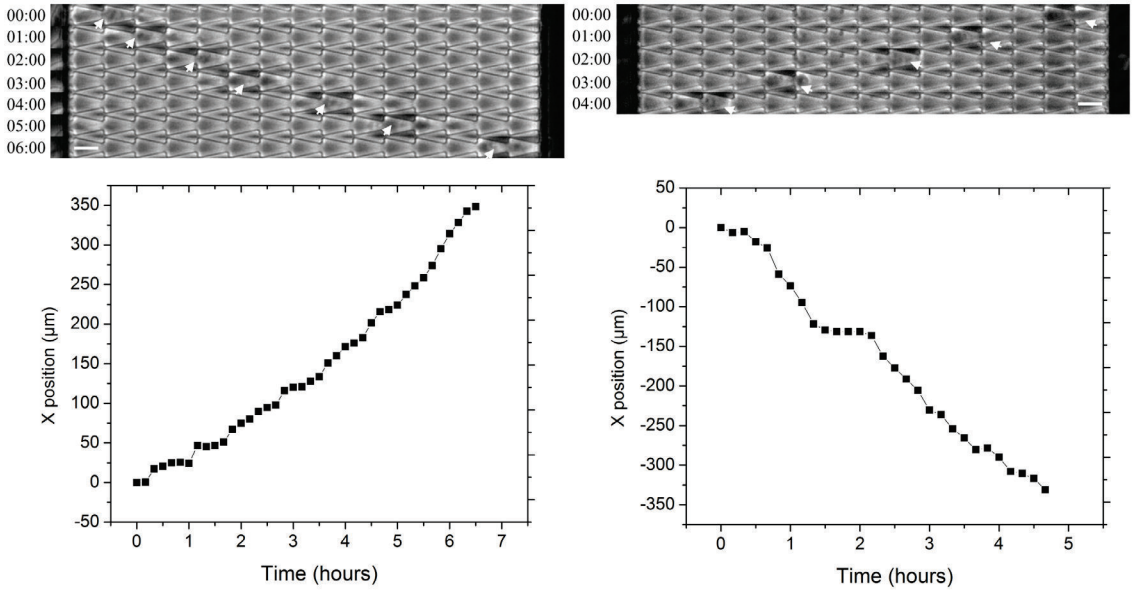

Figure 3.28: Example of a NIH3T3 cell migrating in α24i30 ratchet configuration and its corresponding trajectory. White arrows show the cell position. Left. In the ratchet direction. Right. Against the ratchet direction. Scale bar 20µm. Time in hh:mm. See Movie 13 and Movie 14.

Then, we plot the trajectories of 8 cells tracked in the ratchet direction or against the ratchet direction (Figure 3.29). Here, all of the cells cross the entire microchannels in less than 12h. In fact, in the + direction, the mean total migrating time to cross the microchannels is equal to 7.2±3.6h and 6.4±2.7h against the ratchet direction, there is no statistical difference between the distribution of total migrating time in the ratchet + and ratchet – directions (One-way

ANOVA, p>0.05). We observed here that cells did not change direction of migration. Once cell entered the microchannel, it migrated until the end of the microchannel without changing direction.

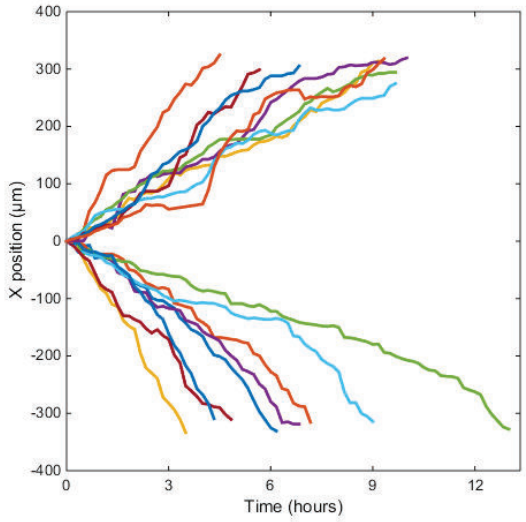

Figure 3.29: Trajectories of cells tracked in the α24i30 ratchet configuration

Then, the persistent length, time and speed of the first persistent cell movement are measured. The distributions of persistent length, time and speed are similar in the ratchet + and – directions (Figure 3.30). In the ratchet + and – directions, respectively, the mean persistent length is equal to 229±109µm and 227±116µm, the mean persistent time is equal to 4.3±2.4h and 4.1±2.3h and the mean persistent speed is equal to 66±34µm/h and 54±27µm/h. There are no statistical differences in the persistent length, time and speed distributions between the + and – directions. Like for α16i20 and α16i30 conditions, we observed a peak in the persistent length distribution between 300-350µm. It corresponds to cells which migrate persistently until the end of the microchannel without pausing. In-between, the distributions in persistent length are homogeneous. We did not observe any preferential direction of migration.

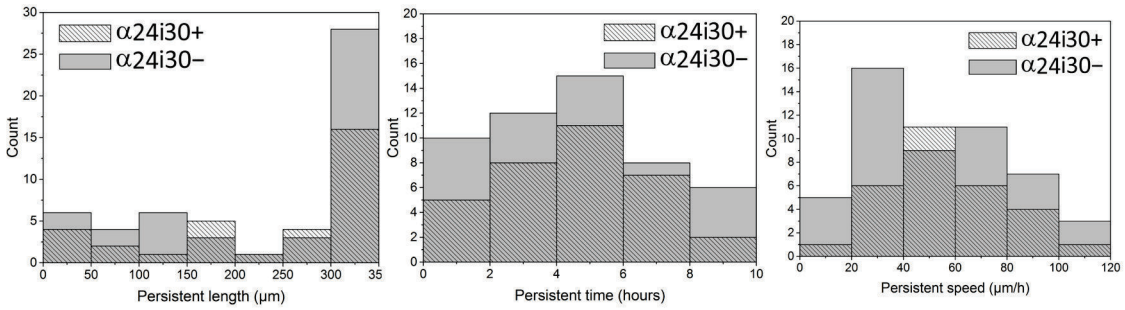

Figure 3.30: Persistent length, time and speed distributions of the first persistent motion of NIH3T3 cells migration in α24i30 microchannels in the ratchet direction (+) and against the ratchet direction (-). 6 independent experiments n+= 33 cells, n-=51 cells.

Compared to α16i30, we modified for α24i30 condition the angle α by keeping connecting area between ratchet units equal to 30µm². As for the previous ratchet conditions, this condition allows some cells to cross the entire microchannels whereas other cells pause in-between. However, the cell migration is impaired the same way in the ratchet + and – directions and no

change of direction of migration is observed, indicating that none of the direction is preferred. We did not observe rectification of cell migration in α24i30 condition.

In this part, we studied persistent length, time and speed distributions as well as the total migrating time of four different ratchet conditions: we modified the bottleneck area between ratchet units i or the angle α. 10µm² bottleneck ratchet microchannels is too constraining and did not allow cell migration over long distances. For the other microchannels ratchet tested, *i.e.* α16i20, α16i30 and α24i30, we did not observe any change in direction. In contrast to 2D flat and topographical surfaces, closed ratchet microchannels did not rectify cell migration[16,23]. However and compared to straight microchannels, we can see that the cell migration is directed but impaired in ratchet microchannels.

In the next section, I will summarize the migration of NIH3T3 cells in the different ratchets and straight microchannels and related it to cell migration on 2D flat surfaces. Then, I will justify the choice of the ratchet condition α16i20 to study cell migration for the rest of the PhD thesis.

3.3.2 Sum up of the closed microchannels conditions presented and choice of α16i20 ratchet microchannels

3.3.2.1 NIH3T3 cells in straight and ratchet microchannels

We studied migration of NIH3T3 cells in straight and ratchet microchannels. We varied the bottleneck area between ratchet units from 10µm², 20µm² to 30µm². As controls, we followed cell migration in straight microchannels whose cross-section area is equal to the ratchet bottleneck, *i.e.* 20µm² and 30µm². In order to compare the different conditions, we measured the total migrating time and the length, time and speed of the first persistent motion. First, I summarized the total migrating time, *i.e.* the time that cells take to cross the microchannels including the potential pauses (Figure 3.31). It includes cells which cross the microchannels without pausing and cells which pause in-between and then migrate until the end of the microchannel.

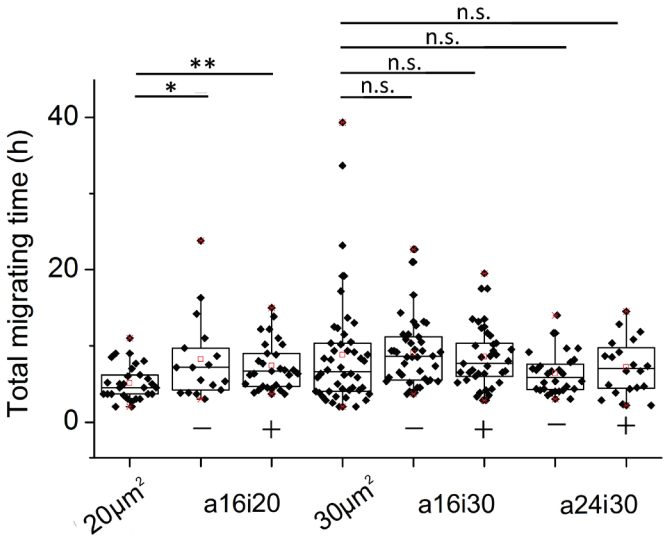

Figure 3.31: Summary of total time NIH3T3 cells need to cross the different microchannels. Red squares indicate the mean. Statistical test: One-Way ANOVA. * p<0.05; **p<0.01, n.s. non significant.

There are no statistical differences in total migrating time distributions for cells migrating in 30µm^2 straight and α16i30 and α24i30 ratchet microchannels. However, in α16i20 conditions, the total migrating time increases compared to 20µm^2 straight microchannels, suggesting that α16i20 impairs cell migration compared to straight and the other ratchet microchannels.

Then, we compared the distributions of the length, time and speed of the first persistent motion of NIH3T3 cells migrating in straight and ratchet microchannels as well as on 2D flat surfaces (Figure 3.32, Figure 3.33 and Figure 3.34). As mentioned previously, the first persistent motion corresponds to the movement of the cell from the first ratchet or equivalent distance in straight microchannels.

Figure 3.32 summarizes the persistent time distribution for NIH3T3 cells. Compared to 2D flat surfaces, confinement increases significantly the persistent time of all the microchannels ($p<0.001$), except for α16i10 condition. In addition, we note no difference in persistent time distributions of cells migrating in 20µm^2 straight and α16i20 ratchet microchannels. In agreement with total migrating time distribution, it strongly suggests the fact that cells need more time to cross the entire α16i20 microchannel, because of their pause in-between.

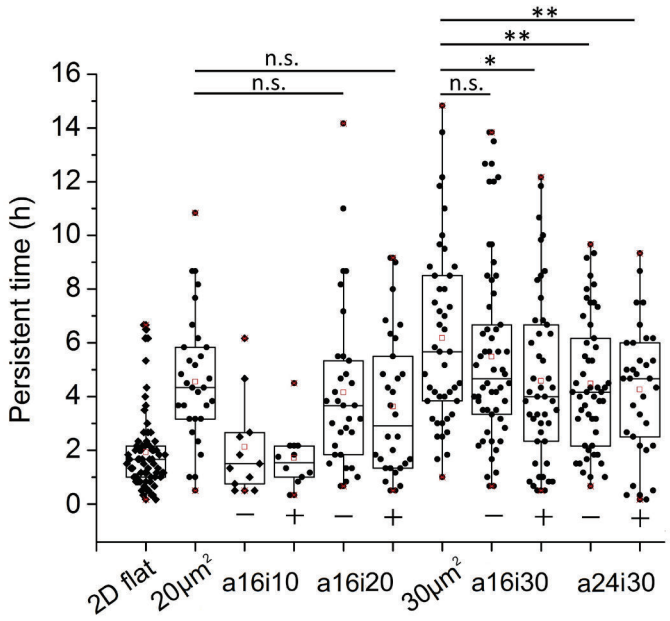

Figure 3.32: Summary of the persistent time distributions of the first NIH3T3 cells persistent motion. Red squares indicate the mean. Statistical test: One-Way ANOVA. * p<0.05; **p<0.01. n.s. non significant

A decrease in persistent time distribution is observed between 30µm^2 straight and α16i30 and α24i30 ratchet microchannels (Figure 3.32). It indicates that cells pause in these ratchet configurations compared to straight microchannels, but the total cell migration time is not affected.

Figure 3.33 summarizes the persistent speed distributions of NIH3T3 cells.

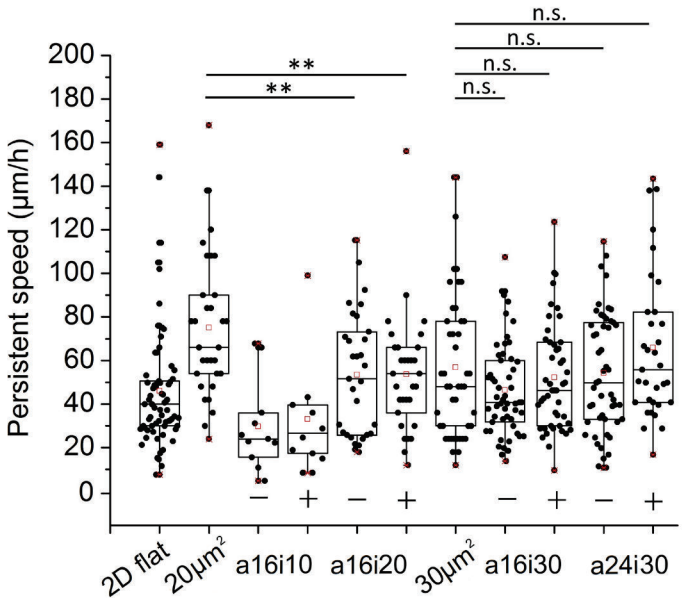

Figure 3.33: Summary of the persistent speed distribution of the first NIH3T3 cells persistent motion. Red squares indicate the mean. Statistical test: One-Way ANOVA. **p<0.01, n.s. non significant.

Compared to 2D flat surfaces, confinement increases significantly the persistent speed of NIH3T3 cells migrating in α16i30 in the ratchet + direction and in 20µm^2 straight microchannels (p<0,01). But no significant differences were observed in the other configurations compared to cells migrating on 2D flat surfaces. In addition, compared to 20µm^2 straight microchannels, the persistent speed is significantly reduced in α16i20 (p<0,01), suggesting again that α16i20 ratchet impairs cell migration. There are no significant differences between persistent speed distributions of 30µm^2 straight and α16i30 and α24i30 ratchet microchannels (Figure 3.33).

The last parameter we measured is the persistent length of NIH3T3 cells migrating in the different microchannels (Figure 3.34).

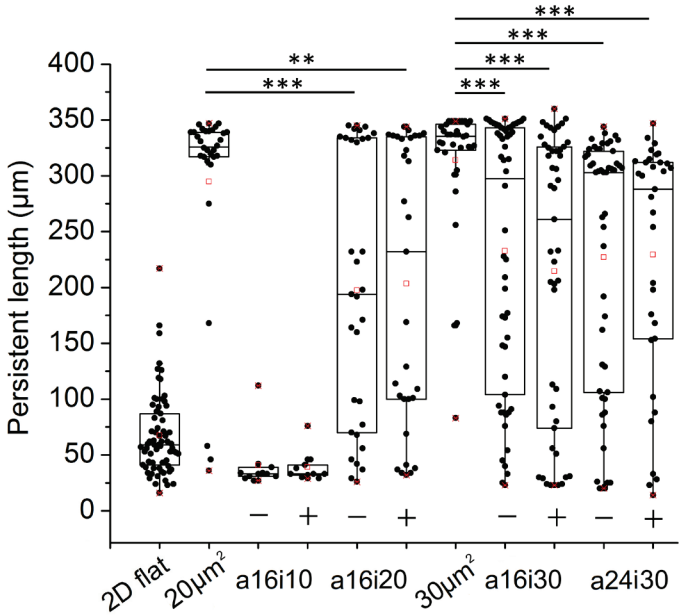

Figure 3.34: Summary of the persistent length distribution of the first NIH3T3 cells persistent motion. Red squares indicate the mean. Statistical test: One-Way ANOVA.; **p<0.01;*p<0.001.**

Compared to 2D flat surfaces, confinement increased significantly the persistent length of NIH3T3 cell ($p<0.001$), excepted for α16i10 condition. In α16i10 condition, cells migrate one ratchet, then pause or die. Previously in the lab, Amélie Godeau measured, in 10µm^2 straight microchannels, a mean persistent length equal to 274±42µm[51]. It indicates that cells can migrate in 10µm^2 straight microchannels. However, the cells cannot migrate in the ratchet configuration with 10µm^2 bottleneck, in which cells have to strongly deform and then relax to move from one ratchet to another one. We observe that in 20µm^2 and 30µm^2 straight microchannels, cells migrate persistently until the end of the microchannels with only few cells which pause in-between. The mean persistent length is closed to 350µm, the length of the microchannels, *i.e.* 295±90µm and 269±77µm in 20µm^2 and 30µm^2 straight microchannels respectively. Interestingly, we observe that persistent length distribution is dispersed in all ratchet microchannels compared to straight microchannels (Figure 3.34). It indicates that ratchet geometry impairs cell migration, because cells pause and sense their topographical environment. The "Pushing off the walls" model is kept to explain cell migration in confined microchannels. In addition, and in contrast to what we expected, none of the direction is favored and no cell rectification is observed, *i.e.* change in direction of migration. On 2D flat and topographical surfaces, ratchetaxis rectified cell motion[15,16]. As we proposed previously, it seems that the entry inside confined microchannels sets the direction of migration.
However, we can see differences between ratchet microchannels: in the ratchet and against the α16i20 microchannels direction, the mean persistent length is lesser than in α16i30 and α24i30 (Figure 3.34. Red squares).

The next point is to determine, for the rest of the study, which configuration affects the most cell migration without preventing it. We saw that α16i10 is too restrictive to allow fast cell migration. Cell migration in α16i20 ratchet is affected in term of total migrating time, persistent speed and length, whereas α16i30 and α24i30 affect cell migration in terms of persistent length and time. According to the ratchet geometry, we can look at how the nucleus has to deform to go to one ratchet to the other one.

By definition, α16i20 condition has 20µm^2 bottleneck area between ratchet units, compared to 30µm^2 in α16i30 and α24i30 ratchet microchannels. In every configuration, nucleus has to deform to fit to a ratchet unit and to pass to the next ratchet. We estimated the nucleus cross-section area roughly at 90µm^2.

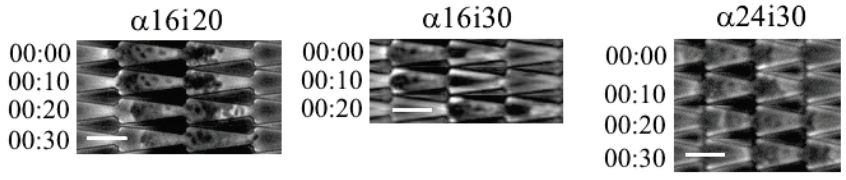

Figure 3.35: Time series of NIH3T3 cell crossing the ratchet bottleneck in α16i20, α16i30 and α24i30 ratchet microchannels. Scale bar 20µm. Time in hh:mm.

Nucleus deformation is more important in α16i20 ratchet microchannels compared to α16i30 and α24i30, *i.e.* 4,5 versus 3 fold cross-section reduction (Figure 3.35).
Altogether, the strong nucleus deformation, increased total migrating time and decreased persistent speed and length of α16i20 ratchet convinced us to probe the efficiency of α16i20

ratchet microchannels to direct NIH3T3 cells migration in the open microchannels configuration and in the presence of chemical gradient. But before presenting this part of the project, we wonder if reducing cell confinement allows changes in the direction of migration. We used dHL60 cells which has a smaller volume to answer this point.

3.3.2.2 dHL60 cells in straight and ratchet microchannels

In the closed configuration, we designed the ratchet unit to fully confined NIH3T3 cells, *i.e.* the ratchet volume is equal to the mean volume of NIH3T3 cell. Results indicate that cells cannot change direction of migration in the closed microchannels. We studied also the migration of dHL60 cells in the same ratchet geometry, α16i10, α16i20, α16i30, α24i20 and α24i30 and straight microchannels. The volume of HL60 cells is half the volume of ratchet unit (HL60 cell: 800±210µm^3, ratchet unit: 1500µm^3), indicating that the cells are not confined in a ratchet unit but are confined while migrating between two ratchets.

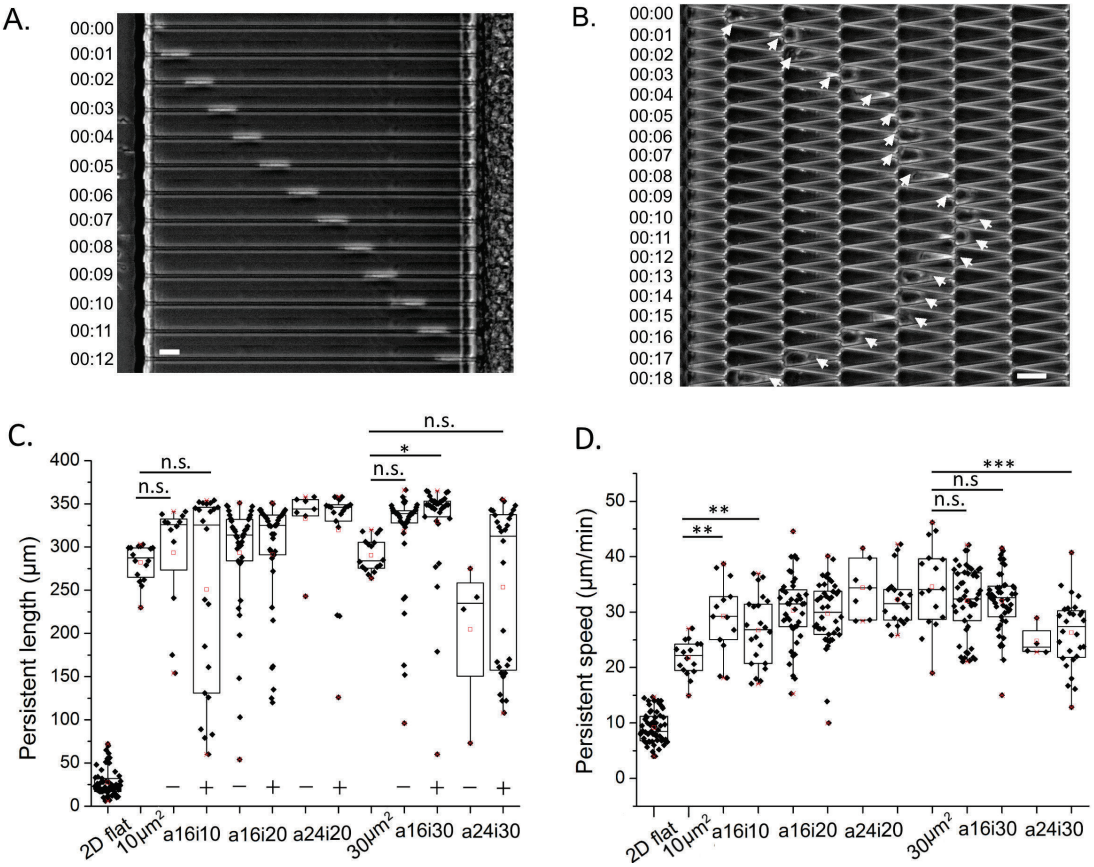

Figure 3.36: dHL60 cells migration in straigth and ratchet microchannels. A. Time series of a dHL60 cell migrating in 10µm² straight microchannel. B. Time series of a dHL60 cell migrating in α16i10 ratchet microchannels. Time in hh:mm. Scale bar 20µm. See Movie 15 and Movie 16. C. Persistent length distributions of dHL60 cells migrating in closed straight and ratchet microchannels. D. Persistent speed distributions of dHL60 cells migrating in closed straight and ratchet microchannels. $n_{2D\ flat}$= 19cells, $n_{\alpha16i10+}$= 22 cells, $n_{\alpha16i10-}$= 12 cells, $n_{\alpha16i20+}$= 42 cells, $n_{\alpha16i20-}$= 42 cells, $n_{\alpha16i30+}$= 35 cells, $n_{\alpha16i30-}$= 46 cells, $n_{\alpha24i20+}$= 18 cells, $n_{\alpha24i20-}$= 7 cells, $n_{\alpha24i30+}$= 28 cells, $n_{\alpha24i30-}$= 4 cells, $n_{10\mu m2}$= 16 cells and $n_{30\mu m2}$= 16 cells. Red squares represent the mean. Statistical test: One-Way ANOVA.; **p<0.01;*p<0.001, n.s. non significant.**

Figure 3.36A and B represents the migration of dHL60 cells in10µm² and α16i10 ratchet microchannels. This condition is the most restrictive one tested. There, dHL60 cell changes

direction of migration whereas NIH3T3 cells were not able to migrate. As for NIH3T3 cells, we measured the persistent length and speed distributions of dHL60 cells migrating in straight and ratchet microchannels in order to compare conditions between them. The persistent length and speed distributions are presented Figure 3.36 C. and D. As for NIH3T3 cells, we clearly observe that confinement increases the persistent length and speed of dHL60 cells compared to 2D flat surfaces (One-Way ANOVA $p<0.001$). α16i20, α24i20 and α16i30 ratchet microchannels do not affect dHL60 cells migration, as the persistent lengths are closed to the maximal length of the microchannel (α16i20+=291±78µm, α16i20-= 293±65µm, α16i30+= 329±59µm, α16i30-= 318±56µm, α24i20+= 333±40µm, α24i20-= 320±64µm, 10µm^2 straight= 282±21µm and 30µm^2 straight= 264±21µm). In α24i30 ratchet microchannels, we observe that cell migration is impaired. However, this phenomenon has to be confirmed with a higher number of cells. In contrast, in α16i10 ratchet microchannels, dHL60 cells migration is impaired in terms of persistent length only in the ratchet direction but not against the ratchet direction, *i.e.* α16i10+= 251±113µm, α16i10-= 293±66µm. It should be confirmed by increasing the number of cell against the ratchet direction.

In fact, we know that these cells are smaller and can highly deform their nucleus compared to NIH3T3 cells. We stained for the nucleus with DAPI while cells are migrating. Figure 3.37 shows examples of two dHL60 cells migrating inside α16i10 ratchet microchannels. The nucleus of the "left" cell is strongly deformed and elongated and the cell crosses two ratchets in 30 seconds. The right cell has a round nucleus, whose shape is comparable to NIH3T3 nucleus. This cell deforms its nucleus while reaching the bottleneck and crosses the ratchet in 5 minutes. These two extreme examples confirm that the nucleus is the factor limiting the cell migration and its strong or weak deformation favors or inhibits cell migration respectively.

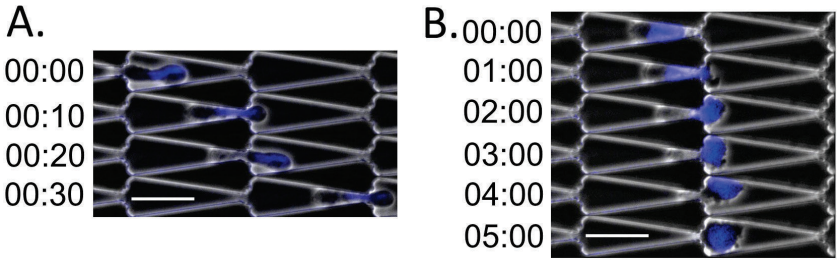

Figure 3.37: Examples of time series of dHL60 cells migrating in α16i10 ratchet microchannels. DAPI in blue stains for the nucleus. Left. Nucleus of the cell is strongly deformed. Right. Nucleus of the cell is round. Time in mm:ss. Scale bar 20µm.

Altogether, we first observed that dHL60 cells not highly confined can change direction of migration. Furthermore, persistent length distributions of dHL60 cells migrating in ratchet microchannels reveals that 20µm^2 and 30µm^2 bottleneck area between ratchet units did not impair cell migration compared to straight microchannels. We observed that cell migration is impaired in the ratchet direction of α16i10 ratchet migration. In addition, the deformation of dHL60 cell nucleus is the key criterion which allows quick cell migration. Moreover, for these reasons, it confirms that α16i20 is the best ratchet condition to potentially rectify NIH3T3 cells migration.

To conclude this first part, we measured the total migrating time, persistent length, time and speed of NIH3T3 and dHL60 cells migrating inside 20µm^2 and 30µm^2 straight and α16i10, α16i20, α16i30 and α24i30 ratchet microchannels. For the rest of the presentation, I will only present persistent length distribution which is the parameter for which we observed striking differences. In every ratchet conditions tested, we saw impairment of cell migration compared to straight microchannels but we did not see any preferential NIH3T3 cells migration in the ratchet or against the ratchet direction. In the next sections, we will focus on the ratchet condition which impairs the most cell migration, *i.e.* α16i20. We will use 20µm^2 cross-section area in straight microchannel as control. In fact, it seems that cells entry into the microchannels sets the direction of migration, potentially prevented the rectification of cell migration. We tried to avoid this problem by designing new microchannels. I will present the new design in the next section.

3.3.3 Closed microchannels: new design to prevent entry-biased cell migration.

To overcome the problem of entry which set cell polarity and then direction of migration, the ideal solution would be to insert cells in the middle of the closed microchannels inside a ratchet unit, then let the cells spontaneously polarize and observe cell migration, as observed in previous ratchetaxis studies [15,16]. Unfortunately, it is technically not possible to do with the microchannels we had at our disposable, because of the micrometer dimensions of a ratchet unit. The best solution would be to design a new closed configuration, in which the cells would have the possibility to enter the microchannels in the ratchet direction or against the ratchet direction. We designed the mask below (Figure 3.38A) and went to microfabrication process to produce the new chip. In this configuration, cells are injected in the central seeding channel following the protocol detailed in the Material & Methods section. Cells adhere to the surface.

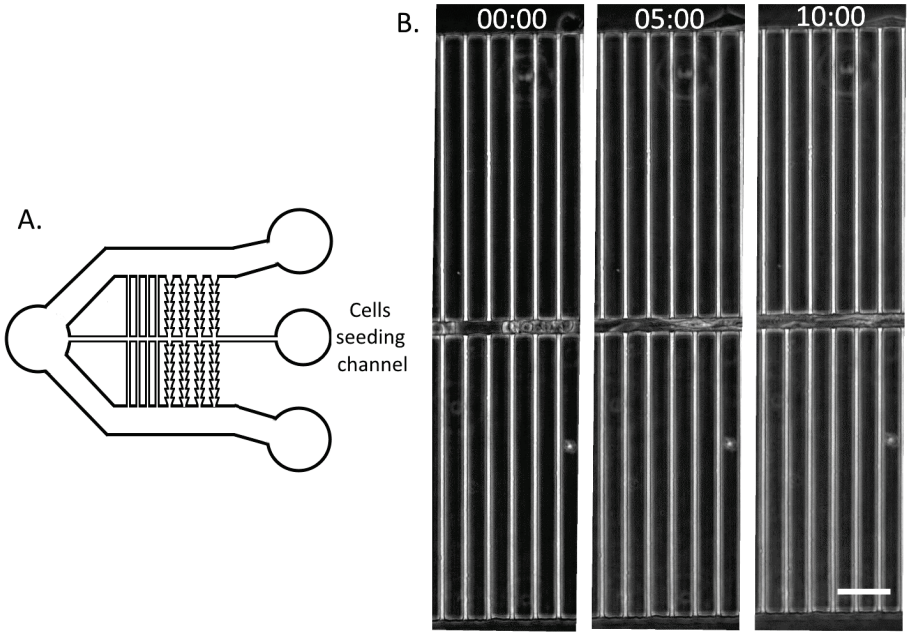

Figure 3.38: New configuration tested to allow spontaneous cells entry inside microchannels. A. Schematic of the new microchannels design. B. Time series of NIH3T3 cells migrating in the seeding channel and not entering in the microchannels. Time in hh:mm. Scale bar 50µm.

However, the expected effect was not observed: cells prefer to migrate in the central channel rather than entering into perpendicular straight microchannels (Figure 3.38B). It shows again that cells accumulation at the microchannels entry in the only way to make them entering without using a chemical gradient.
In fact, if we do not want to set the cell entry, the best option is to simply remove the top layer of the microchannels. The cells will be confined from the sides but not from the top: it is the open microchannel configuration. As explained in the Material & Methods (page 84), we managed to produce the open microchannels configuration and to follow cells migration across time. The configuration and results are presented in the next section.

3.4 Cell migration in the open microchannels configuration

3.4.1 Configuration

In the previous section, we determine α16i20 as the configuration which impairs the most cell migration in the closed microchannels configuration. We then used the same ratchet design to produce ratchet open microchannels and straight open microchannels as a control (Figure 3.39). The microchannels walls are high enough to trap the cells in-between.

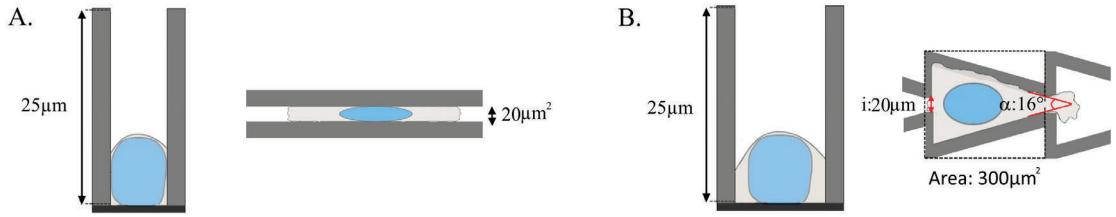

Figure 3.39: Schematics of the open straight (A.) and ratchet (B.) microchannel configurations.

As explained in the Material & Methods section, cells are seeded in the middle of the microchannels. Figure 3.40 schematics the open microchannels. Like in the closed configuration, the + direction is defined as the ratchet direction. There, in contrast to closed microchannels configuration, cells are free to migrate in the ratchet direction or against the ratchet direction in the ratchet and straight microchannels (Figure 3.40).

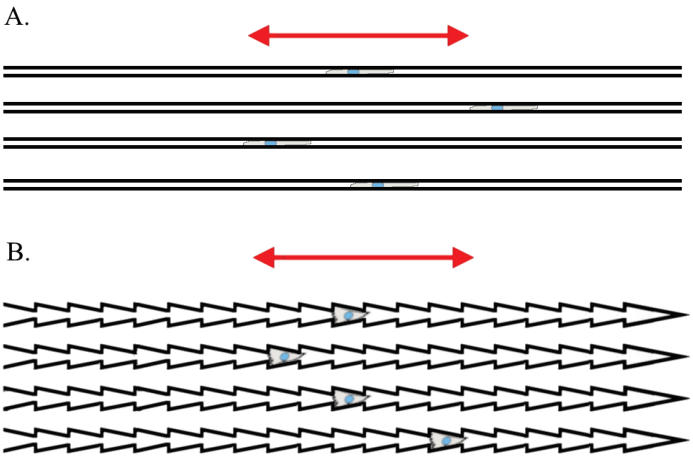

Figure 3.40: Schematics of the open straight (A.) and ratchet (B.) microchannels configurations. Red arrow indicates in which direction cells can migrate.

As explained in the closed microchannel configuration (page 105), we tracked cell migration and the initial cell position is set at 0. We tracked cells which adhere at the center of the microchannels. There, the length of the microchannel (1mm) is long enough to not limit cell migration (Figure 3.40). The cell which start migrating in the ratchet direction will have positive values, whereas the cell which start migrating against the ratchet direction will have negative values. For each configuration, we tracked the cell in straight and ratchet open configurations for 12h and observed any potential directed cell migration. In addition, we measured the persistent length, time and speed distribution of the first persistent cell motion**.** It allows the fair comparison of cell migration between the open and closed configurations.

3.4.2 NIH3T3 cell migration in the open 20µm² straight and α16i20 ratchet microchannels

Figure 3.41 shows example of NIH3T3 cells migrating in straight (Figure 3.41A) and ratchet (Figure 3.41B) open microchannels for 12hours and their corresponding trajectory.

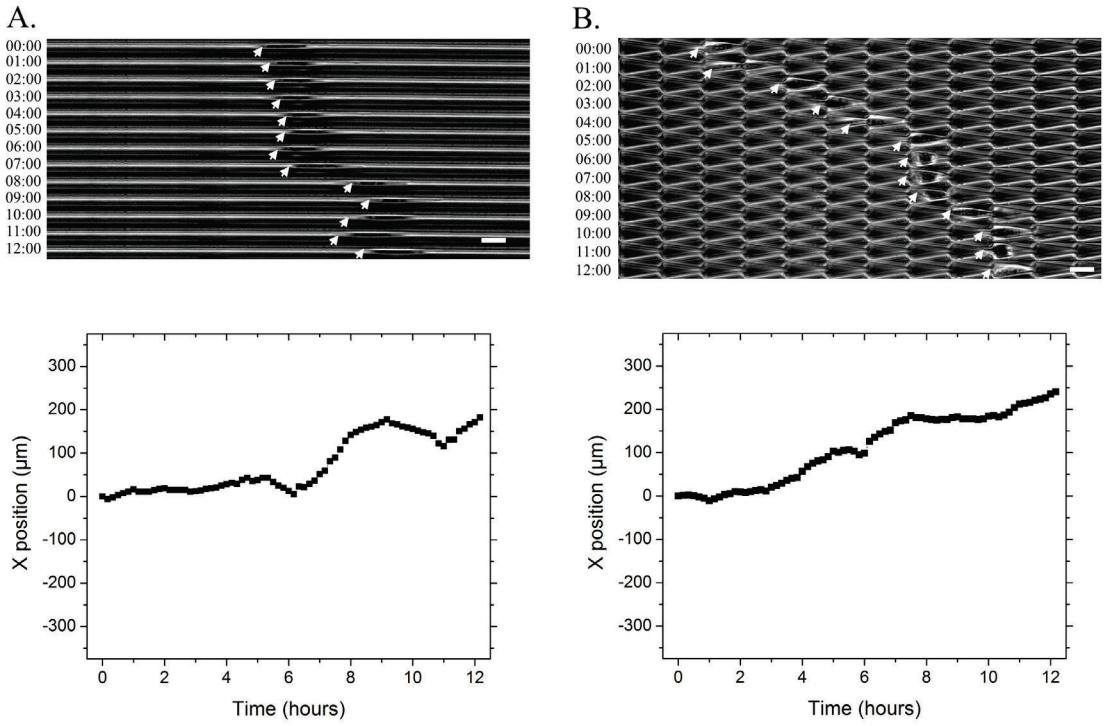

Figure 3.41: Examples of a NIH3T3 cell migrating in open 20µm² straight and α16i20 microchannels and its corresponding trajectory. Scale bar 20µm. Time in hh:mm. See Movie 17 and Movie 18.

Then, we plot the trajectories of 8 cells tracked in straight (Figure 3.42A) and ratchet (Figure 3.42B) microchannels. Here, we observed that cells can change direction of migration in straight and ratchet open microchannels.

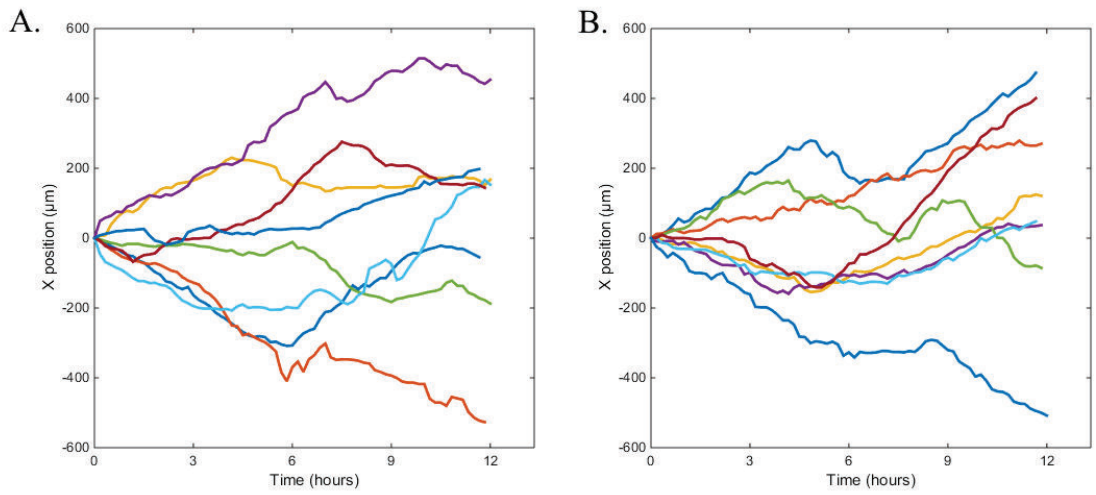

Figure 3.42: Trajectories of 8 cells tracked in straight (A.) and ratchet (B.) open microchannels.

Then, from the 12h trajectories, we can extract information on the cell trajectory such as the angular distribution, *i.e.* angular orientation of migration for each time point, and the mean displacement vector, *i.e*. average vector between the initial and final positions of each cell (Figure 3.43). It shows that in the straight open microchannels, cells migrate in the x-axis in both senses, as revealed by the angular distribution. The mean vector displacement value is in the noise of the measure, indicating that on average, final cells position is close to the initial cell position, *i.e.* no directed cell migration (Figure 3.43A). In contrast, in the ratchet open microchannels, the angular distribution follows the x-axis but is directed towards the + direction. In addition, the mean displacement vector is equal to +84µm and indicates that, 12h after cell migration start, final cells position is on average in the ratchet direction (Figure 3.43B). It highlights that, over long time period, cell migration is rectified in the ratchet direction while we do not observe any rectification in straight open microchannels.

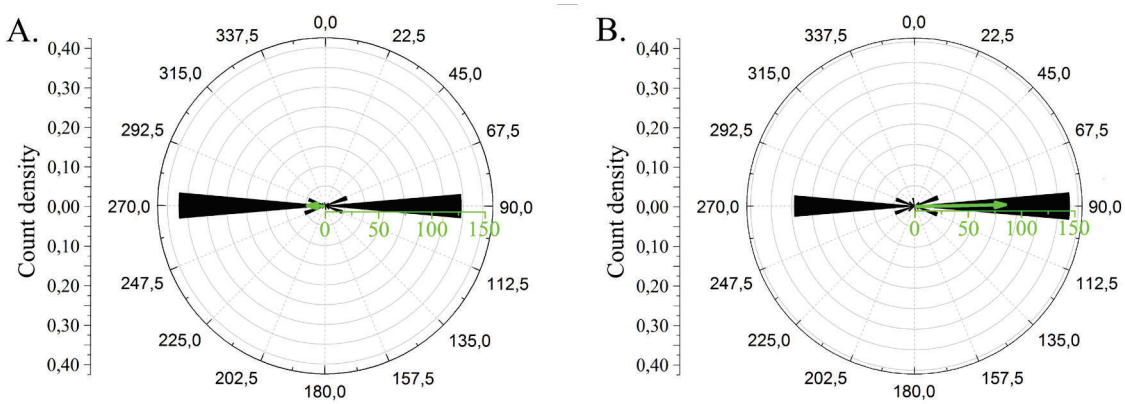

Figure 3.43: Angular distribution and mean displacement of cells migrating in straight (A.) and ratchet (B.) open microchannels. Black plots represent angluar distribution of the cells and green arrows represent mean displacement vector which is the mean vector between initial and final position 12hours later. Scale bar is in µm. (A.) Every 10 min, ni= 2107 steps and n= 31 cells. the mean displacement vector is in the measure noise (B.) Every 10 min, ni= 3625 steps and n= 58 cells. The mean displacement vector is equal to +84µm.

Then, the persistent length, time and speed distributions were measured. Figure 3.44 presents the persistent length distribution. The persistent time and speed distributions are presented in Appendix A.4.3.1.

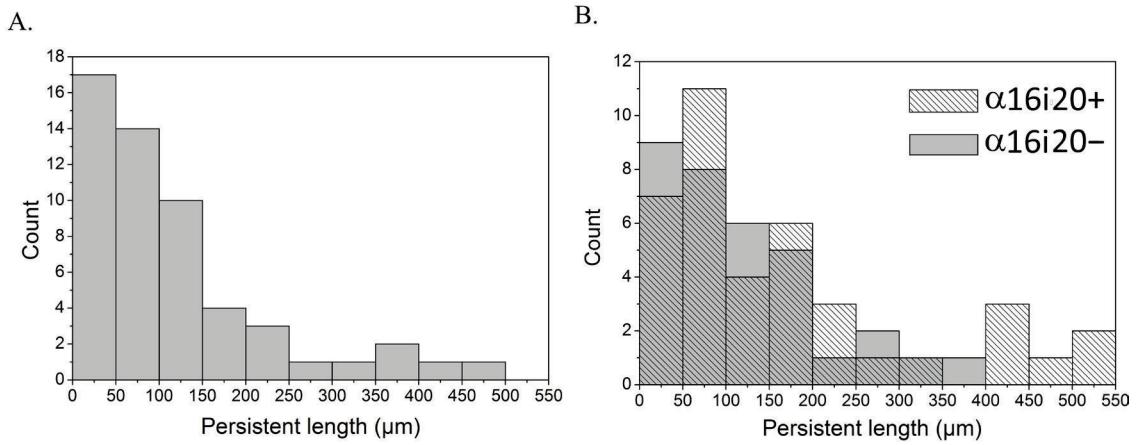

Figure 3.44: Persistent length distributions of the first persistent motion of NIH3T3 cells migration in 20µm² straight (A.) and ratchet (B.) open microchannels. 8 independent experiments $n_{straight}$= 54cells, n+= 39 cells and n-=33 cells.

In the ratchet + and – directions, respectively, the mean persistent length is equal to 169±151µm and 121±95µm. In straight open microchannels, it is equal to 120±106µm. The persistent length distributions in the ratchet microchannels are not statistically different to the straight microchannels. However, even if we did not measure any statistical differences in persistent lengths in ratchet + and – directions, we observed that the persistent length distribution in the ratchet direction is shifted to the highest values (Figure 3.44).

Altogether, it reveals that the open ratchet microchannel configuration directs cell migration in the ratchet direction and more importantly is able to rectify cell migration.

3.4.3 Comparison of cell migration in the closed and open microchannels configurations

In this section, I will compare the migration of NIH3T3 cells in the open and closed straight and α16i20 ratchet microchannels. First, from the cell trajectory, we can extract the percentage of cells which pause and potentially change direction of migration (Figure 3.45). In the open microchannels configurations, 90% of cells pause and half of the cells change direction of migration. In the straight closed microchannels, 20% of cells pause and 3% of the cells changes direction of migration. In the closed ratchet microchannels, 60% of the cells pause and less than 10% of the cells change direction of migration.

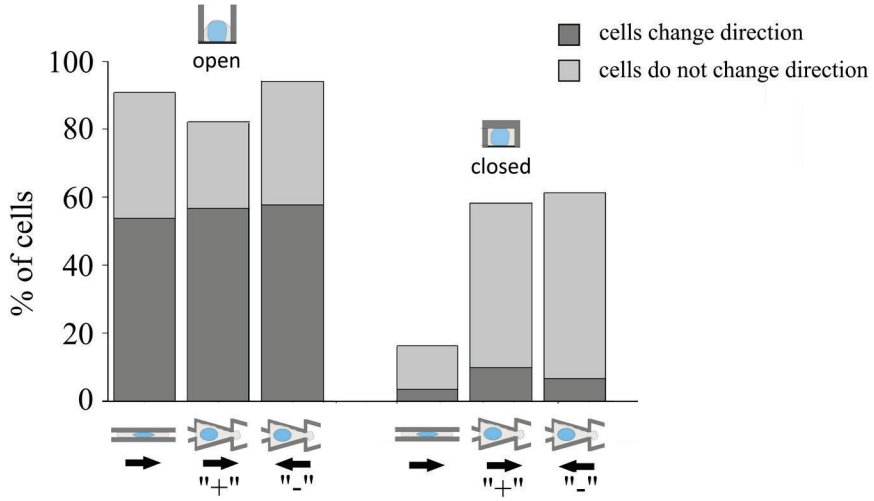

Figure 3.45: Summary of the percentage of NIH3T3 cells which pause during their migration and then migrate in the same direction (light grey) or change direction of migration (dark grey). The open and closed configuration with 20µm² straight and α16i20 ratchet microchannels are represented. Schematics represents top and side views of the cell. Number of cells which change direction over total number of cells: Open straight:29/54, open ratchet +: 22/39, open ratchet -19/33, closed straight: 1/31, closed ratchet +: 3/31, closed ratchet -: 2/31.

It shows that the open microchannels gave the possibility to the cells to change direction whereas the closed microchannels do not allow it. Then, the persistent length of migrating cells in the open and closed microchannels is compared (Figure 3.46). First, we observed that the persistence increases with the confinement. Then, we observed that the ratchet favored the cell migration in the open microchannels whereas it did not in the closed microchannels. The persistent time and speed distributions are presented in Appendix A.4.3.2.

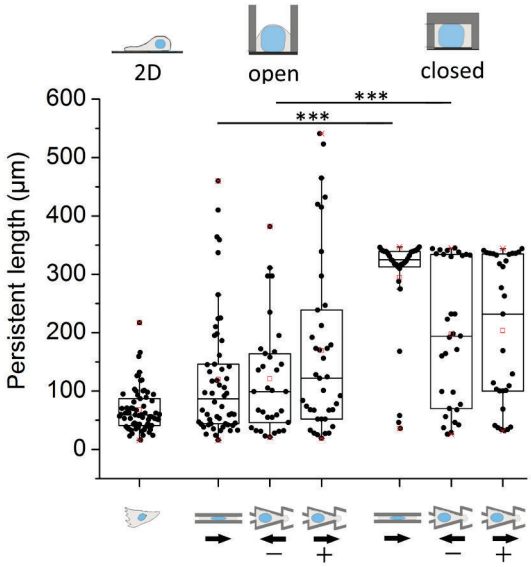

Figure 3.46: Summary of the persistent length distribution of NIH3T3 cells migrating on 2D flat surfaces, in open and closed, 20µm² straight and α16i20 ratchet microchannels configurations. Schematics represents top and side views of the cell. Statistical test: One-Way ANOVA, *** p<0.001. non significant differences between open and closed microchannels in the ratchet direction.

Altogether, we showed that ratchetaxis exists under low confinement, *i.e.* open microchannels. We rectified cell migration under confinement due to the presence of asymmetric motifs in the

cell environment and without ant chemical gradient. Cell polarity is set at the cell entry in closed microchannels and strong confinement did not allow change in direction of migration. I will present in the next paragraph NIH3T3 cells migration in response to serum gradient, with the classical Boyden chamber and pipette experiment, then inside microchannels with the microfluidic we develop in the lab. Finally we studied migration of NIH3T3 cells in closed straight and ratchet microchannels with a serum gradient.

3.5 Chemotaxis experiment: cell migration towards serum gradient

3.5.1 Classical experiments: Pipette and Boyden chamber experiments

We first tested the efficiency of serum gradient to direct NIH3T3 cells migration with classical chemotaxis experiments, *i.e.* Boyden chambers experiment and pipette experiment on 2D flat surfaces. After starving NIH3T3 cells for 4 hours, Boyden experiments were prepared as explained in the Material & Methods section page 89. To check the efficiency of a chemoattractant to direct cell migration, we need a negative control which shows the number of cells migrating in the absence of chemical gradient. In our experiments, 1% serum medium is placed in the upper and lower chambers, it is the negative control. We studied cell migration towards serum gradient: we placed 1% serum medium in the upper chamber and 10%serum medium in the lower chamber. In Boyden chamber experiment, NIH3T3 cells efficiently migrate towards 10% serum and accumulate in the lower membrane with on average 12.4±5.0 cells per fields of view compared to 2.3±1.4 cells per fields of view in 1%serum.
Then, we set-up a pipette experiment which allow the local delivery of chemoattractant at the cell periphery and to follow cell migration on flat surfaces. The protocol is explained in details in the Material & Methods section page 88. We first treated the coverslip with PLL-g-PEG to reduce cell attachment to the coverslip. We observed the directed cell migration of weakly attached cells towards the pipette delivering 10%serum (Figure 3.47). The Dextran-TRITC allows the visualization of the chemical gradient. In contrast, as a control, we only injected Dextran-TRITC. Directed cell migration was not observed.

Figure 3.47: NIH3T3 cell migration towards a pipette delivering 10% serum and TRITC-Dextran. Coverslip is treated with PLL-g-PEG to reduce cell attachment to the surface. Scale bar 20µm. Time in hh:mm. Representative of 4 independent experiments. See Movie 19.

Pipette and Boyden chamber experiments show migration of NIH3T3 cells in the direction of the highest concentration of serum gradient and accumulation of the cells in the lower membrane of the Boyden chamber respectively. NIH3T3 cells respond to serum gradient. However the aim of this PhD thesis is to follow cell migration in confined and controlled environment. In the next section, I will present the microfluidic configuration used to form chemical gradients and follow cell migration.

3.5.2 Chemotaxis in controlled and confined environments

3.5.2.1 Experimental set-up

To form a chemical gradient, the continuous injection of medium is required. To do that, the "ladder" chamber is the simplest design (Figure 3.48)[21]; it contains two channels entries, one channel exit and microchannels in the center in which gradient is formed and where cells are migrating.

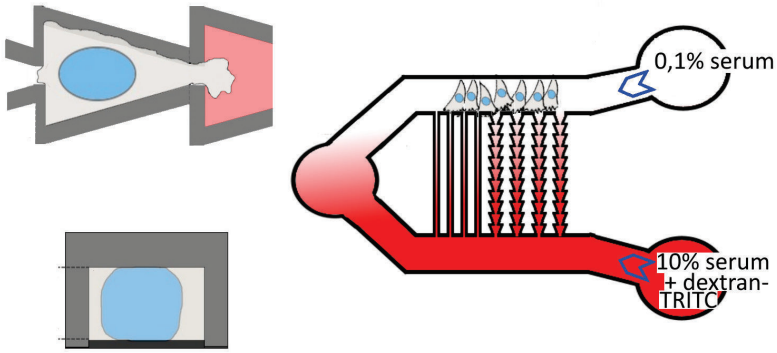

Figure 3.48: Schematics of the experimental set-up used to form chemical gradient inside microchannels. A seringue pump injects 0.1% serum medium and 10% serum + Dextran-TRITC medium (Blue empty arrows).

The two channels entries allow first the injection of the chemoattractant medium, i.e. 10% serum plus Dextran-TRITC medium, and second the injection of medium without chemoattractant. Both solutions are contained in two syringes connected to a syringe pump through tubings. Once the pump start injecting, a chemical gradient forms inside microchannels by diffusion. We can characterize the soluble gradient by measuring the fluorescent intensity of Dextran-TRITC (Figure 3.49).

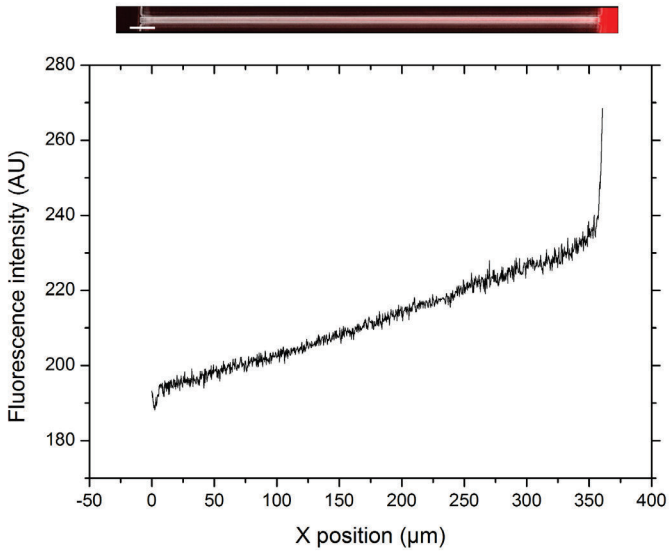

Figure 3.49: Chemical gradient is linear inside microchannels. First row. Image of a 20µm² microchannel and chemical gradient visualized with Dextra-TRITC. Scale bar 20µm. Bottom. Fluorescence intensity of Dextran-TRITC as a function of the position in the microchannel and 10h after the beginning of the acquisition.

We observed that the gradient is stable for up to 20h. The next step is to see if NIH3T3 cells detect the serum gradient and migrate towards the highest concentration under confinement.

3.5.2.2 Directed cell migration in closed microchannels towards 10% serum gradient

We first observed the migration of NIH3T3 cells in 75µm² cross-section area microchannels. Cells are confined from the top but not from the sides. In the presence of 10% serum gradient, cells entered the microchannels and migrated directionally towards the highest concentration of the serum gradient (Figure 3.50).

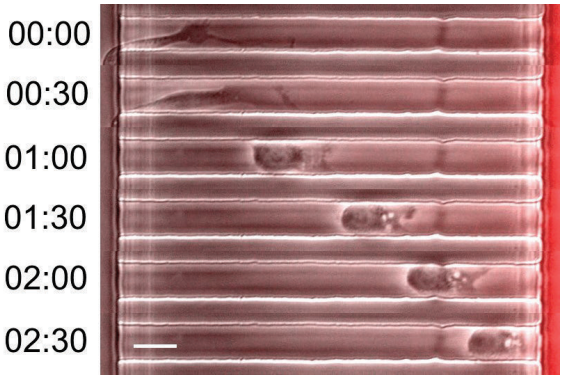

Figure 3.50: Time series of a NIH3T3 cell migrating in 75µm² cross-section area microchannel towards 10% serum gradient visualized by Dextran-TRITC. Scale bar 20µm. Time in hh:mm. See Movie 20.

None of the cells migrate against the chemical gradient. In the next section, I will present the migration of NIH3T3 cells in closed 20µm² straight and α16i20 ratchet microchannels.

3.5.2.3 Directed cell migration in 20µm² straight and α16i20 ratchet closed microchannels towards 10% serum

As for the closed and open microchannels configurations, I will be presenting first an example of NIH3T3 cell migrating in straight and ratchet microchannels, then the plot of its corresponding trajectory (Figure 3.51) and then the persistent length distributions (Figure 3.52).

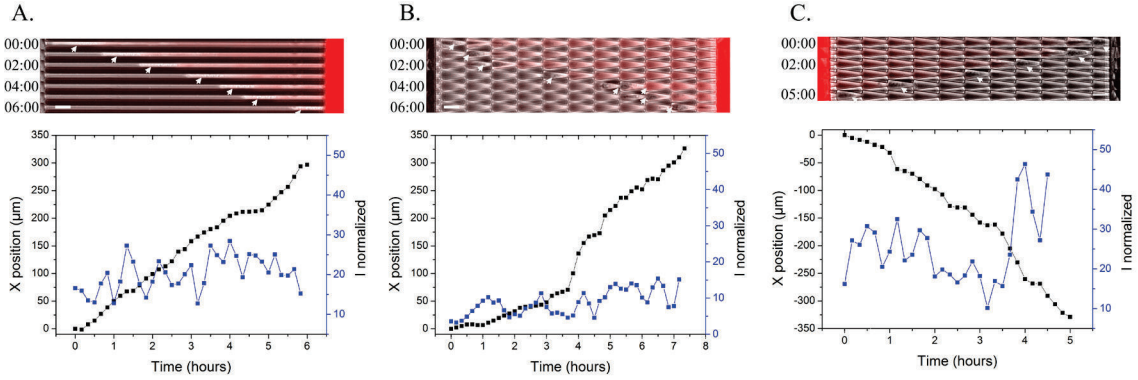

Figure 3.51: Examples of a NIH3T3 cell migrating in 20µm² straight and α16i20 closed microchannels in the presence of 10% serum gradient and its corresponding trajectory. Scale bar 20µm. Time in hh:mm. See Movie 21, Movie 22 and Movie 23.

Figure 3.51 shows the cell trajectory and the Dextran-TRITC fluorescence normalized. We normalized the fluorescence intensity at the cell front by subtracting the fluorescence intensity at the cell back. In fact, once the cell enters the microchannels, the cell is confined and occupies the full microchannels in high and width. In this condition, the Dextran-TRITC and serum accumulate at the cell front, and the difference in intensity is constant. Moreover, cells are always migrating towards 10% serum and none of the cells are migrating against the serum gradient.

In addition, the persistent length distributions indicate that NIH3T3 cells migrate towards the highest serum concentration with a high persistent length, few cells pause before reaching the end of the microchannels. The 10% serum gradient strongly directs cell migration.

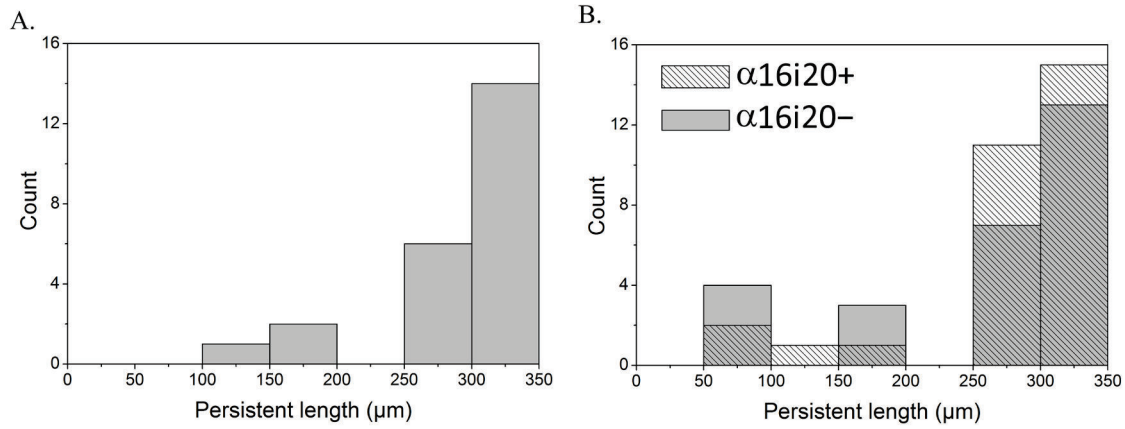

Figure 3.52: Persistent length distributions of NIH3T3 cells migrating in 20μm² straight (A.) and a16i20 ratchet (B.) closed microchannels in the presence of 10% serum gradient, $n_{straight}$=23cells (7 independent experiments), $n_{\alpha16i20+}$=30cells (9 independent experiments), and $n_{\alpha16i20-}$=28cells (6 independent experiments).

In the next section, I will summarize the migration of NIH3T3 cells in the open, closed with and without serum gradient.

3.6 Summary of NIH3T3 cells migration in open, closed microchannels without and with serum gradient

First, we saw that confinement significantly increases the persistent length (Figure 3.53, $p<0.001$ One-Way ANOVA). In the presence of 10% serum gradient, the persistent length significantly increases in the ratchet direction compared to the closed ratchet configuration without gradient. Against the ratchet direction, the mean persistent length increases (263±87μm *versus* 197±121μm) but the difference is not significant. In straight microchannels, there is no significant difference between persistent length of cell migrating with or without serum gradient.

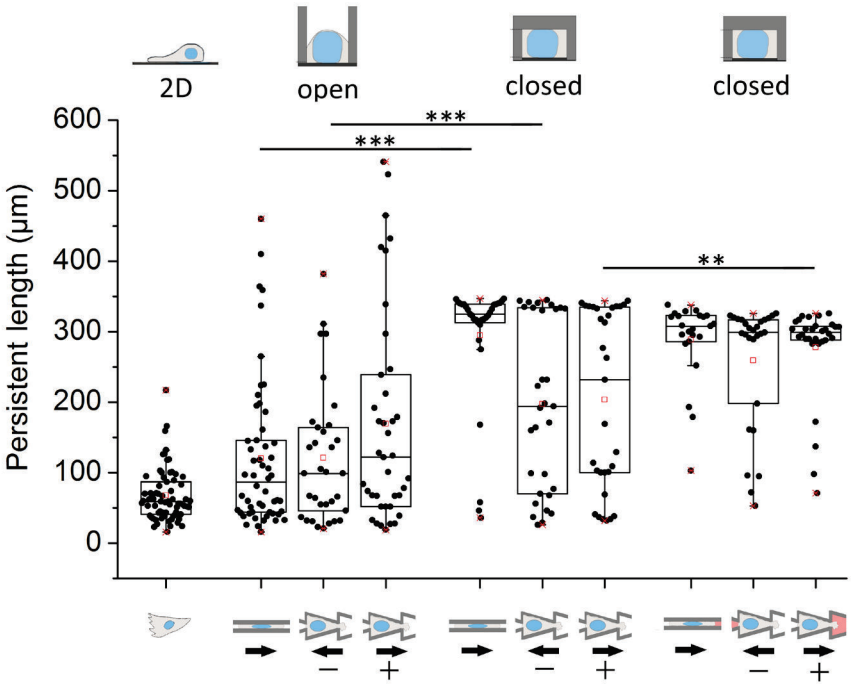

Figure 3.53: Summary of the persistent length distributions of NIH3T3 cells migrating on 2D flat surfaces, in open and closed, 20µm² straight and α16i20 ratchet microchannels with and without 10% serum gradient configurations. Schematics represent top and side views of the cell. Statistical test: One-Way ANOVA, ** p<0.01, *** p<0.001.

In addition, we saw that in the presence of 10% serum gradient, few cells pause and the one who pauses, does not change direction of migration after pausing (Figure 3.53).

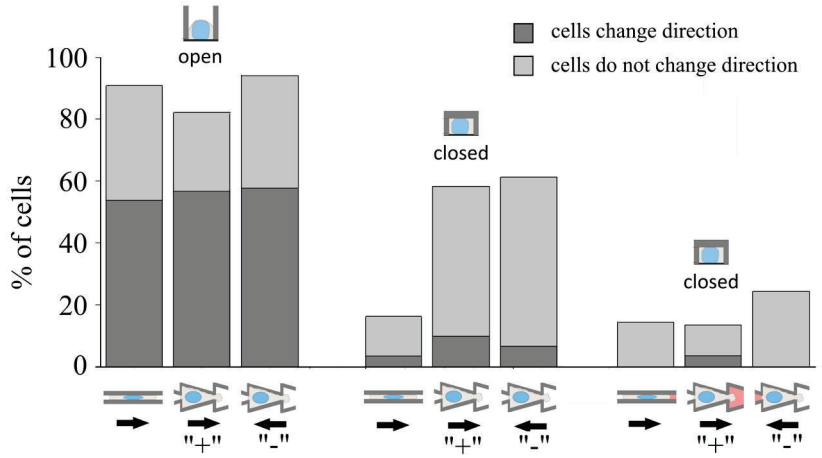

Figure 3.54: Summary of the percentage of NIH3T3 cells which pauses their migration and then migrate in the same direction (light grey) or change direction of migration (dark grey). The open and closed configurations with 20µm² straight and α16i20 ratchet microchannels and with 10% serum gradient are represented. Schematics represent top and side views of the cell. of cells which change direction over total number of cells Open straight:29/54, open ratchet +: 22/39, open ratchet -19/33, closed straight: 1/31, closed ratchet +: 3/31, closed ratchet -: 2/31, gradient straight: 0/23, gradient ratchet +: 1/30, gradient ratchet -: 0/29.

Altogether, the mean persistent length increases with cell confinement. In the open microchannels, NIH3T3 cells are sensitive to the environment geometry and migrate directionally following the ratchet direction. In closed microchannels, cell migration is impaired but cells cannot change direction of migration as compared to open microchannels. The entry in the microchannels sets the direction of migration and the high confinement prevents change

of direction. The 10% serum gradient used directs the cell migration, for any microchannel geometry. The importance of serum gradient slope will be discussed page 156.

Using the same ratchet microchannels and serum gradient, we next challenge the cell persistency by removing the chemical gradient while cells are migrating inside microchannels. How will the cells behave after gradient removal? Will the cells be able to sense the geometry of the ratchets and change its direction of migration after gradient removal?

3.7 Competition and cooperation between ratchetaxis and chemotaxis

To perform these experiments, we first formed a 10% serum gradient inside microchannels and allowed the cell entry and migration from 1 to 6 ratchet units (equivalent to 30 to 200µm).

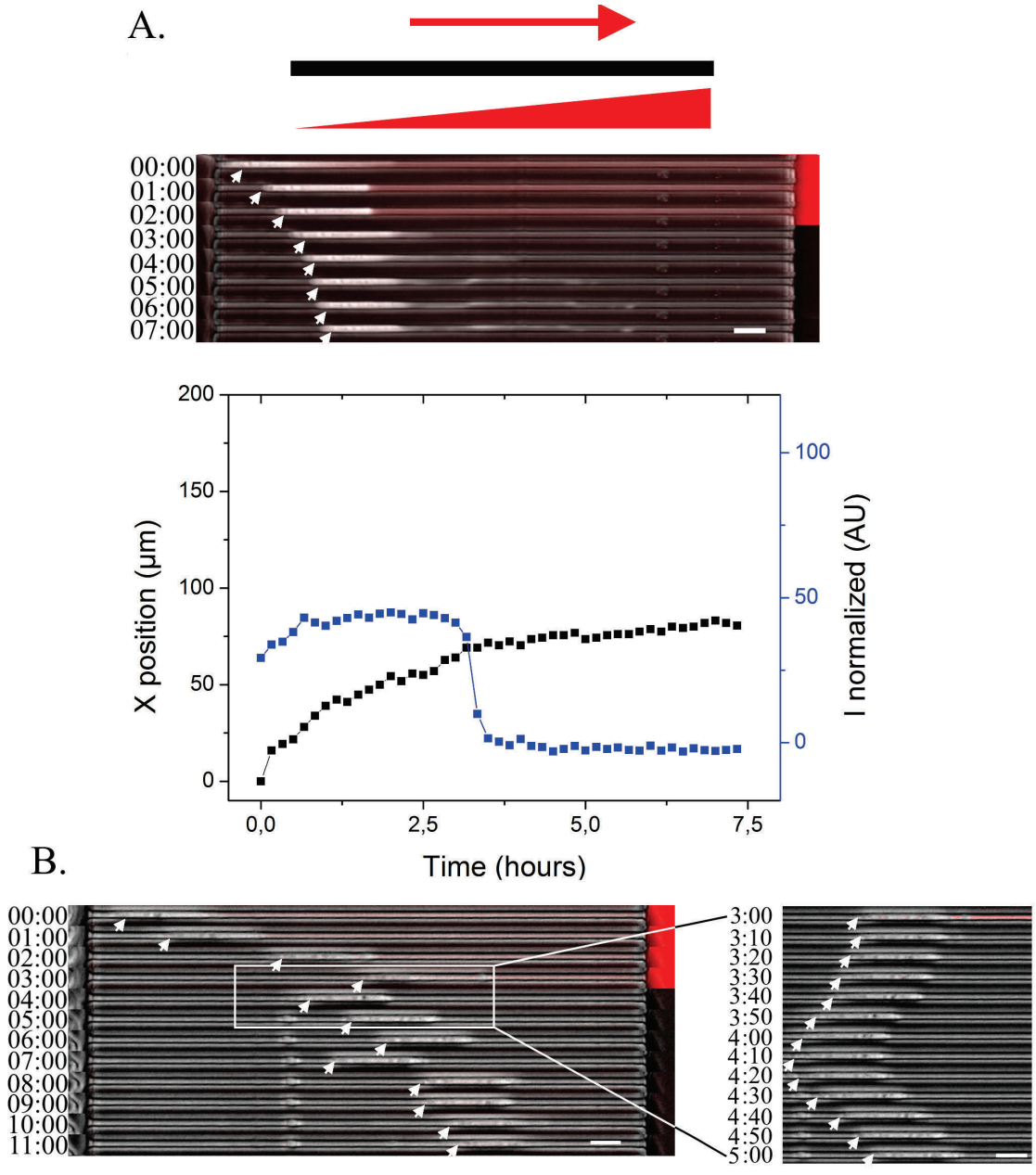

Figure 3.55: A. Example of a NIH3T3 cell migrating in closed straight microchannel before and after gradient removal. Second row. Trajectory of the cell in A. and normalized dextran-TRITC fluorescence intensity are plotted. B. Another example of NIH3T3 cell migrating in straight microchannel before and after gradient removal with 10min interval. White arrows show the cell position. Scale bar 20µm. Time in hh:mm. See Movie 24 and Movie 25.

Then, we removed the 10% serum gradient by removing the syringe containing the serum gradient from the syringe pump. The Dextran-TRITC fluorescence disappears 10min after gradient removal. We then observed cell behaviors after gradient removal in straight microchannels (Figure 3.55), in ratchet microchannels in the ratchet direction (Figure 3.56) and in ratchet microchannels against the ratchet direction (Figure 3.57).

After gradient removal, we observed that the normalized fluorescent intensity drops indicating that gradient has efficiently been removed. In straight channel, after gradient removal, cells migrate mainly in the same direction than previous gradient or fluctuates (Figure 3.55B).

In the example presented in Figure 3.56, cell migrate in the ratchet direction and after gradient removal; *i.e.* visualized by the drop of Dextran-TRITC fluorescent intensity, cell continues to migrate in the ratchet and previous serum gradient direction.

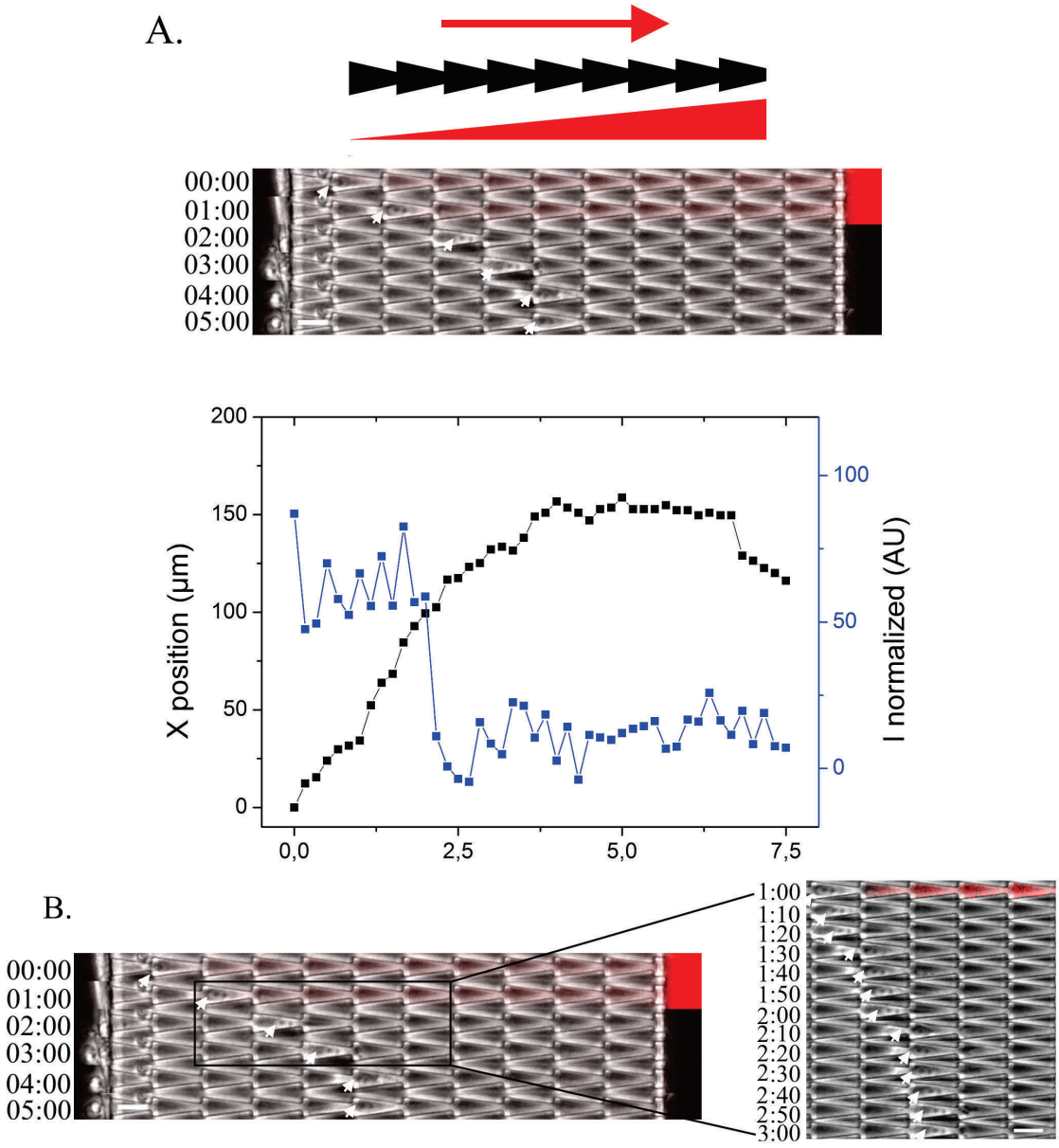

Figure 3.56: A. Example of NIH3T3 cell migrating in closed ratchet microchannel in the ratchet direction before and after gradient removal. Second row. Cell trajectory and normalized Dextran-TRITC fluorescence intensity are plotted. B. Same cell presented in A but with 10min interval between images. White arrows show the cel position. Scale bar 20µm. Time in hh:mm. See Movie 26.

In the examples presented in Figure 3.57, we observed that after gradient removal, cells migrating against the ratchet direction stop their migration. If we look more into details 2h after gradient removal, we observed that the ratchet bottleneck prevented the passage of the cells, and more precisely the passage of the nucleus, to the next ratchet (Figure 3.57B).

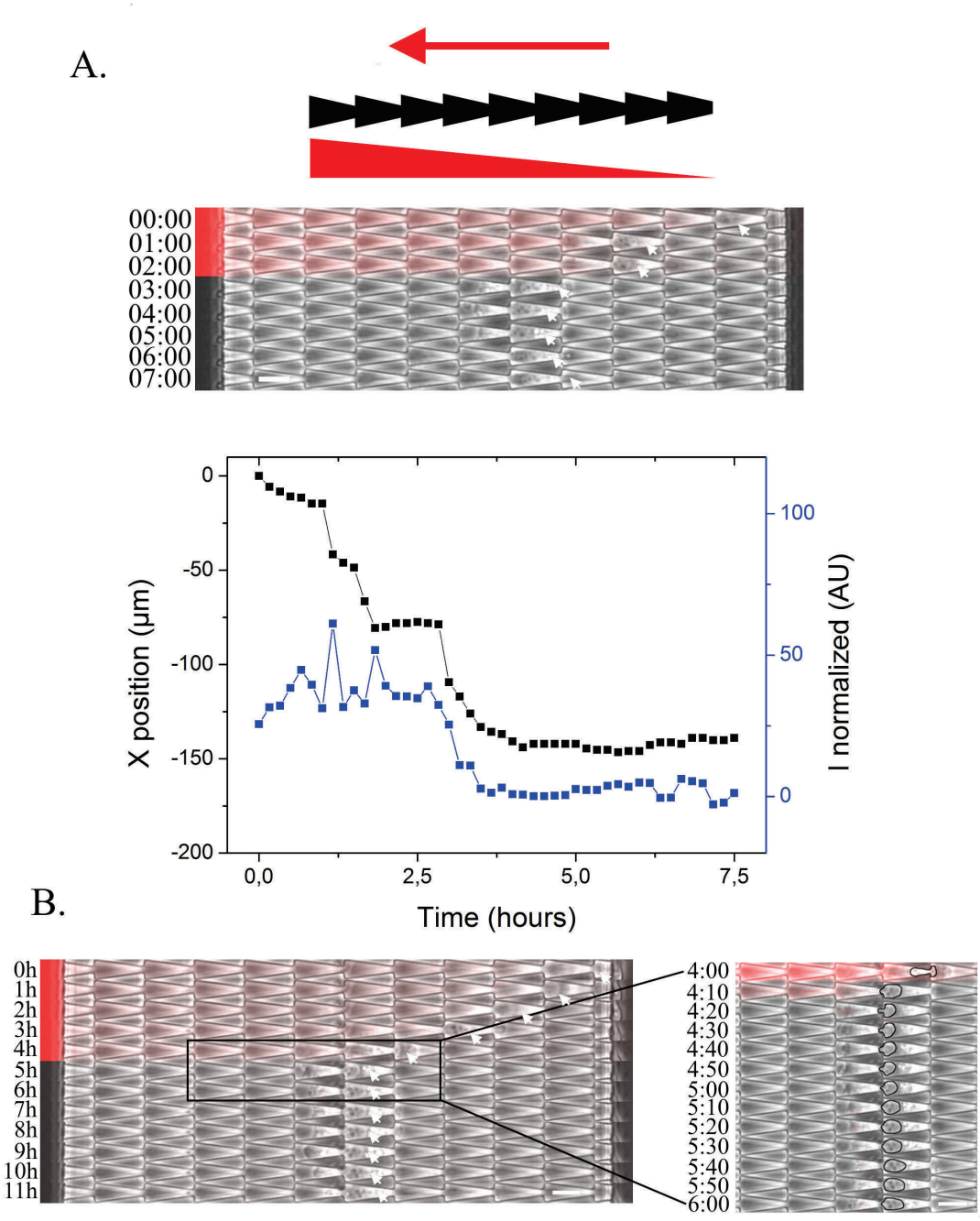

Figure 3.57: A. Examples of NIH3T3 cells migrating in closed ratchet microchannel against the ratchet direction before and after gradient removal. Middle. Trajectory of cell in A. and normalized dextran-TRITC fluorescence intensity are plotted. (B.) Another example of NIH3T3 cell migrating against the ratchet microchannel before and after gradient removal with 10min interval. White arrows show the cell position. Black lines highlight the nucleus. Scale bar 20µm. Time in hh:mm. Scale bar 20µm. Time in hh:mm. See Movie 27 and Movie 28.

For each condition, we measured the persistent length in the presence of the serum gradient and after gradient removal (Figure 3.58).
In straight microchannels, it shows three behaviors: after gradient removal, cells pause, *i.e.* persistent length closed to 0, migrate in the same direction, *i.e.* positive persistent length, or move in the opposite direction, *i.e.* negative persistent length (Figure 3.58A). However, none of the cells migrate a distance large enough to exit the microchannels, in the previous gradient direction or in the opposite direction. Moreover, in the opposite direction of the previous gradient, the persistent lengths are shorter than in the previous gradient direction.
In the ratchet direction, we observed only two behaviors; no cells migration and mainly migration in the previous direction of the gradient (Figure 3.58B). It suggests that ratchet favors the migration in the ratchet direction. In addition, it seems that, less exposed to the gradient and longer are migrated the cells.

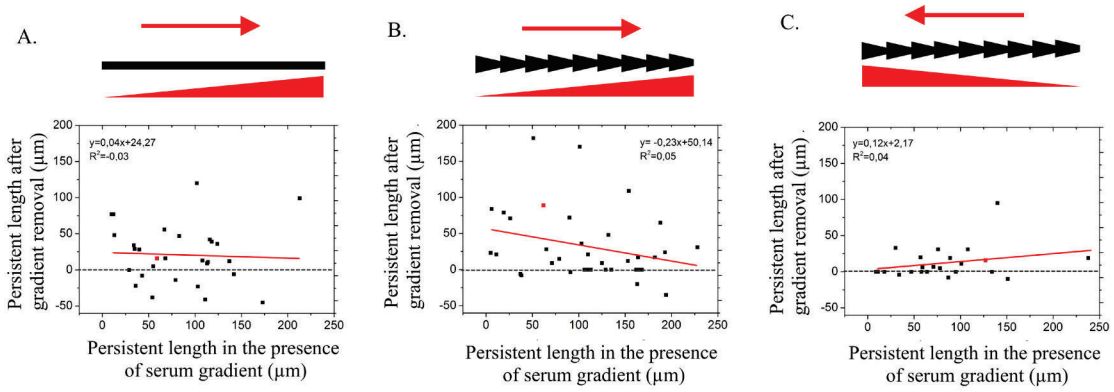

Figure 3.58: Persistent length of NIH3T3 cells after gradient removal as a function of the persistent length in the presence of gradient in closed straight (A.), in the ratchet direction (B.) and against the ratchet direction (C.). Red squares show cell presented in Figure 3.55, Figure 3.56 and Figure 3.57. $n_{straight}$= 29cells, $n_{ratchet\ +}$= 33cells and $n_{ratchet\ -}$= 23cells.

Against the ratchet direction, the majority of the cells are not migrating or migrate small distances, *i.e.* maximum the size of a ratchet (33µm)(Figure 3.58B). It confirms that ratchet geometry prevents the passage of the cells to the next ratchet after gradient removal. Mainly, the nucleus is the obstacle to cell migration.

Altogether, in ratchet closed microchannel and even after gradient removal, cells did not change direction of migration, whereas they did change direction of migration in open microchannels. To have an idea about the polarity status of the cells, we performed preliminary experiments by transfecting NIH3T3 cells with a DNA construct (pACT-mKOI) which marks proteins of the centrosome or by using Sir-tubulin which stain for microtubules. Centrosome is then visualized as a dot in pACT-mKOI transfected cell and highest microtubules intensity, representing the MTOC or centrosome. We observed that the centrosome position (red dot) is located at the cell front in the closed and open microchannels and is moving forward as cells move (Figure 3.59).

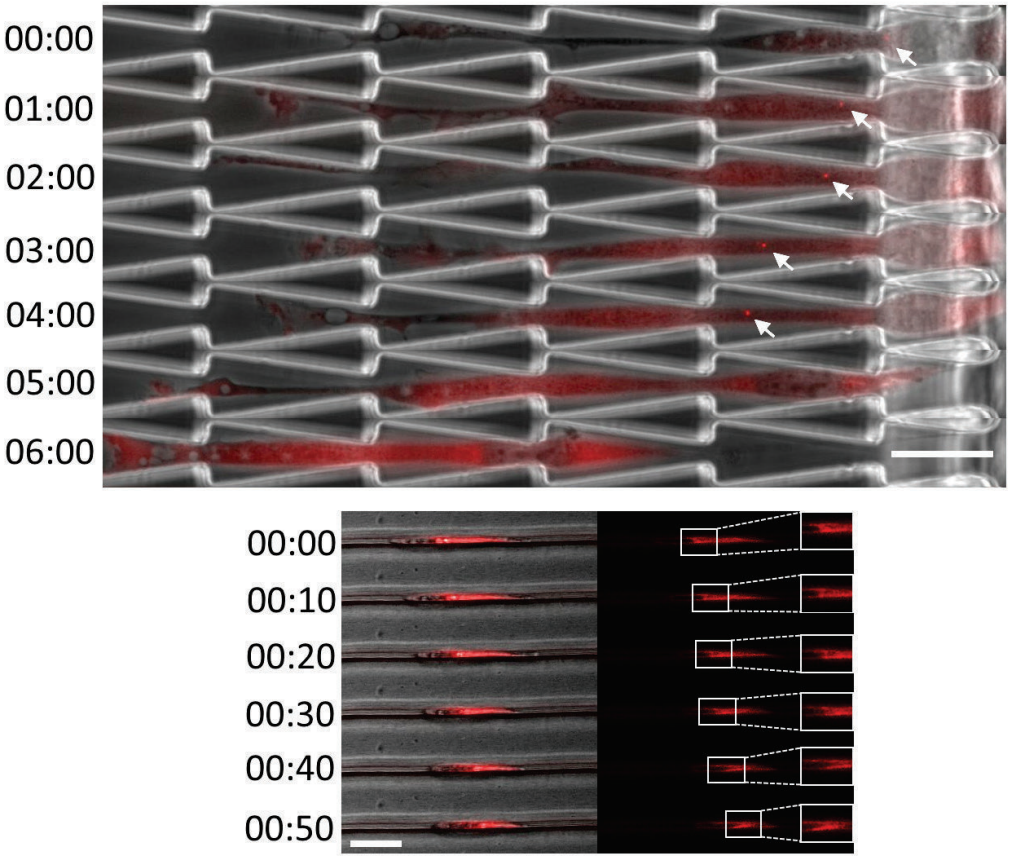

Figure 3.59: NIH3T3 cells migration and centrosome position. First row. NIH3T3 cell migration in α16i20 ratchet microchannels and centrosome position (PACT-mKOI transfected cell) in the presence of 10 % serum gradient. Second row. NIH3T3 cell migration in 20µm² straight open microchannels and centrosome position (SiR-tubulin). White arrows highlight the centrosome position. Time in hh:mm. Scale bar 20µm.

Additional experiments are required to determine first if inside microchannels, centrosome is always located at the cell front while migrating, and second, if we observe change of centrosome position after gradient removal or in the open microchannels.

Altogether, in closed ratchet microchannels, we observed an impaired cell migration but we did not see any rectification of cell migration. The entry in the microchannels sets the cell polarity. In the presence of 10% serum gradient, cell migration is directed in the ratchet and against the ratchet directions as well as in straight microchannels. However, in the open microchannels configuration, migration is rectified towards the ratchet direction. In addition, we observed a ratchet effect when we removed the chemical gradient of migrating cells inside microchannels. In the ratchet direction, cell migration is favored after gradient removal. Against the ratchet direction, cells migration is stopped: the nucleus prevents the cell passage.

To conclude, a 10% serum gradient is able to direct cell migration. In the next part, we want to see if a physiological gradient of CXCL12 is also able to direct cell migration in our configuration. Moreover, the localization of its two membrane receptors CXCR4 and CXCR7 is addressed. A differential localization could explain the symmetry breaking event and give us an indication of cell polarity.

3.8 Using CXCL12 as a physiological gradient

As mentioned in the Introduction (page 72), the chemokine CXCL12 is involved in numerous processes, from development to metastatic spread[14,24]. In the case of metastatic spread, the presence of a CXCL12 gradient at the proximity of organ is widely accepted to be responsible for the directed cell migration of circulating tumor cells towards this organ. However, the presence of the CXCL12 gradient *in vivo* has never been shown. In this part, we want to understand the processes leading to cell migration through CXCL12. First, we observed the localization of the two membranes receptors CXCR4 and CXCR7. Second, we followed the migration of cells towards CXCL12 gradient.

3.8.1 Differential localization of CXCR4 and CXCR7 in NIH3T3 and SW480 cells

We used two methods to observe the localization of CXCR4 and CXCR7 receptors, by immunostaining or by transfecting fluorescent constructs to visualize membrane receptors (Material & Methods page 79 and 81). In NIH3T3 and SW480 cells, we observed the same results: CXCR4 and CXCR7 did not have the same localization. Immunostainings indicate that CXCR4 accumulated at the cell edge and more precisely in the lamellipodia and ruffle region (Figure 3.60 A. and B. white arrows). In contrast, CXCR7 do not localize in the ruffle region of lamellipodia (Figure 3.60).

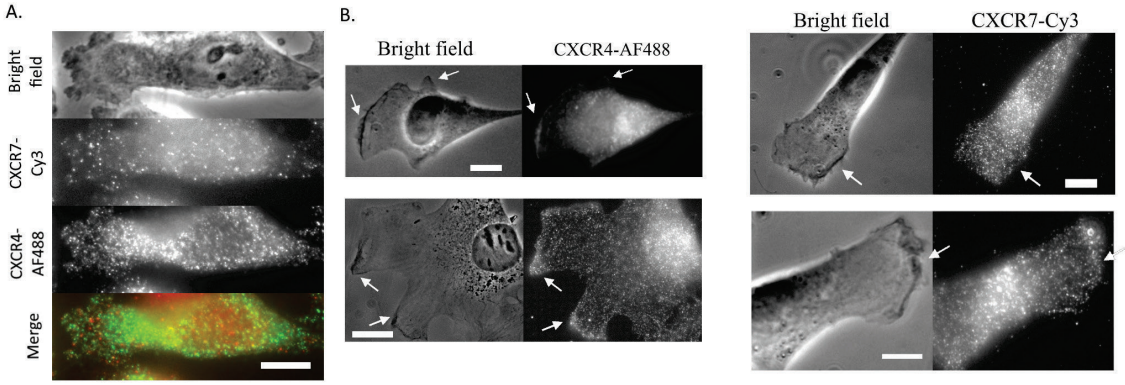

Figure 3.60: Immunostaining of CXCR4 and CXCR7 receptors in SW480 (A.) and NIH3T3 cells (B.). White arrows indicates ruffle lamellipodia. Scale bar 10µm.

It suggests that CXCR4 is linked to lamellipodia activity and actin cytoskeleton whereas CXCR7 is not. This is what we check in the next sections.

3.8.2 CXCR4 is linked to lamellipodia activity

We observed CXCR4 localization together with actin in fixed samples (NIH3T3 and dHL60 cells) and lived samples (SW480 cells) (Figure 3.61). Surprisingly, we observed CXCR4 accumulation at the cell edge overlapping with lamellipodia and actin rich region in fixed and lived samples (Figure 3.61). We measured an actin retrograde flow, *i.e.* actin monomers depolymerization from the leading edge moving retrogradelly to the cell centre. It is associated with CXCR4 retrograde flow (Figure 3.61C). The speed of the retrograde flow has been measured: it is equal

to 34±11nm.s^{-1} in CXCR4 and LifeAct transfected SW480 cells whereas it is equal to 23±3nm.s^{-1} in LifeAct transfected SW480 cells alone. These values are coherent with already published data[161]. Nedeva et al. (2013) measured a retrograde flow of 30nm.s^{-1} in NIH3T3 cells. An increase in retrograde flow speed indicates further a link between CXCR4 and actin cytoskeleton.

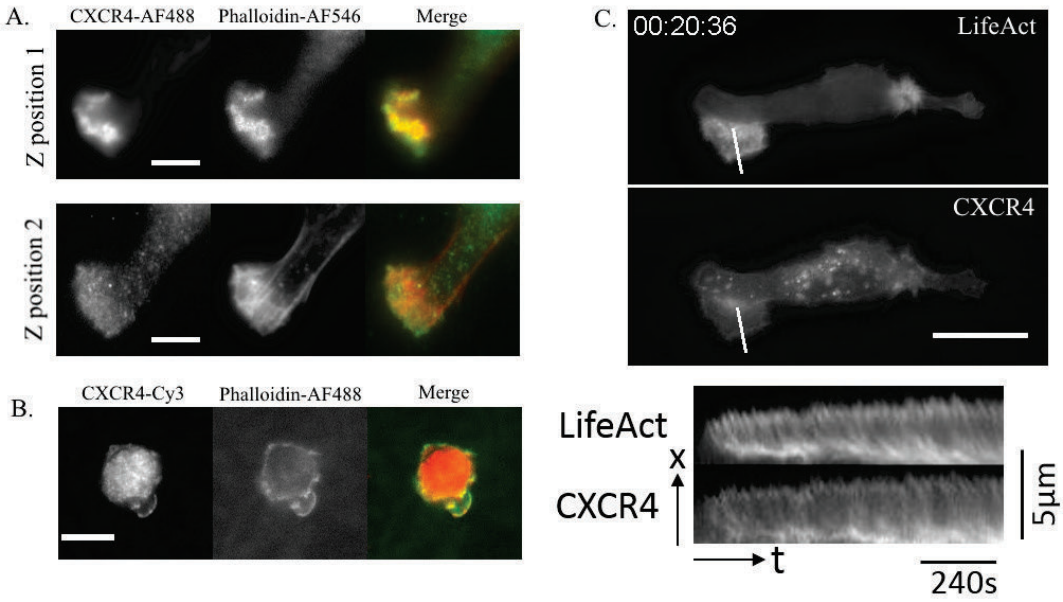

Figure 3.61: CXCR4 is linked to the lamellipodia activity. (A.) Immunostaining of CXCR4 (green) and actin (phalloidin-red) in NIH3T3 cell. Two Z positions are taken. Z position 1 is few µm above the coverslip. Z position 2 is focused on the coverslip. Scale bar 5µm. (B.) Immunostaining of CXCR4 (red) and actin (phalloidin-green) in dHL60 cell. Scale bar 5µm. (C.) First row. Transfection of SW480 cell with CXCR4-GFP and LifeAct-mCherry. Images obtained by Charlotte Alibert. Scale bar 10µm. See Movie 29.Time in hh:mm:ss. Second row. Kymographs along the white lines represented in Top.

Additional experiments are required to confirm CXCR4 and actin retrograde flows measurement in SW480 and NIH3T3 cells. In general, I observed that cells overexpressing CXCR4 have more difficulties to spread, they needed more time compared to non-transfected cells.
Next, we look at CXCR7 localization and its potential link to microtubules networks as it is not linked to actin network.

3.8.3 CXCR7 and microtubule networks

With the overexpression of CXCR7-mRFP and tubulin-GFP, we observed first, a large number of CXCR7 vesicles and second, the directed migration of these CXCR7-vesicles within the cells (Figure 3.62).

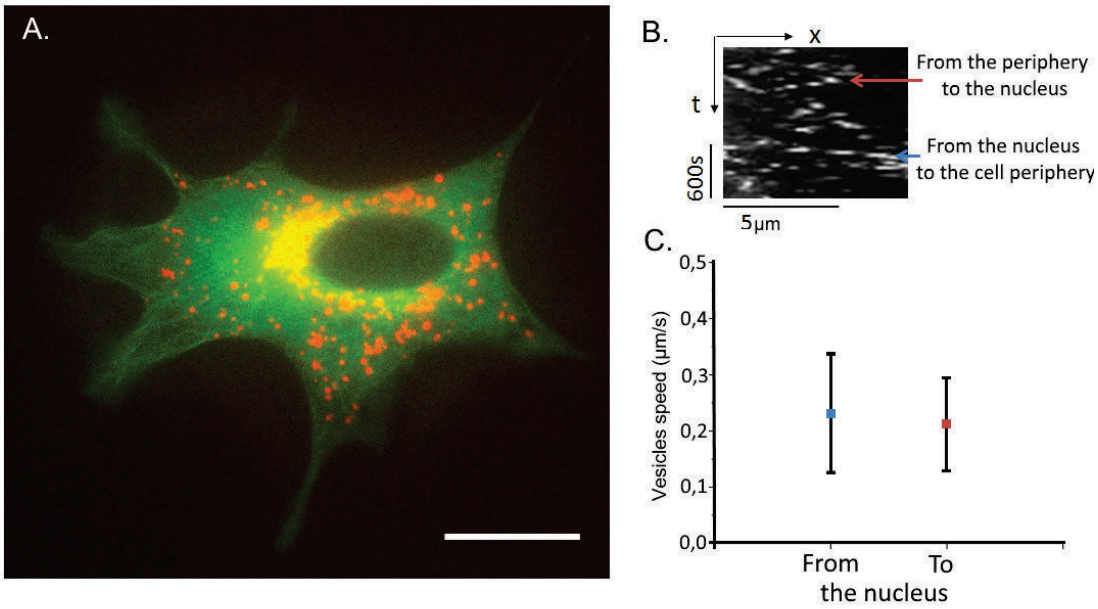

Figure 3.62: CXCR7 and microtubules. (A.) transfection of a NIH3T3 cell with CXCR7-mCherry and tubulin-GFP (microtubules). Scale bar 20µm. See Movie 30. (B.) kymograph of vesicles moving along microtubules. CXCR7 vesicles are moving from the cell periphery to the nucleus (blue arrow) whereas others are moving from the nucleus to the cell periphery (red arrow). (C.) CXCR7 vesicles speed moving from the nucleus (blue) and to the the nucleus (red), $n_{\text{from the nucleus}}$ =19vesicles, $n_{\text{to the nucleus}}$ =22vesicles. 3 independents cells.

The vesicles speed has been quantified (Figure 3.62C). However and in contrast to CXCR4 overexpression, CXCR7 accumulate into vesicles. In fact, it seems that GPCR coupled to red fluorophores, such as mRFP, accumulated into endosomal vesicles (Jean Luc Galzi, unpublished data). For this reason, we transfected NIH3T3 cells with CXCR7 coupled to other fluorophores (Figure 3.63).

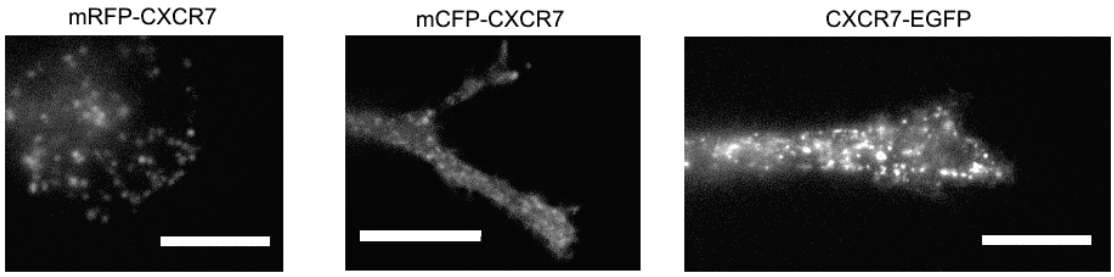

Figure 3.63: Images of CXCR7 overexpression with CXCR7 linked to different fluorophores, intracellular (mRFP-CXCR7 and CFP-CXCR7) or extracellular (CXCR7-EGFP). Scale bar 5µm.

There, we still observed accumulation of CXCR7 into vesicles (Figure 3.63). The vesicles were smaller in size, *i.e.* 0.13±0.04µm for CXCR7-mRFP vesicles and CXCR7-EGFP 0.09±0.02µm. However, these results are preliminary (1 experiment and at least 10 vesicles for each condition) and, to be fully validated need further investigations. Nevertheless, in mCFP-CXCR7 and CXCR7-EGFP transected NIH3T3 cells, we could observe a diffuse signal which is absent in CXCR7-mRFP transfected cells. This diffuse signal is present also in CXCR4-GFP transfected cells. However, directed motion of CXCR7-CFP and CXCR7-EGFP vesicles has been observed, confirming the link between CXCR7 vesicles and microtubules network.

Altogether, we saw that CXCR7 and CXCR4 did not have the same localization within the cell. CXCR4 accumulate at the cell edge and is associated with lamellipodia activity, strongly suggesting a link with actin (Figure 3.61). CXCR7 is not linked to lamellipodia activity but is present within vesicles and move directionally along microtubules suggesting a link between CXCR7 and microtubules (Figure 3.60 and Figure 3.63). In the next sections, we will study the migration of NIH3T3 and MDA-MB-231 cells towards gradients of CXCL12. To do that, different experiments have been performed: pipette, Boyden chamber, gradient in microchannels and microcontact-printing experiments.

3.8.4 NIH3T3 cells migration in CXCL12 gradients

In this PhD thesis, we mainly used NIH3T3 cells for their ability to migrate on flat surfaces and confined microchannels and to respond to chemical gradients. The next step was to study the migration of NIH3T3 cells in response to physiological gradients of CXCL12. First, we locally injected CXCL12 at the cell proximity with a pipette on flat surfaces. We did not observe directed cell migration. Then, we wanted to check if in other configurations, *i.e.* soluble gradients in microchannels and Boyden chamber and adhesive gradients, NIH3T3 cells would be able to migrate. However, we did not observe directed cell migration towards CXCL12. These results will be presented in the next sections. There, different CXCL12 concentrations have been tested, they are in the same magnitude order than in published data[14].

3.8.4.1 Pipette experiment

In the previous section, we showed that pipette experiment was a useful tool to direct cell migration towards a serum gradient (page 126). We saw also that to allow quick cell migration towards 10% serum gradient, the coverslip has to be treated with 0.1mg/ml PLL-g-PEG, a cell repellant. Because we observed that CXCR4 overexpressing NIH3T3 cell have more difficulty to spread, the coverslip coating is modified. For CXCR4 and CXCR7 transfected cell, the amount of PLL-g-PEG is reduced and Fibronectin is added in order to facilitate cell attachment to the coverslip but at the same time allow quick cell migration. Different tests have been performed and a mix of 0.075mg/ml of PLL-g-PEG and 0.025µg/ml of fibronectin is used to study the migration of CXCR4-GFP and CXCR7-mRFP transfected NIH3T3 cell towards a pipette delivering CXCL12 and Dextran-AF647 to visualize the chemical gradient (Figure 3.64).

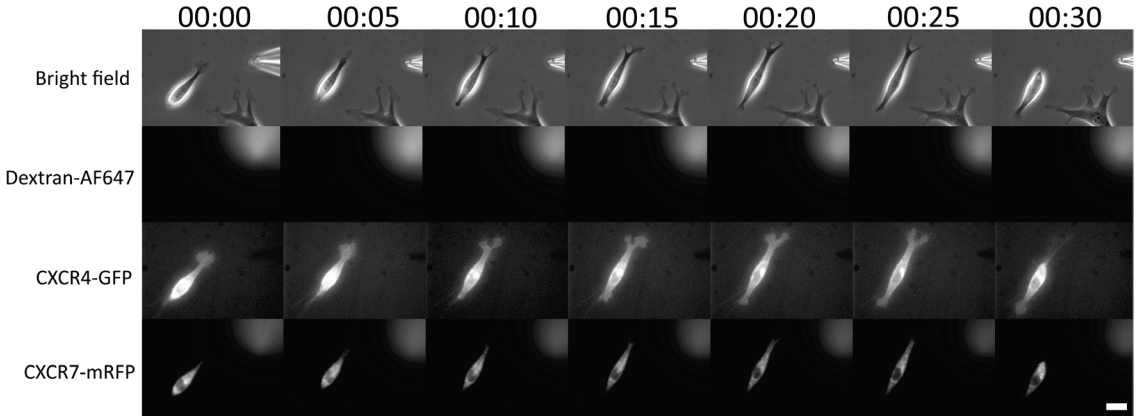

Figure 3.64: NIH3T3 cell transfected with CXCR4-GFP and CXCR7-mRFP. Medium containing CXCL12 (100nM) and Dextran-AF647 (12µg/ml) is delivered by the micropipette. Scale bar 10µm. Time in hh:mm. See Movie 31. Representative of 2 independents experiments.

We can see that a gradient is formed. However, we did not observe migration of NIH3T3 cells towards pipette delivering 100nM CXCL12. In addition, we did not see any relocalization of CXCR4 and CXCR7 after CXCL12 addition.

In order to check if the overexpression of CXCR4 and CXCR7 did not prevent cell response to chemical gradient, we transfected NIH3T3 cells with CXCR4-GFP and CXCR7-mRFP and followed cell migration towards pipette delivering 10% serum gradient (Figure 3.65).

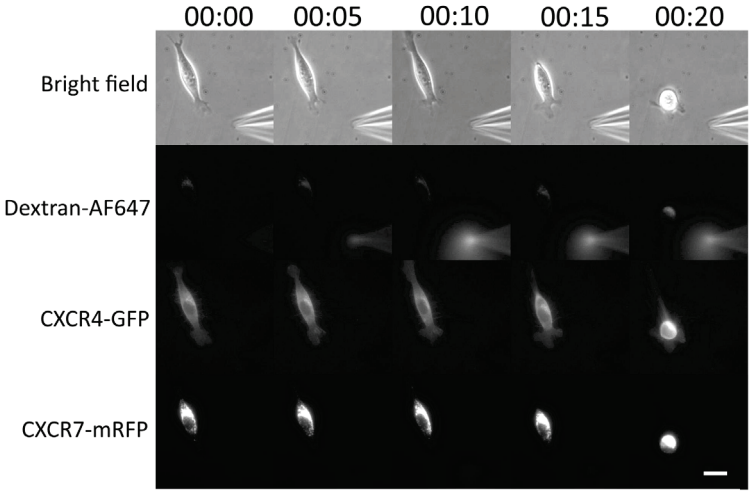

Figure 3.65: NIH3T3 cell transfected with CXCR4-GFP and CXCR7-mRFP. Medium containing 10% serum and dextran-AF647 (12µg/ml) is delivered by the micropipette. Scale bar 10µm. Time in hh:mm. See Movie 32.

There, we saw that NIH3T3 cell transfected with CXCR4-GFP and CXCR7-mRFP are able to migrate towards 10% serum gradient delivered by the micropipette. It reveals that membrane receptors overexpression do not prevent chemotactic cell migration towards 10% serum but that CXCL12 is not able to direct NIH3T3 cell migration on flat surfaces.

In vivo, a potential CXCL12 gradient would form at the organ proximity in narrow capillaries. We next formed CXCL12 gradients inside microchannels to combine confinement and physiological gradient and to observe if NIH3T3 cells migration could be directed. I will be presenting in the next section migration of NIH3T3 cells in two different microchannel configurations in term of length and width, and in the presence of three CXCL12 concentrations.

3.8.4.2 CXCL12 gradients in microchannels

We first studied migration of NIH3T3 cells in 20µm^2 straight microchannels. We previously showed that NIH3T3 cells were able to enter and migrate inside 20µm^2 straight microchannels in the presence of 10% serum gradient (page 128). A 16nM of CXCL12 gradient is first used, visualized with dextran-TRITC. The slope is then equal to the CXCL12 concentration divided by the microchannel length, *i.e.* 0.046nM.µm^{-1}. In this experiment, we did not see NIH3T3 cells entering into microchannels. The cell presented in Figure 3.66A was already inside the microchannel before the formation of CXCL12 gradient. We observed cell migration in the opposite direction of 16nM CXCL12. In the previous section (page 127), we saw that 10% serum gradient was able to direct cell migration in narrow and large microchannels. We wonder if the

slope of the gradient was not too low to attract cells inside microchannels. To overcome this problem, we used another microchannels design where NIH3T3 cells were not confined from the sides, *i.e.* 75µm^2 cross-section instead of 20µm^2, and microchannels are shorter, *i.e.* 100µm instead of 350µm, reducing cell confinement and increasing the gradient slopes. Two gradients of CXCL12 are used, 13nM (Figure 3.66B) and 85nM (Figure 3.66C). There, CXCL12 gradient slopes are respectively equal to 0.13nM.µm^{-1} and 0.85nM.µm^{-1}.

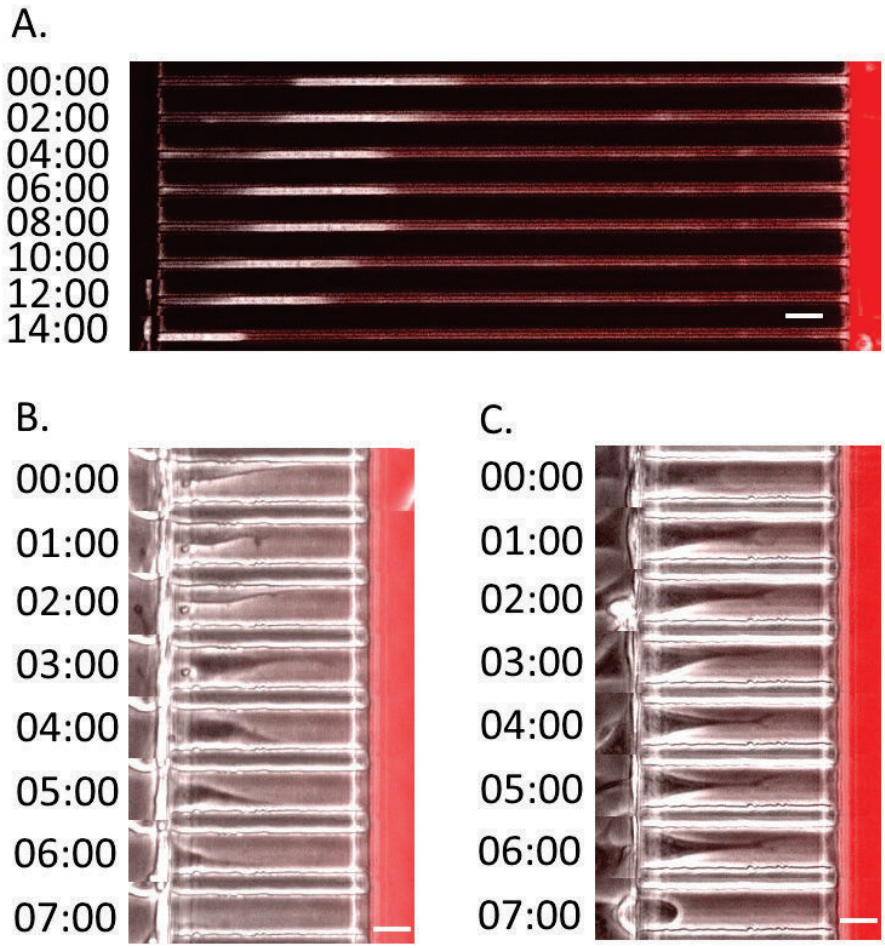

Figure 3.66: Time series of NIH3T3 cells migrating in closed microchannels with CXCL12 gradients. (A.) 20µm^2 cross-section microchannels and 0 to 16nM CXCL12 gradient. (B.) 100µm^2 cross-section microchannels and 0 to 13nM CXCL12 gradient. (C.) 100µm^2 cross-section microchannels and 0 to 85nM CXCL12 gradient.Time in hh:mm. Scale bar 20µm. See Movie 33, Movie 34 and Movie 35.

Again, cells are not entering inside microchannels, and when some cells are already inside microchannels, they migrate in the opposite direction of the highest CXCL12 concentration (Figure 3.66). This has never been observed in the case of 10% serum gradient. We did not manage to induce cell migration towards CXCL12 in confined microchannels, neither with pipette experiment.

However, Zhang et al. (2012) observed the migration of neural progenitor cells towards adhesive lines of CXCL12. Following this line, we wanted to check if NIH3T3 cells would be able to migrate towards adhesive lines of CXCL12. We decided to adapt microcontact-printing protocol, which is a protocol daily used in the lab, to print CXCL12 motifs on coverslip.

3.8.4.3 Microcontact-printing of the chemokine CXCL12

In the lab, microcontact-printing experiments are commonly performed to transfer fluorescent fibronectin motifs with a stamp to a coverslip[15]. Briefly, a stamp containing desired motifs is activated and fibronectin is incubated. After a short drying step, fibronectin motifs are transferred to a coverslip. Microcontact-printing efficiency is checked with the fluorescence of fibronectin motifs. In this PhD thesis, we want to microcontact-print the non-fluorescent protein CXCL12. We needed to adapt the protocol to find a way to visualize CXCL12 proteins transfer to coverslip. The protocol is detailed in the Material & Methods section (page 90). First, we incubated the stamp with a mixture of CXCL12 and Dextran-TRITC in order to visualize the motifs microcontact-printed (Figure 3.67).

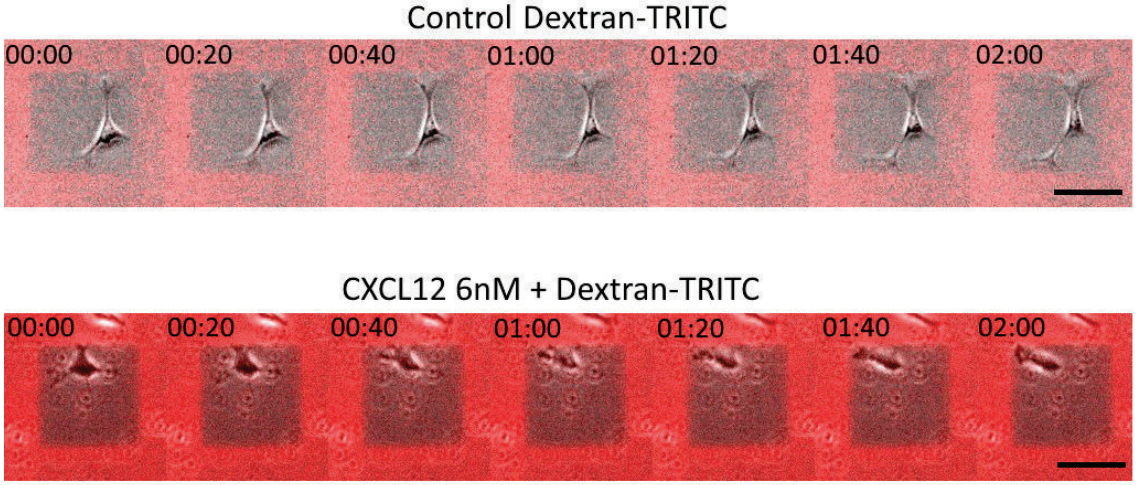

Figure 3.67: Microcontact-printing of Dextran-TRITC without and with CXCL12 (6nM) and effect on NIH3T3 cell migration. Time in hh:mm. Scale bar 100µm. Movie 36 and Movie 37.

Here, I show NIH3T3 cells which are plated on a square surrounding by Dextran-TRITC or Dextran-TRITC plus CXCL12 (6nM) microcontact-printed. We observed in both conditions that NIH3T3 cells sent protrusions towards motifs of Dextran-TRITC and Dextran-TRITC mix with CXCL12 (6nM) microcontact-printed. However, cells do no escape from the square and the cells presents on Dextran-TRITC motifs do not spread. We used Dextran-TRITC as a control to check the efficiency of the microcontact-printing protocol. As a control, the migration of NIH3T3 cells on Dextran-TRITC surfaces should be isotropic, *i.e.* "persistent random walk". However, it looks like Dextran-TRITC microcontact-printed repulse NIH3T3 cells.

Then, we changed the protocol and we first microcontact-printed CXCL12 alone and then stained for CXCL12 using a first antibody targeting CXCL12 and a second antibody coupled to a fluorophore and targeting the primary CXCL12 antibody. It allows the visualization of adhesive CXCL12 patterns, indicating that we successfully managed to transfer CXCL12 to the coverslip. First, the overall cell migration is followed. No accumulation of cells on adhesive CXCL12 was observed. Then, we checked if adhesive CXCL12 would affect the cell polarization. Just after replating, NIH3T3 cells are round. We observed cell polarization 1h30 after cell seeding. We followed the polarization of cells located at the border of adhesive CXCL12 lines, where cells would have the possibility to polarize in the direction of CXCL12 or in the opposite direction.

Two different controls are used: cells plated on surfaces without CXCL12 (Figure 3.68A) and with homogeneous CXCL12 microcontact-printed (Figure 3.68B). Both controls should give isotropic cell migration.

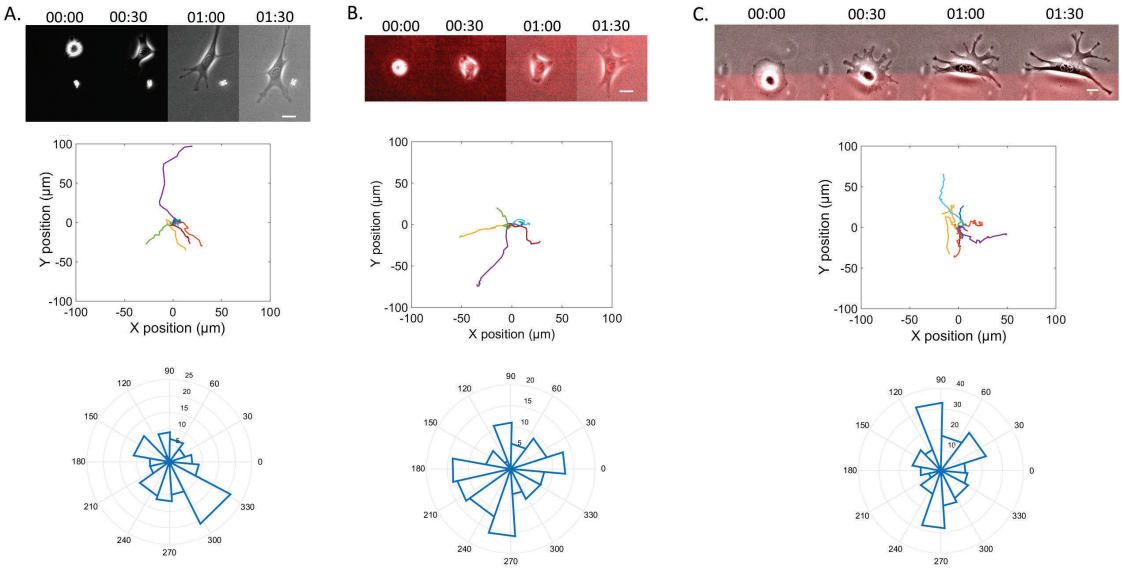

Figure 3.68: Microcontact printing of CXCL12 and effect on cell migration 1h30 after cell polarization on coverslip (A.), homogeneous CXCL12 microcontact printing (B.) and at the border of CXCL12 lines (C.). First row. Time series show the polarization of the cell 1h30 after seeding. Second row. Trajectories of all cells tracked. Third row. Angular distribution of the cell trajectories. (A.) n= 8 cells, (B.) n=7 cells, (C.) n=11 cells. 2 independent experiments. Scale bar 20µm. Time in hh:mm.

Preliminary experiments reveal in both controls, without CXCL12 and in homogeneous CXCL12 environment, a distribution of cell migration roughly isotropic. For cells located at the limit, there is no clear migration neither polarization of NIH3T3 cells towards adhesive CXCL12 (Figure 3.68C). However, additional experiments are required to validate this statement. Moreover, CXCL12 microcontact-printing protocol can be largely improved.

Altogether, pipette, microchannel and microcontact-printing experiments show the absence of directed NIH3T3 cells migration towards CXCL12.

In addition, published data reveal that fibroblasts are CXCL12 producer[22,136]. We suggested that the production of CXCL12 by NIH3T3 cells prevents the chemotactic response to an external gradient of CXCL12. For this reason, we inhibited CXCL12 production by using couples of siRNA which target CXCL12 mRNA. In the next section, I will present the results of CXCL12 down-regulation as well as the response of these cells to CXCL12 gradient in Boyden chamber experiments.

3.8.4.4 NIH3T3 cells migration in Boyden chamber and CXCL12 down-regulation

The CXCL12 down-regulation experiments were performed as described in the Material & Methods section (page 80). Two siRNA couples targeting CXCL12 mRNA and control siRNA, called scramble, have been used. The first siRNA couple (n°10 and 11), has been validated by the company Qiagen, whereas the second one has not been validated. siRNA scramble is a control

which does not target any mRNA. 48h after incubation with siRNA, cells were lysed, mRNA extracted, reverse-transcripted to obtain cDNA and tragetted mRNA quantified by q-PCR. It will allow the quantification of a specific mRNA. Dr. Pencreac'h performed the extraction and quantification. I will briefly explain the principle of q-PCR. Specific primers which target a specific mRNA, here CXCL12 and the gene PBGD as a reference, are used. At each PCR cycle, the number of PCR product double. A PCR curve usually has an exponential phase followed by a plateau. The cycle number, called Cycle threshold (Ct), is measured and is proportional to the initial mRNA level. Larger the Ct, lower the mRNA level. Each siRNA n°10 and siRNA n°11 target a specific sequence of the CXCL12 mRNA. The couple siRNA n°10 and 11 should target a large amount of CXCL12 mRNA. Theoretically, for any treatment, the mRNA level of the reference PBGD should be constant. However, we observed that its mRNA level decrease with siRNA treatments *i.e.* increased Ct (Table 3.1). For example, between the non-treated cells (Ct PBGD=21.45) and siRNA n°10+11 10 nM treated cells (Ct PBGD=26.17), there is almost a difference of 5 PCR cycles. Knowing that at each PCR cycle, the number of PCR product double, a difference of 5 PCR cycles means a 32-fold reduction in PBGD mRNA level between the untreated and CXCL12 siRNA treated cells. In parallel, we observed also an increased number of dead cells in siRNA treated cells, suggesting that siRNA treatment is toxic for NIH3T3 cells.

Table 3.1: Summary of CXCL12 and PBGD mRNA level expression according to the siRNA treatment.

	Ct CXCL12	**Ct PBGD**
Non-treated	27,81	21,45
siRNA scramble 5 nM	28,25	22,37
siRNA scramble 10 nM	29,01	23,12
siRNA n°10 5 nM	30,67	24,56
siRNA n°11 5 nM	31,05	24,77
siRNA n°10+11 5 nM	31,54	24,84
siRNA n°10+11 10 nM	***mRNA degraded***	***26,17***

In addition, we observed that the CXCL12 mRNA level decreased with the siRNA treatment, until becoming undetectable with 10nM siRNA treatment. The reduction of CXCL12 mRNA level being similar to the reduction of PBGD mRNA level, we cannot conclude that siCXCL12 treatment reduced the level of CXCL12 mRNA level within the cell. There, analysis classically performed to compare mRNA level between different treatments cannot be performed as the PBGD control is non-constant. However, the reduction of PGBD mRNA level could indicate that the CXCL12 siRNA treatment itself is toxic for NIH3T3 cells or it is the down-regulation of the protein CXCL12 which is toxic indicating that cells are non-viable without producing CXCL12. Further experiments have to be performed to validate these results: measure the mRNA level of another reference gene and critical points, test the cell viability after siRNA treatment.

Despite these results, we stained for CXCL12 in wild type (WT) cells and cells treated with siRNA n°10 +11 10nM (siCXCL12) (Figure 3.69).

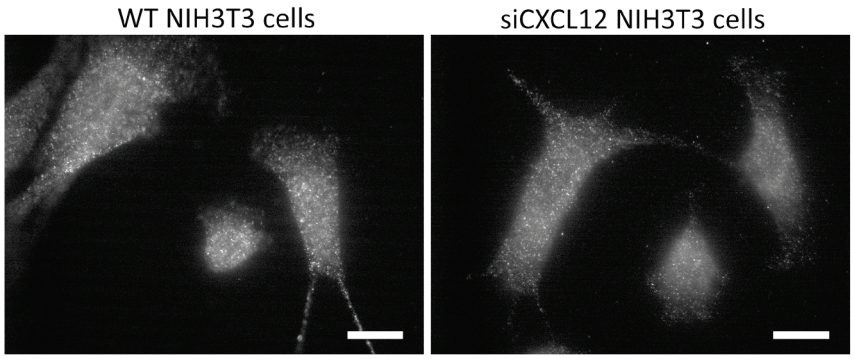

Figure 3.69: CXCL12 immunostaining in WT NIH3T3 cells and cells treated with siRNA targeting CXCL12 mRNA (siCXCL12). Scale bar 20µm.

First, we observed CXCL12 protein expression in WT NIH3T3 cells, confirming that these cells produce and most probably secrete CXCL12. NIH3T3 cells were treated 48h with siRNA targeting CXCL12 mRNA. Cells were then replated on coverslip and stained for CXCL12. We did not observe any differences in CXCL12 signal compared to WT NIH3T3 cells, *i.e.* reduction or absence of CXCL12 proteins.

However, even if we did not observe CXCL12 down-regulation by RT-qPCR and immunostaining, we performed Boyden Chamber experiments with WT and siRNA treated NIH3T3 cells (Figure 3.70).

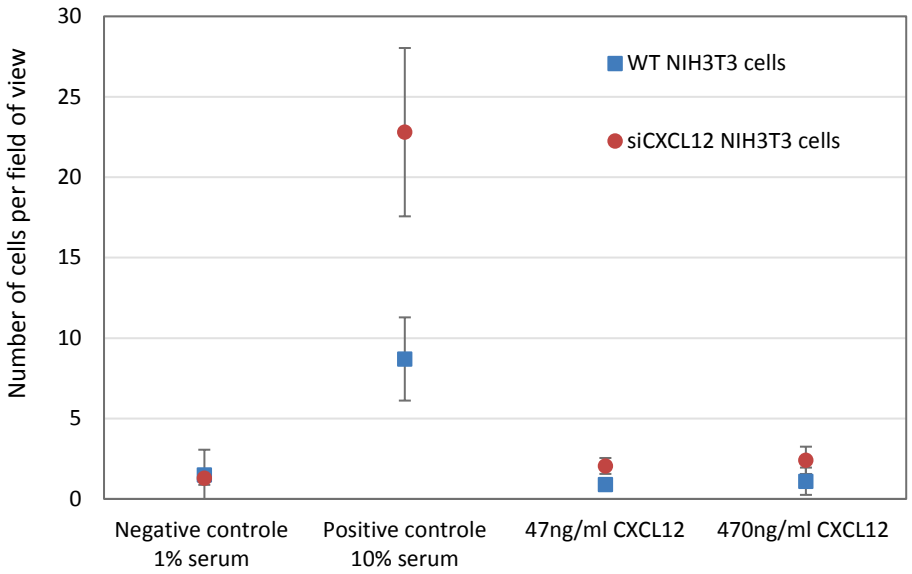

Figure 3.70: Boyden chamber experiments in serum and CXCL12 gradients. Data are presented as the mean number of NIH3T3 cells accumulated in the lower membrane of the Boyden chamber per field of view. Negative control: 1% to 1% serum gradient. Positive control 1% to 10% serum gradient. CXCL12 gradient: 1% serum to 1% serum + 6nM or 60nM CXCL12 gradient. 2 independents experiments for CXCL12 gradient experiments with Wild Type (WT) NIH3T3 cells and siCXCL12 NIH3T3 cells.

First, we did not observe migration of WT NIH3T3 cells towards the CXCL12 but we did observe cell migration towards 10%serum. These results confirm that NIH3T3 cells did not migrate towards CXCL12. NIH3T3 cells treated with siRNA CXCL12 migrate towards 10% serum whereas

they did not migrate towards CXCL12 gradient. Altogether, we did not see NIH3T3 cells migration towards CXCL12 in all the experiments performed.

We conclude that NIH3T3 cells are not a good cell line to study cell migration in response to a physiological CXCL12 gradient. For this reason, we studied migration of the breast cancer cell MDA-MB-231 which have been reported in the literature to response to CXCL12 gradients[14].

3.8.5 Migration of MDA-MB-231 cells towards serum and CXCL12 gradients

I first presented in this report that MDA-MB-231 cells were not able to migrate on 2D flat surfaces, but migrate when confined in 20µm^2 straight microchannels in the absence of chemical gradient (Figure 3.3 and Figure 3.4B). We then exposed the MDA-MB-231 cells to serum and CXCL12 gradients (Figure 3.71). 100nM is the concentration used in Müller et al. (2001) which strongly direct cell migration in Boyden chamber experiments. For this reason, we tested 100nM and 50nM CXCL12 concentrations and 10% serum and 20% serum gradients as controls in 20µm² straight microchannels.

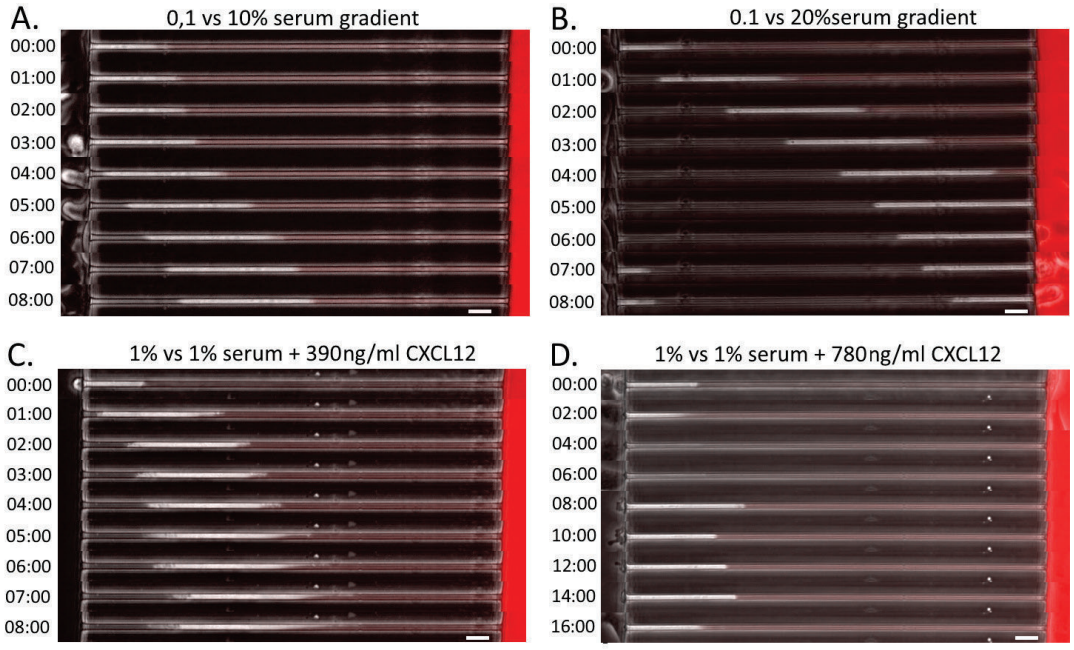

Figure 3.71: Migration of MDA-MB-231 cells in 20µm^2 straight microchannels in the presence of 10% (A.) and 20% (B.) serum gradient and 50nM (C.) and 100nM (D.) CXCL12 gradient. 1 experiment per condition. Time in hh:mm. Scale bar 20µm. See Movie 38, Movie 39, Movie 40 and Movie 41.

First, we observed that 10% serum gradient is able to attract MDA-MB-231 cells inside microchannels but did not efficiently induce cell migration. The cell, showed in Figure 3.71A, did not migrate the all microchannels length in 10% serum gradient (See Movie 38). In contrast, in the absence of serum gradient and during the same period of time, *i.e.* 8h, MDA-MB-231 cell migrate across the 20µm^2 microchannels length (Figure 3.4B and see Movie 4). Moreover, when we increased the serum gradient concentration to 20%, *i.e.* slope of the gradient, the number of cells entering the microchannels increases and the migration of MDA-MB-231 cells is more efficient compared to 10% gradient (Figure 3.71B and Movie 39). 50nM CXCL12 gradient is not able to attract cells into microchannels. The cell showed in Figure 3.71C is already at the

microchannel entry before the formation of CXCL12 gradient, did not migrate towards CXCL12 and started fluctuating 3h after cell entry into the microchannel (Movie 40). In contrast, cells in 10% and 20% serum gradient are more persistent. Moreover, 100nM CXCL12 gradient is also not able to attract cell inside microchannels. In addition, over 11 cells present inside microchannels before forming CXCL12 gradient, 7 cells migrate in the opposite direction of the gradient (Movie 41). As preliminary results, we observed MDA-MB-231 cells migration towards serum gradient, but not towards CXCL12 gradients. However, additional experiments are required to further confirm these results.

Altogether, the chemokine CXCL12 and its membrane receptors localization study reveals that CXCR4 is linked to lamellipodia activity and actin network in NIH3T3, SW480 and dHL60 cell lines; CXCR7 is not linked to lamellipodia and is present within the cell as vesicles. CXCL12 is not able to direct the migration of NIH3T3 cells in 4 different experiments, *i.e.* pipette on flat surfaces, in Boyden chamber, microcontact-printed and in confined microchannels. We supposed that CXCL12 production by NIH3T3 cells would suppress the chemoattractant effect of CXCL12. For this reason, we used MDA-MB-231 cells known to response to CXCL12 in Boyden chamber experiment. Surprisingly, they did not migrate towards CXCL12 gradients in confined microchannels. Therefore, we could doubt the reliability of Boyden chamber to study effective cell migration or of the chemoattractant effect of CXCL12 to direct cell migration.

Altogether, these results will be discussed and criticized in the next section.

4 Discussion

In this PhD thesis, we studied cell migration under confinement, mimicking the environment that cells can find *in vivo*. In addition, we compared two types of directed cell migration, chemotaxis and ratchetaxis. Chemotaxis has been widely studied whereas ratchetaxis has recently been described. They are both able to direct cell migration on 2D flat or topographical surfaces; chemotaxis directs also cell migration under confinement. The novelty of this project is to study ratchetaxis under confinement, combine or compete ratchetaxis with chemotaxis, and observe the overall cell migration. In addition, to be even closer to physiological conditions, we used a physiological gradient of CXCL12 and studied localization of its membrane receptors CXCR4 and CXCR7.

First, we defined the geometry of the ratchet unit. Ratchetaxis in confined environment is in fact a series of connected ratchet unit and it is called closed microchannels configuration. A ratchet unit volume is equal to the volume of a NIH3T3 cell in suspension, in order to confine the cell. Then, the geometry of the ratchet itself is modified: the opening angle α as well as the bottleneck area connecting two ratchets unit i are parameters that we changed. We then studied cell migration in these different configurations in straight microchannels, in the ratchet and against the ratchet directions. We observed than in every case, ratchet microchannels affected the migration of NIH3T3 cells. However, we chose one ratchet geometry for the rest of the study for its ability to impair cell migration and deform cell nucleus in confined microchannels. In addition, this ratchet geometry has been tested in less confined also called open microchannels configuration for its ability to direct cell migration. There, cell migration is clearly rectified. We will detail and discuss the results in the next section.

Next, we developed in the lab a microfluidic system to form soluble chemical gradients inside microchannels. The 10% serum gradient tested directed cell migration in any configuration. However, when we removed the serum gradient of cell inside ratchet microchannels, interesting phenomena occur: ratchet **favors** migration of cell **in the ratchet direction**. Ratchet **prevents** migration of cell **against the ratchet direction**. Altogether, cell migration and ratchetaxis will be discussed in the next section and a model will be proposed to explain ratchetaxis, chemotaxis and combination of both under confinement (Figure 4.1).

Last, we studied potential role of a physiological gradient of CXCL12 to direct cell migration. To date, we did not observe directed cell migration towards CXCL12. However, the study of the localization of the membrane receptors CXCR4 and CXCR7 brought interesting information: CXCR4 is linked to actin and lamellipodia activity whereas CXCR7 is linked to microtubules through the transport of its vesicles.

In this Discussion part, we will analyze the results obtained during this thesis and relate them to already published data. First, we will discuss the choice of the ratchet unit volume. Then, we will analyze the ratchet effect to direct cell migration in high and low confinement and in the presence and the absence of serum gradient. I will also discuss the physiological gradient of CXCL12 and its ability to direct cell migration.

4.1 Confined the cell: ratchet volume and *in vivo* relevance

Cell migration in confined ratchet is based on the measurement of the volume of NIH3T3 cells. We defined the ratchet volume at 1500µm^3, which corresponds to the mean volume of NIH3T3 cells, *i.e*. 1560±520µm^3. This value was deduced from the mean diameter of NIH3T3 cells right after plating and before cell spreading. Along this line, others have measured the volume of fibroblasts after trypsin treatment. Halter et al. (2009) measured a mean volume of NIH3T3 cells equal to 2300µm^3 by using automatic Coulter size measurement whereas Xie et al. (2018) measured a mean volume of NIH3T3 cells equal to 4000µm^3 by confocal microscopy[162,163]. However, it has been shown that fibroblast cell and nucleus volumes reduce after trypsin treatment[164]. It would suggest that in our measurement, we underestimate the cell volume. But surprisingly, two different teams published opposite results: they showed that the cell spreading, *i.e.* increased cell area, is associated with a decreased cell volume[163,165]. It has been observed in lived astrocytes and NIH3T3 cell lines by labelling the cytoplasm and using confocal microscopy[163,165]. They measured a volume of NIH3T3 cells equal to 4000µm^3 in suspension and to 1500µm^3 in adherent cells[163]. However, our data showed that NIH3T3 cells are efficiently confined inside a ratchet unit, *i.e.* 1500µm^3, as we can see in Figure 3.35. In addition to cell volume measurement, we quantified the dimensions of the nucleus of spread cells. The mean nucleus height is equal to 8.4±1.4µm. Therefore, we set the microchannels height to 5µm. The mean nuclear cross-section on 2D flat surfaces is roughly estimated to 90µm^2 from the nucleus height and minor nucleus axis measurement. We designed the ratchet geometry to have a cross-section area of 10µm^2, 20µm^2 and 30µm^2, respectively corresponding to 2µm, 4µm and 6µm opening width between ratchet unit. It is typically the size of blood capillaries or longitudinal tracks which can be found *in vivo*[35,36,39]. Thereby, within any ratchet microchannels, we observed nucleus deformation.

Altogether, the ratchet geometries designed confined the cell and the nucleus and lead to their deformation to fit to the ratchet geometry. In the next section, we will discuss how much the ratchet geometry affect the cell migration.

4.2 From 2D and topographical ratchetaxis to 3D ratchetaxis

4.2.1 Cell polarity in closed microchannels

In closed microchannels, we did not observe change in direction of cell migration. It seems that cell polarity is locked because of the strong confinement. In the open microchannels, *i.e.* low confinement, cells can change direction of migration. We could reduce the cell confinement in closed microchannels by increasing the microchannels height from 5µm to 10µm: the ratchet geometry would still be the same, but the volume of the ratchet unit would be multiplied by two. It would be the intermediate confinement configuration. There, we could propose that cells would be able to change direction of migration. Moreover, it would be interesting to check for polarity markers localization while cells are migrating in closed and open configurations. In fact, it has been shown that centrosome repositions while cells change direction of migration[74]. We have in the lab a DNA construct which allows the visualization of the centrosome and SiR tubulin which fluorescently labelled microtubules.

Preliminary experiments suggested that in the open and closed microchannels, the centrosome is located at the front of NIH3T3 cell nucleus (Figure 3.59). If we observe cell migration and centrosome position in closed microchannels, we could confirm the locked polarity in the closed microchannels and explain the absence of change in direction of migration. In another experiment, we could force the cell to change direction of migration by adding a chemoattractant gradient at the back of cell migrating in the closed microchannels. This experiment is inspired by Prentice-Mott et al. (2015). They observed that 90% of dHL60 cells change direction of migration after addition of the chemoattractant at the back of the cells in confined microchannels. However and in contrast to NIH3T3 cells, dHL60 cells can spontaneously change direction of migration in the absence of chemoattractant gradient. dHL60 are neutrophil-like cells, they form weak adhesions to the substrates, migrate faster than NIH3T3 cells and can highly deform their nucleus. Despite the difference between NIH3T3 and dHL60 cells, it would be interesting to observe if NIH3T3 cells can repolarize and change in direction of migration after addition of the chemoattractant at the cell back. In the absence of change in direction of migration*,* it would suggest, *in vivo,* that once a cancer cell enters a really narrow capillary, such as 6µm in diameter -mean diameter of a human brain capillary[37]- it would migrate persistently in one direction and would not change direction of migration.

4.2.2 Explaining the mechanism of cell migration in confined microchannels

First, we will consider cells migrating in straight microchannels. Once a cell enters straight microchannels, it migrates persistently until the end of the microchannel, *i.e.* 350µm long. To explain this mode of migration, the model of Hawkins is kept[10]. It is also called “pushing off the walls” and we can summarize it by saying that a polarized cell can spontaneously migrate under confinement due to the frictions generated at the interfaces between the cell membrane and the channel walls and the difference in pressure across the cell. As suggested by the model, we observed an increased in persistent speed for NIH3T3 and dHL60 cells in straight microchannels compared to cells migrating on 2D flat surfaces. For NIH3T3 and dHL60 cells, the persistent speed is respectively equal to 43±28µm/h and 9.1±2.9µm/min on 2D flat surfaces and equal to 76±34µm/h and 21.8±3.2µm/min in 20µm² and 10µm² straight microchannels respectively. In our hand, it is associated with an increased in persistent time and length, *i.e.* for NIH3T3 cells persistent time and length on 2D flat surfaces are equal to 1.9±1.5hours and 69±39µm and in 20µm² straight microchannels equal to 4.1±2.6hours and 295±90µm and for dHL60 cells, persistent length on 2D flat surfaces is equal to 26±17µm and in 10µm² straight microchannels 282±21µm. We observed also that the non-motile MDA-MB-231 cells on flat surfaces become motile when confined in microchannels. In fact, Liu et al. (2015) showed that low adhesion and high confinement induce mesenchymal to amoeboid transition and as a result, cells used frictions generated between the cell membrane and the channel walls to migrate[17]. This explains how MDA-MB-231 cells migrate under confinement.

In straight microchannels, we observed the presence of focal adhesions in migrating NIH3T3 cells by immunostaining and by transfecting the cells with the construct Zyxin-RFP (page 101). Preventing cell adhesion in confined environment further increase cell speed by shifting cell migration mode to an amoeboid-like one[17]. We could incubate the microchannels with PLL-g-PEG which is a cell repellant and therefore prevents focal adhesions formation.

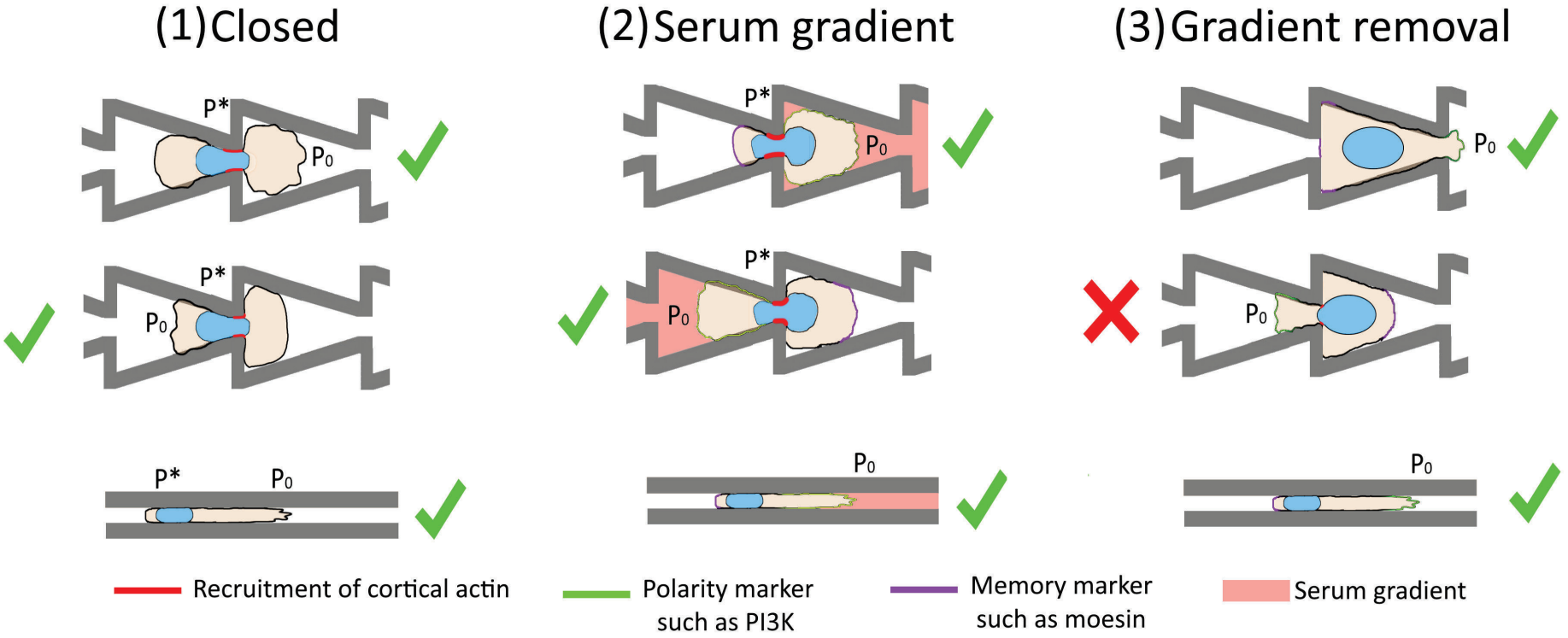

Figure 4.1: Schematics of the proposed mechanisms for cell migration in the closed configuration without and with serum gradient and after gradient removal. (1) In closed straight microchannels, a pressure gradient across the cell generates frictions between plasma membrane and channels walls and leads to cell migration. Theren the pressure gradient is constant. In ratchet microchannels, frictions are still generated but the maximal pressure is reached at the ratchet bottleneck. The pressure gradient varies with the position of the nucleus related to the bottleneck. Actin is recruited at bottleneck to facilitate nucleus passage by exerting pushing forces. However, the absence of actin recruitment prevents the nucleus passage. As a result, mean persistent length is reduced compared to cell migrating in straight microchannels. (2) The serum gradient eases the recruitment of actin at the bottleneck of the ratchet and maintains the cell polarity with asymmetric distribution of proteins associated to actin organisation, such as PI3K at the cell front and moesin at the cell back. As a result, the mean persistent length increases. (3) The cell polarity is maintained for some time. As a result, migration is favoured in the ratchet direction and straight microchannels. Against the ratchet direction, the nucleus prevents the passage through the bottleneck. P_0, pressure equal to 0 at the cell front. P*, pressure maximal reached at the ratchet bottleneck and cell back.

Without focal adhesion and NIH3T3 cells should be able to migrate faster in straight and ratchet microchannels.

Next, we compared cell migration in straight and ratchet microchannels. The "pushing off the walls" mechanism still explained cell migration in confined environment. Cells used frictions to move. However, in contrast to straight microchannels, we observed that the migration of dHL60 and NIH3T3 cells migrating in any ratchet microchannels is impaired: cells are able to detect the irregularity of the environment and as a consequence cell persistency is reduced. In straight microchannel, the pressure gradient is the same along the cell and during cell migration. However, the pressure gradient varies in the ratchet configuration according to the position of the cell inside the ratchet microchannels. At the bottleneck of each ratchet, pressure and frictions are most probably maximal around the nucleus (Figure 4.1). In fact, dendritic cell entering into constriction zone recruits cortical actin around the nucleus, leading to the generation of pushing forces favoring nucleus passage[126]. It is an active process which required actin polymerization and is dependent on actin and Arp2/3 complex integrity[126]. In addition, Thiam et al. (2016) observed that the absence of actin recruitment around the nucleus prevented the cell passage through the constriction[126]. In our configuration, it would be interesting to check if actin is recruited around the nucleus of NIH3T3 cells migrating across the ratchet bottleneck. It could indicate increasing pushing forces at the ratchet bottleneck favoring the nucleus passage and cell migration. The absence of actin recruitment could explain why some cell pauses. Another way to check if the nucleus constriction leads to the recruitment of pushing forces is to measure an increased in cell velocity after the bottleneck passage. As preliminary analysis, I plot the instantaneous velocity as a function of time for NIH3T3 cells migrating in the ratchet and against the ratchet direction and in straight microchannels (Figure 4.2.)

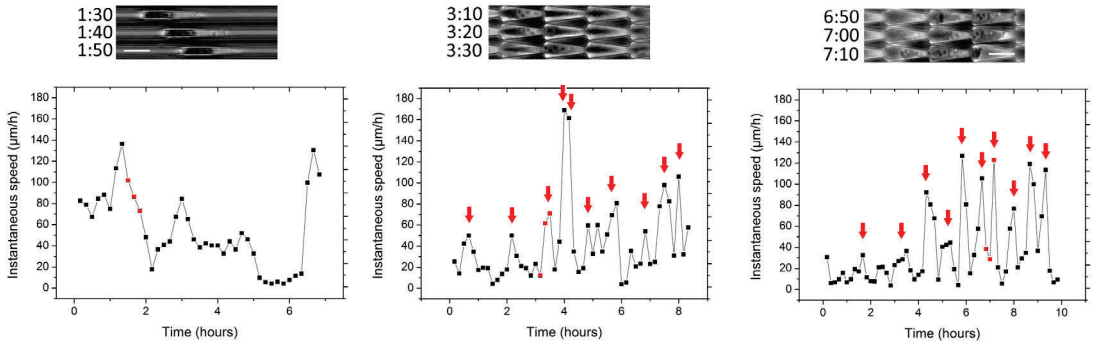

Figure 4.2: Instantaneous cell speed as a function of time. First row. Time series of the cell passage through the ratchet bottleneck. Same cells than in Movie 5, Movie 9 and Movie 10. Second row. The cell speed increases after the passage of the nucleus through the ratchet bottleneck in the ratchet direction and against the ratchet direction. Each red arrow corresponds to the cell passage through one ratchet bottleneck. The red squares represents the time points presented in the first row. As a reminder, one ratchet microchannel contains 10 bottlenecks.

The sudden increase in cell speed after its passage through each bottleneck suggests the existence of pushing forces which form around the nucleus and favors the nucleus deformation and passage. These analyses are preliminary and need to be confirmed with a larger number of cells. In addition, observing the recruitment of actin around the nucleus would further confirm this point. Altogether, we support the idea that frictions and pressure differences across the cell induces cell migration under confinement. In ratchet microchannels, the nucleus has to deform

probably leading to cortical actin recruitment, generating pushing forces and favoring nucleus passage (Figure 4.1). However, we did not explain how cell migration can be directed. In the next section, we will compare the different ratchet microchannels tested and try to explain the mechanisms behind the directed cell migration in ratchet microchannels.

4.2.3 Ratchetaxis under confinement directs cell migration

Different closed ratchet designs have been tested in this project; mainly the cross-section area connecting two ratchet units have been modified. 10µm^2 bottleneck area completely prevents cell migration (Table 4.1). Cells usually migrate one ratchet unit and die or pause for several hours (Figure 3.18, 2.5hours). In contrast, in 10µm^2 straight microchannels, Amélie Godeau showed that NIH3T3 cells were able to migrate on average 282±21µm[51]. It means that it is not the 10µm^2 cross-section area which is preventing cell migration but rather the fact the cell and, critical point, the nucleus have to actively and strongly squeeze to allow its passage. As a reminder, the nucleus cross-section is roughly equal to 90µm^2 on flat surfaces; therefore, a 9-fold reduction of nucleus cross-section is imposed. In fact, it has been reported that breast cancer cells can cross such narrow bottlenecks, down to 6.5µm^2 in cross-section[124,125]. However, we should mention that Denais et al. (2016) reported this migration in the presence of a serum gradient and 10µm^2 bottleneck induced nuclear envelope rupture associated to DNA damages[125]. Moreover, Lautscham et al. (2015) followed cell migration in microchannels containing a series of decreasing bottlenecks. They observed that the proportion of cells at the bottleneck entry is higher than inside or outside the bottleneck. However, they did not highlight the fact that the cells spent at least 5h in front of the narrower bottleneck, *i.e.* 6.5µm^2 in cross-section, before entering the microchannels. Together with our results, it suggests that cells can cross very narrow bottlenecks but this is associated to strong nuclear deformations and would induce DNA damages. 10µm^2 cross-section is too restrictive to allow quick NIH3T3 cell migration, neither directed cell migration. In fact, it shows that the nucleus, which is the stiffest and biggest organelle of the cell, blocks or prevents cell migration[18]. We can clearly see it in the example of the two dHL60 cells migrating in α16i10 ratchet microchannels: the cell with an elongated nucleus migrates much faster than the cell with a round nucleus (Figure 3.37).

Table 4.1: Summary of the persistent length, time and speed of the first persistent motion of NIH3T3 cells in straight and ratchet microchannels.

		Persistent length (µm)	Persistent time (hours)	Persistent speed (µm/h)
α16i10	+	39±14	1.7±1.1	33±26
	-	40±24	2.1±1.8	30±20
20µm²		295±90	4.1±2.6	76±34
α16i20	+	203±126	3.6±2.6	54±27
	-	197±121	4.2±3.1	54±28
30µm²		269±77	5.6±3.6	58±32
α16i30	+	215±127	4.6±3.2	52±25
	-	233±119	5.5±3.3	46±25
α24i30	+	229±109	4.3±2.4	66±34
	-	227±116	4.1±2.3	54±27

We noted that the decreased in mean persistent length of NIH3T3 cells migrating in the different ratchet microchannels is linked to areduced cross-section area (Table 4.1). Ratchet units separated by 20µm² and 30µm² in cross-section impaired cell migration but did not prevent it. This phenomenon has been reported by Le Berre et al. (2013). They studied ratchetaxis and rectification of cell migration placed under tilted pillars which mechanically and asymmetrically deformed the nucleus. The tilted pillars heights vary, changing the nucleus deformation under the tilted pillars. There, it is the nucleus deformation which sets the direction of migration (page 64). They observed that a strong nucleus deformation prevented cell migration[20]. It could correspond in our configuration, to 10µm² bottleneck area, *i.e.* α16i10 ratchet microchannel, where cells cannot migrate. Then, in low nucleus deformation, they did not observe directed cell migration[20]. It could correspond in our configuration, to 30µm² bottleneck area, *i.e.* α16i30 and α24i30 ratchet microchannels which have the highest persistent lengths. However, they observed cell rectification at intermediate nucleus deformation[20]. In our case, the intermediate confinement could correspond to 20µm² bottleneck, *i.e.* α16i20. We did not observe cell rectification in closed α16i20 configuration, however, we observed persistent length reduction associated with a decreased in persistent speed. In fact, we were expecting to see cell rectification in one direction, *i.e.* in the ratchet or against the ratchet directions, where persistent length would be longer or cells would change direction of migration. In contrast, we observed that NIH3T3 cell entry in the microchannel sets the direction of migration and cells did not change direction of migration.

We reduced the cell confinement by preparing the open microchannels configuration. We observed first that cells can change direction of migration and second that cells did preferentially migrate in one direction. We observed an increased in persistent length and biased NIH3T3 cells migration in the open ratchet microchannels. In addition, we observed the migration of dHL60 cells in the closed microchannels. They are smaller in size than NIH3T3 cells and therefore are not confined in a ratchet unit, *i.e.* 1500µm³: volume of a ratchet; 800±210µm³: volume of HL60 cells. These cells can change direction of migration in ratchet microchannels and migrate preferentially against the ratchet direction of closed α16i10 microchannels. Altogether, we confirm previous studies published in the lab: ratchetaxis is able to direct cell migration on flat surfaces, topographical surfaces and under confinement[15,16]. This confirms that the presence of any external gradient is not necessary to direct cell migration. Asymmetric and repetitive motifs present in the environment under confinement can direct cell migration.

To conclude, we suggest that the mechanisms leading to cell migration under confinement are linked to the frictions generated by the cell membrane to the channel walls. In addition, the ratchet configuration leads to nucleus deformation and most probably to the recruitment of actin cortex around the nucleus, facilitating nucleus passage. The second part of this project was to form chemical gradient inside microchannels and to study ratchetaxis in the presence of chemical gradient. The results obtained will be discussed in the next section.

4.3 Chemotaxis in confined and unconfined environment

4.3.1 Importance of chemoattractant gradients to direct cell migration

In this PhD thesis, Boyden chamber, pipette and microchannels experiments were performed to study cells chemotaxis. Boyden experiment is the classical experiment to assess cell chemotaxis. Two chambers are separated by a 15µm thick porous membrane. In the presence of a chemoattractant gradient, cells will cross the 15µm thick membrane and accumulate to the lower chamber. Pipette experiment allows the formation of a soluble gradient on 2D flat surfaces[110]. Chemoattractant is delivered by the pipette and the gradient is visualized with a fluorescent dye. Cells attracted by the chemoattractant will migrate towards the pipette, *i.e.* highest chemoattractant concentration.

We then used a microfluidic ladder chamber system to form chemical gradient inside microchannels[21]. In both main channels, medium containing the chemoattractant and medium without chemoattractant are continuously injected. Between the two main channels are placed 350µm length microchannels where cells are migrating under confinement. Chemical gradient forms within the microchannels by diffusion and is stable for up to 24h.
With pipette, Boyden and microfluidic experiments, a 10% serum gradient has been formed and was able to efficiently direct NIH3T3 cells migration. In this PhD thesis, we studied cells migration under confinement, our interest was then focused on gradients formed inside microchannels. We saw that 10% gradient directed cell migration of NIH3T3 cells inside microchannels. However, a 20% serum gradient was necessary to direct migration of MDA-MB-231 cells. We did observe MDA-MB-231 cells attraction to and entry in the microchannels in the presence of 10% gradient, however a 20% serum gradient was more efficient to direct cell migration. The slope of the gradient plays then a key role in the directed cell migration process. In fact, it has been reported that higher is the chemical gradient, more efficient is the cell migration in term of percentage of cells which enter and exit the microchannels[11]. In addition, Tong et al. (2012) observed that the microchannels widths affect the efficiency of directed cell migration. 100% of cells enter in 500µm^2 cross-section microchannels compared to 15% cells entry in 30µm^2 cross-section microchannels for the same serum gradient[11]. Altogether, this highlights the importance of gradients and microchannels geometry to direct cell migration.

4.3.2 Cell migration mechanism in the presence of serum gradient and after gradient removal

It has been reported that the addition of a chemical gradient at the cell proximity induces cell polarization, asymmetric distribution of cellular component and directed cell migration[114,115]. On 2D flat surfaces, PI3K is quickly and asymmetrically distributed in dHL60 cells, *Dictyostelium* cells and fibroblasts after chemoattractant stimulation, less than 30sec for HL60 and *Dictyostelium* cells and around 3min for fibroblasts[114,115,166]. PI3K seems to be the first messenger produced after membrane receptors stimulation and promotes the activation of Rho GTPases, thereby activating actin binding proteins and inducing actin polymerization at the cell front and myosin accumulation at the cell back. It allows also reorganization of actin cytoskeleton and

maintenance of the cell polarity[167]. It was shown that the addition of a chemoattractant induces an increased in F-actin polymerization[14,168]. In confined microchannels, the activation of PI3K at the cell front is also observed in response to chemical stimulation[12]. In straight and ratchet microchannels, we observed cells attraction into the microchannels in response to 10% serum gradient. In straight microchannels without and in the presence of 10% serum gradient the persistent length is close to the maximal length of the microchannels, *i.e*. 295±89µm and 277±96µm with serum gradient. Moreover, in the ratchet microchannels in both directions, we observed an increased in mean persistent length compared to in the absence of serum gradient, in the ratchet direction, 203±126µm and 278±66µm without and with serum gradient respectively and against the ratchet direction, 197±121µm and 263±87µm without and with serum gradient respectively. It indicates that the 10% serum gradient directed cell migration in any microchannel and increased also the persistency. In the presence of 10% serum gradient in confined microchannel, we could think that PI3K located at the cell front would favor actin polymerization and maintain and reinforce the cell polarity. Probably, serum gradient could favor the polymerization of actin around the nucleus, favoring the nucleus passage at the bottleneck of the ratchet (Figure 4.1). As a result, migration in ratchet microchannels would be facilitated, as observed with the increased in mean persistent length. It could be verified by observing the recruitment of actin around the nucleus: the speed and/or the localization of the actin recruitment would precise the potential role of cortical actin recruitment in the cell migration process under confinement.

In addition, it would be interesting to test another serum gradient. Preliminary experiments showed that 2% serum gradient attracted NIH3T3 cell inside microchannels. We wonder how much the cell migration would be favored in ratchet microchannels in the presence of 2% serum gradient. Prentice-Mott et al. (2016) showed that lower chemoattractant gradients reduced strongly the persistency of dHL60 cells migrating in straight microchannels. 2% serum gradient would be an intermediate condition between cell migration in ratchet microchannels in the absence and in the presence of 10%serum gradient: an increased mean persistent length would be observed compared to in the absence of serum gradient but the mean persistent length would be lowest than in the presence of 10% serum gradient.

In the last part of the study on NIH3T3 cells ratchetaxis and chemotaxis cell migration, we decided to remove the 10% serum gradient of cells already inside the microchannels. Interestingly, we observed different results after 10% serum gradient removal. In straight and ratchet direction microchannels, the majority of cells migrate after gradient removal in the same direction, *i.e.* previous serum gradient. It indicates that cells are still polarized after gradient removal. However, against the ratchet direction, the majority of the cells stop their migration after gradient removal. Even if the cell is still polarized, it clearly appeared that the nucleus blocked the cell passage. Prentice-Mott et al. (2016) observed, in straight microchannel, the depolarization of dHL60 cells almost instantaneously after gradient removal as observed by the loss of PI3K accumulation at the cell front. It is associated with the arrest of cell migration. In the kymographs presented in the paper, we observed a few seconds delay between gradient removal, loss of cell polarity and arrest of cell migration[12]. In addition, they observed an asymmetric localization of moesin at the back of the cell maintained few minutes after gradient removal and loss of PI3K polarity. They suggested that asymmetric distribution of moesin, which

linked actin cortex to the plasma membrane, is the protein which allows directional memory after chemical gradient removal. This cytoskeletal memory could also exist in NIH3T3 cells. Together with pressure gradient generated by the confinement, it could favor the migration of NIH3T3 cells in the ratchet direction and in straight microchannels. However, the obstacle depicted by the nucleus against the ratchet direction is too important to be overcome by the pressure gradient across the cell or the directional memory of the cell (Figure 4.1). Usually, we formed the serum gradient for 8h, to allow the cell entry and migration into the microchannels. Then the gradient is removed for up to 12hours. It would have been interesting to acquire cell migration for 12h to 24h more. Cells trapped inside microchannels may have started to migrate again. There, we could expect cell migration mainly in the ratchet direction.

Altogether, to explain why the nucleus prevents cell migration against the ratchet direction, we could look at the asymmetric localization of proteins such as moesin and the actin organization after gradient removal.

4.4 The chemokine CXCL12 and the localization of the membrane receptors CXCR4 and CXCR7

CXCL12 is a chemokine involved in physiological and pathological processes such as embryogenesis and cancer spread[131]. It is mainly produced by lungs, lymph nodes and liver[14]. CXCL12 binds two membrane receptors CXCR4 and CXCR7. CXCL12 axis is involved in cell survival, migration and differentiation[131]. We are mainly interested in cell migration, and more precisely in the case of cancer cell migration. In fact, it is widely accepted that breast and colon metastatic cancer cells, which overexpressed CXCR4 and CXCR7, developed metastasis mainly in lungs and liver, organs producer of CXCL12[13,14]. For this reason, the presence of a CXCL12 gradient at lungs and liver proximity which would attract cancer cells into these organs has been proposed. However, there is no proof of this gradient *in vivo*. In this PhD thesis, we first studied the localization of the two membrane receptors. An asymmetric localization of both membranes receptors would be responsible for the symmetry breaking event leading to cell polarization and directed cell migration. Second, we observed the directed cell migration in response to CXCL12 stimulation. The results obtained will be discussed in the next section.

4.4.1 CXCR4 is linked to actin and CXCR7 to microtubules

We observed a differential localization of CXCR4 and CXCR7 in NIH3T3 and SW480 cells, in fixed and lived samples. CXCR4 is linked to lamellipodia and accumulates at the cell edges where lamellipodia are active whereas CXCR7 is not present in lamellipodia and in lived samples, CXCR7 migrate in vesicles along microtubules. This differential localization has been observed in the absence of CXCL12 stimulation. However, CXCL12 has been detected in the serum of healthy patient, about 10ng/ml serum[141]. It could be present also in bovine serum used in the culture medium. In addition, it has been shown that NIH3T3 cells are CXCL12 producer, about 40pg per ml of supernatant[22]. Therefore, it could activate basal signaling pathways. CXCR7 K_D being lowest than CXCR4 k_D (0.4nM versus 3.6nM), in the presence of small concentrations of CXCL12, CXCR7

would be activated and internalized first. It could explain the presence of CXCR7 mainly into vesicles whereas CXCR4 would still be present in the plasma membrane. In fact, study reported the endocytosis of CXCR4 into vesicles after CXCL12 stimulation[169,170]. We observed CXCR7 vesicles motion along microtubules in both directions, most probably due to dyneins and kynesins cargo proteins. In contrast and as mentioned previously, we observed accumulation of CXCR4 at the cell edges and more precisely in lamellipodia and actin-rich region. In lived images we observed actin and CXCR4 retrograde flow, *i.e.* actin depolymerization at the cell leading edge, equal to 34±11nm.s^{-1}. This process has widely been studied and retrograde flow measured. Our measurements are in agreement with already published data[161]. The retrograde flow speed is inversely proportional to the traction forces applied by the focal contacts[171]. When CXCR4 is overexpressed, actin retrograde flow is higher compared to control actin retrograde flow, *i.e.* 23±3nm.s^{-1}. It could indicate that at the lamellipodia level, CXCR4 overexpression leads to less traction forces exerted to the substrates. Altogether, it suggests that CXCR4 is linked to the actin network. In fact, such link has been investigated: after CXCL12 stimulation, an increased in F-actin polymerization is observed, CXCR4 colocalized with the formin mDia at the cell periphery, CXCR4 internalization is dependent on myosin IIA integrity or can lead to Rac1 activation[14,135,149,168,170].

To conclude, both membrane receptors integrity is required to induce collective cell migration *in vivo*[24,111,172]. The asymmetric distribution of CXCR4 and CXCR7 could explain the symmetry breaking event leading to directed cell migration. In the next section, we will discuss the results obtained for NIH3T3 and MDA-MB-231 cells migration in response to CXCL12 stimulation.

4.5 Physiological CXCL12 gradients

4.5.1 Migration of NIH3T3 cells towards CXCL12

In this PhD thesis, we wanted to study the migration of NIH3T3 cells under confinement and in the presence of the physiological gradients of CXCL12. As mentioned in the results section page 139, we challenged the migration of NIH3T3 cells in different environments, on flat surfaces, *i.e.* pipette experiments and adhesive lines of CXCL12, under confinement, *i.e.* microchannels and in Boyden chambers. We did not manage to observe NIH3T3 cells migration towards CXCL12. These results will be discussed in the following part and I will talk more about the microcontact-printing experiments which allow the formation of adhesive lines of CXCL12.

The formation of soluble gradients of CXCL12 failed to attract NIH3T3 cells. For this reason, we decided to form adhesive lines of CXCL12 and observed the migration of NIH3T3 cells through a haptotatic process. Along this line, Zhang et al. (2015) observed the directed migration of neural progenitor cells towards adhesives lines of CXCL12[120]. In our lab, microcontact-printing is a protocol daily used[15]. For this reason, we first decided to adapt the protocol by microcontact-printing the protein CXCL12 mix with fluorescent molecule, such as Dextran-TRITC. Dextran-TRITC is used to visualize the motifs microcontact-printed. We microcontact-printed also Dextran-TRITC alone as a control. We did not observe NIH3T3 cells migration towards CXCL12 but more importantly we observed that Dextran-TRITC motifs repulse NIH3T3 cells. In fact, it has been shown that Dextran-coated surfaces reduce the adhesion and spreading of NIH3T3 cells[173].

In addition, Dextran prevents the adhesion of T cells to endothelial cells by inhibiting integrin clusterization[174]. Altogether, it explained why NIH3T3 cells did not migrate isotropically on Dextran-TRITC surfaces and could be the reason why we did not observe directed cell migration towards CXCL12. To overcome this problem, we then decided to first microcontact-print CXCL12 alone and second visualize CXCL12 motifs by immunostaining. We managed to observe fluorescent patterns on the coverslip, confirming that CXCL12 has been transferred. However, we visualized CXCL12 through an indirect way. Following the immunostaining, we do not know how much CXCL12 is transferred to the coverslip, neither if immunostaining protocol affects cell migration. In addition microcontact-printing is not an easy protocol to master: it needs a lot of experiences and skills to make it reproducible. However, the protocol could be optimized by first using fluorescent-coupled CXCL12 protein. Altogether, preliminary experiment on cell migration studies did not reveal accumulation of NIH3T3 cells on CXCL12 lines, neither directed cell migration towards CXCL12, in contrast to Zhang et al (2015) observations for neural progenitor cells[120,148]. Adherent CXCL12 was not able to direct NIH3T3 cells migration.

We proposed that NIH3T3 cells did not migrate towards CXCL12 because they are CXCL12 producer[22]. However, we thought that NIH3T3 cells could still be sensitive to an external gradient of CXCL12. In Schiraldi et al. (2012) study, they observed the migration of NIH3T3 cells in Boyden chamber experiment in response to the chemoattractant HMGB1 (high mobility group box1). This migration is dependent on CXCL12 and CXCR4 activation. In fact, CXCL12 and HMGB1 form a heterocomplex and bind to CXCR4[22]. They did not measure the migration of NIH3T3 cells towards CXCL12 in Boyden chamber. However, they highlighted the fact that CXCL12-CXCR4 axis could be involved in the migration of NIH3T3 cells in response to specific chemical gradient. In our straight microchannels, it would be interesting to study NIH3T3 cells migration in response to HMGB1 gradient. In this case, we suppose that directed NIH3T3 cell migration would be associated to membrane receptors relocalization at the cell front. In contrast, we tried to down-regulate CXCL12 production in NIH3T3 cells and to follow cell migration towards CXCL12. However, preliminary experiments of down-regulation were not conclusive and we preferred to study the migration of the breast cancer cells MDA-MB-231 towards physiological gradients of CXCL12.

4.5.2 Migration of the breast cancer cell MDA-MB-231 cells towards CXCL12

Studies report that CXCL12 axis plays a key role in the metastatic spreading of breast cancer, in particular by inducing the migration of the breast cancer cell MDA-MB-231 cells in response to CXCL12 in Boyden chambers[14,175]. In both studies, inhibition of CXCR4 and CXCR7 leads to a reduction of MDA-MB-231 cells migration. For this reason, we followed the migration of MDA-MB-231 cells in 20µm² microchannels and with two gradients of CXCL12, 50nM and 100nM, concentrations used in Müller et al. (2001) study. Surprisingly, we did not observe MDA-MB-231 cells migration. Moreover and in contrast to serum gradient, cells were not attracted inside microchannels and cells present in the microchannels before CXCL12 gradient formation escaped from the microchannels in the opposite direction of the CXCL12 gradients. As a reminder, straight microchannel used are 20µm² in cross-section and 350µm long, whereas pores in the membrane of Boyden chamber are 50µm² in cross-section and 15µm long.

Altogether, these results are in opposition to the one obtained in Boyden chamber in Müller et al. (2001) and Qian et al. (2018). There, they observed a dose-dependent effect of CXCL12 on cells migration, the optimal CXCL12 concentration is respectively 100nM and 100ng/ml (12nM)[14,175]. Different hypotheses can be formulated to explain the absence of directed cell migration in our configuration: 1) 20µm² straight microchannels are too confined and do not allow the optimal MDA-MB-231 cells migration. In the presence of serum gradient, it is known that percentage of MDA-MB-231 cell which enter and exit from a microchannel decreased when the confinement increases[11]. 2) We should reproduce Boyden chambers experiments which would confirm in our hands, the directed MDA-MB-231 cells migration towards CXCL12. In addition, we could change the microchannels dimensions in terms of length and cross-section area and vary CXCL12 concentrations to see if a potential directed MDA-MB-231 cells migration could be observed. 3) We can speculate that CXCL12 is not a chemoattractant molecule for MDA-MB-231 cells, but play other roles to promote cancer progression. It can induce angiogenesis, favor cell adhesion or promote cell extravasation[48,135,136,156,159,175].

Altogether, we observed an asymmetric distribution of CXCR4 and CXCR7 in NIH3T3, SW480 and dHL60 cells. CXCR4 are linked to actin network and lamellipodia activity whereas CXCR7 are linked to microtubules. Asymmetric distribution of cellular components such as CXCR4 and CXCR7 leads to directed cell migration. However, we did not manage to observe NIH3T3 and MDA-MB-231 cells migration towards physiological gradients of CXCL12. More experiments have to be performed to determine if the microchannels conditions used or CXCL12 concentrations tested were the optimal ones. We cannot deny the fact that CXCL12 may not be able to direct cell migration over long distances in confined environment. *In vivo,* cancer cells accumulation into the organs producer of CXCL12 may not be due to the presence of a gradient of CXCL12. In contrast, cancer cells arrest at organs proximity would first be due to size restriction and second, optimal environment would favor tumor growth. CXCL12 may favor tumor spreading through the activation of CXCL12-mediated pathways promoting angiogenesis, cell adhesion or extravasation.

5 Conclusion and outlook

The objective of this PhD thesis was to direct cell migration under confinement through ratchetaxis and in the absence of chemical gradient. To be closer to *in vivo* conditions, we designed closed microchannels whose dimensions mimic blood capillaries. Cells are confined from the top and sides. In addition, the ratchet unit had the volume of a NIH3T3 cell. We first proved that the geometry of the ratchet affect the migration of NIH3T3 cells. The nucleus is the stiffest and largest organelle of the cell. It strongly deformed to fit to the ratchet geometry. Its large squeezing drastically impaired cell migration*, i.e.* 10µm² area bottleneck, whereas intermediate and small squeezing, *i.e.* 20µm² and 30µm² area bottleneck, impaired cell migration without preventing it. In addition, we observed that under strong confinement, cells cannot change direction of migration. The cell entry in the microchannel sets the direction of migration. We produced open microchannels to reduce cell confinement. Cells are confined from the sides. There, we successfully managed to direct cell migration under confinement. Altogether, we proved that ratchetaxis is a powerful tool to direct cell migration in the absence of chemical gradient. The combination of ratchetaxis and chemotaxis reveals that the 10% serum gradient used increases the cell persistency. However, after serum gradient removal, a clear effect of the ratchet appeared. Against the ratchet, the migration is completely suppressed after gradient removal, the nucleus being blocked by the ratchet. In contrast, in the ratchet direction, cell migration is favored due to the memory of the previous gradient. In the future, it would be interesting to understand in confined ratchet microchannels why cell migration is impaired. First, we could observe if there is recruitment of actin cortex at the ratchet bottleneck, which would exert pushing forces around the nucleus facilitating its passage. We propose that the absence of actin recruitment prevents cell migration whereas serum gradient favors its formation. Second, serum gradients play a key role in directing cell migration. An increased serum gradient would improve the cell memory and favor cell migration after gradient removal.

In this PhD thesis, we criticized the use of Boyden chamber as classical experiments to study cell migration. Boyden chambers conditions are far from *in vivo* conditions: cells have to migrate distances smaller than their size and in addition the stability of the gradient cannot be ensured during the time of the experiment. We still used Boyden chamber to validate our microchannels set-up. In contrast to published data in Boyden chamber, we did not observe breast cancer cell migration towards CXCL12 gradients in our microchannels. We can both doubt the reliability of Boyden chamber and CXCL12 gradients to direct cell migration over long distances.

Our results suggest that *in vivo,* a cell which migrates into narrow capillaries would not be able to change direction of migration. It supports studies which report that cancer cell are arrested at the organ proximity by size restriction. In addition, *in vivo*, the environment is complex and heterogeneous and cells migrate mainly under confinement. The presence of any repetitive motifs in the environment along perineural tracks or myofibers could lead to directed cell migration. Moreover, *in vitro* we saw that in a chemically changing environment, the geometry of the environment could favor or prevent cell migration. *In vivo*, it could suggest that cells would be both sensitive to the disappearance of chemical cues at the cell proximity and to the asymmetric environment which would influence the overall cell migration.

BIBLIOGRAPHY

1. Niethammer, P., Grabher, C., Look, A. T. & Mitchison, T. J. A tissue-scale gradient of hydrogen peroxide mediates rapid wound detection in zebrafish. *Nature* **459,** 996–999 (2009).
2. Bénazéraf, B. *et al.* A random cell motility gradient downstream of FGF controls elongation of an amniote embryo. *Nature* **466,** 248–252 (2010).
3. Chambers, A. F., Groom, A. C. & Macdonald, I. C. Dissemination and growth of cancer cells in metastatic sites. *Nat. Rev. Cancer* **2,** 563–572 (2002).
4. Yamauchi, K. *et al.* Development of real-time subcellular dynamic multicolor imaging of cancer-cell trafficking in live mice with a variable-magnification whole-mouse imaging system. *Cancer Res.* **66,** 4208–4214 (2006).
5. Yamauchi, K. *et al.* Real-time in vivo dual-color imaging of intracapillary cancer cell and nucleus deformation and migration. *Cancer Res.* **65,** 4246–4252 (2005).
6. Boyden, S. The chemotactic effect of mixtures of antibody and antigen on polymorphonuclear leucocytes. *J. Exp. Med.* **115,** 453–466 (1962).
7. Petrie, R. J., Gavara, N., Chadwick, R. S. & Yamada, K. M. Nonpolarized signaling reveals two distinct modes of 3D cell migration. *J. Cell Biol.* **197,** 439–455 (2012).
8. Hung, W. C. *et al.* Distinct signaling mechanisms regulate migration in unconfined versus confined spaces. *J. Cell Biol.* **202,** 807–824 (2013).
9. Lämmermann, T. *et al.* Rapid leukocyte migration by integrin-independent flowing and squeezing. *Nature* **453,** 51–55 (2008).
10. Hawkins, R. J. *et al.* Pushing off the walls: A mechanism of cell motility in confinement. *Phys. Rev. Lett.* **102,** 1–4 (2009).
11. Tong, Z. *et al.* Chemotaxis of cell populations through confined spaces at Single-Cell resolution. *PLoS One* **7,** 1–10 (2012).
12. Prentice-Mott, H. V. *et al.* Directional memory arises from long-lived cytoskeletal asymmetries in polarized chemotactic cells. *Proc. Natl. Acad. Sci.* **113,** 1267–1272 (2016).
13. Romain, B. *et al.* Hypoxia differentially regulated CXCR4 and CXCR7 signaling in colon cancer. *Mol. Cancer* **13,** 58–69 (2014).
14. Müller, A. *et al.* Involvement of chemokine receptors in breast cancer metastasis. *Nature* **410,** 50–56 (2001).
15. Caballero, D., Voituriez, R. & Riveline, D. Protrusion fluctuations direct cell motion. *Biophys. J.* **107,** 34–42 (2014).
16. Comelles, J. *et al.* Cells as active particles in asymmetric potentials: Motility under external gradients. *Biophys. J.* **107,** 1513–1522 (2014).
17. Liu, Y. J. *et al.* Confinement and low adhesion induce fast amoeboid migration of slow mesenchymal cells. *Cell* **160,** 659–672 (2015).
18. McGregor, A. L., Hsia, C. R. & Lammerding, J. Squish and squeeze - the nucleus as a physical barrier during migration in confined environments. *Curr. Opin. Cell Biol.* **40,** 32–40 (2016).
19. Mahmud, G. *et al.* Directing cell motions on micropatterned ratchets. *Nat. Phys.* **5,** 606–612 (2009).
20. Le Berre, M. *et al.* Geometric friction directs cell migration. *Phys. Rev. Lett.* **111,** 1–5 (2013).
21. Saadi, W. *et al.* Generation of stable concentration gradients in 2D and 3D environments using a microfluidic ladder chamber. *Biomed. Microdevices* **9,** 627–635 (2007).
22. Schiraldi, M. *et al.* HMGB1 promotes recruitment of inflammatory cells to damaged tissues by forming a complex with CXCL12 and signaling via CXCR4. *J. Exp. Med.* **209,** 551–

563 (2012).
23. Caballero, D., Comelles, J., Piel, M., Voituriez, R. & Riveline, D. Ratchetaxis: Long-Range Directed Cell Migration by Local Cues. *Trends Cell Biol.* **25,** 815–827 (2015).
24. Donà, E. *et al.* Directional tissue migration through a self-generated chemokine gradient. *Nature* **503,** 285–9 (2013).
25. Radtke, A. J. *et al.* Lymph-Node Resident CD8+ Dendritic Cells Capture Antigens from Migratory Malaria Sporozoites and Induce CD8+ T Cell Responses. *PLoS Pathog.* **11,** 1–23 (2015).
26. Russo, E. *et al.* Intralymphatic CCL21 Promotes Tissue Egress of Dendritic Cells through Afferent Lymphatic Vessels. *Cell Rep.* **14,** 1723–1734 (2016).
27. Costa, G. *et al.* Asymmetric division coordinates collective cell migration in angiogenesis. *Nat. Cell Biol.* **18,** 1292–1301 (2016).
28. Beerling, E., Ritsma, L., Vrisekoop, N., Derksen, P. W. B. & van Rheenen, J. Intravital microscopy: new insights into metastasis of tumors. *J. Cell Sci.* **124,** 299–310 (2011).
29. Domanska, U. M. *et al.* A review on CXCR4/CXCL12 axis in oncology: No place to hide. *Eur. J. Cancer* **49,** 219–230 (2013).
30. Paget, S. The distribution of secondary growths in cancer of the breast. *Lancet* **133,** 571–573 (1889).
31. Ewing, J. *Neoplastic diseases. A treatise on tumors*. (1928).
32. Riihimaki, M., Hemminki, A., Sundquist, J. & Hemminki, K. Patterns of metastasis in colon and rectal cancer. *Sci. Rep.* **6,** 1–9 (2016).
33. Luzzi, K. J. *et al.* Multistep nature of metastatic inefficiency: dormancy of solitary cells after successful extravasation and limited survival of early micrometastases. *Am. J. Pathol.* **153,** 865–873 (1998).
34. Paul, C. D., Mistriotis, P. & Konstantopoulos, K. Cancer cell motility : lessons from migration in confined spaces. *Nat. Rev. Cancer* **17,** 131–140 (2017).
35. Ivanov, K. P., Kalinina, M. K. & Levkovich, Y. I. Blood Flow Velocity in Capillaries of Brain and Muscles Physiological Significance. *Microvacular Res.* **22,** 143–155 (1981).
36. Potter, R. F. & Groom, A. C. Capillary diameter and geometry in cardiac and skeletal muscle studied by means of corrosion casts. *Microvasc. Res.* **25,** 68–84 (1983).
37. Cassot, F., Lauwers, F., Fouard, C., Prohaska, S. & Lauwers-Cances, V. A novel three-dimensional computer-assisted method for a quantitative study of microvascular networks of the human cerebral cortex. *Microcirculation* **13,** 1–18 (2006).
38. Hosokawa, M. *et al.* Size-Based Isolation of Circulating Tumor Cells in Lung Cancer Patients Using a Microcavity Array System. *PLoS One* **8,** 1–7 (2013).
39. Weigelin, B. *et al.* Intravital third harmonic generation microscopy of collective melanoma cell invasion. *Intravital* **1,** 32–43 (2012).
40. Wolf, K. *et al.* Collagen-based cell migration models in vitro and in vivo. *Semin. Cell Dev. Biol.* **20,** 931–941 (2009).
41. Erdogan, B. *et al.* Cancer-associated fibroblasts promote directional cancer cell migration by aligning fibronectin. *J. Cell Biol.* **216,** 3799–3816 (2017).
42. Petri, R. J. A minor modification of the plating technique of Koch. *Milestones Microbiol.* **1,** 279–280 (1887).
43. Paňková, K., Rösel, D., Novotný, M. & Brábek, J. The molecular mechanisms of transition between mesenchymal and amoeboid invasiveness in tumor cells. *Cell. Mol. Life Sci.* **67,** 63–71 (2010).
44. Lämmermann, T. & Sixt, M. Mechanical modes of 'amoeboid' cell migration. *Curr. Opin. Cell Biol.* **21,** 636–644 (2009).
45. Alberts, B. *et al.* in *Molecular biology of the cell. 4th Edition.* Chapter 19: Integrin. (2002).
46. Petrie, R. J., Doyle, A. D. & Yamada, K. M. Random versus directionally persistent cell migration. *Nat. Rev. Mol. Cell Biol.* **10,** 538–549 (2009).
47. Huang, S. Where to Go: Breaking the Symmetry in Cell Motility. *PLoS Biol.* **14,** 1–10

(2016).
48. Wang, B. *et al.* SDF-1/CXCR4 axis promotes directional migration of colorectal cancer cells through upregulation of integrin αvß6. *Carcinogenesis* **35,** 282–291 (2014).
49. Wolf, K. *et al.* Physical limits of cell migration: Control by ECM space and nuclear deformation and tuning by proteolysis and traction force. *J. Cell Biol.* **201,** 1069–1084 (2013).
50. Fitzpatrick, L. E. & McDevitt, T. C. Cell-derived matrices for tissue engineering and regenerative medicine applications. *Biomater. Sci.* **3,** 12–24 (2015).
51. Godeau, A. Cyclic deformations contribute to 3D cell motility. PhD thesis (2016).
52. Faure-André, G. *et al.* Regulation of dendritic cell migration by CD74, the MHC class II-associated invariant chain. *Science* **322,** 1705–10 (2008).
53. Risler, T. in *Encyclopedia of Complexity and System Science* **6701,** 1738–1774 (2007).
54. Cooper, G. in *The Cell: a Molecular Approach. 2nd Edition.* Chapter 11: Structure and organization of actin filaments (2000).
55. Le Clainche, C. & Carlier, M.-F. Regulation of actin assembly associated with protrusion and adhesion in cell migration. *Physiol. Rev.* **88,** 489–513 (2008).
56. Riveline, D. *et al.* Focal contacts as mechanosensors: Externally applied local mechanical force induces growth of focal contacts by an mDia1-dependent and ROCK-independent mechanism. *J. Cell Biol.* **153,** 1175–1185 (2001).
57. Winder, S. J. & Ayscough, K. R. Actin-binding proteins. *J. Cell Sci.* **118,** 651–654 (2005).
58. Small, J. V., Stradal, T., Vignal, E. & Rottner, K. The lamellipodium: Where motility begins. *Trends Cell Biol.* **12,** 112–120 (2002).
59. Vicente-Manzanares, M., Ma, X., Adelstein, R. S. & Horwitz, A. R. Non-muscle myosin II takes centre stage in cell adhesion and migration. *Nat. Rev. Mol. Cell Biol.* **10,** 778–790 (2009).
60. Akhmanova, A. & Steinmetz, M. O. Control of microtubule organization and dynamics: Two ends in the limelight. *Nat. Rev. Mol. Cell Biol.* **16,** 711–726 (2015).
61. Tse, J. R. & Engler, A. J. Stiffness gradients mimicking in vivo tissue variation regulate mesenchymal stem cell fate. *PLoS One* **6,** 1–5 (2011).
62. Hall, A. Rho GTPases and the Actin Cytoskeleton. **279,** 509–513 (1998).
63. Hanna, S. & El-Sibai, M. Signaling networks of Rho GTPases in cell motility. *Cell. Signal.* **25,** 1955–1961 (2013).
64. Raftopoulou, M. & Hall, A. Cell migration: Rho GTPases lead the way. *Dev. Biol.* **265,** 23–32 (2004).
65. Palazzo, A. F., Cook, T. A., Alberts, A. S. & Gundersen, G. G. mDia mediates Rho-regulated formation and orientation of stable microtubules. *Nat. Cell Biol.* **3,** 723–729 (2001).
66. Etienne-Manneville, S. & Hall, A. Cdc42 regulates GSK-3 b and adenomatous polyposis coli to control cell polarity. *Nature* **421,** 753–756 (2003).
67. Berzat, A. & Hall, A. Cellular responses to extracellular guidance cues. *EMBO J.* **29,** 2734–2745 (2010).
68. Servant, G. *et al.* Polarization of chemoattractants receptor signaling during neutrophil chemotaxis. *Science.* **287,** 1037–1040 (2000).
69. Funamoto, S., Meili, R., Lee, S., Parry, L. & Firtel, R. A. Spatial and temporal regulation of 3-phosphoinositides by PI 3-kinase and PTEN mediates chemotaxis. *Cell* **109,** 611–623 (2002).
70. Qian, Y. *et al.* PI3K induced actin filament remodeling through Akt and p70S6K1: implication of essential role in cell migration. *Am. J. Physiol. - Cell Physiol.* **286,** 153–163 (2003).
71. Wang, Artemenko, Y., Cai, W. J., Iglesias, P. A. & Devreotes, P. N. The directional response of chemotactic cells depends on a balance between cytoskeletal architecture and the external gradient. *Cell Rep.* **9,** 1110–1121 (2014).

72. Luxton, G. W. G. & Gundersen, G. G. Orientation and function of the nuclear-centrosomal axis during cell migration. *Curr. Opin. Cell Biol.* **23,** 579–588 (2011).
73. Schütze, K., Maniotis, A. & Schliwa, M. The position of the microtubule-organizing center in directionally migrating fibroblasts depends on the nature of the substratum. *Proc. Natl. Acad. Sci. U. S. A.* **88,** 8367–71 (1991).
74. Zhang, J. & Wang, Y. Centrosome defines the rear of cells during mesenchymal migration. *Mol. Biol. Cell* **28,** 3240–3251 (2017).
75. Chen, B., Kumar, G., Co, C. C. & Ho, C.-C. Geometric Control of Cell Migration. *Sci. Rep.* **3,** 2827 (2013).
76. Kumar, G., Co, C. C. & Ho, C. C. Steering cell migration using microarray amplification of natural directional persistence. *Langmuir* **27,** 3803–3807 (2011).
77. Jiang, X., Bruzewicz, D. A., Wong, A. P., Piel, M. & Whitesides, G. M. Directing cell migration with asymmetric micropatterns. *Proc. Natl. Acad. Sci. USA* **102,** 975–8 (2005).
78. Pouthas, F. *et al.* In migrating cells, the Golgi complex and the position of the centrosome depend on geometrical constraints of the substratum. *J. Cell Sci.* **121,** 2406–2414 (2008).
79. Earman, J. Curie's principle and spontaneous symmetry breaking. *Int. Stud. Philos. Sci.* **18,** 173–198 (2004).
80. Li, R. & Bowerman, B. Symmetry Breaking in Biology. *Cold Spring Harb. Perspect. Biol.* **2,** 1–5 (2010).
81. Turing, A. M. The chemical basis of morphogenesis. *Bull. Math. Biol.* **237,** 153–197 (1952).
82. Kondo, S. & Miura, T. The Reaction-Diffusion Model as a Framework for Understanding Biological Pattern Formation. **329,** 1616–1621 (2010).
83. Paluch, E., Piel, M., Prost, J., Bornens, M. & Sykes, C. Cortical actomyosin breakage triggers shape oscillations in cells and cell fragments. *Biophys. J.* **89,** 724–733 (2005).
84. Chugh, P. *et al.* Actin cortex architecture regulates cell surface tension. *Nat. Cell Biol.* **19,** 689–697 (2017).
85. Feynman, R. in *Lectures on Physics* 1–9 (1963).
86. Ramalingam, N. *et al.* A resilient formin-derived cortical actin meshwork in the rear drives actomyosin-based motility in 2D confinement. *Nat. Commun.* **6,** 1–15 (2015).
87. Lopez-Fagundo, C., Bar-Kochba, E., Livi, L. L., Hoffman-Kim, D. & Franck, C. Three-dimensional traction forces of Schwann cells on compliant substrates. *J. R. Soc. Interface* **11,** 1–9 (2014).
88. Wang, F. The signaling mechanisms underlying cell polarity and chemotaxis. *Cold Spring Harb. Perspect. Biol.* **1,** 1–16 (2009).
89. Niggli, V. A membrane-permeant ester of phosphatidylinostiol 3,4,5-triphosphate (PIP 3) is an activator of human neutrophil migration. *FEBS* **473,** 217–221 (2000).
90. Cramer, L. P. Forming the cell rear first: breaking cell symmetry to trigger directed cell migration. *Nat. Cell Biol.* **12,** 628–632 (2010).
91. Yam, P. T. *et al.* Actin-myosin network reorganization breaks symmetry at the cell rear to spontaneously initiate polarized cell motility. *J. Cell Biol.* **178,** 1207–1221 (2007).
92. Zhao, M. *et al.* Electrical signals control wound healing through phosphatidylinositol-3-OH kinase-g and PTEN. *Nat. Lett.* **442,** 457–460 (2006).
93. Geiger, B., Spatz, J. P. & Bershadsky, A. D. Environmental sensing through focal adhesions. *Nat. Rev. Mol. Cell Biol.* **10,** 21–33 (2009).
94. Teixeira, A. I., Abrams, G. ., Bertics, P. J., Murphy, C. J. & Nealey, P. F. Epithelial contact guidance on well-defined micro- and nanostructured substrates. *J. Cell Sci.* **116,** 1881–1892 (2003).
95. Dickinson, R. B., Guido, S. & Tranquillo, R. T. Biased cell migration of fibroblasts exhibiting contact guidance in oriented collagen gels. *Ann. Biomed. Eng.* **22,** 342–356 (1994).
96. Kubow, K. E., Shuklis, V. D., Sales, D. J. & Horwitz, A. R. Contact guidance persists under myosin inhibition due to the local alignment of adhesions and individual protrusions. *Sci. Rep.* **7,** 1–15 (2017).

97. Ramirez-San Juan, G. R., Oakes, P. W. & Gardel, M. L. Contact guidance requires spatial control of leading-edge protrusion. *Mol. Biol. Cell* **28,** 1043–1053 (2017).
98. Caballero, D., Palacios, L., Freitas, P. P. & Samitier, J. An Interplay between Matrix Anisotropy and Actomyosin Contractility Regulates 3D-Directed Cell Migration. *Adv. Funct. Mater.* **27,** 1–12 (2017).
99. Pelham, R. J. & Wang, Y.-L. Cell locomotion and focal adhesions are regulated by substrate flexibility. *Proc. Am. Thorac. Soc.* **94,** 13661–13665 (1997).
100. Lo, C. M., Wang, H. B., Dembo, M. & Wang, Y. L. Cell movement is guided by the rigidity of the substrate. *Biophys. J.* **79,** 144–152 (2000).
101. Hartman, C. D., Isenberg, B. C., Chua, S. G. & Wong, J. Y. Vascular smooth muscle cell durotaxis depends on extracellular matrix composition. *Proc. Natl. Acad. Sci.* **113,** 11190–11195 (2016).
102. Engler, A. J., Sen, S., Sweeney, H. L. & Discher, D. E. Matrix Elasticity Directs Stem Cell Lineage Specification. *Cell* **126,** 677–689 (2006).
103. Rowlands, A. S., George, P. A. & Cooper-White, J. J. Directing osteogenic and myogenic differentiation of MSCs: interplay of stiffness and adhesive ligand presentation. *AJP Cell Physiol.* **295,** C1037–C1044 (2008).
104. Du Bois Reymond, E. Untersuchungen über thierische Electricität. *Reimer* **2,** 245–230 (1849).
105. Cao, L., Pu, J. & Zhao, M. GSK-3b is essential for physiological electric field-directed Golgi polarization and optimal electrotaxis. *Cell. Mol. Life Sci.* **68,** 3081–3093 (2011).
106. Lin, F. *et al.* Lymphocyte Electrotaxis In Vitro and In Vivo. *J. Immunol.* **181,** 2465–2471 (2008).
107. Sroka, J. *et al.* Lamellipodia and membrane blebs drive efficient electrotactic migration of rat walker carcinosarcoma cells WC 256. *PLoS One* **11,** 1–23 (2016).
108. Bonner, J. T. Evidence for the formation of cell aggregates by chemotaxis in the development of the slime mold Dictyostelium discoideum. *J. Exp. Zool.* **106,** 1–26 (1947).
109. Bonner, J. T. *et al.* Acrasin, Acrasinase, and the Sensitivity to Acrasin in Dictyosteliun discoideum. *Dev. Biol.* **20,** 72–87 (1969).
110. Cai, H., Huang, C. H., Devreotes, P. N. & Iijima, M. Analysis of chemotaxis in Dictyostelium. **757,** 1–17 (2012).
111. Venkiteswaran, G. *et al.* Generation and dynamics of an endogenous, self-generated signaling gradient across a migrating tissue. *Cell* **155,** 674–687 (2013).
112. Muinonen-Martin, A. J. *et al.* Melanoma Cells Break Down LPA to Establish Local Gradients That Drive Chemotactic Dispersal. *PLoS Biol.* **12,** 1–17 (2014).
113. Wyckoff, J. *et al.* A paracrine loop between tumor cells and macrophages is required for tumor cell migration in mammary tumors. **64,** 7022–7029 (2004).
114. Lee, S., Shen, Z., Robinson, D. N., Briggs, S. & Firtel, R. A. Involvement of the Cytoskeleton in Controlling Leading-Edge Function during Chemotaxis. *Mol. Biol. Cell* **21,** 1810–1824 (2010).
115. Weiner, O. D. *et al.* Spatial control of actin polymerization during neutrophil chemotaxis. *Nat Cell Biol.* **1,** 75–81 (1999).
116. Carter, S. B. Principles of cell motility: The direction of cell movement and cancer invasion. *Nature* **208,** 1183–1187 (1965).
117. McCarthy, J. B. & Furcht, L. T. Laminin and fibronectin promote the haptotactic migration of B16 mouse melanoma cells in vitro. *J. Cell Biol.* **98,** 1474–1480 (1984).
118. Gupton, S. L. & Waterman-Storer, C. M. Spatiotemporal Feedback between Actomyosin and Focal-Adhesion Systems Optimizes Rapid Cell Migration. *Cell* **125,** 1361–1374 (2006).
119. Smith, J. T., Elkin, J. T. & Reichert, W. M. Directed cell migration on fibronectin gradients: Effect of gradient slope. *Exp. Cell Res.* **312,** 2424–2432 (2006).
120. Zhang, M. *et al.* Applications of stripe assay in the study of CXCL12-mediated neural

progenitor cell migration and polarization. *Biomaterials* **72,** 163–171 (2015).
121. Schwarz, J. *et al.* A microfluidic device for measuring cell migration towards substrate-bound and soluble chemokine gradients. *Sci. Rep.* **6,** 1–12 (2016).
122. Kumar, G., Ho, C. C. & Co, C. C. Guiding cell migration using one-way micropattern arrays. *Adv. Mater.* **19,** 1084–1090 (2007).
123. Biselli, E. *et al.* Organs on chip approach: A tool to evaluate cancer-immune cells interactions. *Sci. Rep.* **7,** 1–12 (2017).
124. Lautscham, L. A. *et al.* Migration in Confined 3D Environments Is Determined by a Combination of Adhesiveness, Nuclear Volume, Contractility, and Cell Stiffness. *Biophys. J.* **109,** 900–913 (2015).
125. Denais, C. M. *et al.* Nuclear envelope rupture and repair during cancer cell migration. *Science (80-.).* **352,** 353–358 (2016).
126. Thiam, H.-R. *et al.* Perinuclear Arp2/3-driven actin polymerization enables nuclear deformation to facilitate cell migration through complex environments. *Nat. Commun.* **7,** 1–14 (2016).
127. Li, J., Zhu, L., Zhang, M. & Lin, F. Microfluidic device for studying cell migration in single or co-existing chemical gradients and electric fields. *Biomicrofluidics* **6,** 1–13 (2012).
128. Mishra, S. & Vazquez, M. A Gal-MμS Device to Evaluate Cell Migratory Response to Combined Galvano-Chemotactic Fields. *Biosensors* **7,** 54–70 (2017).
129. Sundararaghavan, H. G., Saunders, R. L., Hammer, D. A. & Burdick, J. A. Fiber alignment directs cell motility over chemotactic gradients. *Biotechnol. Bioeng.* **110,** 1249–1254 (2013).
130. Prentice-Mott, H. V *et al.* Biased migration of confined neutrophil-like cells in asymmetric hydraulic environments. *Proc. Natl. Acad. Sci. U. S. A.* **110,** 21006–21011 (2013).
131. Teixidó, J., Martínez-Moreno, M., Díaz-Martínez, M. & Sevilla-Movilla, S. The good and bad faces of the CXCR4 chemokine receptor. *Int. J. Biochem. Cell Biol.* **95,** 121–131 (2017).
132. Feng, Y., Broder, C. C., Kennedy, P. E. & Berger, E. A. HIV-1 Entry Cofactor: Functional cDNA Cloning of a Seven-Transmembrane, G Protein-Coupled Receptor. *Science (80-.).* **272,** 872–877 (1996).
133. Sánchez-Martín, L., Sánchez-Mateos, P. & Cabañas, C. CXCR7 impact on CXCL12 biology and disease. *Trends Mol. Med.* **19,** 12–22 (2013).
134. Sun, X. *et al.* CXCL12 / CXCR4 / CXCR7 chemokine axis and cancer progression. *Cancer Metastasis Rev.* **29,** 709–722 (2010).
135. Gassmann, P. *et al.* CXCR4 Regulates the Early Extravasation of Metastatic Tumor Cells In Vivo. *Neoplasia* **11,** 651–661 (2009).
136. Izumi, D. *et al.* CXCL12/CXCR4 activation by cancer-associated fibroblasts promotes integrin b1 clustering and invasiveness in gastric cancer. *Int. J. Cancer* **138,** 1207–1219 (2016).
137. Gu, X. L., Liu, L., Lu, X. D. & Liu, Z. R. Serum CXCL12 Levels as a Novel Predictor of Future Stroke Recurrence in Patients with Acute Ischemic Stroke. *Mol. Neurobiol.* **53,** 2807–2814 (2016).
138. Duan, X.-X. *et al.* The diagnostic and prognostic value of serum CXCL12 levels in patients with ischemic stroke. *Neurol. Sci.* **36,** 2227–2234 (2015).
139. Franchini, S. *et al.* Serum CXCL12 levels on hospital admission predict mortality in patients with severe sepsis/septic shock. *Am. J. Emerg. Med.* **33,** 1802–1804 (2015).
140. Łukaszewicz-Zając, M., Mroczko, B., Kozłowski, M. & Szmitkowski, M. The serum concentrations of chemokine cxcl12 and its specific receptor cxcr4 in patients with esophageal cancer. *Dis. Markers* **2016,** 1–7 (2016).
141. Ella, K., Csépányi-Kömi, R. & Káldi, K. Circadian regulation of human peripheral neutrophils. *Brain. Behav. Immun.* **57,** 209–221 (2016).
142. Spinosa, P. C., Luker, K. E., Luker, G. D. & Linderman, J. J. The CXCL12/CXCR7 signaling axis, isoforms,Circadian Rhythms , and Tumor Cellular Composition Dictate Gradients in

Tissue. *PLoS One* **3100,** 1–17 (2017).
143. Teicher, B. A. & Fricker, S. P. CXCL12 (SDF-1)/CXCR4 pathway in cancer. *Clin. Cancer Res.* **16,** 2927–2931 (2010).
144. Nishita, M., Aizawa, H. & Mizuno, K. Stromal cell-derived factor 1alpha activates LIM kinase 1 and induces cofilin phosphorylation for T-cell chemotaxis. *Mol. Cell. Biol.* **22,** 774–783 (2002).
145. Dart, A. E. *et al.* The drebrin / EB3 pathway drives invasive activity in prostate cancer. **36,** 4111–4123 (2017).
146. Ketschek, A. *et al.* Drebrin coordinates the actin and microtubule cytoskeleton during the initiation of axon collateral branches. *Dev. Neurobiol.* **76,** 1092–1110 (2016).
147. Lysko, D. E., Putt, M. E. & Golden, J. A. SDF1 reduces interneuron leading process branching through dual regulation of actin and microtubules. *J. Neurosci.* **34,** 4941–62 (2014).
148. Chen, Q. & Zheng, J. C. CXCR7 Mediates Neural Progenitor Cells Migration to CXCL12 Independent of CXCR4. *Stem Cells* **33,** 2574–2585 (2015).
149. Wyse, M. M., Goicoechea, S., Garcia-Mata, R., Nestor-Kalinoski, A. L. & Eisenmann, K. M. mDia2 and CXCL12/CXCR4 chemokine signaling intersect to drive tumor cell amoeboid morphological transitions. *Biochem. Biophys. Res. Commun.* **484,** 255–261 (2017).
150. Zhao, X. & Guan, J. L. Focal adhesion kinase and its signaling pathways in cell migration and angiogenesis. *Adv. Drug Deliv. Rev.* **63,** 610–615 (2011).
151. Alekhina, O. & Marchese, A. β-arrestin1 and Signal-transducing Adaptor Molecule 1 (STAM1) cooperate to promote focal adhesion kinase autophosphorylation and chemotaxis via the chemokine receptor CXCR4. *J. Biol. Chem.* **291,** 26083–26097 (2016).
152. Tachibana, K. *et al.* The chemokine receptor CXCR4 is essential for vascularization of the gastrointestinal tract. *Nature* **393,** 591–594 (1998).
153. Nagasawa, T. *et al.* Defects of B-cell lymphopoiesis and bone-marrow myelopoiesis in mice lacking the CXC chemokine PBSF/SDF-1. *Nature* **382,** 635–638 (1996).
154. Ali, M. M. *et al.* Effects of Tyrosine Kinase Inhibitors and CXCR4 Antagonist on Tumor Growth and Angiogenesis in Rat Glioma Model: MRI and Protein Analysis Study. *Transl. Oncol.* **6,** 660–669 (2013).
155. Dillenburg-Pilla, P. *et al.* SDF-1/CXCL12 induces directional cell migration and spontaneous metastasis via a CXCR4/Gαi/mTORC1 axis. *FASEB J.* **29,** 1056–1068 (2015).
156. Orimo, A. *et al.* Stromal fibroblasts present in invasive human breast carcinomas promote tumor growth and angiogenesis through elevated SDF-1/CXCL12 secretion. *Cell* **121,** 335–348 (2005).
157. Ma, J.-C. *et al.* Fibroblast-derived CXCL12/SDF-1α promotes CXCL6 secretion and co-operatively enhances metastatic potential through the PI3K/Akt/mTOR pathway in colon cancer. *World J. Gastroenterol.* **23,** 5167–5178 (2017).
158. O'Boyle, G. *et al.* Inhibition of CXCR4-CXCL12 chemotaxis in melanoma by AMD11070. *Br. J. Cancer* **108,** 1634–1640 (2013).
159. Wendel, C. *et al.* CXCR4/CXCL12 participate in extravasation of metastasizing breast cancer cells within the liver in a rat model. *PLoS One* **7,** 1–13 (2012).
160. Jiang, X., Bruzewicz, D. A., Wong, A. P., Piel, M. & Whitesides, G. M. Directing cell migration with asymmetric micropatterns. *Proc. Natl. Acad. Sci. U. S. A.* **102,** 975–8 (2005).
161. Nedeva, I. *et al.* Synthetic polyamines promote rapid lamellipodial growth by regulating actin dynamics. *Nat. Commun.* **4,** 2165–2176 (2013).
162. Halter, M., Elliott, J. T., Hubbard, J. B., Tona, A. & Plant, A. L. Cell volume distributions reveal cell growth rates and division times. *J. Theor. Biol.* **257,** 124–130 (2009).
163. Xie, K., Yang, Y. & Jiang, H. Controlling Cellular Volume via Mechanical and Physical Properties of Substrate. *Biophys. J.* **114,** 675–687 (2018).

164. Kim, D.-H. *et al.* Volume regulation and shape bifurcation in the cell nucleus. *J. Cell Sci.* **129,** 457–457 (2016).
165. Guo, M. *et al.* Cell volume change through water efflux impacts cell stiffness and stem cell fate. **114,** 8618–8627 (2017).
166. Ivetac, I. *et al.* Regulation of PI(3)K/Akt signalling and cellular transformation by inositol polyphosphate 4-phosphatase-1. *EMBO Rep.* **10,** 487–493 (2009).
167. Callan-Jones, A. C. & Voituriez, R. Actin flows in cell migration: From locomotion and polarity to trajectories. *Curr. Opin. Cell Biol.* **38,** 12–17 (2016).
168. Brand, S. *et al.* CXCR4 and CXCL12 are inversely expressed in colorectal cancer cells and modulate cancer cell migration, invasion and MMP-9 activation. *Exp. Cell Res.* **310,** 117–130 (2005).
169. Gómez-Moutón, C. *et al.* Filamin A interaction with the CXCR4 third intracellular loop regulates endocytosis and signaling of WT and WHIM-like receptors. *Blood* **125,** 1116–1125 (2015).
170. Rey, M. *et al.* Myosin IIA is involved in the endocytosis of CXCR4 induced by SDF-1alpha. *J. Cell Sci.* **120,** 1126–1133 (2007).
171. Gardel, M. L. *et al.* Traction stress in focal adhesions correlates biphasically with actin retrograde fl ow speed. *J. Cell Biol.* **183,** 999–1005 (2008).
172. Wang, Y. *et al.* CXCR4 and CXCR7 Have Distinct Functions in Regulating Interneuron Migration. *Neuron* **69,** 61–76 (2011).
173. Massia, S. P., Stark, J. & Letbetter, D. S. Surface-immobilized dextran limits cell adhesion and spreading. *Biomaterials* **21,** 2253–2261 (2000).
174. Termeer, C. C., Weiss, J. M., Schöpf, E., Vanscheidt, W. & Simon, J. C. The low molecular weight Dextran 40 inhibits the adhesion of T lymphocytes to endothelial cells. *Clin. Exp. Immunol.* **114,** 422–426 (1998).
175. Qian, T. *et al.* CXCR7 regulates breast tumor metastasis and angiogenesis in vivo and in vitro. *Mol. Med. Rep.* **17,** 3633–3639 (2017).

A. Appendix

A.1 Abbreviation

Table A.1: Table of abbreviations

Abbreviation	Full name	Abbreviation	Full name
3D	3 Dimensions	GTP	Guanine TriPhosphate
ABP	Actin-Binding Proteins	FBS	Fetal Bovine Serum
ADF	Actin-Depolymerizing Factor	LPA	lysophosphatidic acid
ADP	Adenosine DiPhosphate	MLC	Myosin Light Chain
ATP	Adenosine TriPhosphate	MMP	Matrix MetalloProteinases
BCS	Bovine Calf Serum	MTOC	Microtubules Organized Center
CAF	Cancer associated-fibroblasts	PDMS	PolyDiMethylSiloxane
Ct	Cycle threshold	PBS	*Phosphate-buffered saline*
BSA	Bovin Serum Albumin	PFA	Paraformaldehyde
CDM	Cell-Derived Matrix	PH	pleckstrin homology domain
CHO	Chinese Hamster Ovary	PIP3	Phosphotidylinositol(3,4,5)phosphate
CXCR4	C-X-C chemokine receptor type 4	PI3K	Phosphotidylinositol(3,4,5)phosphate kinase
CXCR7	C-X-C chemokine receptor type 7	PLL-g-PEG	Poly-l-lysine-g-PolyEthylene Glycol
CXCL12 or SDF-1	C-X-C motif chemokine 12 or Stromal cell-Derived Factor 1	PTEN	Phosphatase and TENsin homolog
DAPI	4',6-diamidino-2-phénylindole	q-PCR	quantitative Polymerase Chain Reaction
ECM	ExtraCellular Matrix	ROCK	Rho-associated protein kinase
FACS	Fluorescence-activated cell sorting	RPE-1	retinal pigment epithelial
For A	formin (Dictyostelium cell)	siRNA	small interfering RNA
GAP	GTPase Activating Proteins	SEM	Scanning Electron Microscopy
GDP	Guanine DiPhosphate	SHG	Second Harmonic Generation
GDI	Guanine nucleotide Dissociation inhibitors	THG	Third Harmonic Generation
GEF	Guanine nucleotide exchange factors	TRITC	Tetramethylrhodamine isothiocyanate
GPCR	G-protein coupled receptors family	WT	Wild type

A.2 Supplementary information: products

Table A.2: Products and references used for mammalians cells culture:

Product name	Brand	Reference
DMSO	Sigma Aldrich	D8418
BCS	Sigma Aldrich	C8056
DMEM (4.5g/l glucose)	Gibco	41965062
DMEM (1g/L glucose)	Gibco	31885049
RPMI 1640 w/o HEPES	Gibco	22409031
Leibovitz L-15 medium	Gibco	11540556
Trypsin	Gibco	11570626
Poly-l-lysine-g-PolyEthylene Glycol	SuSoS AG	SZ33-15
Lipofectamine™ 2000 Transfection Reagent	Invitrogen	11668500
CXCL12α	Almac	CN-11-B-1
Fibronectin	Sigma Aldrich	F1141
human fibronectin	Sigma Aldrich	F0895
Petri dish	Greiner Bio-One	628161
Cell culture flask	CellStar	690170
Suspension culture growing flask	CellStar	690190
Glass coverslip	Deckgläser	0111650
Lipofectamine™ RNAiMAX Transfection Reagent	Invitrogen	13778030
siRNA CXCL12 validated	Qiagen	Hs CXCL12 n°10 and n°11
siRNA CXCL12 non-validated	Qiagen	Hs CXCL12 n°7 and n°16
scramble-siRNA	Eurogentec	SR-CL000-005
SiR-Actin and SiR-Tubulin	Cytoskeleton	CY-SC006

Tableau A.1: List of plasmid used in this study, their antibiotic resistance and origin

Plasmid name	Antibiotic resistance	Origin
SP-GFP-CXCR4	Ampicillin/Geneticin	Jean-Luc Galzi
SP-mRFP1-CXCR7	Kanamycin/Geneticin	Jean-Luc Galzi
CXCR7-eGFP	Ampicillin/Geneticin	Jean-Luc Galzi
Tubulin-GFP		
LifeAct-mCherry	Kanamycin/Geneticin	Ewa Paluch
pCAGGS-PACT-mKOI	Kanamycin	Juliette Godin

SP: signal peptide. Allow the addressing of the protein to the plasma membrane.

Table A.3: Table of antibodies, references and concentrations used

Product name	Concentration/ dilution	Type Species	Brand	Reference
DAPI (4',6-diamidino-2-phenylindole)	1/1000		Sigma Aldrich	32670
Hoescht 33342	0.4µg/ml		Thermo Fisher Scientific	10150888
AlexaFluor488-Phalloidin	1/200		Invitrogen	A12379
Anti-h/mCXCL12	1/100	Monoclonal mouse	R&D system	MAB350
Anti-CXCR4	1/50	Polyclonal rabbit	Cusabio	CSB-PA006254YA01HU
Anti-CXCR7	1/100	Monoclonal mouse	R&D system	MAB42273
Cy3-conjugated Anti-rabbit	1/200	Polyclonal goat	Jackson ImmunoResearch	111-166-047
AlexaFluo 488 anti-mouse	1/200	Polyclonal goat	Molecular Probe	A-11034

Table A.4: Table of products

Product name	Brand	Reference
3-(mercaptopropyl)trimethoxy silane	Fluorochem	S10475
AlexaFluor647-dextran (10kDa)	Invitrogen	D-22914
FocalCheck microspheres	Molecular probe	F-24634
Capillary	Harvard Apparatus	30-0035
chlorotrimethylsilane	Sigma Aldrich	92360
Cell Culture insert/Boyden chamber	Greiner Bio-One product	662638
Celltram® Vario	Eppendorf	5176000084
Tetramethylrhodamine isothiocyanate Dextran (20kDa)	Sigma Aldrich	73766
Tygon tubing	Saint-Gobain	AAD04103
Microloader	Eppendorf	5242956003
Chlorotrimethylsilane	Sigma Aldrich	92360

Table A.5: Table of products for microfabrication

Product name	Brand	Reference
SU8-2005 photoresist	MicroChem	
SU8-2025 photoresist	MicroChem	
Silicon Wafer	Si-Mat	PRIME
PDMS – Sylgard 184	Dow Corning	DC184-1.1,0002-01-000032
Photomask	Selba	
Su-8 developer	Chimie Tech Services	DevSU8/4

A.3 Supplementary information: protocols

A.3.1 RNA extraction and quantification protocols

Extraction ARN

Régler **la centrifugeuse** à **4°C** en avance
Mettre à **-20°C** de l'**isopropanol** et de l'**éthanol 70%** de façon à l'utiliser très froid.
ARN/cellules toujours dans la glace avant le TRIzol
Trizol au frais dans le réfrigérateur, et à remettre rapidement au froid

Séparation ADN/ARN :

1. Ajouter **1mL de TRIzol** (=1volume) pour **5.10^6 cellules**, de la façon suivante :
2. Aspirer le milieu de culture des puits et faire un rinçage au PBS froid stérile.
3. Une fois les puits vide, mettre **la plaque dans la glace** et sortir de la salle de culture pour travailler sous la sorbonne
4. **Ajouter** le volume de **TRIzol**
5. **Gratter** les puits avec un cône à l'envers
6. **Regrouper le lysat** dans « un coin du puits » puis aspirer avec la pipette pour le mettre dans les tubes eppendorf 1,5mL préparés précédemment.
7. Incuber **5 min** à **température ambiante** (TA) afin de favoriser la dissociation des complexes nucléoprotéiques
8. (Possibilité de stocker à -80°C à cette étape
9. Ajouter **200µL** de **Chloroforme** pour 1mL de TRIzol
10. Vortexer vigoureusement pendant 15 s
11. Laisser reposer 2 à 15 min à Température ambiante (TA)
12. **Centrifuge**r à **12000 g (13rpm)** à **4°C** durant **15 min** : on obtiendra 3 phases : La phase inférieure (organique) contenant l'ADN, l'interphase contenant l'ADN et les protéines et la phase supérieur (aqueuse) contenant l'ARN

Précipitation de l'ARN :

13. **Récupérer la phase aqueuse qui contient l'ARN** (=350uL : 30-40% du volume de TRIzol) et la transvaser dans un nouveau tube annoté (= tube final) Remarque : conserver le tube avec la phase organique et l'interphase si ce sont des échantillons précieux et que l'extraction ne se passe pas bien : il sera alors possible de récupérer l'ARN.
14. Ajouter **400uL** de **Chloroforme** pour 1mL de TRIzol
15. Vortexer vigoureusement pendant 15 s
16. Laisser reposer 2 à 15 min à TA
17. Centrifuger à 12000 g (13rpm) à 4°C durant 15 min
18. Récupérer la phase aqueuse.
19. Ajouter **500µL d'isopropanol glacé** (pour 1mL de TRIzol) à la phase aqueuse.
20. Vortexer.
21. Laisser reposer 5 à 10 min à TA.
22. **Centrifuger** à **12000 g (13rpm)** à **4°C** durant **8 min**. L'ARN précipité forme un petit filament (presque invisible) au fond du tube.
23. **Eliminer le surnageant** par renversement (poubelle « déchet isopropanol + égoutter le tube sur du papier absorbant).

Lavage de l'ARN :

24. Ajouter **1 mL d'éthanol 70% glacé** (pour 1 mL de TRIzol) au culot d'ARN précipité de façon à laver celui-ci.
25. Centrifuger à 8000 g (9rpm) à 4°C durant 5 min.
26. **Eliminer le surnageant** par renversement (poubelle « déchet isopropanol + égoutter le tube sur du papier absorbant).
27. **Répéter 1 fois** les étapes de lavages
28. **Laisser sécher** à l'air libre.

Solubilisation de l'ARN :

29. Le culot est repris dans **20µL d'eau RNAase Free**. (Si peu ou beaucoup d'ARN : adapter le volume).
30. Conservation à -80°C.

Remarque : Il est préférable de doser l'ARN après avoir fait 1 cycle de congélation/décongélation.

31. **Dosage** au NanoDrop : voir protocole « Dosage ARN »

Rattrapage : (Si ARN contaminés)

1. Ajouter de l'eau ultra pure (qsq 80µL)
2. Ajouter 11µL de sodium acétate 3M pH 5,2
3. Ajouter 300µL d'EtOH 100%

4. Laisser minimum **30 min à -20°C** (1h30 ou O/N)
5. Centrifuger à 12000 g pendant 30 min à 4°C
6. Retirer le surnageant à la pipette et **laver 2x EtOH 70%** (ajouter **1mL d'EtOH Froid 70%** ou **500µL** (=Volume TRIzol départ), Vortexer rapide et centrifuger 5 min 9000g 4°C, Enlever le surnageant à la pipette (poubelle EtOH) + Tips par capillarité)
7. Solubiliser dans 20µL d'eau ultra pure
8. Conserver **1h30** à **-20°C**
9. **Dosage** au NanoDrop

Protocol RT-qPCR

ARN à -80°C à décongeler (tapoter puis légère centri des tubes)
Toujours laisser les ARN sur glace
Toujours utiliser des cônes avec des filtres

Reverse transcription

A savoir :
RT- : tube avec le plus d'ARN utilisé, pas d'enzyme donc s'il y a de l'ADN lors de la qPCR = contamination
Prévoir une réaction et une RT - **en rab**

Préparation du mix RT :
Préparer les 2 tubes 0,5 des mix (RT+ et RT-) dans l'ordre :
POUR 1 REACTION
Eau : 4,2µL (RT+) ou **5,2µL (RT-)**
10X RT **Buffer** : 2µL
10X RT Random Primers : 2µL
25X **dNTP** Mix (100mM) : 0,8µL
Reverse transcriptase : 1µL (RT+) ou 0µL (RT-) (ATTENTION : enzyme visqueuse donc tapoter le cône dans le tube quand on prélève)
Mettre les tubes dans la glace

Préparation des échantillons :
Annoter les tubes 0,2 puis les mettre sur glace
Préparer les tubes 0,2 : eau (même tube d'eau que pour le mix) puis ARN **(1µg) → vf = 10µL**
Centrifuger les mix pour homogénéiser
Déposer 10µL du mix/tube puis centrifuger
Mettre les échantillons d'ARN de départ au congel (-20°C ou -80°C)
Réaction de PCR:
Hybridation : 25°C pdt 5min
RT : 37°C pdt **2h**

Dénaturation : 85°C pdt 5min
Conserver au froid : 15°C à l'infini
Congeler les tubes (-20°C ou -80°C) ou faire la qPCR directement (dilution au 1/5)

qPCR (cônes à filtre)

Préparation des échantillons RT dilués:
Diluer les tubes de RT au 1/5 : 20µL des échantillons + 80µL d'eau (même tube d'eau que pour les mix) (conserver à -80°C uniquement si besoin)
Centrifuger les tubes pour homogénéiser

Préparation des mix qPCR :
Si nouveaux primer : solubilisation dans de l'eau MilliQ puis une congélation nécessaire
Si pas d'aliquot dispo : 20µL de primer sens + 20µL de primer anti-sens + 60µL d'eau MilliQ (**pour invitrogen**) / 10µL de primer sens + 10µL de primer anti-sens + 80µL d'eau MilliQ (**pour Sigma**) du jour même (écrire le gène, le nom du couple d'amorces, la dilution, la date → compléter le tableau + serveur)
Sous hotte, préparer **1 mix/primer** (prévoir 5/6 réactions de plus) dans l'ordre :
POUR 1 REACTION
Syber Green Mix : 10µL
Eau MilliQ : 5,5µL
Primer (500nM) : 0,5µL
Centrifuger les mix pour homogénéiser
Mettre les tubes dans la glace

Préparation des plaques :
Préparer la plaque : déposer la plaque transparente (sans trop la toucher) sur le support bleu
Déposer 16µL des mix/puits avec le dispatcher
Déposer 4µL des échantillons RT dilués avec des cônes à filtre (utiliser une nouvelle boîte de cônes pour faire une plaque complète) **(ATTENTION : changer de cône à chaque fois !)**
Déposer le filtre sans faire de bulle
Centrifuger à 1200rpm pdt 1 à 2min (program 1)

A.3.2 PDMS spin coated speed

PDMS thickness VS spin-coating speed

Problematic: What is the thickness of a spin coated PDMS layer?

The final thickness of a PDMS layer mainly depends of spin speed and spinning duration. Important parameters to get reproducible thickness of PDMS layer are:

- Spinning speed
- Spinning duration
- Type of PDMS
- Ratio of reticulating agent and PDMS
- Duration between mixing of PDMS/reticulating agent and spin-coating.
- Room temperature

Several publications give the thickness of the deposited layer depending on these conditions for example [1] (fig. 1), or [2] and [3] (fig. 2).

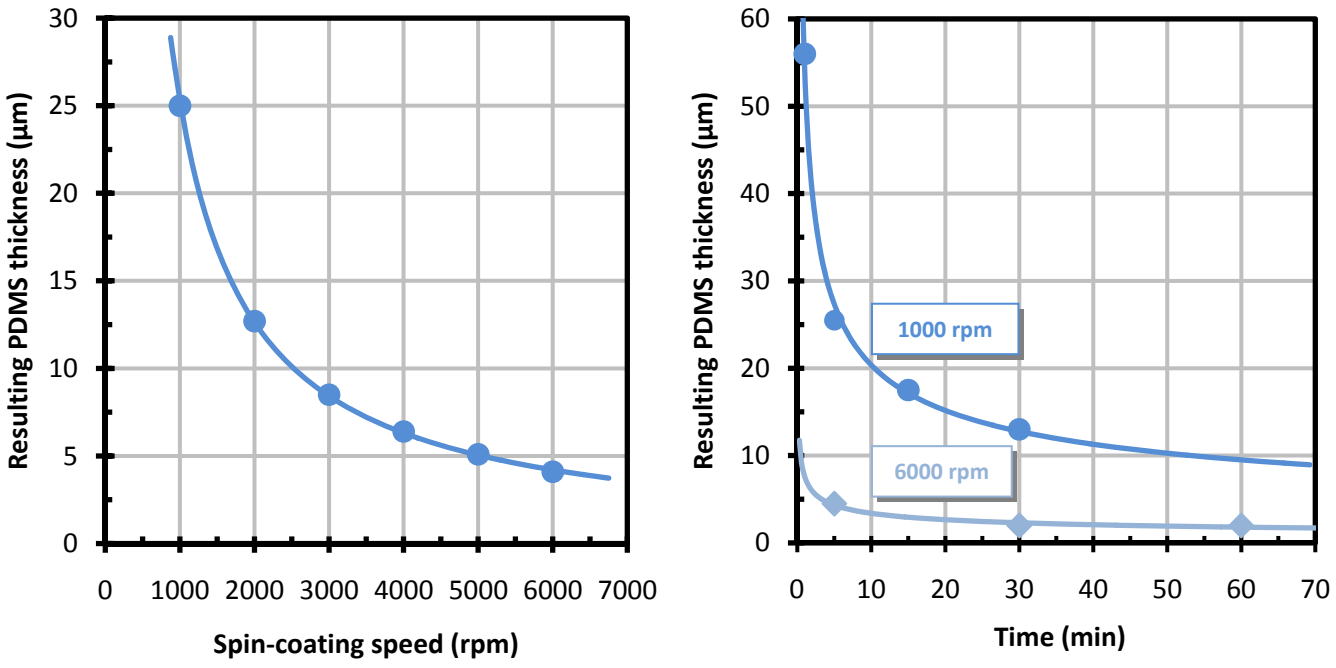

Figure 1: Dependence of the PDMS layer thickness as a function of spin speed for a rotation time of 5 min (left) and as a function of rotation time (right).

PDMS part A and part B (Sylgard 184, Dow Corning) mixed in a 10:1 (weight:weight) ratio and steered during 2 minutes. The PDMS was placed in vacuum desiccators for degassing (10–13 minutes). Total preparation time: 15 minutes, figure modified from [1]

Another source gives similar results on the thickness of the PDMS layer as a function of the spinning speed [3]:

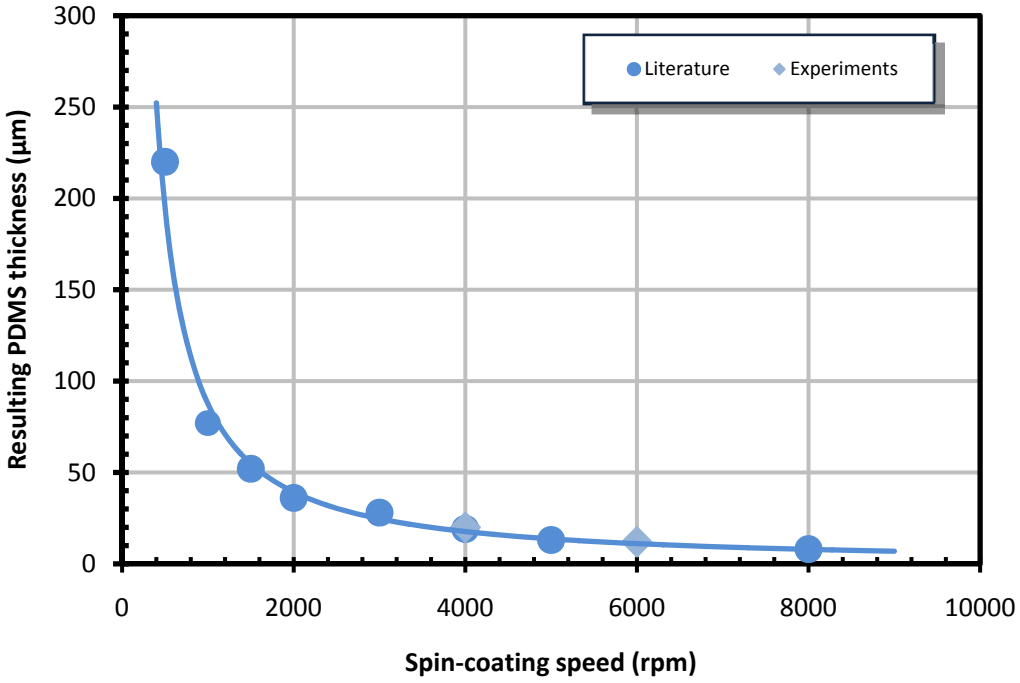

Spin-coating speed (rpm)		500	1000	1500	2000	3000	4000	5000	6000	8000
PDMS thickness (µm)	Balagadde et al. (2005)	220	77	52	36	28	19	13		8
	Measurements						20		12	

Figure 2: PDMS thickness as a function of spin speed, (Sylgard-184 PDMS just after base and agent were mixed in a 10:1 ratio). Closed circles are measurements with a spin time of t=30s, open circles are data points from [2] with t=60s, and the solid line is the theoretical fit $W=0.23\ \omega^{-1.14}$ (W in meters, ω in rpm). The inset shows the same plot on logarithmic scales [3].

References:

[1]: J. H. Koschwanez, R. H. Carlson, D. R. Meldrum, *PLoS ONE* **4**:2 (2009)
[2]: F. K. Balagadde, L. You, C. L. Hansen, F. H. Arnold, S. R. Quake, *Science* **309**:5731, 137-140 (2005)
[3]: http://willem.engen.nl/uni/intern-mbx/material/Sylgard-184-spincoat.php

Form's authors: G. Velvé Casquillas, M. Le Berre, E. Terriac, F. Bertholle
For any comment or suggestions: contact@elveflow.com

A.4 Supplementary information: results

A.4.1 Cell diameter distribution

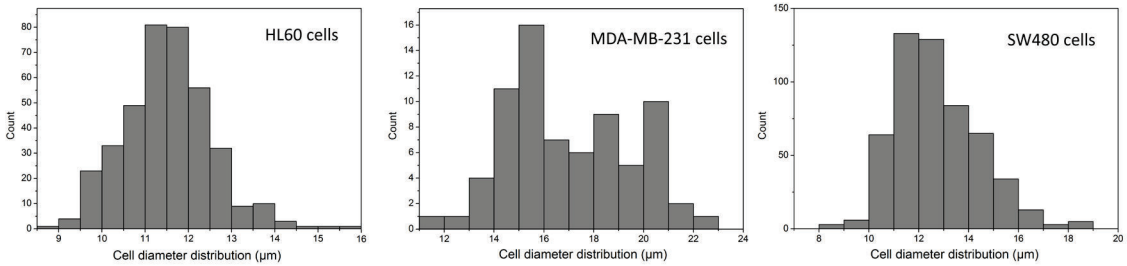

Figure A.1: Nucleus diameter distributions of HL60, MDA-MB-231 and SW480 cells. Hl60 cells n=384 cells; MDA-MB-231 cells n=73 cells; SW480 cells n=533 cells.

The mean HL60 cells diameter is equal to 11.5±1.0µm corresponding to a mean volume of 800±210µm^3. The mean MDA-MB-231 cells diameter is equal to 17.0±2.5µm corresponding to a mean volume of 2590±1140µm^3. The mean SW480 cells diameter is equal to 12.1±1.8µm corresponding to a mean volume of 940±420µm^3. Note that diameter of perfectly roun cells have been measured. For SW480 cells, a large number of irregular and big cells were present. The diameter of the cells were not measured, as a consequence, the mean SW480 cells diameter is underestimated.

Inside 1500µm^3 ratchet channel, HL60 cells were not confined whereas MDA-MB-231 and SW480 cells were more confined that NIH3T3 cells.

A.4.2 NIH3T3 cells migration in closed microchannels

A.4.2.1 α8i20

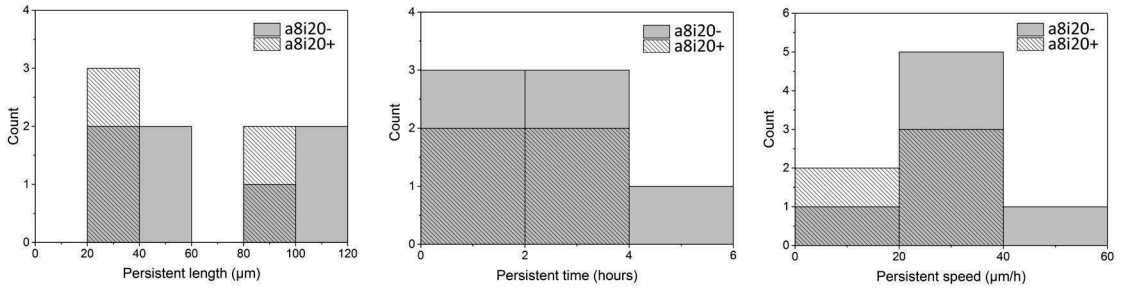

Figure: Persistent length, time and speed distributions of the first persistent motion of NIH3T3 cells migration in α8i20 microchannels in the ratchet direction (+) and against the ratchet direction (-). 3 independent experiments n+= 5cells, n-=7cells.

In the ratchet + and - directions, the persistent length, time and speed are similar (Figure 3.20). In the ratchet + and – direction, respectively, the mean persistent length is equal to 68±41µm and 65±41µm, the mean persistent time is equal to 3.3±3.2h and 2.2±1.8h and the mean persistent speed is equal to 19±14µm/h and 29±10µm/h.

A.4.2.2 α8i30

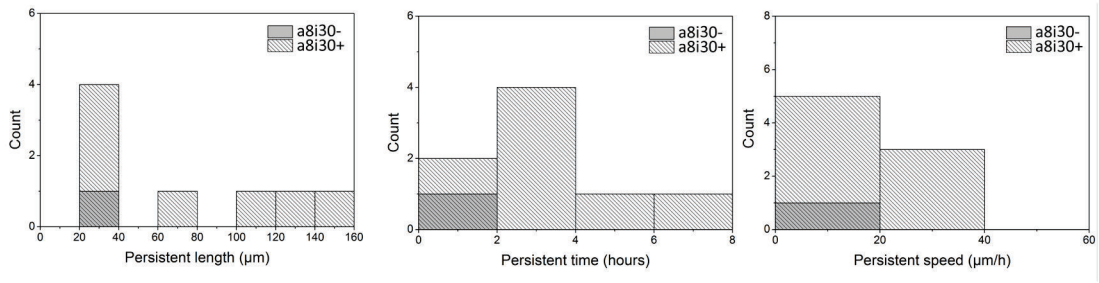

Figure: Persistent length, time and speed distributions of the first persisten motion of NIH3T3 cells migration in α8i30 microchannels in the ratchet direction (+) and against the ratchet direction (-). 1 experiment n+= 8cells, n-=1cell.

In the ratchet +, the mean persistent length is equal to 71±51µm, the mean persistent time is equal to 3.6±1.9h and the mean persistent speed is equal to 19±7µm/h.

A.4.2.3 α24i20

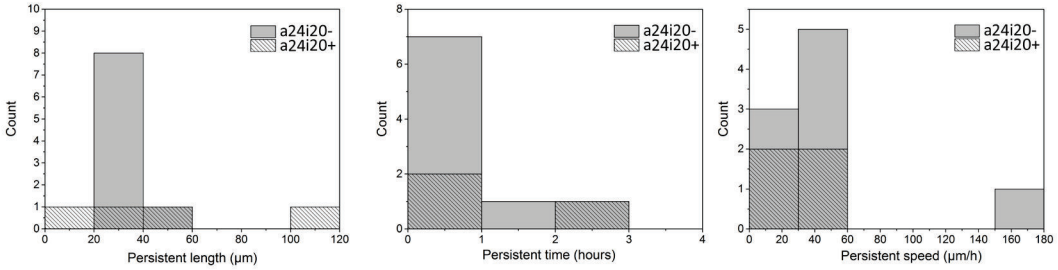

Figure: Persistent length, time and speed distribution of the first move of NIH3T3 cells migration in a24i30 microchannels in the ratchet direction (+) and against the ratchet direction (-). 1 experiment n+= 4 cells, n-=9 cells.

In the ratchet + and – directions, respectively, the mean persistent length is equal to 53±44µm and 29±11µm, the mean persistent time is equal to 2.3±2.3h and 0.9±0.8h and the mean persistent speed is equal to 28±8µm/h and 47±40µm/h.

A.4.3 Persistent time and speed distribution of the different configurations tested

A.4.3.1 Persistent time and speed distribution of NIH3T3 cells migrating in the open configuration

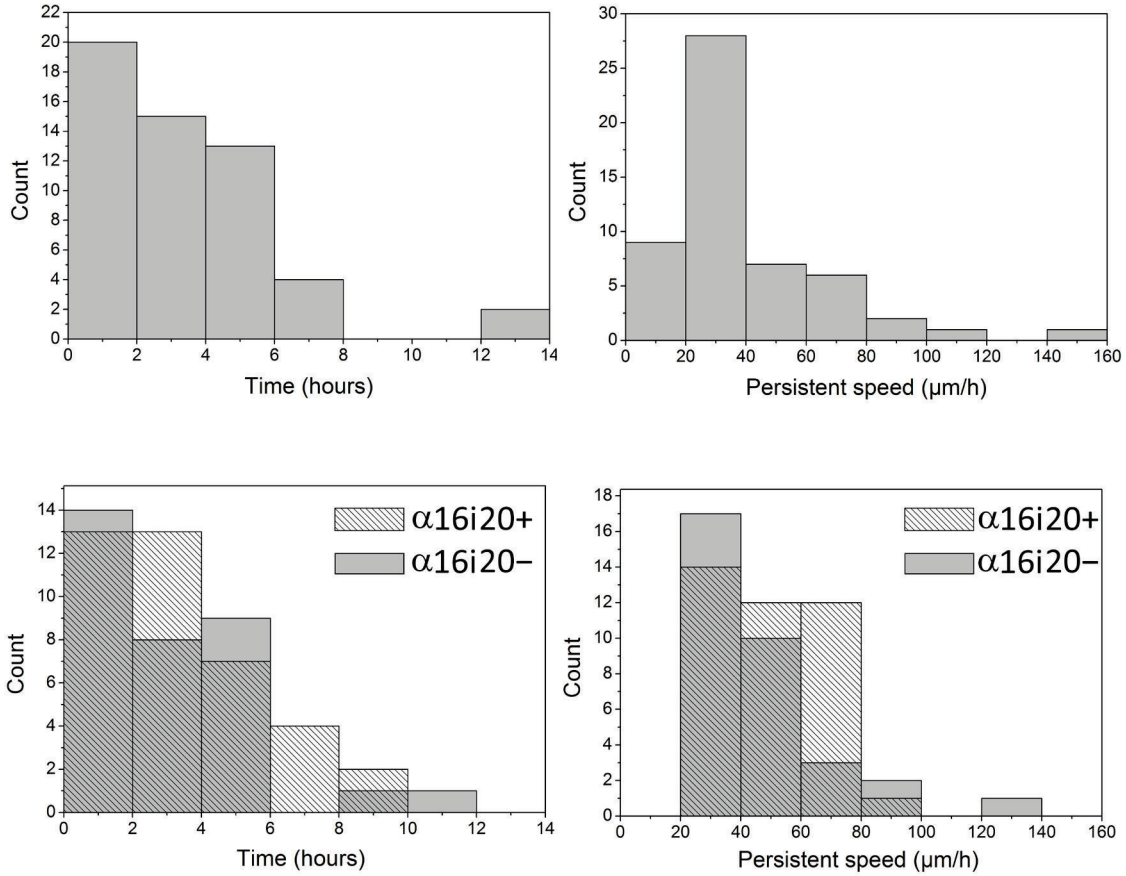

Figure: Persistent time and speed distributions of NIH3T3 cells migrating in straight (A.) and a16i20 ratchet (B.) closed microchannels in the presence of 10% serum gradient.

A.4.3.2 Persistent time distributions of NIH3T3 cells in open, closed and with serum gradient

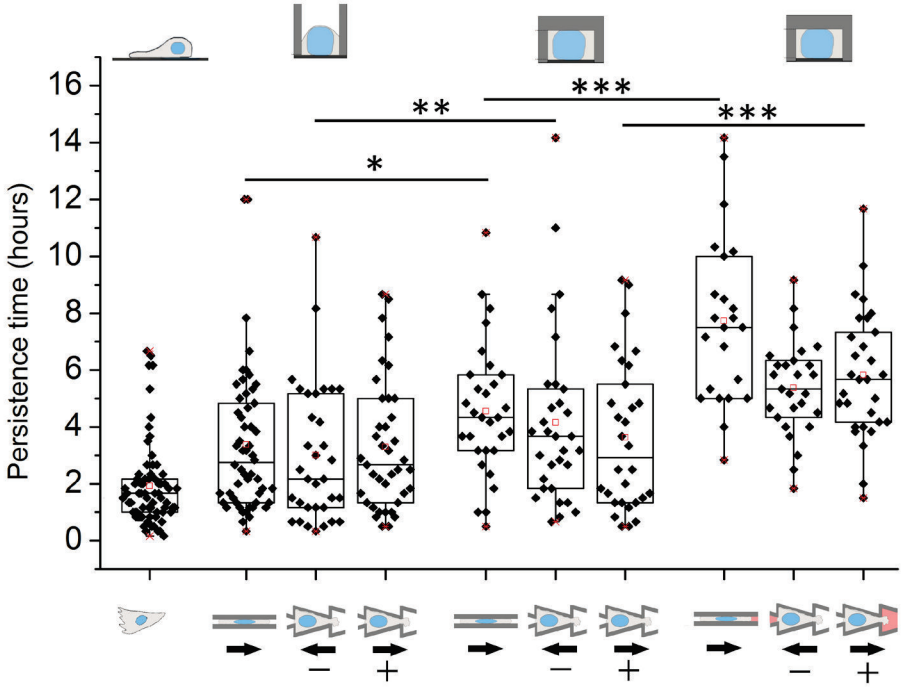

Figure: Summary of persistent time distributions of NIH3T3 cells migrating in 2D flat surfaces, open, closed with and without 10% serum gradient in straight and α16i20 ratchet microchannel configurations. Statistical test: One-Way ANOVA *p<0.05, **p<0.01 and ***p<0.001

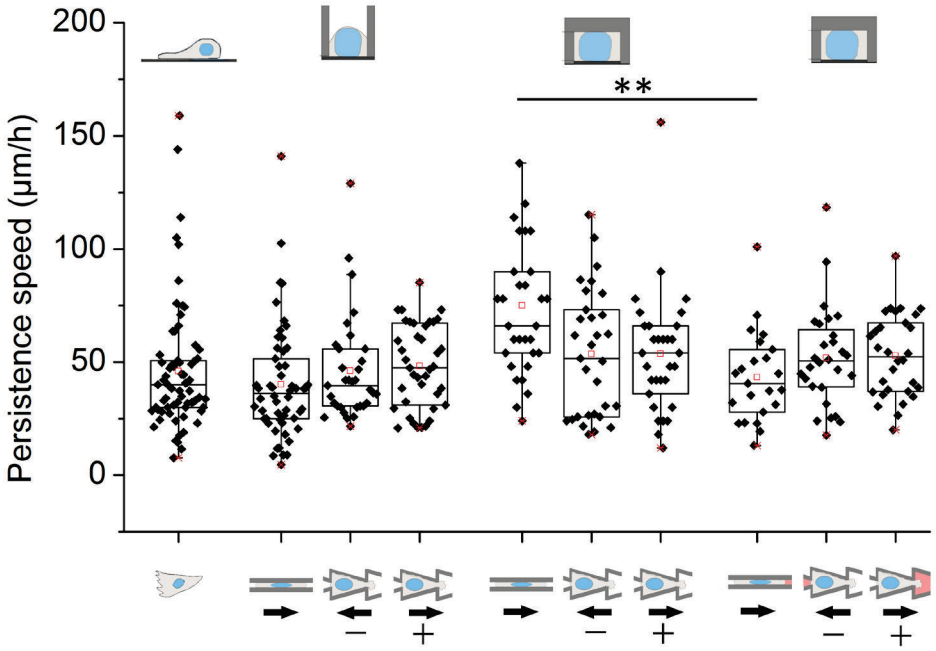

Figure: Summary of persistent speed distributions of NIH3T3 cells migrating on 2D flat surfaces, open, closed with and without 10% serum gradient in straight and α16i20 ratchet microchannel configurations. Statistical test: One-Way ANOVA **p<0.01

A.4.4 Migration distance in the presence of serum gradient

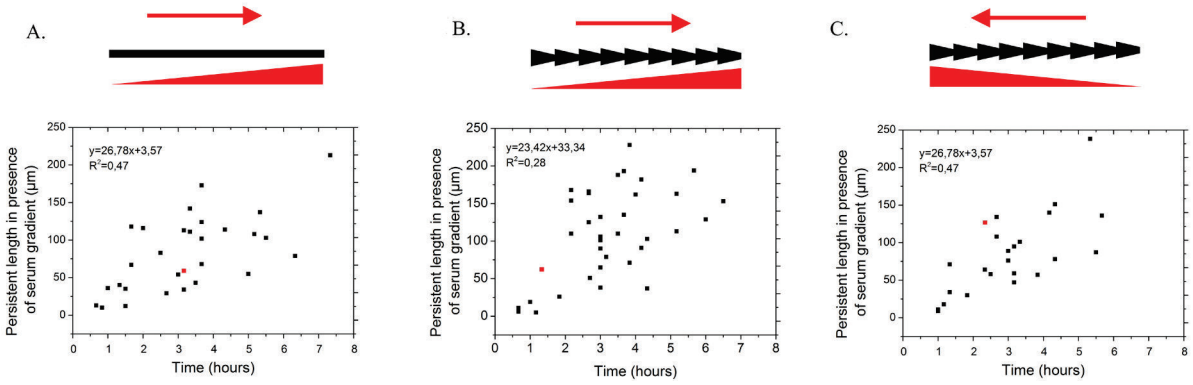

Figure: Persistent length in closed straight (A.), in the ratchet direction (B.) or against the ratchet direction (C.) as a functionof time exposed to the 10% serum gradient

A.5 Publication

LE MAOUT, E., LO VECCHIO, S., BHAT, A, RIVELINE, D. Directing cell migration on flat substrates and in confinement with microfabrication and microfluidics. Chapter 10: Cell guidance by physical cues, Microfluidics in Cell Biology Part B - Microfluidics in single cells. under review

Directing cell migration on flat substrates and in confinement with microfabrication and microfluidics

Short title: Microfabrication and microfluidics to control cell motion

Emilie LE MAOUT[1-5], Simon LO VECCHIO[1-5], Alka BHAT[1-5], Daniel RIVELINE[1-5*]

[1]Laboratory of Cell Physics ISIS/IGBMC, CNRS and University of Strasbourg, Strasbourg, France
[2]Institut de Génétique et de Biologie Moléculaire et Cellulaire, Illkirch, France
[3]Centre National de la Recherche Scientifique, UMR7104, Illkirch, France
[4]Institut National de la Santé et de la Recherche Médicale, U964, Illkirch, France
[5]Université de Strasbourg, Illkirch, France

**Correspondence: riveline@unistra.fr*

1 Introduction

Cell motility plays a key role during development (Helvert, Storm, & Friedl, 2018). When its normal mode of operation is altered, defects appear in tissues, and they can be involved in diseases such as cancer progression. Many genes and pathways have been shown to be important for regulating cell motions *in vivo*, and their roles were further characterized *in vitro*.

Indeed cell motion can be recapitulated on 2D flat coverslips or on Petri dishes: a polarized cell migrates in one direction, pauses, potentially changes polarity and migrates in another direction. Their typical motions over days are represented in Figure 1. Five parameters can encode cell motility. Persistence length is the length travelled 'straight' by the cell during a certain time with no pause. This time is called persistence time. Persistence speed is deduced from the ratio of these two values (see Figure 1B). Next, cell pauses and this phase can be characterized by its duration time; the number of turn per unit time captures the changes in directions. Measurements of these 5 parameters can lead to interesting results to characterize cell motion in a generic way (see Figure 1C and Caballero, Voituriez, and Riveline 2014).

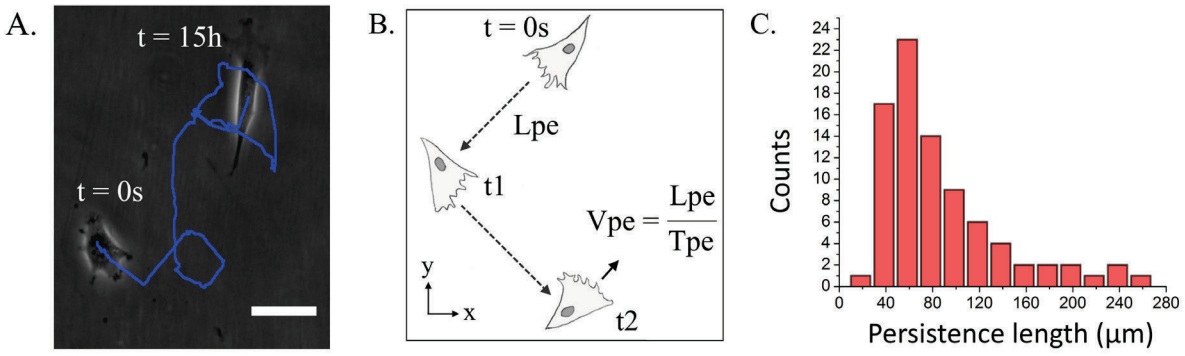

Figure 1: Characterization of NIH3T3 fibroblast migration on a 2D flat substrate**.** A. Typical trajectory of a cell moving randomly on a flat coverslip, the blue trace shows the trajectory; Scale bar 100 µm. B. Schematics showing the migration of a cell, Lpe represents the persistence length, Tpe the persistence time and Vpe the persistence speed; pausing time and number of turns per unit time can also be measured. C. Distribution of a parameter, here the persistence length, for NIH3T3 fibroblasts migrating on flat surface (n=84 trajectories).

1.1 Petri dishes and Boyden chambers: their limits

Experiments have been mainly performed so far in conditions which can be viewed as 'artificial' compared to *in vivo* conditions. For example, cells are cultured and observed in flat Petri dishes (see Figure 1A and 2A), and this method was kept probably for historical reasons (Petri 1887). In this setup, cells have random shapes and this can alter their migration; also, they evolve on 2D flat substrates which constitute an important difference with 3D physiological environments. At the stage of plating, cells can appear as single cells or as groups of cells with an ill-controlled number of cells per group. These varying initial conditions can lead to bias in the study of motility. Other assays using Boyden chambers, for example, can also generate artificial conditions (see Figure 2C and Boyden, 1962): cells are placed in an upper chamber and are exposed to a membrane with cavities of controlled dimensions, typically 10 µm in diameter and 10 µm in depth. In the presence of chemical gradients between the top and bottom compartments, cells eventually migrate. However, the motion itself is restricted to a small fraction of the cell size. This 10 µm cavity limits considerably the potential extrapolation to *in vivo* situations. As a result, with Petri dishes and Boyden chambers, the study of cell migration lacks control and the assays can be far from reproducing physiological conditions.

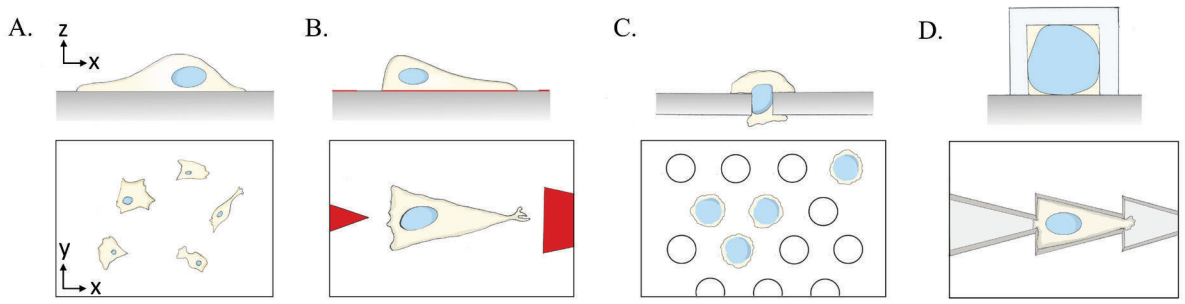

Figure 2: Cell motility on different configurations: A. Cell on Petri dish/flat 2D substrate, B. Cell on 2D ratchet, C. Cell on a 'membrane' in a Boyden chamber experiment, D. Cell in 3D confined ratchet. The nucleus is depicted in blue. In all panels, we represent x-z plane (top) and x-y plane (bottom).

1.2 The microfabrication revolution and its impacts

The usage of techniques developed through microfabrication and microfluidics (Whitesides, 2006) have opened a new era for the study of cell migration (Cramer 2010; Caballero, Voituriez, and Riveline 2014; Hawkins et al., 2009; Prentice-Mott et al., 2013; Jiang et al. 2005). When studying 2D cell migration, the shape of cells can be imposed on surfaces through adhesive micro-contact printing proteins surrounded by cell repellent (see Figure 2B and Théry & Piel, 2009). Cell symmetry and its effect on migration can be analyzed quantitatively and encoded in physical models (Figure 5 and Caballero, Voituriez, and Riveline 2014; Hawkins et al. 2009). In addition, cells can be confined in 3D through the appropriate preparation of microchannels (see Figure 2D); this can reproduce conditions where single cells are trapped in blood vessels with diameters smaller than the cell dimensions. This configuration can also lead to controlled cell symmetries (see Figure 7 and 8). In both cases, on flat 2D printed substrates and in 3D confined geometries, motions can be acquired in the presence of chemical gradients (Comelles et al. 2014; Prentice-Mott et al. 2013).

These developments have been possible because Polydimethylsiloxane (PDMS) the main material to prepare these assays is biocompatible and easy to manipulate. The material is still liquid right after addition of the cross-linker and can be deposited on molds and cured in a 65ºC oven. The PDMS solid mold can be replicated with negative/positive combinations with up to nanometer resolutions in the reproduction of motifs (Qin, Xia, & Whitesides, 2010). Altogether, cell shapes and dimensions are now controlled with microfabrication, and these methods have shown to be essential for obtaining new standardized tests.

We report below the experimental procedures to prepare these assays for the same cell type, *i.e.* NIH 3T3 fibroblasts. Any cell can be used, but the fact of probing the same cell line allows to identify changes in behaviors between experimental conditions set by the assay, such as speeds and directions.

1.3 Designing the motifs: scaling arguments

In order to match the motility assays to each cell type, cell dimensions need to be determined first. The mean area of resting cells on flat coverslips allows to evaluate the optimal surface area needed to micro-contact print adhesive motifs on 2D flat surfaces. Cells will spread on these motifs with their spontaneous resting shape (Figure 2B). In addition, measure of the mean cell diameter after trypsinization and before cells start spreading, helps to evaluate the cell volume and this can guide the design of motifs for 3D confinements (Figure 2D). As reported above, the cell symmetry can also be modified: cells can adopt disk shapes (2D, Caballero, Voituriez, and Riveline 2014) or move along straight channels (3D; Prentice-Mott et al. 2013), and their symmetry can be broken while keeping the projected area/volume constant in 2D/3D assays respectively. In fact, several studies have reported that the presence of asymmetric patterns in the environment can direct cell motion. This kind of motion has been named *ratchetaxis* (Caballero, Comelles, Piel, Voituriez, & Riveline, 2015). In 2D configuration, lines of periodic triangles can be generated to simplify the ratchetaxis motion along a single direction. For the 3D case, lines of periodic connected triangles can be generated to study the motion in confined environments with a local broken symmetry. In addition, the junction/gap between subsequent motifs can be controlled. In 2D, a cell on a motif will have different dynamics depending on the gap between the neighboring motifs. In 3D confined situations, the opening width of connecting triangles will test different regimes in cell motility.

Altogether, cell area in 2D and cell volume in 3D will set rules for the design of the microfabricated unit. Junctions/gaps between motifs will test cell probing and confinement respectively. The sum of microfabricated unit length and junction's length can be integrated in a lattice unit or in cell dimension to compare between conditions and between cell types ($L<100\mu m$ for NIH 3T3 cells, see Figure 1A). Cells trajectory can be then calculated as lattice unit/cell length dimensions. Symmetry/asymmetry will be generated by keeping constant area/volume in 2D/3D respectively.

Finally, the cell velocity should be taken into account for the design of experiments. Specifically, trajectories should be sufficiently long to acquire reliable statistics; this can be evaluated with cell velocity. For example, let us say that cells move at 10 µm/h speed with a typical cell dimension of 100 µm. If we want to follow the cell migration for 10 times the length of a cell (around 1 000 µm), taking into account the frequent pauses on 2D flat surfaces (see Figure 1A), this would require an acquisition of at least 24 hours. In turn, the number of

periodic lattice units should be prepared accordingly to allow cells to potentially move along this 1 000 μm long trajectory.
With these simple orders of magnitude in mind, the masks containing the motifs can be designed for microfabrication.

2 Designing the motifs

Designing of the mask can be done using different softwares, *e.g.* Clewin (Freeware) or Autocad®. A light sensitive material called *photoresist* is used during microfabrication: it is spin-coated on a wafer before exposure of the wafer to UV light when wafer and mask are in close contact (Figure 3).
Motifs are designed depending on the type of photoresist (positive or negative) in use. Here in our study, epoxy based photoresist SU-8 (MicroChem) was used. SU-8 being a 'negative' photoresist becomes insoluble to the SU-8 developer when exposed to UV light. The unexposed regions will be stripped off during the development process leaving behind the micro-structures. Masks have to be designed accordingly, in order to fabricate either holes or pillars on the wafer. It is important to have dark motifs ("+" polarity) on the mask, so that the UV light cannot pass through, in turn fabricating holes on the wafer. Similarly for fabricating pillars, transparent motifs ("-" polarity) have to be designed, which would allow the UV light to pass through the motifs, cross-linking the exposed photoresist. Structures fabricated in such a way have excellent thermal and mechanical stability.
After the masks with the desired dimensions are printed, motifs are prepared through microfabrication (see below; method).

Materials

- Silicon wafers
- Wafer tweezers
- Chromium/plastic photomask (with printed desired motifs to micro-fabricate)
- SU-8 photoresist (2005 and 2025)
- SU-8 developer
- Acetone
- 2-propanol
- Ethanol

Equipment

- Mask aligner
- Spin-coater
- Hot plates (65 °C and 95 °C)
- Disposable graduated dropper (for removal of bubbles)

Method

Two sets of motifs are required for the processes reported in sections II, III and IV. Section II: micro-contact printing requires one layer of the photoresist (25 μm). The depth is tuned to have an optimal aspect ratio: if the pillars are too high and the motif area is too small, pillars will bend during stamping and the quality of the printed patterns will not be optimum. Section III: open microchannel configuration requires one layer of the photoresist (25 μm): height of the photoresist pillars is tuned to have an optimal aspect ratio and PDMS should be high enough to trap the cells (see Figure 7A). Section III and IV: closed microchannel

configuration requires two layers; a first layer of 5 µm thickness and a second layer of 50 µm thickness. The first layer is the microchannel and confines the cells from the top, whereas the second layer constitutes the reservoir for cells and should be high enough to allow cell circulation and positioning.

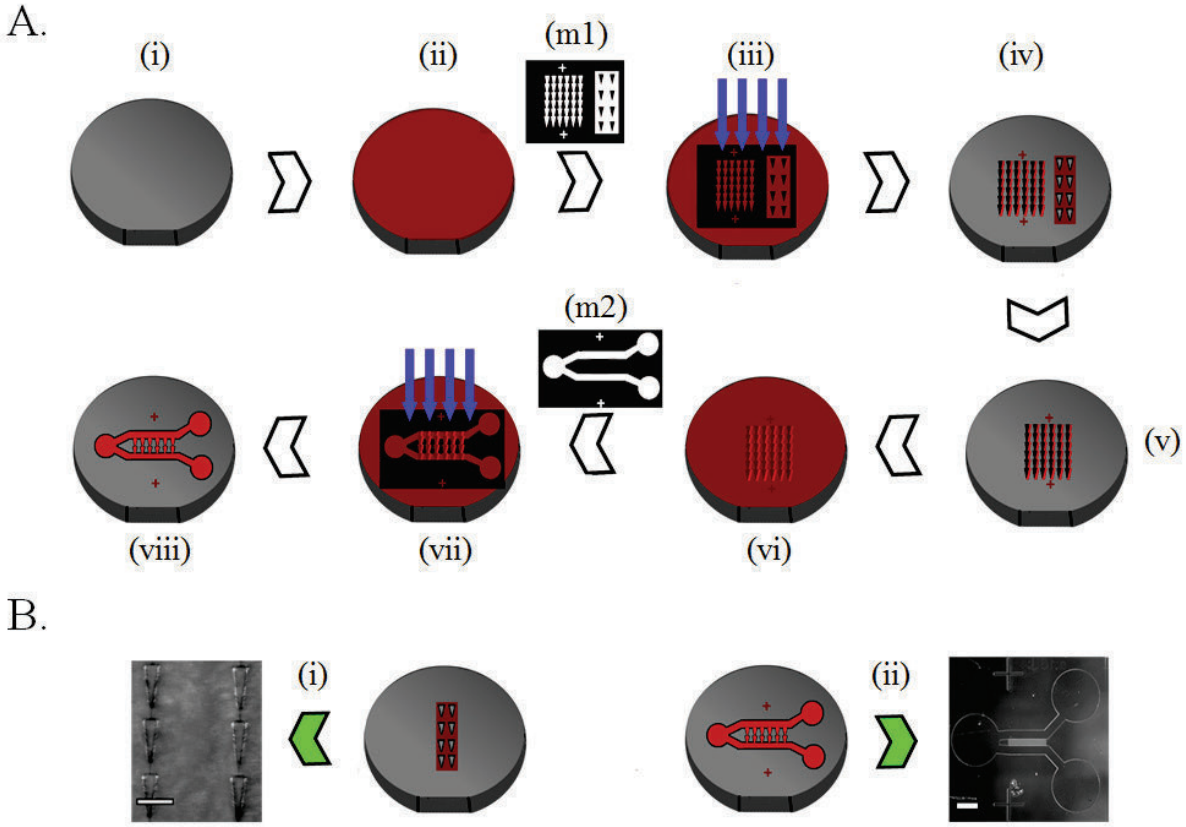

Figure 3: Microfabrication for the study of 2D and 3D ratchetaxis: A. Steps followed to obtain motifs. (i) Silicon wafer (ii) spin-coated with SU-8 (2005, 2025) according to the required height/depth. (iii) UV exposure of the spin-coated wafer through the desired mask (m1) for the first layer. (iv) Developed motifs of the first layer with 5 µm high connected triangles; left side of the wafer and 25 µm deep first layer of separated triangles; right side of the wafer. (v) Wafer with 5 µm high connected triangles (vi) spin-coated with photoresist; SU-8 2025 for 50 µm thickness. (vii) UV exposure of the spin-coated wafer through the desired mask (m2) for the second layer. (viii) Developed motifs of the second layer; connected triangles with the reservoir. B. Developed resin motifs on a Si wafer of (i) 25 µm thick first layer of separated triangles (right side: holes on wafer; left side: image of the wafer, scale bar 100 µm); and (ii) 5 µm thick connected triangles with 50 µm thick reservoir (left side: pillars on wafer: right side, image of the wafer, scale bar 1 mm).

The following steps are performed in a clean room, if available (see Figure 3):

1. Clean the silicon wafers with first acetone and then ethanol. Dry the wafer using a nitrogen stream after each solvent cleaning. Solvent cleaning insures the complete removal of oils and organic residues from the surface of silicon wafers; while they do remove contaminants, solvents themselves actually leave residues on the surface of wafers as well. For this reason, a two-solvent method is implemented to ensure that the wafer is contaminant-free. After this step, heat up the wafers at 200 °C for 15-30 minutes for a complete removal of humidity from the surface of the wafer.
2. Spin-coat the first photoresist layer according to the target thickness. To obtain separated triangular patterns for micro-contact printing (see Figure 4) and open micro-channels (see Figure 7), pour the photoresist (SU-8 2025) on the wafer and remove air bubbles with the aid of a plastic dropper. Set a two-step spinning process on the spin-

coater. Spin at 500 rpm for 10 s with an acceleration of 100 rpm/s during the first step to homogenize the layer over the wafer. Next, spin the wafer containing the resin at 3 000 rpm for 30 s with acceleration of 300 rpm/s for the second step. This should result in a photoresist layer of 25 µm thickness (see Figure 3A (ii)).

3. To obtain the first layer for the closed connected triangular microchannel (see Figure 8), a 5 µm thick layer is required. After repeating step (2) using the desired photoresist (SU-8 2005), spin at 3 000 rpm for 30 s with acceleration of 300 rpm/s for the second spin step. This should result in a photoresist thickness of 5 µm (see Figure 3A (ii)).
4. After obtaining the evenly spread photoresist, pre-bake has to be done to ensure a firm attachment of the photoresist to the wafer. For a 25 µm thick layer, this step has to be done during 5 min at 95 °C and for a 5 µm thick layer during 2 min at 95 °C.
5. After pre-bake, make a firm contact between the wafer and the mask containing the respective motifs. A defective contact will lead to ill-defined motifs (see Troubleshooting Tr.1, Figure 10A). The masks should have negative polarity for 25 µm thick layer (Separated Triangles) to give holes and positive polarity for 5 µm thick layer (Connected Triangles) to obtain pillars on photoresist (SU-8) layer. After tight contact with the desired mask (see Figure 3A; (m1)) cross-link the photoresist by exposing the wafer to UV irradiation with a dose of 150 mJ/cm^2 for 25 µm thick Separated Triangles and 105 mJ/cm^2 for 5 µm thick Connected Triangles (see Figure 3A (iii)). The time of exposure will depend on the power/wavelength of the device (*e.g.* mask aligner) for the UV light exposure.
6. As soon as the exposure is over, for Separated Triangles: follow a post-bake of 1 min at 65 °C and then 5 min at 95 °C; and for Connected Triangle: 3 min at 95 °C. An image of the mask should be visible on the (SU-8) photoresist coating.
7. After post-bake, develop the structures by immersing them in the SU-8 developer solution, while gently agitating the container; 4 min for 25 µm thick Separated Triangles and 1 min for 5 µm thick Connected Triangles layer. This would strip off the non-crosslinked resin, leaving behind the required motifs (see Figure 3A; (iv)). Finally, rinse the surface with 2-propanol to remove the leftover photoresist.
8. Dry the wafer containing motifs, using a nitrogen stream after rinsing with 2-propanol.
9. After preparing a 5 µm thick layer of Connected Triangles (see Figure 3A; (v)), a second layer has to be prepared in order to obtain a microchannel of connected triangles with a reservoir for cells on either sides of the Connected Triangles, in order to introduce cells in microchannels (see Figure 8B).
10. The second layer (for reservoir) is recommended to be 50 µm thick for easy entry of cells with the cell culture media. For this purpose, follow step (2) and spin the wafer containing the resin (SU-8 2025) at 1 700 rpm for 30 s with acceleration of 300 rpm/s for the second spin step (see Figure 3A (vi)).
11. Then follow a pre-bake of 6 min at 95 °C.
12. Before the next step of UV exposure for crosslinking with the desired mask, check on the silicon wafer that the mask for the second layer containing motif for reservoir (see Figure 3A; (m2)) is perfectly aligned with the developed first layer of Connected Triangles. For alignment purpose, it is recommended to design masks with two crosses each, on both mask 1 (containing microchannel motif) and mask 2 (containing the reservoir motif) exactly at the same position. During microfabrication and alignment process, both crosses should superimpose between first photoresist (SU-8) layer and second mask to ensure optimal alignment of first and second layers (see Troubleshooting; Tr. 2)

13. Once the alignment is performed, secure the tight contact between the wafer and the mask (for reservoir). Crosslink the photoresist by exposing the wafer to UV irradiation with a dose of 150-155 mJ/cm^2 for a 50 µm layer of reservoir (see Figure 3A (vii)).
14. As soon as exposure is over, follow a post-bake of 1 min at 65 °C and then 6 min at 95 °C. After post-bake at 95 °C, an image of the mask should be visible on the photoresist coating.
15. Next, develop the structures by immersing the sample in the SU-8 developer solution while gently agitating the container for 5 min. This would strip off the non-crosslinked resin, leaving behind desired motifs (see Figure 3A (viii)). Finally, rinse the surface with 2-propanol to remove the leftovers of photoresist.
16. After the silicon wafers are ready with desired motifs (with 1 or 2 layers), do a 'hard bake' step at 150 °C for a couple of minutes. This is useful for annealing any surface cracks that may have appeared after development; this step is relevant to all layer thicknesses.
17. After obtaining the desired motifs for Separated Triangles (25 µm thick layer) and Connected Triangles (1st layer: 5 µm, 2nd layer: 50 µm), cover the wafers with PDMS (crosslinker:prepolymer [1:10]).
18. Remove all air bubbles through desiccation and finally cure it overnight at 65 °C on a leveled surface.
19. Once cured, peel off the PDMS and obtain the chips (containing the desired motifs) for Separated Triangles and Connected Triangles with the reservoir.

3 Rectifying cell motion with asymmetrical patterns: micro-contact printing of adhesive motifs.

3.1 The design of pattern

The scaling arguments are presented in Caballero et al. (2014) for this assay.

3.2 Micro-contact printing

3.2.1 Protocol

In this section, we detail the protocol for printing adhesive motifs on a glass coverslip. We use fluorescent fibronectin to visualise the motifs with microscopy (other proteins could also be used). Poly-l-lysine-g-PolyEthylene Glycol (PLL-g-PEG) is used for surface passivation (see Figure 4).

Materials

- 'Piranha' solution (sulfuric acid : hydrogen peroxide [7:3])
- Glass coverslips (N°1 – 25 mm diameter)
- 3-(Mercapto)propyltrimethoxysilane
- Phosphate-buffered saline 1x (PBS)
- 10µg/ml Rhodamine labelled Fibronectin (FN) in PBS
- 0.1 mg/ml PLL-g-PEG (diluted in HEPES 10mM)
- PDMS
- Milli-Q Water
- Ethanol 70%

- Parafilm

Equipment

- Plasma Cleaner
- Oven
- Sonicator
- Vacuum pump
- Desiccator

Methods

1. Clean the coverslips inside "Piranha" solution during 10 min (this step should be performed cautiously under a hood). Bubbles will form, check that coverslips stay immersed throughout the process. Carefully rinse the glass coverslips with Milli-Q water. Then, sonicate one by one each coverslip in beakers during 5 min and dry them with a nitrogen stream. Finally, put them in an oven at 65 °C for 10 min.
2. Place the "Piranha" cleaned coverslips inside the desiccator with a small Petri dish filled with 100 µl of 3-(Mercapto)propyltrimethoxysilane. Generate a vacuum, then close the pump and let the silane deposit on the substrates for 1 h.
3. Place the silanized coverslips for at least 90 min at 65 °C (up to 4 h); note that non-bound silane is very sensitive to temperature and humidity.
4. Meanwhile, cut the PDMS to have 1 cm x 1 cm stamps; sonicate them for 5 min in ethanol and dry them with a nitrogen stream.
5. Activate the surface of each stamp with oxygen plasma (air can also be used). This step will make sure that the surface is hydrophilic and suitable for protein incubation and binding. Be sure that patterns face up during activation.
6. Incubate activated stamps with a 100 µl drop of 10 µg/ml solution of Rhodamine labelled FN for 1 h.
7. After incubation, remove the drop with a pipette and quickly dry the stamp with a nitrogen stream. It should take only few seconds. You can also let the stamp dry at room temperature for about 5 min. This step is critical and differences in drying will impact the overall quality of the patterns (see Troubleshooting; Tr.3 and Tr.4).
8. Put the stamp (face with the patterns down) on the silanized coverslip with a 50 g weight on top of it. Wait for 30 min and gently remove the weight and the stamp from the coverslip. Store the patterned glass coverslips in PBS at 4 °C. At this point, patterns can be stored up to one week, even if immediate usage is recommended.
9. Deposit a 100 µl drop of PLL-g-PEG on a piece of Parafilm and put the patterned face of the coverslip on the drop. Incubate for 20 min. This step will passivate the surface and will decrease adhesion of cells outside the patterns.

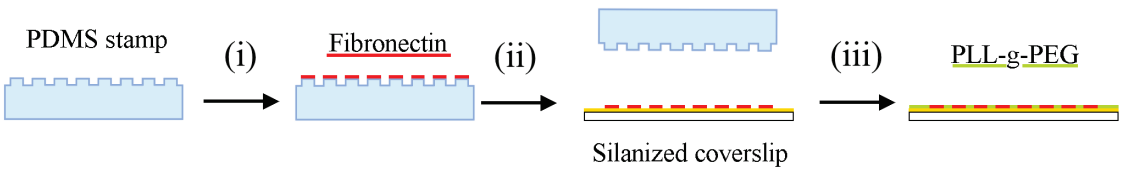

Figure 4: Micro-contact printing procedure: (i) incubation of the PDMS stamp with fibronectin. (ii) Stamping. (iii) Passivation with PLL-g-PEG.

3.2.2 2D cell migration experiment:

The cells should be carefully placed on the micro-contact printed motifs. Proper washing allows to generate samples with cells exclusively on motifs. Cells should be plated at low density. This will help prevent them to migrate along the same path and in turn potentially 'collide'. Such phenomenon would interfere with cells trajectories. Finally, low serum condition allows to keep standard cell motility while preventing cell division during migration.

Materials

- NIH3T3 cells (or other migratory fibroblasts)
- Dulbecco's Modified Eagle Medium (DMEM) 4.5g/l glucose 1% Penicillin-streptomycin
- Bovine Calf Serum (BCS)
- Leibovitz's (L-15) medium
- Trypsin-EDTA
- Cell counter
- Pipettes
- 5 ml Petri dishes (60mm in diameter)

Equipment

- Epifluorescence microscope with phase contrast and temperature control
- Sterile hood
- Incubator with CO_2
- Centrifuge

Methods

At this stage, all steps should be performed under a sterile hood with a laminar flow.

1. Trypsinize a 5 ml Petri dish with adherent cells 3 min, and add 3 ml of DMEM 10% BCS.
2. Centrifuge cells at 500 rpm during 3 min and re-suspend the pellet in 5 ml of DMEM 10% BCS.
3. Count cells and place 2 000 cells on the micro-patterned coverslip.
4. Incubate cells for 30 min at 37 °C with 5% CO_2. Wash out the sample to remove non adherent cells and replace the medium by L-15 with 1% BCS. This low serum condition will ensure standard cell motility while reducing cell division during the 48 h experiments.
5. Go to the microscope and image patterns and cells (See Troubleshooting; Tr.5).

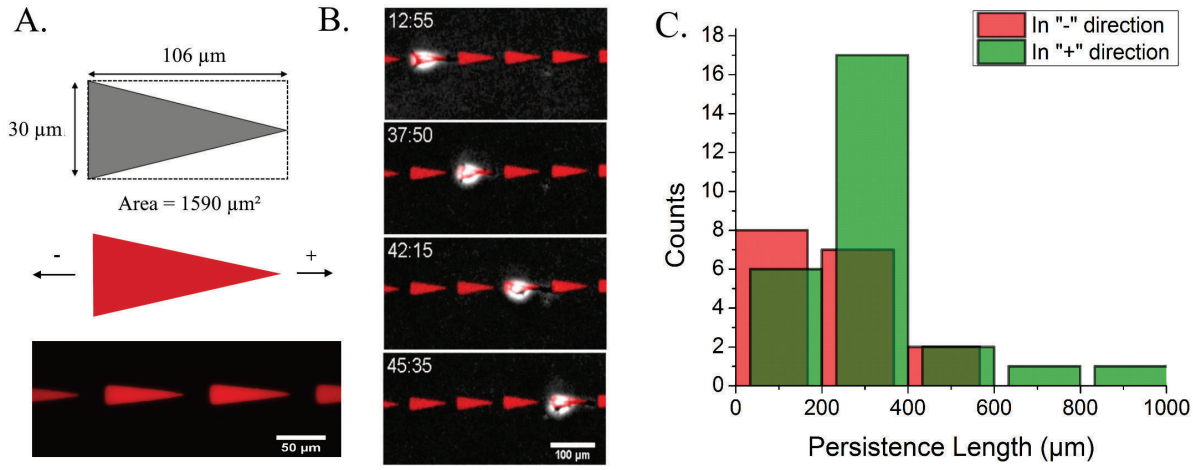

Figure 5: A. Pattern characteristics and dimensions (up) and motifs printed on a surface with micro-contact printing (bottom). Patterns are stamped with rhodamine labelled fibronectin. For clarity, tip direction is set as "+" and triangle base direction as "-" (middle). B. Sequence of a NIH3T3 cell moving on triangles separated by 22 µm gaps. T=0 corresponds to the beginning of acquisition (shortly after plating). Migration is directed towards the "+" direction in this sequence; Scale bar 50 µm. Time in hh:mm. C. Persistence length distribution of NIH3T3 cells migrating in "+" direction and in "-" direction. Motion is directed, or *rectified*, to the + direction on average.

4 Control of cell migration in confined 3D environment

4.1 The design of pattern

Along the scaling arguments (see Introduction), we measured cell volumes after trypsinization. We obtained a mean diameter for individual rounded cells D_{cell}=14.4±1.6 µm (n=388 cells, s.d.), which corresponds to a mean volume of V_{cell}=1560±520 µm^3. Nuclei were stained on spread cells using Hoechst, and their volume and height were measured. The mean volume was $V_{nucleus}$=740±180 µm^3 (n=199 nuclei, s.d.) and the mean height $H_{nucleus}$=8.5±1.4 µm (n=199 nuclei, s.d.). Altogether, we used V_{cell}, $V_{nucleus}$, $H_{nucleus}$ to design the 3D triangle channel motif: each triangular motif has the volume of a NIH3T3 fibroblast (1500 µm^3). Taking into account these values, we designed the height of the microchannel as 5 µm to allow confinement of the cell and nucleus. We calculated the xy area for each triangle to be 300 µm^2: we selected an angle of 16° similar to the angle used in triangles on 2D ratchetaxis and to further confine the nucleus, we selected an opening width of 4 µm between connected ratchets. Using the following parameters (area: 300 µm^2, angle: 16° and opening width: 4 µm), base and length of a ratchet were calculated. They are equal respectively to 14 µm and 34 µm (see Figures 7 and 8). In ratchetaxis experiments, we used this motif in a closed microchannel configuration, where cells were confined from the top and sides (see Figure 8); and in open microchannel configuration, cells were confined only from the sides (see Figure 7).

In order to have a large number of trajectories per experiment, we designed a mask with 50 rows of connected triangles. For the closed configuration, two layers of SU-8 are required. The first layer contains connected ratchets of 5 µm height. The second layer allows to fabricate the reservoir of 50 µm height for the cells. In order to generate chemical gradients, the second layer has a Y-shaped channel of 50 µm height (see Figure 3 and 9B). For the open microchannel configuration, a layer of 25 µm height SU-8 is required in order to trap cells (see Figure 7A).

4.2 Confined open microchannel configuration

4.2.1 Protocol

Materials

- Masks/Silicon wafer
- PDMS
- Glass coverslips (N°1 – 25 mm diameter)
- Chlorotrimethylsilane (Sigma ref 92360)
- 2 ml Petri dish (35mm in diameter)

Equipment

- Plasma cleaner
- Tweezer
- Blade
- Oven
- Spin-coater
- Vacuum pump
- Desiccator

Methods

1. Pour PDMS (crosslinker:prepolymer [1:10]) on a silicon wafer. Remove air bubbles by placing the wafer into desiccator for 1 h. Cure at 65 °C for at least 4 h.
2. Cut PDMS with a blade and remove the PDMS 1 stamp from the wafer (see Figure 6A (i)).
3. Activate the surface of PDMS stamp 1 with oxygen plasma. Put it inside the desiccator with a small Petri dish filled with 100 µl of chlorotrimethylsilane. Generate a vacuum, then close the pump and let the silane deposit on the substrate for 30 min.
4. Pour PDMS (crosslinker:prepolymer (1:10)) on PDMS 1 placed on Petri dish. Check that patterns are 'face up'. Remove air bubbles by placing the wafer into desiccator for 1 h. Cure at 65 °C for at least 4 h (see Figure 6A (ii)).
5. Cut PDMS with a blade and remove the PDMS stamp 2 from the Petri dish containing PDMS stamp 1.
6. Activate with oxygen plasma the surface of PDMS stamp 2. Put it inside the desiccator with a small Petri dish filled with 100 µl of chlorotrimethylsilane. Generate a vacuum, then close the pump and let the silane deposit on the substrate for 30 min.
7. Spin liquid PDMS on PDMS stamp 2. Set a two-step spinning process on the spin-coater. Spin at 500 rpm for 10 s during the first step to homogenize the PDMS layer over the PDMS stamp 2. The speed used in the second step will define the height of PDMS stamp 3. Spin-coating at a speed of 2 000 rpm allows the spreading of PDMS at a height of approximately 40 µm. Cure at 65 °C for at least 4 h (see Figure 6A (iii)).
8. Activate both coverslip and PDMS stamp 3 (see Figure 6A (iv); blue side) with oxygen plasma. Bind the blue surface side of PDMS stamp 3 to the coverslip. Incubate them at 65 °C overnight to secure the binding between the PDMS stamp 3 and the glass coverslip.
9. With a tweezer, gently peel off the PDMS stamp 2 from the PDMS stamp 3 (which is attached to the coverslip).

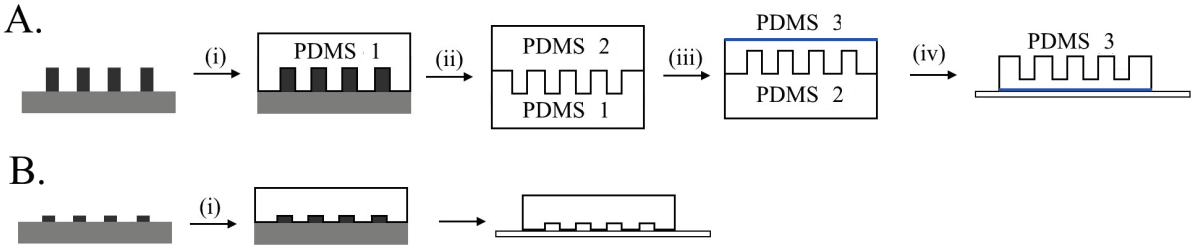

Figure 6: Schematics of the method to obtain closed A. and open B. microchannel configuration. (i) PDMS is poured on SU-8 wafers and cured 4 h at 65 °C. In closed configuration, microchannels are 5 µm height. (ii) After activation of PDMS and coverslip with oxygen plasma, they are both bonded together. In open configuration, microchannels are 25 µm height. (ii) PDMS 1 is cut, activate with oxygen, treated with chlorotrimethylsilane and PDMS is poured on it and cured 4 h at 65 °C. (iii) PDMS 2 is cut, activated with oxygen, treated with chlorotrimethylsilane and PDMS is spin-coated on top of PDMS 2 at 2 000 rpm to obtain 40 µm PDMS layer. (iv) After curing at 65 °C for 4 h and activate with oxygen plasma, PDMS 3 is bonded to a coverslip and incubated overnight at 65 °C to consolidate the bonding. PDMS 2 is then peeled off.

4.2.2 Cell migration experiment:

Materials

- NIH3T3 cells (or other migratory fibroblasts)
- DMEM 4.5g/l glucose 1% Penicillin-streptomycin
- BCS
- L-15 medium
- Trypsin-EDTA
- Cell counter
- Pipettes
- 5 ml Petri dishes (60mm in diameter)

Equipment

- Epifluorescence microscope with phase contrast and temperature control
- Sterile hood
- Incubator with CO_2
- Centrifuge

Methods

At this stage, all steps should be performed under a sterile hood with a laminar flow. We report now how to place the cells in the sample.

1. Prior experiment, activate the surface of the stamp with oxygen plasma. This step will make the surface hydrophilic and facilitate media distribution within the sample. Place the open microchannel sample under UV for 10 min sterilization.
2. Trypsinize a 5 ml Petri dish with adherent cells 3 min and add 4 ml of DMEM 10% BCS. Count cells.
3. Centrifuge cells at 500 rpm during 3 min and re-suspend the cells in DMEM 10% BCS at a density of 100 000 cells/ml.
4. Place 100 µl of the cell suspension on the open microchannel configuration.
5. Incubate 30 min at 37 °C with 5% CO_2. Wash out the sample to remove non adherent cells and replace the medium with L-15 containing 1% BCS.
6. Go to the microscope and acquire cell migration with a 10 min interval.

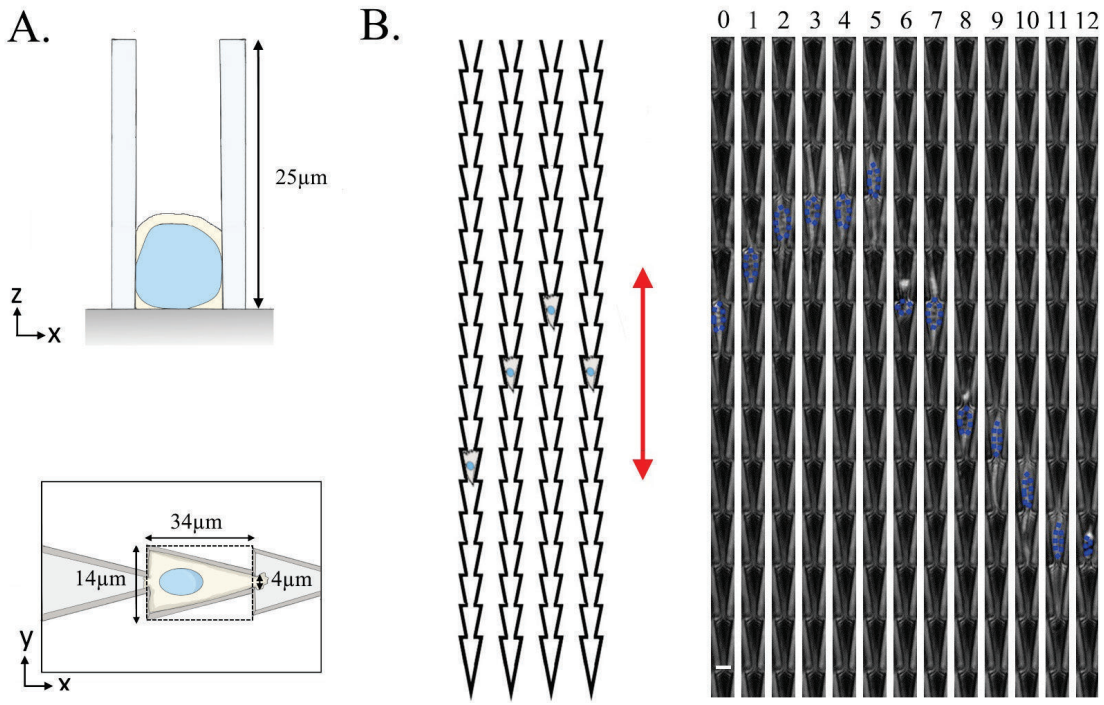

Figure 7: A. Dimension of the triangular 3D open configuration, xz plane (top) and xy plane (bottom). B. Left; schematic of the experimental setup. Cells are seeded in the middle of open ratchet microchannel. Right; Time-lapse images of a NIH3T3 fibroblast migrating in the open ratchet microchannel configuration. Blue dots outline the nucleus over time. Scale bar 10 µm, time in hour.

In open ratchet microchannel configuration, cells seeded in channels migrate longer and preferentially in the "+" direction after probing in both directions (see a typical example Figure 7B (manuscript in preparation).

4.3 Confined closed microchannel configuration

4.3.1 Protocol

Materials

- Masks/Silicon wafer
- PDMS
- Glass coverslips (N°1 – 25 mm diameter)
- Holes puncher

Equipment

- Plasma cleaner
- Tweezer
- Blade
- Oven

Methods

1. Pour PDMS (crosslinker:prepolymer (1:10)) on a silicon wafer. Remove air bubbles by placing the wafer into desiccator for 1 h.
2. Cure at 65 °C for at least 4 h.

3. Cut PDMS with a blade and remove the PDMS stamp from the wafer (see Figure 6B (i)).
4. Punch holes in the reservoirs with a 0.75 mm diameter puncher.
5. Use adhesive tape to remove dusts and PDMS residues deposited on the motifs.
6. Activate the surface the coverslip and PDMS stamp with oxygen plasma. Bind PDMS to the coverslip (see Figure 6A (ii')).
7. Incubate the chip at 65 °C overnight to secure the binding between the PDMS stamp and the glass coverslip.

4.3.2 Cell migration experiment:

At this stage, all steps should be performed under a sterile hood with a laminar flow. To place cells in the sample, we follow this protocol.

Materials

- NIH3T3 fibroblasts (or other migratory fibroblasts)
- Trypsin-EDTA
- DMEM 4.5g/l glucose 1% Penicillin-streptomycin
- Leibovitz's L-15 medium
- BCS
- Pipettes
- Petri dishes
- Eppendorf micro-loader ™

Equipment

- Laminar flow hood
- Incubator
- Centrifuge
- Epifluorescence microscope with phase contrast and temperature control
- Metallic holder

Method

1. Activate the chip with oxygen plasma to make it hydrophilic. Fill in the PDMS chip with L-15 with 10% BCS.
2. Trypsinize a 5 ml Petri dish with adherent cells for 3 min, and add 4 ml of DMEM 10% BCS. Count cells.
3. Centrifuge for 3 min at 500 rpm. Cells will form a pellet. Remove the supernatant and re-suspend cells in L-15 10% BCS at a density of 30 million cells/ml.
4. With an Eppendorf micro-loader, inject 20 µl of the cells suspension into one inlet (see Figure 8B). Slowly aspirate L15 medium from the second inlet to allow accumulation of cells at the entry of channel.
5. Immerse the PDMS chip in L-15 containing 10% BCS.
6. Incubate for 2 h at 37 °C to let cells adhere and spread.
7. Transfer the chip into sterile holder and start the time-lapse acquisition with a 10X objective and 10 min interval. Note that due to the presence of a thin layer of PDMS in the optical path, phase contrast images might not be perfect. To improve the phase contrast, use an objective with a numerical aperture (N.A.) of a minimum 0.40 N.A.

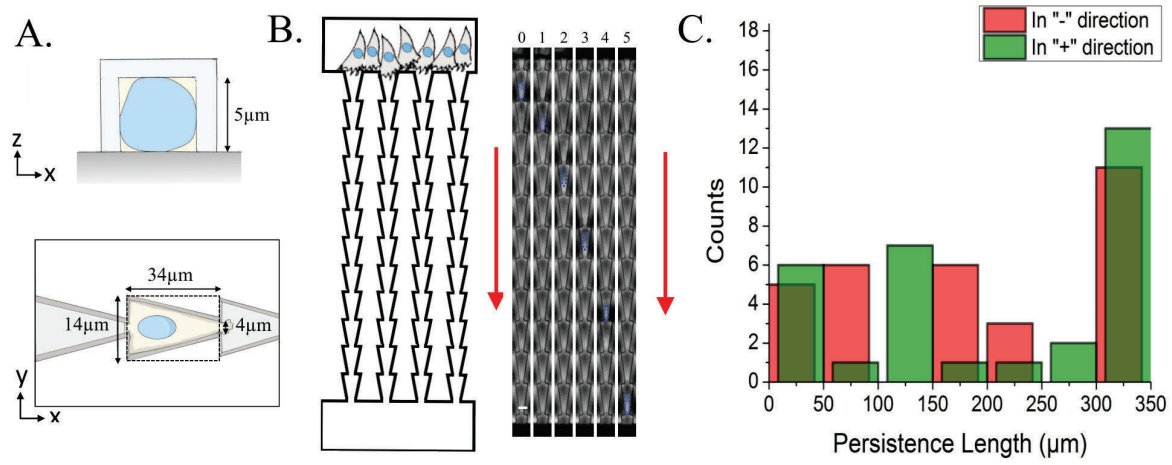

Figure 8: Dimension of the triangle 3D confined motifs. A. Schematic of a ratchet unit with its dimensions, xz axis (top) and xy axis (bottom). B. Left: Schematics of the experimental setup. Cells are seeded in one side of the channel allowing the entry and migration of the cells in the "+" direction (red arrow). Right: Time-lapse images of a NIH3T3 fibroblast migrating in a ratchet microchannel in the "+" direction (red arrow). Blue dots outline the nucleus over time. Scale bar 10 µm, time in hours. C. Persistence length distributions of cells migrating in "+" direction and in "-" direction. Experiments in B. was repeated with cells plated on the other side of the channel. Altogether, the confined configuration forces cells to follow the polarity set at the entry of channels (data in preparation).

5 Control of cell migration in 3D with chemotaxis

With this setup, the motion of cells can be challenged by a chemical gradient when the sample is closed (see Figure 9B). We report now the protocol.

5.1.1 Protocol:

Materials

- Masks/Silicon wafer
- PDMS
- Glass coverslips (N°1 – 25 mm diameter)
- Holes puncher

Equipment

- Plasma cleaner
- Tweezer
- Blade
- Oven

Methods

1. Pour PDMS (crosslinker:prepolymer (1:10)) on a silicon wafer. Remove air bubbles by placing the wafer into desiccator for 1 h.
2. Cure at 65 °C for at least 4 h.
3. Cut PDMS with a blade and remove the PDMS stamp from the wafer (see Figure 6A (i)).
4. Punch holes in the inlets-outlet with a 0.75 mm diameter puncher.
5. Use adhesive tape on the motifs to remove any residual dusts and/or PDMS residues.

6. Activate the surface the coverslip and PDMS stamp with oxygen plasma. Bind PDMS to the coverslip (see Figure 6A (ii)).
7. Incubate the chip at 65 °C overnight to secure the binding between the PDMS stamp and the glass coverslip.

5.1.2 Cell migration experiment:

At this stage, all steps should be performed under a sterile hood with a laminar flow. To place cells in the sample, we follow this protocol.

Materials

- NIH3T3 fibroblasts (or other migratory fibroblasts)
- Trypsin-EDTA
- DMEM 4.5g/l glucose 1% Penicillin-streptomycin
- Leibovitz's L-15 medium
- BCS
- Petri dishes
- Eppendorf micro-loader ™
- Tetramethylrhodamine isothiocyanate–Dextran, Molecular weight 20kDa (Sigma ref 73766)
- 1ml syringe (Henke-Sass Wolf Soft-Ject ref 5010-A00V0)
- 20Gx1" needle (Terumo 0.9x25mm Luer)
- 23Gx1" needle (Terumo 0.6x25mm Luer)
- Tygon tubing (Saint Gobain ref AAD04103)

Equipment

- Laminar flow hood
- Incubator
- Centrifuge
- Epifluorescence microscope with phase contrast and temperature control
- Metallic holder
- Syringe pump

Method

1. Activate the chip with oxygen plasma to make it hydrophilic. Fill in the PDMS chip with L15 with no BCS (0% BCS).
2. Trypsinize a 5 ml Petri dish with adherent cells 3 min, and add 4 ml of DMEM containing 10% BCS. Count cells.
3. Centrifuge for 3 min at 500 rpm. Cells will form a pellet. Remove the supernatant and re-suspend cells in L15 0% BCS at a density of 30 million cells/ml. Cells are re-suspended in L15 0% BCS in order to starve cells prior stimulation to the serum gradient.
4. With an elongated tip, inject 20 µl of cell suspension into the outlet. Slowly aspirate L-15 medium from inlet 1 to allow accumulation of cells at the channels entry (see Figure 9B).
5. Immerse the PDMS chip in L-15 0% BCS.
6. Incubate for 2 h at 37 °C to let cells adhere and spread.
7. Transfer the chip into the sample holder.

8. To form the serum gradient, two 1 ml syringes are prepared with L-15 0.1% BCS or L-15 containing 10% BCS and fluorescent dextran, enabling the visualization of the chemical gradient.
9. Connect syringes to syringe needles (23Gx1") and Tygon tubing which have previously been rinsed with L-15.
10. Make sure that there are no bubbles into the tubing during experiment. This can prevent a good flow and detach cells if bubbles enter the microfluidic device (see Troubleshooting; Tr.6 and Figure 10F).
11. Connect tubing to the two inlets of the chip by using cut syringe needles (20Gx1"). The outer diameter of the needles (0.9 mm) is slightly larger than the diameter of the punched holes (0.75 mm). This makes sure that upon insertion the connection is sealed securely (see Figure 9C).
12. Place syringes on the pump. Flow the two solutions at a rate of 10 µl/h. After few minutes, a stable gradient forms into microchannels which can be visualized with fluorescent dextran as seen in Figure 9D and E.

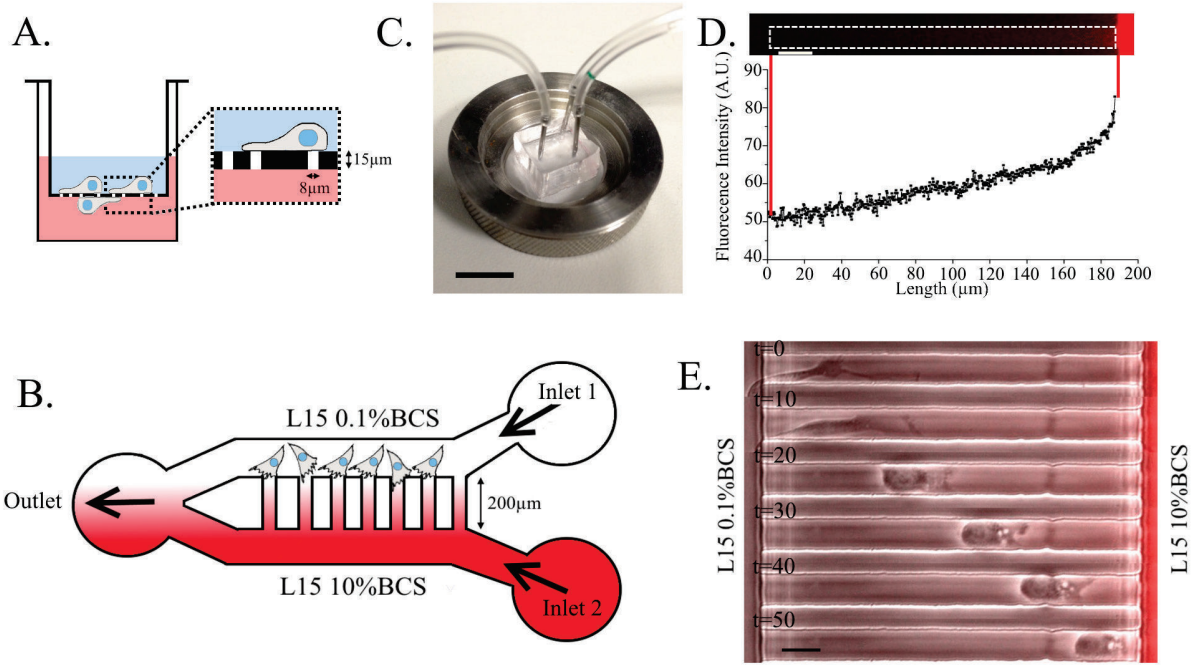

Figure 9: Boyden and microfluidics experiments to study chemotaxis. A. Schematic of a Boyden chamber. Typically, a Boyden chamber is composed of two chambers separated by a 15 µm thickness membrane with 8 µm pores (Boyden, 1962). Cells are seeded in the upper chamber in medium without chemo-attractant. The lower chamber is filled with medium containing the chemo-attractant. After incubation for 12 h, migration is stopped and migrating cells which crossed the membrane are counted. B. Schematic of the microfluidic chip used to follow the migration of cells across time in response to a chemical gradient. Cells are seeded in the microfluidics chamber. Gradient is formed in the micro-channels by connecting two syringes, one with the chemo-attractant and fluorescent dye and the other one without. A syringe pump is necessary to form stable gradient up to 24 h. C. Image of the device. Scale bar 1 cm. D. Top, fluorescent image of the microchannel and the chemical gradient visualized with the fluorescent dye. Bottom, corresponding fluorescent intensity profile along the microchannel. Scale bar 20 µm. E. Time-lapse images of a NIH3T3 fibroblast migrating in a microchannel in a gradient of 10% serum. Scale bar 20 µm, time in minutes.

Conclusion: With this method, chemical gradients can be generated in closed configurations - but not in open configurations. They can be imposed in competition or in cooperation with other external cues such as confinement and ratchetaxis. The net results can be reported through the analysis of trajectories like in the other examples presented above.

6 Troubleshooting

Many issues can appear in the preparation of samples, during the microfabrication, micro-patterning, or even during the acquisition under the microscope. We follow the order of their appearances below.

6.1 Microfabrication:

Tr. 1: During microfabrication process, a critical step is to obtain well defined structures, for example, triangles should have sharp edges. Ill-defined structures will appear, if there is not a firm contact maintained between SU-8 and mask (see step in Figure 3(iii) and Figure 10A). To prevent this, make sure that the contact is tight enough. This can also happen during the development step when motifs are underdeveloped. To avoid this, immerse back the wafer in SU-8 developing solution for 30 s, rinse with isopropanol and check the motifs.

Tr. 2: If two layers are required, they need to be perfectly aligned. A misalignment is observed when crosses on the wafer of layer 1 do not overlap with crosses on the mask for the layer 2 (see Figure 10B filled arrows). This results in disconnected structures from the first and second SU-8 layers (see Figure 10B empty arrow). To prevent this, be patient and pay attention during alignment step that both crosses are aligned. During the design of the mask, it is possible to insert more asymmetric motifs in both masks (for the layers 1 and 2) along the motifs to make sure that there is optimal alignment, before UV exposure.

6.2 Micro-contact printing:

Tr. 3: Drying time critically depends on humidity, the ambient temperature in the room and on patterns characteristics (area, aspect ratio and spacing between motifs). It can vary from 2 min to 6 min depending on the design. Drying the stamps with a nitrogen stream can prevent these problems but this method is more difficult to control. Drying too much the stamp will impede fibronectin transfer to the glass surface (Figure 10C). On the other hand, a stamp too wet gives ill-defined patterns (Figure 10E). This is the most critical step.

Tr. 4: Double stamping (Figure 10D) usually happens when the stamp moves while applying pressure or when it touches again the coverslip while removing it. Using two tweezers to remove the stamp (one on the coverslip, the other one holding the stamp) is a good solution to carefully release the PDMS stamp from the coverslip.

Tr. 5: Cell death during acquisition might happen for the following reasons:

- Coverslips are not well rinsed after ‘piranha’ treatment.
- Stability of PLL-g-PEG: it is recommended not to use the diluted solution after 2-3 weeks.
- Cells are too confluent on the plate, prior deposition on patterns: contact inhibition might affect cell motility and prevent motion leading to death on the motifs (especially for large gap distances).

6.3 Microfluidics:

Tr. 6: While imaging, air bubbles can affect the stability of chemical gradients (see Figure 10F), and can lead to detachment of cells from the coverslip. Typically, this type of

experiments cannot be analyzed. To prevent this, make sure that there are not bubbles in the tubing while preparing them and before starting experiment.

Tr. 7: Even after the sealing of PDMS stamps to the coverslip, sometimes detachment can occur. A proper binding is particularly important for generating the chemical gradient. In this situation, check that plasma binding is properly achieved. Also, check if PDMS and coverslips are clean and without dusts, which if present could prevent proper sealing.

Optimal z -focus: In order to image cells during typical timescales relevant for reliable measures *i.e.* days, cells need to remain within the same focal plane. When acquiring for longer time periods at 37 °C, microscopes might exhibit some drift due to thermal gradients, in particular along the z-direction. A good solution involves placing the entire experimental set-up in an environment with temperature control ahead of time, prior the experiment to generate a good mechanical stability. Alternatively, feedback loops to control the objective-sample distance can be used to keep focus throughout acquisition. Also µm size beads can be deposited on the sample, and images can be realigned after experiments using these fiducial markers.

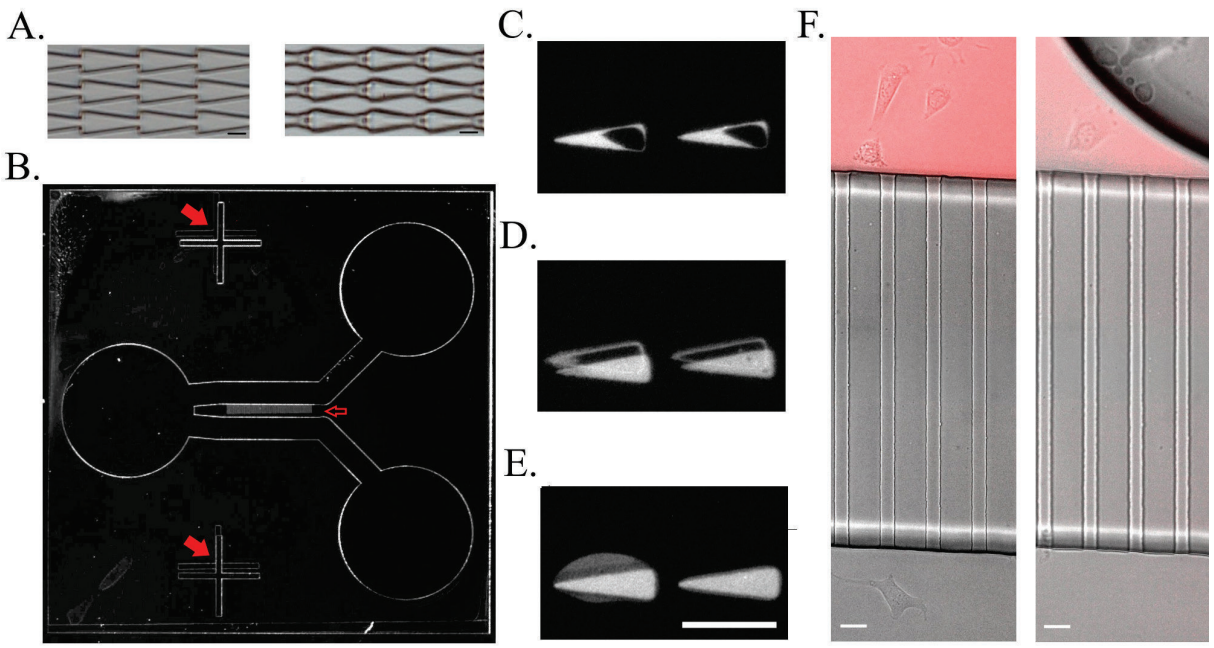

Figure 10: Issues encountered during microfabrication (A. and B.) and micro-contact printing process (C., D. and E.) and microfluidics experiments (F.). A. Images of two wafers. Left: image of connected ratchet microchannel properly defined. Right: image of ill-defined connected ratchet microchannel due to poor contact between SU-8 on wafer and mask. Scale bar 20 µm. B. Image of a wafer where first and second layers are misaligned. Filled red arrows show non-aligned crosses, empty red arrow show that micro-channels are not connected to the main channel at the bottom side. Scale bar 100 µm. C. Patterns with over-dried stamp. D. Double stamping. E. Wet patterns. F. Appearance of bubbles during chemical gradient experiment in microchannel. Chemical gradient is removed in the presence of bubble. Scale bar 20 µm**.**

7 Conclusion:

The methods reported in this article show how cell migration can be controlled specifically for a quantitative study. Their implementations do not require large and expensive equipment and these assays can be used in any laboratories. Designs of 2D and 3D cellular controls have allowed to reveal new modes of migrations (Bergert et al., 2015; Caballero et al., 2015; Liu et al., 2015). With such setups, more migration modes could appear and the associated signaling

networks could be studied. Finally these microfabrication techniques could also open potential new methods for diagnosis at cellular scales in diseases where migration is impaired, in cancer for example (Mitchell, Jain, & Langer, 2017).

References

We apologize for not quoting an exhaustive list of references on these quickly expanding approaches.

Bergert, M., Erzberger, A., Desai, R. A., Aspalter, I. M., Oates, A. C., Charras, G., … Paluch, E. K. (2015). Force transmission during adhesion-independent migration. *Nature Cell Biology*, *17*(4), 524–529.

Boyden, S. (1962). The chemotactic effect of mixtures of antibody and antigen on polymorphonuclear leucocytes. *Journal of Experimental Medicine*, *115*(3), 453–466.

Caballero, D., Comelles, J., Piel, M., Voituriez, R., & Riveline, D. (2015). Ratchetaxis: Long-Range Directed Cell Migration by Local Cues. *Trends in Cell Biology*, *25*(12), 815–827.

Caballero, D., Voituriez, R., & Riveline, D. (2014). Protrusion fluctuations direct cell motion. *Biophysical Journal*, *107*(1), 34–42.

Comelles, J., Caballero, D., Voituriez, R., Hortigüela, V., Wollrab, V., Godeau, A. L., … Riveline, D. (2014). Cells as active particles in asymmetric potentials: Motility under external gradients. *Biophysical Journal*, *107*(7), 1513–1522.

Cramer, L. P. (2010). Forming the cell rear first: breaking cell symmetry to trigger directed cell migration. *Nature Cell Biology*, *12*(7), 628–632.

Hawkins, R. J., Piel, M., Faure-Andre, G., Lennon-Dumenil, A. M., Joanny, J. F., Prost, J., & Voituriez, R. (2009). Pushing off the walls: A mechanism of cell motility in confinement. *Physical Review Letters*, *102*, 058103-1–058103-4

Helvert, S. Van, Storm, C., & Friedl, P. (2018). Mechanoreciprocity in cell migration. *Nature Cell Biology*, *20*(1), 8-20.

Jiang, X., Bruzewicz, D. A., Wong, A. P., Piel, M., & Whitesides, G. M. (2005). Directing cell migration with asymmetric micropatterns. *Proceedings of the National Academy of Sciences of the United States of America*, *102*(4), 975–978.

Liu, Y. J., Le Berre, M., Lautenschlaeger, F., Maiuri, P., Callan-Jones, A., Heuzé, M., … Piel, M. (2015). Confinement and low adhesion induce fast amoeboid migration of slow mesenchymal cells. *Cell*, *160*, 659–672.

Mitchell, M. J., Jain, R. K., & Langer, R. (2017). Engineering and physical sciences in oncology: challenges and opportunities. *Nature Reviews. Cancer*, *17*, 659–675.

Petri, J.R (1887). Eine kleine Modification des Koch'schen Plattenverfahrens. *Centralblatt für Bakteriologie und Parasitenkunde*, 1, 279-280.

Prentice-Mott, H. V, Chang, C.-H., Mahadevan, L., Mitchison, T. J., Irimia, D., & Shah, J. V. (2013). Biased migration of confined neutrophil-like cells in asymmetric hydraulic environments. *Proceedings of the National Academy of Sciences of the United States of America*, *110*(52), 21006–11.

Qin, D., Xia, Y., & Whitesides, G. M. (2010). Soft lithography for micro- and nanoscale patterning. *Nature Protocols*, *5*(3), 491–502.

Théry, M., & Piel, M. (2009). Adhesive micropatterns for cells: A microcontact printing protocol. *Cold Spring Harbor Protocols*, *4*(7), 1–12.

Whitesides, G. M. (2006). The origins and the future of microfluidics. *Nature*, *442*, 368–373.

Emilie LE MAOUT

Ratchetaxie et chimiotaxie, ou comment diriger la migration des cellules sous confinement

Résumé

La migration des cellules individuelles est un phénomène clé d'un point de vue physiologique ou pathologique. *In vitro*, la migration des cellules est par défaut étudiée sur surface plane. Dans cette thèse, nous avons étudié la migration cellulaire dans un espace confiné, appelé microcanal, dont les dimensions miment les capillaires sanguins. Deux types de migration dirigée ont été étudiés, la chimiotaxie, qui dirige la migration des cellules avec un gradient chimique et la ratchetaxie, qui dirige la migration des cellules grâce à la présence de motifs asymétriques et répétés dans leur environnement. Nous avons prouvé que la ratchetaxie est capable de diriger et rectifier la migration des cellules sous confinement. Nous avons aussi rapporté l'importance de la déformation du noyau pour diriger la migration cellulaire. Cette thèse met en évidence l'importance de l'étude de la motilité des cellules sous confinement ainsi que le rôle de l'environnement pour orienter sa migration.

Mots-clés: migration cellulaire sous confinement, ratchetaxie, chimiotaxie, rectification de la migration

Résumé en anglais

Single cell migration is a key phenomenon involved in physiological and pathological processes. *In vivo*, cells migrate under confinement. *In vitro,* for simplicity reasons, cell migration is studied on flat surfaces. In this PhD thesis, we studied cell migration in confined environment, called microchannel, whose dimensions are similar to blood capillaries. Two types of directed cell migration have been studied, chemotaxis, which is the way to direct cell migration with chemical gradients and ratchetaxis, recently discovered being able to direct cell migration due to the presence of asymmetric and repetitive motifs in the cell environment. We showed that ratchetaxis directs cell migration under confinement. We reported also the importance of nucleus deformation to direct cell migration. Altogether, this PhD thesis highlights the importance of studying cell migration under confinement and the key role of the environment to direct cell migration.

Key-words: cell migration under confinement, ratchetaxis, chemotaxis, cell rectification